Investigating Neurovascular Function in Pre-Clinical Models of Alzheimer's Disease & Atherosclerosis

Osman Shabir

A thesis submitted for the degree of Doctor of Philosophy (PhD)

Neuroimaging in Cardiovascular Disease (NICAD) Network Studentship

August 2020

Abstract

Background: Neurovascular coupling (NVC) is essential to brain health and the breakdown of NVC is proposed to be a key pathological factor in the development of Alzheimer's disease (AD), vascular dementia (VaD) and other cerebrovascular diseases. Importantly; as we age, the presence of two or more comorbidities is common and this often leads to clinical complications. Whilst preclinical models of human disease are numerous and have supported basic and translational neuroscience immensely over the past few decades, models of comorbidity are few and often neglected when it is important to study comorbidity to reflect clinical presentations in patients. This project will focus on examining neurovascular function in 3 different preclinical models of AD, atherosclerosis (ATH) and comorbid AD & ATH (MIX).

Aims & Objectives: I) To investigate neurovascular function at an early-AD timepoint (6m) in the J20-hAPP model of AD (J20-AD); when amyloid-beta deposits begin to form, using a chronic surgery recovered animal protocol. Neurovascular function will be assessed by 2D-optical imaging spectroscopy (2D-OIS) to measure cortical haemodynamics, in addition to using multichannel microelectrodes to obtain neural multi-unit activity (MUA). II) To investigate neurovascular function in a novel experimental model of ATH using the rAAV8-mPCSK9-D377Y + Western Diet model (PCSK9-ATH). III) To create a mixed comorbid model of AD and ATH (J20-PCSK9-MIX) and to investigate neurovascular function in this novel model. IV) To assess neuropathology and neuroinflammation from brain tissue in the 3 disease models.

Results: Firstly, at an early stage, J20-AD mice exhibit enhanced evoked-haemodynamic responses associated with neural hyperexcitability. They also display a unique time-dependent elevation of baseline blood volume under normobaric hyperoxia. Secondly, PCSK9-ATH display reduced evoked-responses and show signs of neurovascular dysfunction associated with increased IL1β & TNFα-neuroinflammation. Thirdly, J20-PCSK9-MIX comorbid mice have a trebling of Aβ plaques in the hippocampus, although, without any further worsening of neurovascular function in the cortex compared to J20-AD mice, although all 3 disease models show a trend towards the reduced washout of HbR, which indicates metabolic inefficiency and inadequate oxygen delivery to neurons. Finally, electrode insertion into the brain (causing mild brain injury) leads to cortical spreading depression (CSD) to occur in all mice, with the most severe CSD occurring in J20-AD and PCSK9-ATH mice, and this may be related to levels of IL1β neuroinflammation, though this needs to be confirmed.

Conclusions: These results provide novel insights in all 3 disease models which have important translational implications by highlighting distinct therapeutic targets and strategies. The results also show the importance of neurovascular function in dementia and targeting impairments to neurovascular function early on may be key to slowing down the onset and progression of dementia.

Declaration

I, Osman Shabir, confirm that the thesis is my own work. I am aware of the University's Guidance on the Use of Unfair Means (www.sheffield.ac.uk/ssid/unfair-means). This work has not been previously been presented for an award at this, or any other, University.

This thesis is in a **publication format** and comprises of the following **published papers**:

1. **Chapter 1a (A Review) – Shabir et al, 2018.** Neurovascular dysfunction in vascular dementia, Alzheimer's and atherosclerosis. BMC Neuroscience 19(1):62. In addition to Shabir et al, 2018, there is further commentary in chapter 1 that is not published.

- **Chapter 1b (A Review) – Shabir et al, 2020.** Preclinical Models of Disease and Multimorbidity with Focus upon Cardiovascular Disease and Dementia. Mechanisms of Ageing and Development 192:111361 as part of special issue on multimorbidity. *Only my section of models of cardiovascular disease and cerebrovascular disease has been included in this thesis. The other sections were not relevant to the thesis and have been omitted.*

2. **Chapter 3 – Shabir et al, 2020.** Enhanced Cerebral Blood Volume Under Normobaric Hyperoxia in the J20-hAPP Mouse Model of Alzheimer's Disease. Scientific Reports 10(1):7518.

In addition, the following experimental chapters include papers in submission, and/or currently on *bioRxiv* (biorxiv.org) the preprint server:

- **Chapter 5 – Shabir et al, 2020.** Assessment of Neurovascular Coupling & Cortical Spreading Depression in Mixed Models of Atherosclerosis & Alzheimer's Disease (submitted to journal at time of submission) – preprint on bioRxiv (2020.08.13.249987).

At the start of each chapter, a full acknowledgment and reference of the publication and its format is given, in addition to any full permissions, my contribution, as well as that of my co-authors and collaborators is stated. All chapters are formatted according the submitted journals guidelines and the format may vary between chapters. Some of the chapters contain additional data and commentary that is not in the submitted manuscripts.

Acknowledgments

I am hugely thankful to Dr Jason Berwick for his constant excitement & enthusiasm about the data and the project, his blunt & honest manner, his sense of humour and his friendship. Jason not only has helped me massively with the data analysis, but also being heavily involved with the experiments themselves given that we had a limited number of animals and resources. *Maybe I will learn MATLAB, at some point, but a huge thanks for all the help.* Also, a very special thank you to Prof Sheila Francis who has been one of the most supportive mentors and her constant guidance and thorough feedback has been hugely important in improving my writing and presentations skills as well as becoming a better scientist all round. I'm also hugely thankful to Sheila for believing in my abilities and applying for a project grant to the BHF to continue our work with me as the named post-doc that I am very excited to begin. I couldn't have asked for 2 better supervisors than Jason & Sheila, who have both given me freedom during my PhD to do my own experiments & to support me in fellowship applications.

The PhD would not have been the same without the Neurovascular Lab members, namely Dr Clare Howarth, Llywelyn Lee & Beth Eyre. Firstly, I want to thank Llywelyn for his friendship right from the start, him training me on the surgeries and imaging experiments, and for being an incredibly supportive friend throughout the PhD. Secondly, I want to thank Clare for all the help she has given me throughout the 3 years, especially with data analysis, proofreading scripts and applications, helping with experiments as well as all the chats we've had in our office! Finally, I want to thank Beth for her continuous optimistic outlook on life; which has actually rubbed off on me now, and for her rather crude sarcasm – which is lovely.

I would like to thank Monica (Ale) Rebollar for her help in brain dissections. I would also like to thank all of the lovely BSU staff, in particular Michelle & Barry Bird (great couple!), Beka Armstrong & Rachel Sandy for all their help with the animals, and all the lovely chats we've had over the last 3 years. I also want to thank all my friends and colleagues across SITraN, Psychology, IICD and BMS for their support, laughter and good times along the way (including the 'enemies' I may have made!). I fear that if I start listing names, I may accidentally miss off some, so to all of you – thank you! (Oh, and a special shout out to Toby, Jordon and Lorna!).

Finally, a huge thanks to my family; especially my mum, my dad and my brother who have supported me immensely during my PhD (and before), even though they don't quite understand a) what I actually do & b) what I am going to do with my PhD – neither do I! It was their encouragement from childhood that has led to me where I am to today. Also, a huge shout out to the COVID-19 pandemic for really putting a fantastic end to the PhD (not)! But also, hugely thankful to the University for granting me a 2 month fully paid extension.

Table of Contents

List of Figures

List of Tables

List of Abbreviations

2D-OIS	2D-Optical Imaging Spectroscopy
AAV	Adeno-Associated Virus
Aβ	Amyloid Beta
AD	Alzheimer's Disease
ApoE	Apolipoprotein E
APP	Amyloid Precursor Protein
AQP4	Aquaporin-4
ATH	Atherosclerosis
BBB	Blood Brain Barrier
BOLD	Blood Oxygen Level Dependent
CAA	Cerebral Amyloid Angiopathy
CBF	Cerebral Blood Flow
CbVD	Cerebrovascular Disease
CSD	Cortical Spreading Depression
CSF	Cerebrospinal Fluid
CVD	Cardiovascular Disease
EMCI	(Early) Mild Cognitive Impairment
EOAD	Early-Onset Alzheimer's Disease
HbO	Oxyhaemoglobin
HbR	Deoxyhaemoglobin
HbT	Total Haemoglobin
IHC	Immunohistochemistry
IL1β	Interleukin 1-beta
LDL	Low Density Lipoprotein
LDLR	Low Density Lipoprotein Receptor
MCA	Middle Cerebral Artery

MUA	Multi-Unit Activity
NOS	Nitric Oxide Synthase (e; endothelial, n; neuronal)
NVC	Neurovascular Coupling
NVU	Neurovascular Unit
PCSK9	Proprotein Convertase Subtilisin/Kexin Type 9
PDGFRβ	Platelet-Derived Growth Factor Receptor Beta
qRT-PCR	Quantitative Reverse-Transcriptase Polymerase Chain Reaction
ROI	Region of Interest
ROS	Reactive Oxygen Species
SEM	Standard Error of Mean
SVD	Small Vessel Disease
TBI	Traumatic Brain Injury
TNFα	Tumour Necrosis Factor-alpha
VaD	Vascular Dementia
VSMC	Vascular Smooth Muscle Cell

Chapter 1 – Introduction

This chapter contains 2 published review articles:

Shabir et al, 2018. BMC Neuroscience. 19:62 & Shabir et al, 2020. Mechanisms of Ageing and Development. 192:111361

1.1 – Paper Title and Authors

Neurovascular Dysfunction in Vascular Dementia, Alzheimer's and Atherosclerosis.

Osman Shabir[1]*, Jason Berwick[1] & Sheila E Francis[2]

[1]The Neurovascular & Neuroimaging Group, Alfred Denny Building, University of Sheffield, Western Bank, Sheffield, S10 2TN

[2]Department of Infection, Immunity & Cardiovascular Disease, University of Sheffield, Medical School, Beech Hill Road, Sheffield, S10 2RX

**Corresponding Author.*

Author emails: oshabir1@sheffield.ac.uk, j.berwick@sheffield.ac.uk & s.francis@sheffield.ac.uk

I, Osman Shabir, am the author of this manuscript and made all the figures. JB & SF proofread and edited the manuscript. This review was published at the end of my first year to set the groundwork for my project and to highlight the research gaps in the field.

1.2 – Abstract

Efficient blood supply to the brain is of paramount importance to its normal functioning and improper blood flow can result in potentially devastating neurological consequences. Cerebral blood flow in response to neural activity is intrinsically regulated by a complex interplay between various cell types within the brain in a relationship termed neurovascular coupling. The breakdown of neurovascular coupling is evident across a wide variety of both neurological and psychiatric disorders including Alzheimer's disease. Atherosclerosis is a chronic syndrome affecting the integrity and function of major blood vessels including those that supply the brain, and it is therefore hypothesised that atherosclerosis impairs cerebral blood flow and neurovascular coupling leading to cerebrovascular dysfunction. This review will discuss the mechanisms of neurovascular coupling in health and disease and how atherosclerosis can potentially cause cerebrovascular dysfunction that may lead to cognitive decline as well as stroke. Understanding the mechanisms of neurovascular coupling in health and disease may enable us to develop potential therapies to prevent the breakdown of neurovascular coupling in the treatment of vascular brain diseases including vascular dementia, Alzheimer's disease and stroke.

1.3 – Introduction

The human brain accounts for just 2% of total body weight, yet receives between 15-20% of total cardiac output[1]. It is therefore evident that the brain requires an efficient and adequate blood supply to support the metabolic demands it exerts. Unlike the majority of organs and tissues, the brain has a tightly regulated blood brain barrier (BBB), which prevents leakage of blood into the parenchyma and protects the brain from toxic agents and infection. Neurons, therefore, are not in direct association with the blood, but are functionally and structurally connected to a network of cell types within a structure called the neurovascular unit (NVU)[2]. The NVU facilitates cerebral blood flow (CBF) changes in response to the metabolic activity of neurons in a relationship termed neurovascular coupling[3]. Neurovascular coupling ensures that the brain has a proportionally matched CBF in response to neural activity, however dysfunction of neurovascular coupling, either caused by pathology or ageing itself, can cause further cerebral pathologies and neurological disorders. This review will focus on the neurophysiology of neurovascular coupling, how it is impaired in certain neurological conditions, how to study it and will discuss how cardiovascular disease may affect the regulation of CBF and neurovascular coupling.

1.4 – Neurovascular Coupling

1.4.1 – The Neurovascular Unit and the Blood Brain Barrier

The NVU consists of neurons, astrocytes, microglia, interneurons, pericytes, vascular smooth muscle cells (VSMCs) and endothelial cells[3]. It includes the different cell types involved in the

structural and functional connection between neurons and blood vessels in the brain, including cells involved in the formation of the BBB, refer to ***Figure 1.1***. The BBB is formed due to the specialised functions of tight-junctions of endothelial cells in cerebral vasculature, astrocytes, with some evidence suggesting a crucial role for pericytes[4]. The BBB is a specialised structure in the cerebral vasculature and is not seen in many other organs. It serves to limit the entry of pathogens, toxic agents and blood cells into the parenchyma[5], protecting the brain from infection, whilst allowing controlled transport of nutrients back and forth from the brain. However, there are natural pathogens that can penetrate the BBB including group B streptococci, which can cause meningitis[6]. Generic or specialised dysfunction of the NVU is associated with an increasing list of pathologies, including stroke, Parkinson's disease, Alzheimer's disease, multiple sclerosis, amyotrophic lateral sclerosis and vascular dementia[2]. Specific pathologies as a result of NVU and BBB dysfunction will be discussed later.

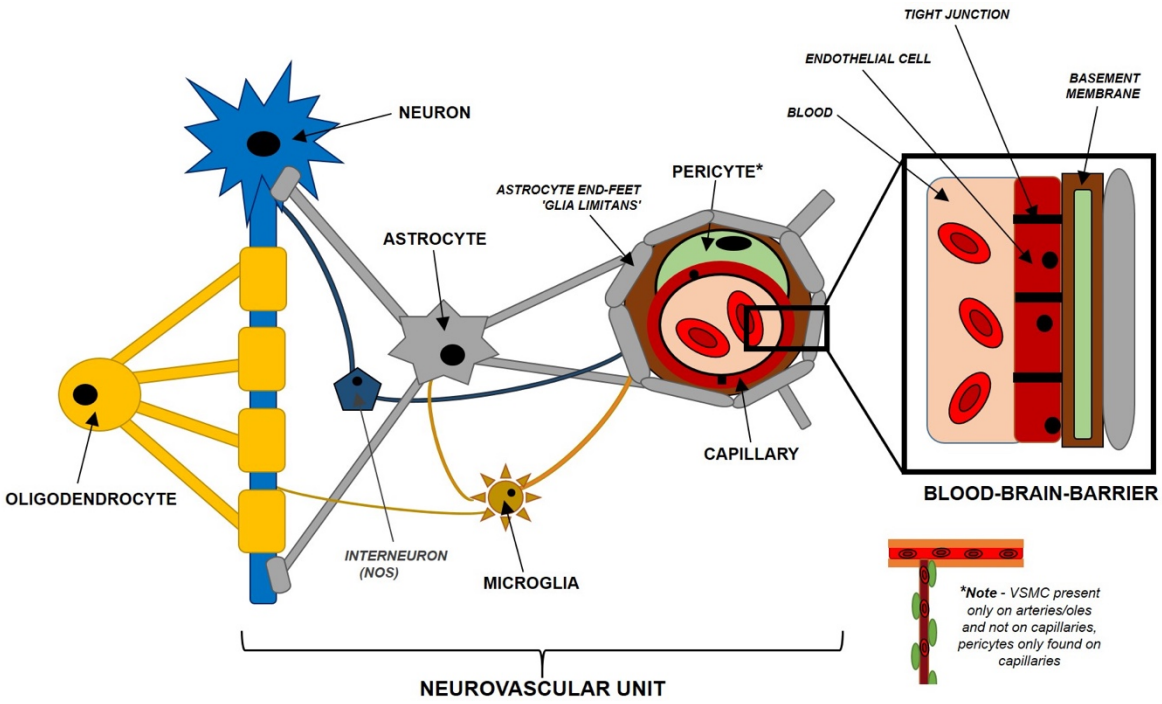

Figure 1.1 - The Neurovascular Unit and the BBB at a capillary. Cerebral arteries have extensive vascular smooth muscle cell (VSMC) coverage regulating vasoconstriction. Capillaries on the other hand lack vascular smooth muscle cells and are instead covered by small pericytes which maintain the integrity of the BBB, as well as regulate their diameter. Cerebral vessels receive inputs from astrocytes by their end-feet to regulate arteriolar diameter, as well as inputs from various interneuron groups.

1.4.2 – Neurophysiology of Neurovascular Coupling

The NVU facilitates haemodynamic changes (alteration in CBF) in response to neural activity. This relationship is termed neurovascular coupling or functional hyperaemia, and is essential for normal metabolic functioning of neurons and the brain as a whole[3], ***Figure 1.2***. Neurovascular coupling is thought to be governed by direct neural and endothelial interactions, or through complex neurogliovascular signalling pathways (of which some are highlighted in *Figure 2*). Neural activation causes neurotransmitter release from synaptic terminals (e.g. glutamate), which bind to N-methyl-D-aspartate receptors (NMDARs) or metabotropic glutamate receptors (mGlutRs) on nNOS-expressing interneurons initiates the synthesis of nitric oxide (NO)[7]. NO can directly cause vasodilation in the endothelium by stimulating cGMP in VSMCs. NO also inhibits CYP4A, which is needed to produce 20-HETE; a prominent vasoconstrictor[8].

Most neurons do not directly innervate the overall vasculature; rather glial intermediaries make the majority of neural-mediated inputs (refer to ***Figure 1.1***). With respect to neurogliovascular signalling, the most important players are thought to be astrocytes whose terminal processes called vascular end-feet, wrap around blood vessels in the brain to contribute to BBB integrity, as well as facilitating neurovascular coupling. Calcium, sodium and potassium signalling via the astrocytic-endothelial axis within the NVU may promote a slow and prolonged vasodilation compared to neural outputs, however this is contested by Lauritzen's group who suggest that astrocytes are involved in the initial vasodilation[9]. On the other hand, rapidly induced transient vasodilation caused by neural NO[10], ensures that CBF change is sufficient to match the demands of metabolic expenditure. Furthermore, it has been shown that a transient loss of oxygen and glucose (as in ischaemia) causes excitotoxicity in neurons leading to delayed neuronal death[11]. At the centre of this excitotoxicity is a delayed mitophagy response (loss of mitochondria) from astrocyte end-feet, leading to a toxic increase in intracellular calcium $[Ca^{2+}]_{IC}$ and glutamatergic activation[11], leading to neuronal death. Although functional neurovascular coupling is related to increased neural activity (i.e. stimulation of brain areas), the brain at rest also requires an efficient steady supply of blood flow. Astrocytes have been shown to influence arteriolar tone by a steady low-level efflux of prostaglandin-E_2 (PGE_2) as a result of basal $[Ca^{2+}]_{IC}$ fluctuations in astrocytic end-feet[12]. This basal tonic influence of arteriolar diameter is independent from stimulus-evoked neural activity-dependent haemodynamic changes, without affecting stimulus-evoked functional hyperaemia. It is therefore assumed that astrocyte dysfunction is key to the breakdown of neurovascular coupling and therefore many neurological conditions.

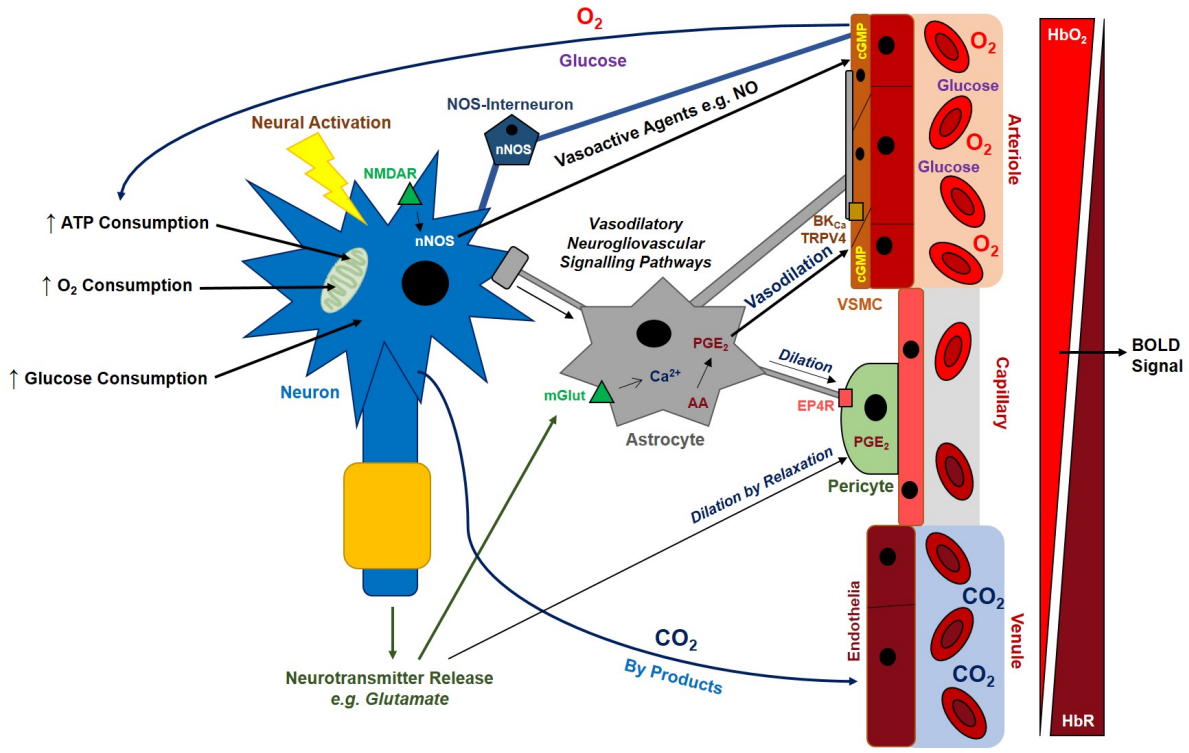

Figure 1.2 - Neurophysiology of Neurovascular Coupling Overview. Neural activity is metabolically expensive demanding a high consumption of glucose and oxygen (from arterial blood). Simultaneously, CO_2 and other by products are also produced, which need to be removed by diffusion into venous blood in order to prevent hypercapnia and acidosis. In order to achieve this, neurons regulate blood flow via neurovascular coupling. Vasoactive agents such as NO directly cause vasodilation of arterial smooth muscle cells. Significant neurogliovascular signalling involving glutamate and calcium signalling causes vasodilation via channels on VSMCs e.g. BK_{Ca}, TRPV4, to stimulate cGMP[13]. There are indeed multiple and complex signalling pathways (including ATP and VIP signalling) also involved in neurovascular coupling. In addition to vasodilator signals, vasoconstrictive signals are also produced, namely 20-HETE, however this is thought to be pathological and as a result of ageing[14]. Pericytes regulate capillary diameter by responding to glutamate release, in addition to PGE_2 produced by astrocytes.

In addition to astrocytes, interneurons also play a role in neurovascular coupling. Interneurons in the cortex come in distinct varieties: VIP/ChAT, NOS/NPY, SOM[7] as well as paravalbumin-GABAergic interneurons[15]. Depending on the input these interneurons receive, they have different outputs with respect to vasoconstriction or vasodilation. For example, acetylcholine (ACh) binding to muscarinic receptors on NOS-interneurons causes the release of NO to facilitate vasodilation on nearby micro vessels, however a serotonergic (5-HT) input on the same interneurons can cause the release of NPY, which can facilitate vasoconstriction[7]. The role of interneurons in neurovascular coupling is still poorly understood and elucidating the mechanistic pathways involved is still to be fully investigated.

As arterioles turn into capillaries in the parenchyma, cerebral vessels no longer have a coverage of VSMCs and instead have a scattered covering of specialised contractile cells called pericytes[16]. Pericytes are an important component of the BBB and maintain its integrity by regulating adherens junction proteins on endothelial cells[17]. The exact function and role of pericytes in the adult CNS is highly controversial. For example, Hall and colleagues published that pericytes are critically involved in the regulation of CBF[18] which was also supported by Kisler et al[19]. However, Hill et al[20] found that arteriolar smooth muscle cells; and not pericytes, regulate regional blood flow. Furthermore, recent evidence has suggested that there may be several types of pericytes with differing roles such as pre-capillary pericytes with smooth muscle actin (SMA), and capillary pericytes without SMA expression[21–24]. Some evidence suggests that astrocytes may regulate pericyte tone and therefore vascular tone[24]. Although pericytes may be involved in capillary alterations, it is true that the arteries and arterioles, which are covered with VSMCs, need to be regulated to bring about a substantial change to CBF. It is evident from contradictions in the literature that regulation of CBF is not a simple mechanism (or as illustrated in ***Figure 1.2***); rather it is a complex interplay between various cell types and signalling pathways with many gaps still remaining in our understanding of the exact mechanisms behind neurovascular coupling in health and disease.

1.5 – Neuroimaging Techniques to Study Neurovascular Coupling

In order to study and measure neurovascular coupling as well as structural alterations to the NVU in vivo, live neuroimaging techniques are used. Neuroimaging techniques allow (largely) non-invasive visualisation of the brain and are typically employed clinically to aid the diagnosis of disease, as well as in research to understand brain function physiologically and pathologically. Many of the clinical techniques can also be effectively used in pre-clinical imaging of animal models in vivo in studies of neurovascular coupling and cerebrovascular pathologies.

1.5.1 – fMRI

Functional magnetic resonance imaging (fMRI) has been the neuroimaging technique of choice for studying brain function in humans and to some extent in rodent models[25]. Briefly, fMRI is based on nuclear magnetic resonance related to proton alignment with a magnetic field[26]. The most commonly used detection paradigm is that of blood oxygen level dependent (BOLD) contrast. BOLD exploits the magnetic differences between oxyhaemoglobin (HbO) and deoxyhaemoglobin (HbR). In a resting state, the relative ratio between HbO:HbR is equal, therefore the magnetic field is unaffected[27]. Upon neural activation and consequent increased CBF, the proportion of HbO increases relative to HbR therefore creating an inhomogeneity in the magnetic field[27], which can be detected by a fMRI scanner. A positive BOLD signal generally reflects increased neural activation, whereas a negative BOLD signal may reflect decreased neural activity, and therefore blood flow[28], although this relationship is not always truly reflective of underlying neural activity especially in cases of pathology or specific cell type activation. fMRI can be used in both human subjects for psychiatric/psychological studies of brain function, clinically in the diagnosis of neurological disease, as well as pre-clinically in animal models. fMRI and related BOLD-based imaging techniques make inferences of neural activity by measuring corresponding haemodynamic changes and do not measure neural activity directly. Neural activity can be recorded by directly measuring action potentials (spiking activity), or the summation of electrical activity determined by local field potentials (LFPs). In order to measure the electrical activity of neurons in vivo, multichannel microelectrodes are implanted in the brain region of interest, or on top of the scalp, producing electrical waveform data[29]. Correlating electrical neural activity to haemodynamic data enables direct association of neural events to corresponding haemodynamics in the study of neurovascular coupling, and is important to do so as blood flow may or may not be directly related to changes in neural activity.

To overcome some of the limitations of individual techniques and to provide a comprehensive representation with respect to brain activity, a multimodal approach is typically used in the study of neurovascular coupling with the combination of two or more techniques. For example, 2D-OIS (optical imaging spectroscopy) or BOLD-fMRI can be combined simultaneously with a micro-electrode implant for electrophysiology, or surface electroencephalography (EEG) in to give both a haemodynamic and neural response[28,30]. For example, a recent study has shown that multiple sclerosis (MS) patients show reductions in gamma power (through magnetoencephalography; MEG) as well as a reduction in BOLD (by fMRI) and CBF responses to visual stimulation[31]. It is important to consider not only a BOLD (blood oxygen level dependent)-related haemodynamic response in neuroimaging, but the source of neural

activity itself, as blood flow changes often lag with respect to neural activity and may even decouple substantially in neurological disorders such as Alzheimer's disease (AD)[19,32].

1.5.2 – 2-Photon Microscopy and Calcium Imaging

At rest, neurons typically have a low basal [Ca^{2+}] concentration of appropriately 50nM, which is kept constant due to the action of several calcium ion channels and pumps such as the efflux plasma membrane calcium ATP-ase (PMCA)[33]. Upon neural activation (propagation of an action potential), influx calcium channels such as voltage gated calcium channels (VGCCs) and glutamate-mediated NMDA receptors, allow a significant influx of intracellular calcium with levels rising to 100-fold higher than baseline[34]. Therefore, neural activity directly correlates with changes to [Ca^{2+}] levels. These indicators can be virally injected into the brain, or genetically engineered. Genetically encoded calcium indicators (GECIs) are bioluminescent protein complexes with integral fluorophores, which when stimulated emit a resonance signal in the form of visible light which can be detected by a camera, allowing quantification of neural activity based on the level of luminescence emitted by the fluorophore. Examples of common GECIs include Yellow Cameleon 3.60 (YC3.60), which contains an enhanced cyan fluorescent protein (ECFP) donor fluorophore, bound to a Venus protein acceptor fluorophore, linked by a calcium-binding domain, calmodulin[35]. More recent GECIs include modifications to the GCaMP family, such as GCaMP6, which is a class of single-fluorophore GECI, where calcium binding causes a conformational change in the integral fluorophore (EGFP) to increase its own intensity[36]. Specific GECIs and other fluorescent proteins can be used to label specific and multiple cell types of the neurovascular unit simultaneously. This can also be achieved by 2D-OIS by measuring GCaMP-labelled neuronal activity, whilst simultaneously measuring haemoglobin reflectance changes, as done in Hillman's group[37] amongst others.

2-photon microscopy is a technique in which a single laser emits two infrared (low-energy) photons to a focused region to cause excitation in fluorophores to a higher-energy state[38]. As the fluorophores return to their resting ground state they emit a light signal which is detected by a scanner. Calcium labelling of neurons and glial cells allows quantification of neural activity by measuring transient changes in spiking activity[34]. Fluorescent labelling of other cell types, including endothelium allows simultaneous blood flow measurements (RBC velocity), and therefore neurovascular coupling at the cellular level[39]. Multi-labelling in live animals eliminates the need to attach electrodes to the area of interest, therefore allowing neural and haemodynamic measurements to be taken by 2-photon microscopy over long periods of time. For example, it has been shown that amyloidosis (visualised by Methoxy-X04) around cerebral vasculature (visualised by TRITC-Dextran) disrupts the NVU function by a displacement of astrocytic-end-feet (visualised by Rhod-2 AM-loaded astrocytes) by reducing overall CBF

(determined by RBC velocity) in an AD mouse model[40]. Despite robust neural activity being present, the slow-down of CBF marks a decoupling of neurovascular coupling in AD.

Most stimulation paradigms in pre-clinical research involves the mechanical stimulation of either whiskers or fore/hind-paws to evoke a neural and haemodynamic response in the somatosensory cortex to study neurovascular coupling. Optogenetics involves expressing light-responding proteins such as channelrhodopsin 2 (ChR2), a blue-light sensitive protein which upon stimulation causes labelled cells to become active[41]. Neurons, as well as astrocytes, interneurons or even pericytes can be tagged with ChR2 in the cell-specific optogenetic stimulation approach. Adapting the correct filters in the 2D-OIS setup can allow the simultaneous optogenetic stimulation by blue light whilst also measuring haemodynamic changes as well as GECI-labelled neurons, in a shift to an all-optical approach to studying neurovascular coupling in vivo.

1.6 – Neurovascular Dysfunction in Neurological Disorders

Many neurological conditions including the common neurodegenerative disorders display some level of neurovascular dysfunction; which either initiates or contributes to their pathogenesis, or is caused as a consequence. The neurovascular dysfunction seen in disorders such as Alzheimer's and stroke can be directly attributed to cardiovascular deficits, however in some cases it may also not be directly associated with any underlying cardiovascular pathology, rather a functional breakdown of the neurovascular unit and signalling pathways.

1.6.1 – Dementia (Alzheimer's Disease)

For the first time since medical records began, dementia has become the single-most leading cause of death in the UK surpassing heart disease, strokes and major cancers[42]. With an ever-ageing population, higher life expectancy and advances in diagnosis techniques, dementia currently affects as many as 1 in 6 in the UK[42]. Of the dementias, AD is the most prevalent followed by vascular dementia, whereas the remainder of cases comprise of frontotemporal dementia (FTD), dementia with Lewy bodies (DLBs) and early-onset dementia. In most of these cases, a mild cognitive impairment stage usually occurs much earlier on before the onset of dementia.

AD is an age-related neurodegenerative disorder and the most frequent form of dementia worldwide[43]. The primary pathological hallmarks of AD consist of extracellular β-amyloid (Aβ) plaques and intracellular neurofibrillary tangles (NFTs) of hyper-phosphorylated tau[44]. Familial cases of AD arise in an autosomal dominant inheritance pattern due to mutations to either

amyloid precursor protein (APP), presenilin 1 (PSEN1) and presenilin 2 (PSEN2)[45–47]. Familial AD is usually relatively early-onset, however only accounts for around 10% of all AD cases worldwide[48]. Although genetic mutations in AD account for a small proportion of all AD cases, most of our understanding of AD pathology and mechanisms have come from animal models with these genetic mutations, for example the J20 mouse (PDGFB-hAPPSwInd) harbours the more common APP mutation called the Swedish K670N/M671L mutation as well as the Indiana V717F mutation, which both increase β-secretase activity[49,50]. The increased production of the toxic form of amyloid, Aβ42, as well as Aβ40, coupled with the decreased ability to clear aggregates is the primary cause of Aβ-plaque build-up in the pathogenesis of AD[51]. ***Figure 1.3*** illustrates the amyloidgenic processing pathway in the formation of Aβ plaques.

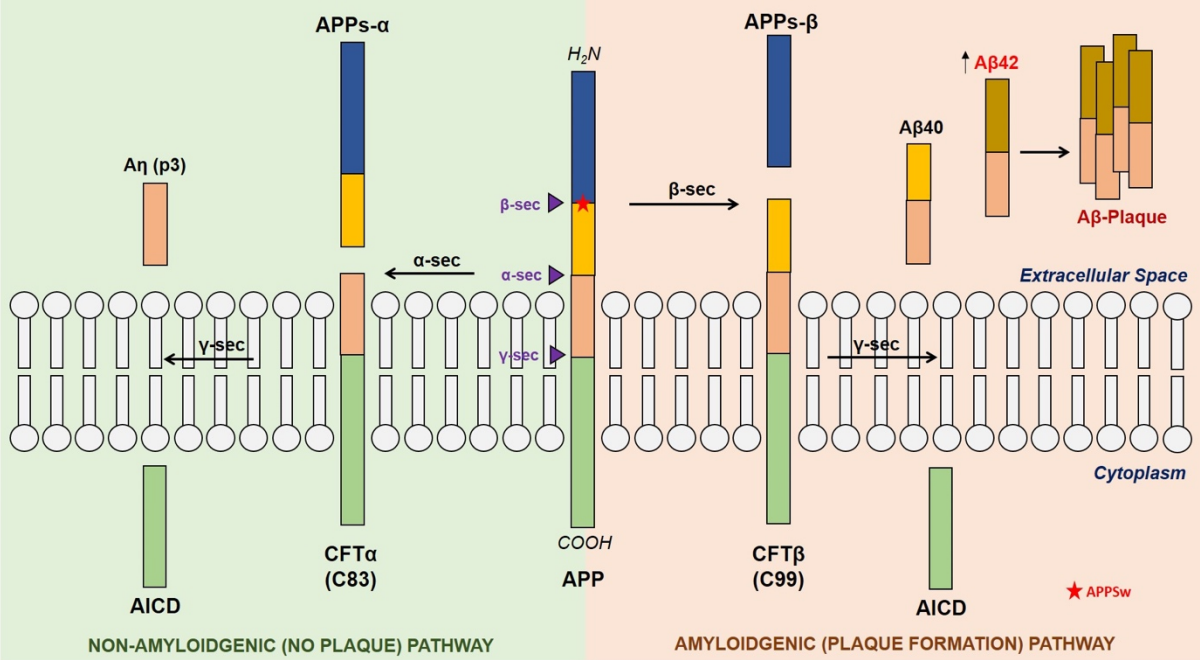

Figure 1.3 - Overview of Aβ processing. APP can be processed via the α-secretase pathways (non-amyloidgenic pathway) producing the soluble APPs-α fragment and a small p3 fragment. The amyloidgenic pathway utilises β-secretase to produce the soluble APPs-β fragment followed by γ-secretase producing Aβ40 or lower in a much higher ratio than the production of Aβ42. Mutations to PSEN1/2 and APP (such as the Swedish mutation, marked by a red star on APP) often favour the production of the more toxic Aβ42 fragment which forms oligomers leading to the formation of Aβ-plaques. (Adapted from Schmechel et al, 1993[52]).

The vast majority of AD cases are sporadic (~90%) and are relatively later-onset, and are therefore not attributable to inherited genetic mutations to amyloid processing genes. It is important to note that even in sporadic AD cases, β-amyloid plaques are still present, and has many similarities to familial AD. Amongst the common risk factors already associated with cardiovascular disease and dementia such as age, hypertension, hypercholesterolaemia, diabetes etc., there are several risk factor gene polymorphisms which greatly enhance the likelihood of developing AD. The most common is the APOEε4 allele which is attributed to up to approximately 50-60% of all AD cases[53] as carrying the allele (found in around 15% of the population) increases the risk of developing AD 4-fold, and homozygous inheritance of the APOEε4 increases the risk 9-fold[53]. APOEε4 AD-patients have amyloid-β plaques as well as phosphorylated-tau NFTs similar to familial AD[52,54]. The knowledge gained from the use of genetic models of AD therefore also applies to a vast proportion of all AD cases where amyloid is present.

There is a growing body of evidence which suggests that neurovascular coupling may be impaired in AD[23,32,55,56]. It is postulated that impaired blood flow responses to neural activity as a result of neurovascular disarray may cause a mismatch between neural activity and provision of oxygen and glucose to meet sufficiently adequate metabolic demands. Consequentially, neural activity is reduced and thus correlates with impaired cerebral function, manifested clinically as cognitive decline[32]. As discussed previously, pericytes are critical in the integrity and maintenance of the BBB and therefore the NVU. Recent evidence has shown that patients with AD carrying the APOEε4-allele have a BBB breakdown attributed to pericyte degeneration in which patients/carriers have up to 50% less pericyte coverage correlating with almost 300-400mm/mm3 total capillary length reduction compared to control subjects without the APOEε4 allele[57]. This study is further supported by Kisler et al[19] in which they found that PDGFRB$^{-/-}$ (pericyte deficient) mice have a reduced cerebral oxygenation level compared to controls as well as neurovascular uncoupling leading to neuronal death[19]. More recent evidence has directly implicated pericyte degeneration in extensive white matter pathology characterised by hypoxia and loss of myelination, leading to the loss of structural and functional connections within the brain which are typically present in some AD cases[58]. The breakdown of the NVU (pericytes amongst other cell types within the NVU) and the BBB is evident in Alzheimer's patients, and may contribute to exacerbated pathology seen in AD, as well as initiating neuropathology. This can be further explained in the 2-hit vascular hypothesis model of AD proposed by Zlokovic[59] (***Figure 1.5***). The first 'hit' refers to vascular dysfunction caused by various risk factors including atherosclerosis leading to a breakdown of vascular integrity causing reduced CBF which in itself can cause stroke (discussed below), cognitive decline and vascular dementia. The second 'hit' refers to the increased Aβ levels (by a

reduction in clearance) which further exacerbates neuronal dysfunction and adding further insult to the pathogenesis of AD[59]. It is therefore becoming increasingly more apparent that AD is not solely a neurodegenerative disorder, rather it is a complex multifactorial disease with a large neurovascular element which needs to be investigated further both in disease initiation and in potential therapeutic strategies.

1.6.2 – Stroke

Vascular dementia and other forms of cognitive impairment can be caused directly by having a stroke. Strokes can arise as a direct consequence of arterial pathology with profound changes to the neurovascular unit and the normal physiology of neurovascular coupling. This impaired blood flow to the brain can lead to the death of neural tissue in specific regions where blood flow is disrupted to cause a stroke. Depending on the severity of the stroke, symptoms can be mild ranging from a transient ischaemic attack to a potentially fatal in a stroke where a large are of the brain is affected[60]. Strokes can fall into two broad categories: ischaemic, where occlusion of vessels leads to death of tissue; or haemorrhagic as a result of a ruptured vessel[60]. As a consequence of stroke, cognitive and motor function can become impaired, sometimes permanently leading to vascular dementia for example.

Subarachnoid haemorrhages (SAH) as a result of cerebral aneurysm rupture can cause a devastating stroke which usually results in death a few days after the initial rupture, if not fatal during the initial stroke[61]. It has been demonstrated that in such haemorrhagic episodes, there tends to be an inversion of neurovascular coupling in response to calcium-signalling mediated by astrocytes[61]. Instead of Ca^{2+}-mediated vasodilation, post-stroke, there is a switch in the polarity of neurovascular coupling in which Ca^{2+} actually causes vasoconstriction pathologically. This then limits CBF and functional hyperaemia to the brain parenchyma resulting in progressive ischaemia after the stroke takes place usually resulting in death of the patient a few days after the stroke[61]. A potential mechanism as to why this may occur may be due to the upregulation of astrocytic endothelin-1 (ET-1); a vasoconstrictor, after SAH[62]. ET-1 binds to ETB1 receptors on endothelial cells to reduce overall synthesis of endothelial nitric oxide synthase (eNOS), and hence NO levels. ET-1 also binds to ETA receptors on the tunica media of vessels to upregulate PKC-α, which in turn inhibits the function of K^+ channels to contribute to vasospasm, and BBB breakdown causing oedema[62]. These studies highlight the importance of astrocytes in neurovascular coupling by alluding to the critical signalling pathways between neurons-astrocytes-endothelial cells in facilitating vasodilation, as well as providing insight into the complexity of stroke pathophysiology.

1.6.3 – Physiological Ageing

Ageing is itself the biggest risk factor in the development of many diseases including cardiovascular disease, Alzheimer's and vascular dementia. Normal physiological ageing itself results in progressive neurovascular dysfunction, primarily marked by a reduction of overall CBF[63,64]. A key reason why many age-related disorders begin is due to the accumulation of reactive-oxygen species (ROS) coupled with impaired ROS-scavenging. Indeed, it has been shown that an enhanced production of ROS leads to an overall reduction in NO within the vasculature, therefore impacting NO signalling to cause vasoconstriction over time[10]. This arises as a direct result of aged vessels affecting their structure and function.

A recent study by Duncombe and colleagues explored the pathophysiology of neurovascular coupling associated with ageing[65]. They found that aged mice show key differences in the NVU compared to younger mice. Firstly, pericyte coverage is markedly reduced in older mice[65]. However, this study did not find any correlative effects of the loss of pericytes with CBF and alterations to neurovascular coupling. This is contradicted by another study by Kisler and colleagues[19], which found that the loss of pericytes directly causes neurovascular uncoupling, in addition to reduced oxygen perfusion in the brain[23]. As alluded to earlier, studying the role of pericytes in neurovascular coupling is a challenging task, mainly as there are few specific markers for pericytes, as well as limited scope to study blood flow in capillaries in vivo, which is acknowledged by Duncombe. Secondly, Duncombe and colleagues found that aged mice exhibit astrocyte end-feet abnormalities by the marked reduction in the expression of AQP4[65], which impairs the cell-cell communication between astrocytes and endothelial cells via the neurogliovascular signalling pathways (as shown in *Figure 2*). Ageing, therefore, progressively impairs functional hyperaemia by a wide variety of pathophysiological changes associated with the NVU, in addition to the loss of key signalling pathways, which may be further worsened in AD through excitotoxic calcium signalling due to Aβ plaque pathology[66].

1.7 – Atherosclerosis

One key pathological change associated with ageing is that of atherosclerosis. Atherosclerosis is a chronic inflammatory syndrome resulting in the progressive thickening and hardening (arteriosclerosis) of major artery walls[67]. This continual narrowing of the lumen restricts blood flow over time, and is causative in millions of deaths worldwide each year with the commonest causes of death being stroke, myocardial infarction and dementia[68]. The aetiology of atherosclerosis is complex with a combination of genetic, lifestyle (e.g. dietary), environmental and immunological factors contributing towards its pathogenesis and progression.

Atherosclerosis can take decades to take full effect with patients being largely asymptomatic until their mid-50s, although initiation of disease takes place in early adulthood. The initiation of atherosclerosis is still not fully understood, although general consensus is that atherosclerosis begins with inflammatory changes within the endothelium caused by low-density lipoproteins (LDLs) being deposited[69,70], and internalised by endothelial cells. However, what is becoming increasingly clearer is that deposition of LDLs into the arterial walls is not sufficient to cause atherogenesis, rather it is the subsequent immune response facilitated by monocytes and leukocytes that initiates the syndrome[71]. LDLs have been shown to deposit more readily in atherosclerotic-prone and low blood flow areas of an arterial branch, where they undergo oxidation by reactive oxygen species (ROS), stimulating an immune-response[72]. The arterial branches susceptible to LDL deposition and atherosclerosis tend to be near areas of major curvatures (e.g. carotid sinus) which have a high shear index compared to laminar areas of the same arterial tree, that tend to be more athero-reistant[73].

The solidifying step in atherogenesis is when invading monocytes differentiate into macrophages in the intima after binding to endothelial receptors such as VCAM1 and P-Selectin[74], ***Figure 1.4***. Once differentiated into macrophages, oxidised-LDLs are subsequently engulfed, slowly transforming normal macrophages into 'foam-cells' with a large accumulation of lipids intracellularly[75]. Over time, clusters of foam cells form visible 'fatty-streaks' inside the intima of the endothelium. Simultaneous to fatty-streak formation, endothelial VSMCs also begin to proliferate and migrate from the media into the intima and form a ring around the fatty-streaks further stabilising the forming plaque[76]. Over time some of the VSMCs begin to calcify and harden adjacent to the atheromatous endothelium, forming a solid core in the intima of the endothelium, which begins to enlarge and partially occlude the vessel to cause a progressive narrowing (stenosis) of the artery[77]. The atheromatous plaque (atheroma) may in itself cause an obstruction of blood flow, or more commonly the atheroma may rupture and form a thrombus with platelets, which can be repeated to form a stable cap disrupting blood flow over time further exacerbating stenosis, or rupturing within the vessel wall to cause either an embolism or haemorrhage. Either of these can contribute to coronary heart disease, myocardial infarction (if in the heart), or a stroke if in the carotid or cerebral arteries.

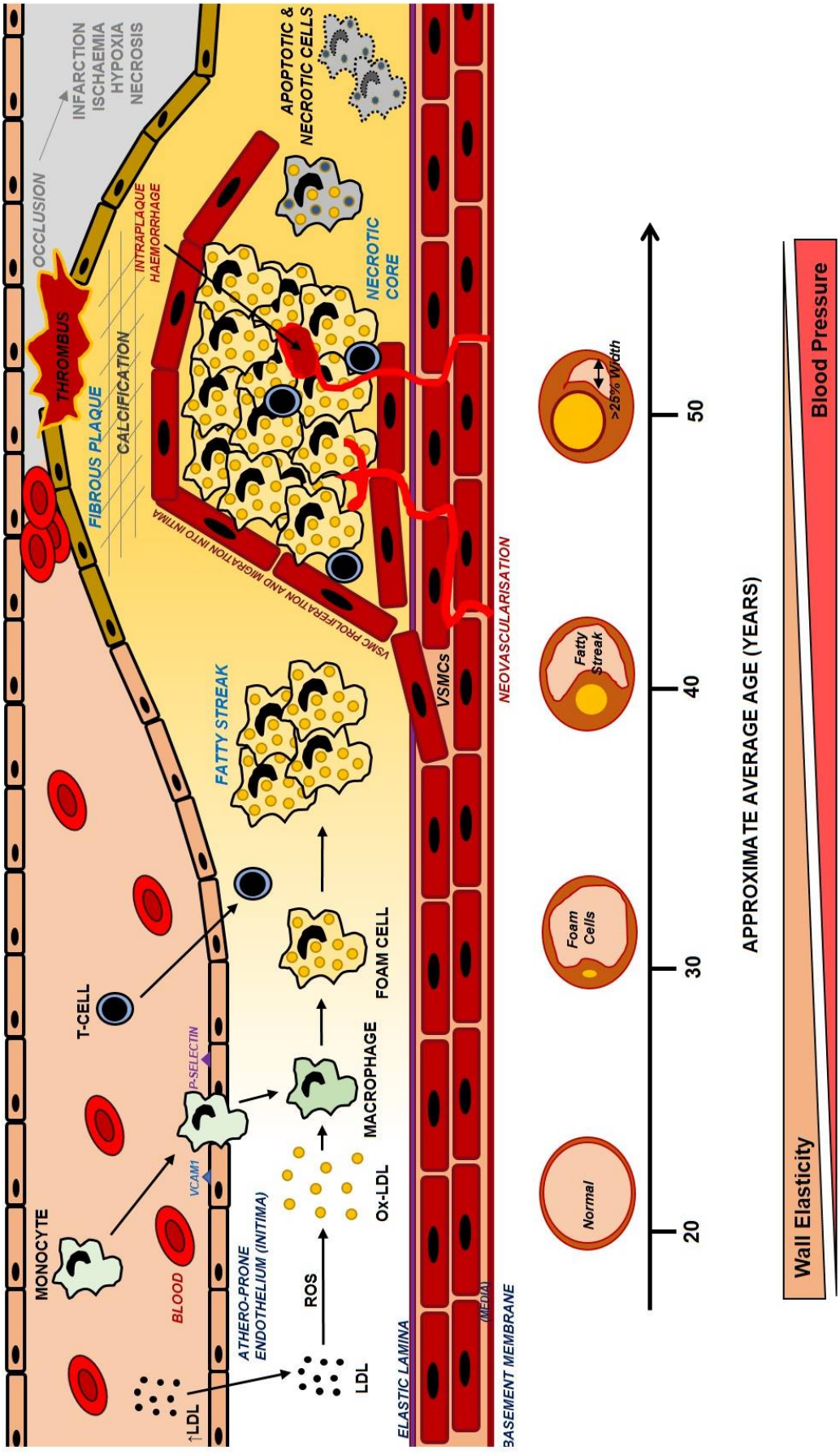

Figure 1.4 - Overview of the Pathogenesis of Atherosclerosis

Figure 1.4 - Overview of the Pathogenesis of Atherosclerosis. Accumulation of LDLs in the blood leads to LDLs being transported into the endothelium, where they become oxidised. Infiltrating monocytes become activated and differentiate into macrophages and begin to ingest oxidised-LDLs to become foam cells. Over time, foam cells conglomerate to form fatty streaks. Simultaneously, due to inflammation and stimulant factors, VSMCs begin to proliferate and migrate into the intima and form a cap around the fatty streak. Endothelial cells overlying the growing plaque become calcified, with reduced elasticity. Over time this cap restricts blood flow due to a luminal constriction. If the plaque ruptures, a thrombus forms and obstructs the lumen completely, or partially. This can lead to ischaemia downstream leading to an ischaemic attack in the brain, or rupture to cause a haemorrhagic stroke. (Adapted from Madamanchi et al, 2005[78]).

1.8 – Atherosclerosis and Neurovascular Dysfunction

Atherosclerosis affects most large to medium sized systemic arteries including those supplying the cerebral circulation, namely the internal carotid and vertebral arteries[60]. Progressive plaque build-up and stenosis of cranial arteries can cause strokes as well as contribute to the development of dementia either directly or as a consequence of stroke. Strokes can either be ischaemic or haemorrhagic in nature, and can both trace their origins to underlying vascular pathologies, such as luminal stenosis as a consequence of atherosclerosis in the arteries supplying the brain and cranium[60]. Here, only the relationship between cardiovascular disease and cognitive impairment will be discussed.

Atherosclerosis and related cardiovascular diseases and risk factors can cause a wide array of simple and complex vascular lesions in the brain. For example, bilateral carotid occlusion directly affects the blood supply to the brain, and is commonly associated with stroke and vascular dementia[79]. Some of the key vascular lesions commonly found in patients with cardiovascular pathology range from microbleeds, microinfarcts (lacunar multi-infarct or strategic) and lipohyalinosis; the deposition of hyaline in the connective tissue walls to disrupt the integrity of the vasculature, affecting the smaller vessels within the white matter termed cerebral small vessel disease[80], refer to ***Figure 1.5***. These lesions arise directly as a consequence of arterial stiffness and inflammation caused by atherosclerosis and vascular risk factors including hypertension, hypercholesterolaemia, smoking, diet and advanced age[81]. Cerebral small vessel disease is directly associated with the onset of dementia, primarily vascular dementia as well as Alzheimer's-like pathology and other milder forms of cognitive impairment as well as stroke. Depending on where in the brain these vascular lesions occur, different symptoms may manifest clinically. Pre-symptomatic (subclinical) carotid atherosclerosis (determined by increased endothelial swelling, *Figure 5.3*) is associated with early cognitive impairment, in which pathologic mechanisms have been attributed to cerebral microvascular dysfunction (*as shown in Figure 5*) in the frontal and temporal lobes[82].

Lipohyalinosis is a brain-specific vessel disease characterised by vascular wall disruption and occurs as a result of systemic atherosclerosis, especially due to extensive inflammation occurring through the accumulation of ROS, in addition to gliosis involving astrocytes, oligodendrocyte precursor cells and microglia which themselves in their reactive state produce ROS[83]. As discussed previously, atherosclerosis is an inflammatory syndrome which initiates as a result of an immune response against oxidised-LDLs in the intima. Monocyte infiltration into the vessel wall followed by differentiation into macrophages which subsequently engulf the oxidised-LDLs forming foam cells is the primary inflammatory trigger[71]. In addition to monocyte infiltration at sites of LDL retention, TH1 (CD4+) lymphocytes are also involved in

the inflammatory response[74,84]. TH1 cells bind to antigen sites on LDL molecules and subsequently produce inflammatory mediators including tumour necrosis factor (TNF) and interferons e.g. IFNγ[74], which all promote the pathogenesis and development of atherosclerosis. Cholesterol crystals activate the NOD-like receptor protein 3 (NLRP3), which together with caspase-1 and apoptosis-associated speck-like protein containing a caspase activation and recruitment domain (CARD) forms an inflammasome[85]. This stimulates the production of the proinflammatory IL-1β chemokine. IL-1β has been shown to be implicated in the pathogenesis of atherosclerosis and thrombosis by the downstream stimulation of IL-6 and C-reactive protein (CRP)[86]. Recent evidence has suggested that targeting the inflammatory pathways in atherosclerosis irrespective of reducing LDL-C levels, may actually be therapeutically beneficial in patients with atherosclerosis, by reducing the frequency and strength of major cardiovascular incidents[86,87]. Clinical trials involving canakinumab, a monoclonal antibody against IL-1β, has shown a significant reduction of major cardiovascular incidents in patients with atherosclerosis, by reducing the total levels of plasma IL-6 & CRP compared to those given a placebo[86].

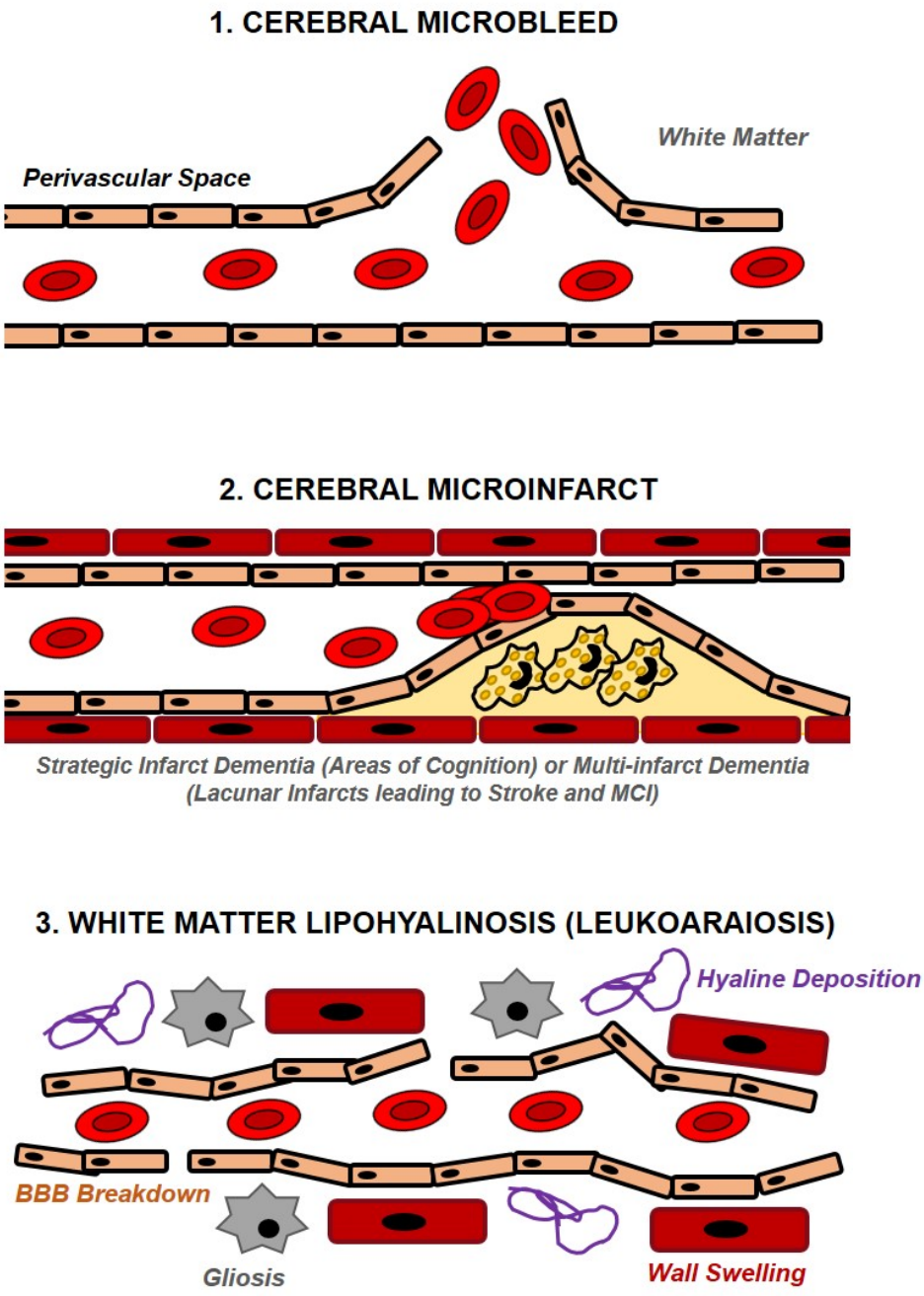

Figure 1.5 - Vascular Lesions in Small Vessel Disease. Key types of vascular lesions found in the brain as a result of small vessel disease (SVD) leading to cognitive impairment (vascular dementia) and stroke include microbleeds, microinfarcts; where fatty deposits accumulate to restrict luminal diameter, and inflammatory white matter pathology such as lipohyalinosis, where hyaline deposits within connective tissue in addition to astrocytic gliosis (scarring) and wall swelling to disrupt the uniformity of vessel walls within the brain (Adapted from Iadecola, 2013[79]).

Vascular dysfunction caused by atherosclerosis and lifestyle/genetic risk factors can directly lead to cerebral vascular damage to cause small vessel disease and a breakdown of the BBB, marked by inflammation and hyper-connectivity[23]. This vascular damage leads to neurovascular dysfunction marked by CBF decrease (oligemia), as well as potentially initiating Aβ pathology by a reduction in clearance. ***Figure 1.6*** illustrates how AD can develop (including the 2-hit vascular model proposed by Zlokovic[59]) as a result of vascular dysfunction leading to amyloid production, in addition to the pathogenesis of vascular dementia at the level of neurovascular dysfunction, independent of amyloid pathology. ***Figure 1.6*** also summarises the key processes involved in atherogenesis and vascular dysfunction, including inflammation, showing the complex overlap between disease conditions.

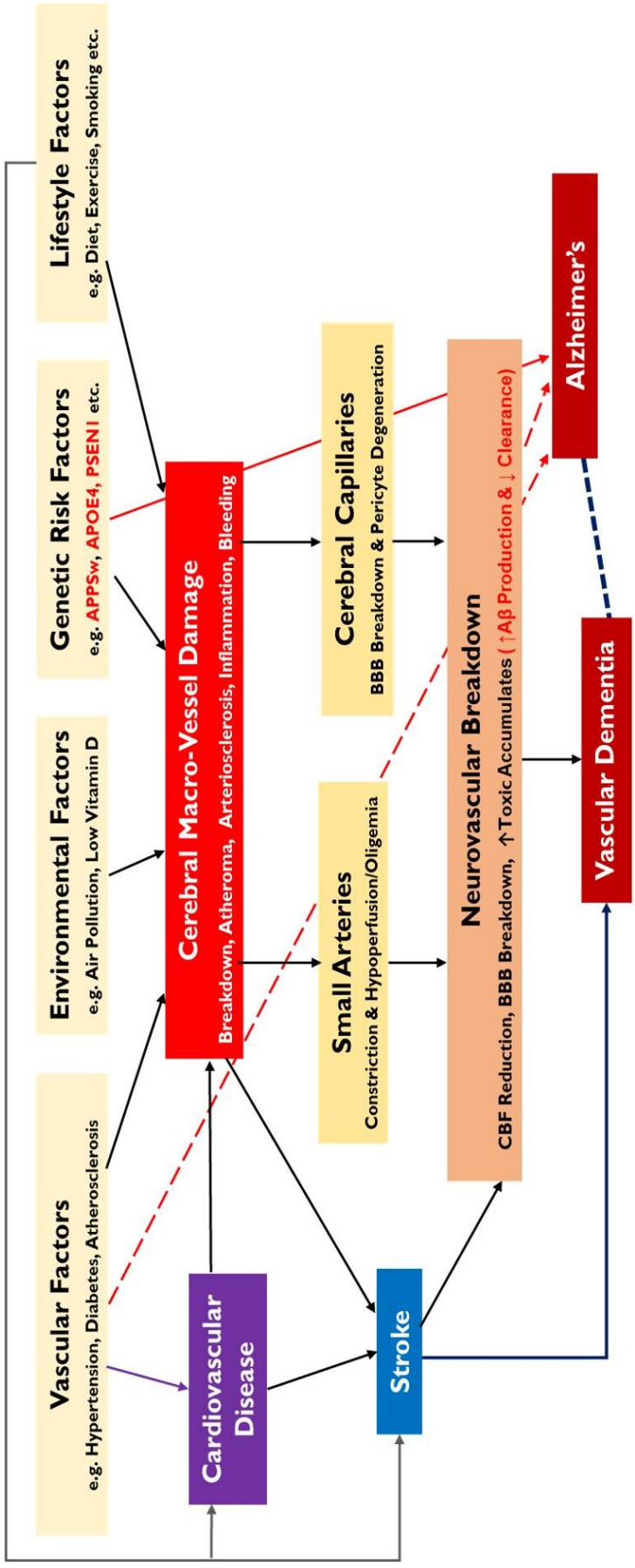

Figure 1.6 - Summary of Vascular Pathologies in CVD, Stroke & Dementia

Figure 1.6 - Summary of Vascular Pathologies in CVD, Stroke & Dementia. Vascular dysfunction pathway for stroke, vascular dementia and AD; AD-specific factors in red text (incorporating the 2-hit hypothesis for AD – hit 1 being at vessel damage and hit-2 being Aβ increase). CVD can directly cause cerebral vessel damage to cause either strokes and/or vascular dementia, in addition to initiating AD pathology if certain risk factors are present. Adapted from Kisler et al, 2017[23] & Zhao et al, 2015[88].

1.8.1 – LDLR, ApoE & PCSK9

LDL molecules comprise of an apolipoprotein B-100 protein, in addition to other lipids (including up to 1500 cholesterol molecules), triglycerides and structural protein complexes[89]. LDLs bind to the LDL-receptors (LDLRs) in hepatocytes, primarily, via the ApoB segment to stimulate endocytosis of the LDLR/LDL complex[90]. The closely related ApoE protein, which also binds to LDLR, is involved in the selective transport of lipoproteins systemically, especially in the transport of chylomicron and LDL remnants[91]. Genetic mutations that cause a loss of function to either the LDLR, ApoE or ApoB of an LDL molecule result in the reduced clearance of LDL from the plasma, therefore increasing the circulating plasma levels of cholesterol[92]. Whilst mutations to these genes may cause familial hypercholesterolemia from a much earlier age, affecting as many people as around 1:500 (heterozygotic)[92], non-affected individuals can naturally develop hypercholesterolemia and therefore atherosclerosis with elevated LDL levels either through dietary intake of trans and saturated fats, being obese, in addition to having diabetes, or simply being male[92]. ApoE-/- and LDLR-/- knockout mice can develop hypercholesterolemia and atherosclerosis and disease severity and progression is exacerbated by being fed a high-fat diet[93,94]. ApoE-/- mice also develop BBB leakage which worsens over time, and may contribute to a breakdown of neurovascular coupling[95,96].

More recently, an rAAV8 D377Y-mPCSK9 ($PCSK9^{DY}$) mouse model (on a male C57BL/6 background) has been used to study atherosclerosis[97–99], where a single injection of AAV-$mPCSK9^{DY}$ is sufficient to cause long-term atherosclerosis in mice comparable to $LDLR^{-/-}$ strains, without the need to create a transgenic mutant knock-in line[97]. The proprotein convertase subtilisin/kexin type 9 (PCSK9) gene on chromosome 1 (1p32.3) has been shown to homeostatically regulate cholesterol levels in the plasma by directly interacting with the LDL-receptor (LDLR) and the related APOE-receptor ($ApoER_2$) by causing their internalisation and degradation within a cell[100,101]. Over-time, the degradation of LDLR with respective increased plasma cholesterol levels may be causative to atherosclerosis in ordinary individuals[102]. Gain of function mutations to PCSK9 (e.g. D374Y) are associated with patients that have genetic hypercholesterolemia, in particular, familial autosomal dominant hypercholesterolemia (FADHC)[103]. In the case of the human $PCSK9^{D374Y}$ mutation, plasma concentrations of cholesterol can exceed 500mg/dL, where normal levels would be less than 200mg/dL and pathological being above 250mg/dL[103]. Recently it has been shown that there is significantly increased PCSK9 within the CSF of Alzheimer's patients carrying the APOEε4 allele, with a yet unknown pathway[104], further adding support to the notion that hypercholesterolaemia is a major risk factor for AD. With the knowledge that PCSK9 is involved in elevated cholesterol levels both physiologically and pathologically, monoclonal antibodies and selective inhibitors, such as alirocumab (against PCSK9), have been approved

by the FDA for the treatment of patients with hypercholesterolemia and atherosclerosis by halting the progression of cardiovascular disease[105]. ***Figure 1.7*** illustrates the physiological and pathological mechanisms of PCSK9 in the regulation of plasma cholesterol levels. It has been shown that a high-fat diet exacerbates atherogenesis by elevating total cholesterol levels in $PCSK9^{DY}$ mice, much like the $LDLR^{-/-}$ strains, however normal rodent chow can also result in moderate atherogenesis[99]. As this is a relatively novel atherosclerosis model, not much is known about the effect on the brain or neurovascular coupling. This viral injection method of inducing atherosclerosis in any strain of mouse is far cheaper than breeding and maintaining inbred colonies, and it is becoming the model of choice due to its rapid induction (including in any genetic model), reliable and consistent atherosclerotic profiles as well as cost. Compared to the artificially high serum cholesterol levels seen in the $ApoE^{-/-}$ mice, and having the added benefit of not maintaining knockout lines, the rAAV-$PCSK9^{DY}$ model is certainly the more economical and more effective model in terms of induction of atherosclerosis as well as a comparable LDL-C profile to that of patients.

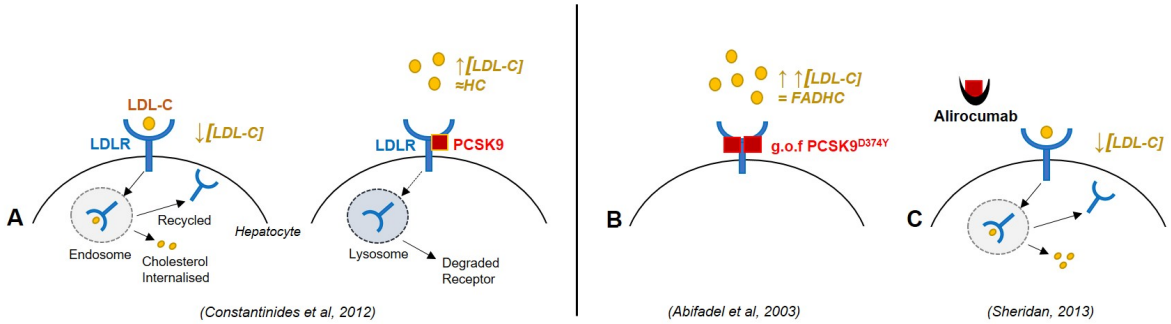

Figure 1.7 - PCSK9 Mechanisms.

Keywords: LDL, low-density lipoprotein; LDL-C, cholesterol; LDLR, low-density lipoprotein receptor; PCSK9 proprotein convertase subtilisin/kexin type 9; HC, hypercholesterolemia; g.o.f, gain of function; FADHC; familial autosomal dominant hypercholesterolemia

A (left) – Physiological homeostatic regulation of LDL-C by LDLR

A (right) – Physiological homeostatic regulation of LDLR by PCSK9 (which may lead to HC)

B – Genetic mutant (g.o.f) variant of PCSK9 causing FADHC

C – PCSK9 inhibitor mechanism to reduce LDL-C levels in patients with HC

It is important to note that all animal models of human disease can never completely replicate human disease in vivo, due to species-specific physiologies; therefore, the models that we do have are our best insight into a more complex scenario with respect to human disease, and results must be interpreted with some level of caution before generalising both in terms of knowledge gained and potential for therapeutics. Although animal models can model human disease and provide insights into disease mechanisms effectively, sometimes the same model may provide conflicting evidence in the hands of other researchers. Studies have found a link between hypercholesterolemia and the onset of vascular dysfunction causing Alzheimer's (-like) pathology in patients[106], as well as in high-fat diet mouse models[107]. However, in a study by Hohsfield and colleagues[108], it was shown that hypercholesterolemia does not increase amyloid-deposition and Alzheimer's like pathology in the same 3xTg-AD mouse model. However, unlike in the previous studies, the 3xTg-AD mice in Hohsfield's study did not survive long enough, therefore probably did not gain enough cumulative amyloid/tau deposition to manifest as Alzheimer's-like pathology. They did not consider more regular behavioural assays such as Morris maze tests to establish whether their mice displayed any early mild cognitive deficits.

1.9 – Conclusions and Future Directions

Neurovascular coupling is critical to the proper functioning of the brain, ensuring that increased neural activity, which itself is incredibly metabolically demanding, is matched with an appropriate change to CBF to both nourish the parenchyma with oxygen and glucose as well as the quick and efficient removal of carbon dioxide and waste products. In order to achieve this, neurons communicate with endothelial cells via the neurogliovascular signalling pathways within the NVU. Pathological changes to the NVU and endothelia impairs the signalling pathways involved in neurovascular coupling, leading to brain pathologies ranging from subtle cognitive deficits to severe AD. Although our knowledge and understanding of the mechanisms behind neurovascular coupling in health, ageing and disease has vastly improved in recent years, much is still to be investigated, especially with respect to the effect of atherosclerosis on cerebral vasculature and neurovascular coupling. Although there are many established models of atherosclerosis, the new rAAV-PCSK9^{DY} method has many benefits over the conventional knock-out lines of ApoE$^{-/-}$ & LDLR$^{-/-}$, including the ability to induce atherosclerosis in any mouse model including AD-mouse models. In future studies, tracking haemodynamic changes over time combined with cellular, genetic and in vivo imaging would provide a comprehensive overview and mechanistic insight into how cardiovascular disease affects neurovascular coupling and the brain as a whole in mouse models of atherosclerosis and mixed models of dementia.

1.10 – References

1. Clark. *Basic Neurochemistry: Molecular, Cellular and Medical Aspects*. (1999).
2. Maki, T. *et al.* Biphasic Mechanisms of Neurovascular Unit Injury and Protection in CNS Diseases. *CNS Neurol. Disord. - Drug Targets* (2013) doi:10.2174/1871527311312030004.
3. Pasely, B. & Freeman, R. Neurovascular Coupling. *Scholarpedia* **3**, 5340 (2008).
4. Armulik, A. *et al.* Pericytes regulate the blood-brain barrier. *Nature* (2010) doi:10.1038/nature09522.
5. Winkler, E. A., Bell, R. D. & Zlokovic, B. V. Central nervous system pericytes in health and disease. *Nature Neuroscience* (2011) doi:10.1038/nn.2946.
6. Nizet, V. *et al.* Invasion of brain microvascular endothelial cells by group B streptococci. *Infect. Immun.* (1997) doi:10.1203/00006450-199704001-01351.
7. Cauli, B. *et al.* Cortical GABA interneurons in neurovascular coupling: Relays for subcortical vasoactive pathways. *J. Neurosci.* (2004) doi:10.1523/JNEUROSCI.3065-04.2004.
8. Gebremedhin, D. *et al.* Production of 20-HETE and its role in autoregulation of cerebral blood flow. *Circ. Res.* (2000) doi:10.1161/01.RES.87.1.60.
9. Lind, B. L., Brazhe, A. R., Jessen, S. B., Tan, F. C. C. & Lauritzen, M. J. Rapid stimulus-evoked astrocyte Ca2+ elevations and hemodynamic responses in mouse somatosensory cortex in vivo. *Proc. Natl. Acad. Sci. U. S. A.* (2013) doi:10.1073/pnas.1310065110.
10. Park, L., Anrather, J., Girouard, H., Zhou, P. & Iadecola, C. Nox2-derived reactive oxygen species mediate neurovascular dysregulation in the aging mouse brain. *J. Cereb. Blood Flow Metab.* (2007) doi:10.1038/sj.jcbfm.9600491.
11. O'Donnell, J. C., Jackson, J. G. & Robinson, M. B. Transient oxygen/glucose deprivation causes a delayed loss of mitochondria and increases spontaneous calcium signaling in astrocytic processes. *J. Neurosci.* (2016) doi:10.1523/JNEUROSCI.4518-15.2016.
12. Rosenegger, D. G., Tran, C. H. T., Wamsteeker Cusulin, J. I. & Gordon, G. R. Tonic local brain blood flow control by astrocytes independent of phasic neurovascular coupling. *J. Neurosci.* (2015) doi:10.1523/JNEUROSCI.1780-15.2015.
13. Fernandes, J. *et al.* IP3 sensitizes TRPV4 channel to the mechano-and osmotransducing messenger 5′-6′-epoxyeicosatrienoic acid. *J. Cell Biol.* (2008) doi:10.1083/jcb.200712058.
14. Cheng, J. *et al.* 20-Hydroxy-5,8,11,14-eicosatetraenoic acid mediates endothelial dysfunction via IκB kinase-dependent endothelial nitric-oxide synthase uncoupling. *J. Pharmacol. Exp. Ther.* (2010) doi:10.1124/jpet.109.159863.
15. Hu, H., Gan, J. & Jonas, P. Fast-spiking, parvalbumin+ GABAergic interneurons: From cellular design to microcircuit function. *Science* (2014) doi:10.1126/science.1255263.
16. Armulik, A., Genové, G. & Betsholtz, C. Pericytes: Developmental, Physiological, and Pathological Perspectives, Problems, and Promises. *Developmental Cell* (2011) doi:10.1016/j.devcel.2011.07.001.
17. Daneman, R., Zhou, L., Kebede, A. A. & Barres, B. A. Pericytes are required for bloodĝ€"brain barrier integrity during embryogenesis. *Nature* (2010) doi:10.1038/nature09513.
18. Hall, C. N. *et al.* Capillary pericytes regulate cerebral blood flow in health and disease. *Nature*

(2014) doi:10.1038/nature13165.

19. Kisler, K. *et al.* Pericyte degeneration leads to neurovascular uncoupling and limits oxygen supply to brain. *Nat. Neurosci.* (2017) doi:10.1038/nn.4489.
20. Hill, R. A. *et al.* Regional Blood Flow in the Normal and Ischemic Brain Is Controlled by Arteriolar Smooth Muscle Cell Contractility and Not by Capillary Pericytes. *Neuron* (2015) doi:10.1016/j.neuron.2015.06.001.
21. Damisah, E. C., Hill, R. A., Tong, L., Murray, K. N. & Grutzendler, J. A fluoro-Nissl dye identifies pericytes as distinct vascular mural cells during in vivo brain imaging. *Nat. Neurosci.* (2017) doi:10.1038/nn.4564.
22. Fernández-Klett, F. & Priller, J. Diverse functions of pericytes in cerebral blood flow regulation and ischemia. *Journal of Cerebral Blood Flow and Metabolism* (2015) doi:10.1038/jcbfm.2015.60.
23. Kisler, K., Nelson, A. R., Montagne, A. & Zlokovic, B. V. Cerebral blood flow regulation and neurovascular dysfunction in Alzheimer disease. *Nature Reviews Neuroscience* (2017) doi:10.1038/nrn.2017.48.
24. Hamilton, N. B. Pericyte-mediated regulation of capillary diameter: a component of neurovascular coupling in health and disease. *Front. Neuroenergetics* (2010) doi:10.3389/fnene.2010.00005.
25. Glover, G. H. Overview of functional magnetic resonance imaging. *Neurosurgery Clinics of North America* (2011) doi:10.1016/j.nec.2010.11.001.
26. Ogawa, S., Lee, T. M., Kay, A. R. & Tank, D. W. Brain magnetic resonance imaging with contrast dependent on blood oxygenation. *Proc. Natl. Acad. Sci. U. S. A.* (1990) doi:10.1073/pnas.87.24.9868.
27. Thulborn, K. R., Waterton, J. C., Matthews, P. M. & Radda, G. K. Oxygenation dependence of the transverse relaxation time of water protons in whole blood at high field. *BBA - Gen. Subj.* (1982) doi:10.1016/0304-4165(82)90333-6.
28. Boorman, L. *et al.* Negative blood oxygen level dependence in the rat: A model for investigating the role of suppression in neurovascular coupling. *J. Neurosci.* (2010) doi:10.1523/JNEUROSCI.6063-09.2010.
29. Rivnay, J., Wang, H., Fenno, L., Deisseroth, K. & Malliaras, G. G. Next-generation probes, particles, and proteins for neural interfacing. *Science Advances* (2017) doi:10.1126/sciadv.1601649.
30. Kennerley, A. J., Mayhew, J. E., Boorman, L., Zheng, Y. & Berwick, J. Is optical imaging spectroscopy a viable measurement technique for the investigation of the negative BOLD phenomenon? A concurrent optical imaging spectroscopy and fMRI study at high field (7T). *Neuroimage* (2012) doi:10.1016/j.neuroimage.2012.03.015.
31. Stickland, R. *et al.* Neurovascular Coupling During Visual Stimulation in Multiple Sclerosis: A MEG-fMRI Study. *Neuroscience* (2019) doi:10.1016/j.neuroscience.2018.03.018.
32. Tarantini, S. *et al.* Demonstration of impaired neurovascular coupling responses in TG2576 mouse model of Alzheimer's disease using functional laser speckle contrast imaging.

GeroScience (2017) doi:10.1007/s11357-017-9980-z.

33. Berridge, M. J., Bootman, M. D. & Roderick, H. L. Calcium signalling: Dynamics, homeostasis and remodelling. *Nature Reviews Molecular Cell Biology* (2003) doi:10.1038/nrm1155.
34. Grienberger, C. & Konnerth, A. Imaging Calcium in Neurons. *Neuron* (2012) doi:10.1016/j.neuron.2012.02.011.
35. Nagai, T., Yamada, S., Tominaga, T., Ichikawa, M. & Miyawaki, A. Expanded dynamic range of fluorescent indicators for Ca2+ by circularly permuted yellow fluorescent proteins. *Proc. Natl. Acad. Sci. U. S. A.* (2004) doi:10.1073/pnas.0400417101.
36. Tian, L. *et al.* Imaging neural activity in worms, flies and mice with improved GCaMP calcium indicators. *Nat. Methods* (2009) doi:10.1038/nmeth.1398.
37. Bouchard, M. B., Chen, B. R., Burgess, S. A. & Hillman, E. M. C. Ultra-fast multispectral optical imaging of cortical oxygenation, blood flow, and intracellular calcium dynamics. *Opt. Express* (2009) doi:10.1364/oe.17.015670.
38. Svoboda, K. & Yasuda, R. Principles of Two-Photon Excitation Microscopy and Its Applications to Neuroscience. *Neuron* (2006) doi:10.1016/j.neuron.2006.05.019.
39. Shih, A. Y. *et al.* Two-photon microscopy as a tool to study blood flow and neurovascular coupling in the rodent brain. *Journal of Cerebral Blood Flow and Metabolism* (2012) doi:10.1038/jcbfm.2011.196.
40. Kimbrough, I. F., Robel, S., Roberson, E. D. & Sontheimer, H. Vascular amyloidosis impairs the gliovascular unit in a mouse model of Alzheimer's disease. *Brain* (2015) doi:10.1093/brain/awv327.
41. Rungta, R. L., Osmanski, B. F., Boido, D., Tanter, M. & Charpak, S. Light controls cerebral blood flow in naive animals. *Nat. Commun.* (2017) doi:10.1038/ncomms14191.
42. ARUK. Alzheimer's Research UK - Dementia Figures. (2017).
43. Alzheimer's Society. Alzheimer's disease. (2018).
44. Masters, C. L. *et al.* Alzheimer's disease. *Nature Reviews Disease Primers* (2015) doi:10.1038/nrdp.2015.56.
45. Chartier-Harlin, M. C. *et al.* Early-onset Alzheimer's disease caused by mutations at codon 717 of the β-amyloid precursor protein gene. *Nature* (1991) doi:10.1038/353844a0.
46. Levy-Lahad, E. *et al.* Candidate gene for the chromosome 1 familial Alzheimer's disease locus. *Science (80-.).* (1995) doi:10.1126/science.7638622.
47. Rogaev, E. I. *et al.* Familial Alzheimer's disease in kindreds with missense mutations in a gene on chromosome 1 related to the Alzheimer's disease type 3 gene. *Nature* (1995) doi:10.1038/376775a0.
48. Campion, D. *et al.* Early-onset autosomal dominant Alzheimer disease: Prevalence, genetic heterogeneity, and mutation spectrum. *Am. J. Hum. Genet.* (1999) doi:10.1086/302553.
49. Mucke, L. *et al.* High-level neuronal expression of Aβ(1-42) in wild-type human amyloid protein precursor transgenic mice: Synaptotoxicity without plaque formation. *J. Neurosci.* (2000) doi:10.1523/jneurosci.20-11-04050.2000.
50. Hall, A. M. & Roberson, E. D. Mouse models of Alzheimer's disease. *Brain Research Bulletin*

(2012) doi:10.1016/j.brainresbull.2011.11.017.

51. McGowan, E. *et al.* Aβ42 is essential for parenchymal and vascular amyloid deposition in mice. *Neuron* (2005) doi:10.1016/j.neuron.2005.06.030.
52. Schmechel, D. E. *et al.* Increased amyloid β-peptide deposition in cerebral cortex as a consequence of apolipoprotein E genotype in late-onset Alzheimer disease. *Proc. Natl. Acad. Sci. U. S. A.* (1993) doi:10.1073/pnas.90.20.9649.
53. Corder, E. H. *et al.* Gene dose of apolipoprotein E type 4 allele and the risk of Alzheimer's disease in late onset families. *Science (80-.).* (1993) doi:10.1126/science.8346443.
54. Harris, F. M. *et al.* Carboxyl-terminal-truncated apolipoprotein E4 causes Alzheimer's disease-like neurodegeneration and behavioral deficits in transgenic mice. *Proc. Natl. Acad. Sci. U. S. A.* (2003) doi:10.1073/pnas.1434398100.
55. Shin, H. K. *et al.* Age-dependent cerebrovascular dysfunction in a transgenic mouse model of cerebral amyloid angiopathy. *Brain* (2007) doi:10.1093/brain/awm156.
56. Tarantini, S., Tran, C. H. T., Gordon, G. R., Ungvari, Z. & Csiszar, A. Impaired neurovascular coupling in aging and Alzheimer's disease: Contribution of astrocyte dysfunction and endothelial impairment to cognitive decline. *Experimental Gerontology* (2017) doi:10.1016/j.exger.2016.11.004.
57. Halliday, M. R. *et al.* Accelerated pericyte degeneration and blood-brain barrier breakdown in apolipoprotein E4 carriers with Alzheimer's disease. *J. Cereb. Blood Flow Metab.* (2016) doi:10.1038/jcbfm.2015.44.
58. Montagne, A. *et al.* Pericyte degeneration causes white matter dysfunction in the mouse central nervous system. *Nat. Med.* (2018) doi:10.1038/nm.4482.
59. Zlokovic, B. V. Neurovascular pathways to neurodegeneration in Alzheimer's disease and other disorders. *Nature Reviews Neuroscience* (2011) doi:10.1038/nrn3114.
60. Donnan, G. A., Fisher, M., Macleod, M. & Davis, S. M. Stroke. *The Lancet* (2008) doi:10.1016/S0140-6736(08)60694-7.
61. Pappas, A. C., Koide, M. & Wellman, G. C. Astrocyte Ca2+ signaling drives inversion of neurovascular coupling after subarachnoid hemorrhage. *J. Neurosci.* (2015) doi:10.1523/JNEUROSCI.1551-15.2015.
62. Yeung, P. K. K., Shen, J., Chung, S. S. M. & Chung, S. K. Targeted over-expression of endothelin-1 in astrocytes leads to more severe brain damage and vasospasm after subarachnoid hemorrhage. *BMC Neurosci.* (2013) doi:10.1186/1471-2202-14-131.
63. Balbi, M. *et al.* Dysfunction of mouse cerebral arteries during early aging. *J. Cereb. Blood Flow Metab.* (2015) doi:10.1038/jcbfm.2015.107.
64. Toth, P., Tarantini, S., Csiszar, A. & Ungvari, Z. Functional vascular contributions to cognitive impairment and dementia: Mechanisms and consequences of cerebral autoregulatory dysfunction, endothelial impairment, and neurovascular uncoupling in aging. *American Journal of Physiology - Heart and Circulatory Physiology* (2017) doi:10.1152/ajpheart.00581.2016.
65. Duncombe, J. *et al.* Ageing causes prominent neurovascular dysfunction associated with loss of astrocytic contacts and gliosis. *Neuropathol. Appl. Neurobiol.* (2017)

doi:10.1111/nan.12375.

66. Lee, L., Kosuri, P. & Arancio, O. Picomolar amyloid-β peptides enhance spontaneous astrocyte calcium transients. *J. Alzheimer's Dis.* (2014) doi:10.3233/JAD-130740.
67. Lusis, A. J. Atherosclerosis. *Nature* (2000) doi:10.1038/35025203.
68. Mozaffarian, D. *et al.* Heart disease and stroke statistics-2015 update : A report from the American Heart Association. *Circulation* (2015) doi:10.1161/CIR.0000000000000152.
69. Williams, K. J. & Tabas, I. The response-to-retention hypothesis of early atherogenesis. *Arteriosclerosis, Thrombosis, and Vascular Biology* (1995) doi:10.1161/01.atv.15.5.551.
70. Tabas, I., García-Cardeña, G. & Owens, G. K. Recent insights into the cellular biology of atherosclerosis. *Journal of Cell Biology* (2015) doi:10.1083/jcb.201412052.
71. Hansson, G. K. & Hermansson, A. The immune system in atherosclerosis. *Nature Immunology* (2011) doi:10.1038/ni.2001.
72. Tabas, I., Williams, K. J. & Borén, J. Subendothelial lipoprotein retention as the initiating process in atherosclerosis: Update and therapeutic implications. *Circulation* (2007) doi:10.1161/CIRCULATIONAHA.106.676890.
73. Gimbrone, M. A. & García-Cardeña, G. Vascular endothelium, hemodynamics, and the pathobiology of atherosclerosis. *Cardiovascular Pathology* (2013) doi:10.1016/j.carpath.2012.06.006.
74. Frostegård, J. *et al.* Cytokine expression in advanced human atherosclerotic plaques: Dominance of pro-inflammatory (Th1) and macrophage-stimulating cytokines. *Atherosclerosis* (1999) doi:10.1016/S0021-9150(99)00011-8.
75. Spann, N. J. *et al.* Regulated accumulation of desmosterol integrates macrophage lipid metabolism and inflammatory responses. *Cell* (2012) doi:10.1016/j.cell.2012.06.054.
76. Alexander, M. R. & Owens, G. K. Epigenetic Control of Smooth Muscle Cell Differentiation and Phenotypic Switching in Vascular Development and Disease. *Annu. Rev. Physiol.* (2012) doi:10.1146/annurev-physiol-012110-142315.
77. Glagov, S., Weisenberg, E., Zarins, C. K., Stankunavicius, R. & Kolettis, G. J. Compensatory Enlargement of Human Atherosclerotic Coronary Arteries. *N. Engl. J. Med.* (1987) doi:10.1056/NEJM198705283162204.
78. Madamanchi, N. R., Vendrov, A. & Runge, M. S. Oxidative stress and vascular disease. *Arteriosclerosis, Thrombosis, and Vascular Biology* (2005) doi:10.1161/01.ATV.0000150649.39934.13.
79. Iadecola, C. The Pathobiology of Vascular Dementia. *Neuron* (2013) doi:10.1016/j.neuron.2013.10.008.
80. Gorelick, P. B. *et al.* Vascular contributions to cognitive impairment and dementia: A statement for healthcare professionals from the American Heart Association/American Stroke Association. *Stroke* (2011) doi:10.1161/STR.0b013e3182299496.
81. Saji, N., Toba, K. & Sakurai, T. Cerebral Small Vessel Disease and Arterial Stiffness: Tsunami Effect in the Brain? *Pulse* (2016) doi:10.1159/000443614.
82. Matsumoto, L. *et al.* Association of subclinical carotid atherosclerosis with immediate memory

and other cognitive functions. *Geriatr. Gerontol. Int.* (2018) doi:10.1111/ggi.13142.

83. Caplan, L. R. Lacunar infarction and small vessel disease: Pathology and pathophysiology. *Journal of Stroke* (2015) doi:10.5853/jos.2015.17.1.2.
84. Stemme, S. *et al.* T lymphocytes from human atherosclerotic plaques recognize oxidized low density lipoprotein. *Proc. Natl. Acad. Sci. U. S. A.* (1995) doi:10.1073/pnas.92.9.3893.
85. Weber, C. & Noels, H. Atherosclerosis: Current pathogenesis and therapeutic options. *Nature Medicine* (2011) doi:10.1038/nm.2538.
86. Ridker, P. M. *et al.* Antiinflammatory therapy with canakinumab for atherosclerotic disease. *N. Engl. J. Med.* (2017) doi:10.1056/NEJMoa1707914.
87. Ridker, P. M. *et al.* Effect of interleukin-1β inhibition with canakinumab on incident lung cancer in patients with atherosclerosis: exploratory results from a randomised, double-blind, placebo-controlled trial. *Lancet* (2017) doi:10.1016/S0140-6736(17)32247-X.
88. Zhao, Z., Nelson, A. R., Betsholtz, C. & Zlokovic, B. V. Establishment and Dysfunction of the Blood-Brain Barrier. *Cell* (2015) doi:10.1016/j.cell.2015.10.067.
89. Segrest, J. P., Jones, M. K., De Loof, H. & Dashti, N. Structure of apolipoprotein B-100 in low density lipoproteins. *Journal of Lipid Research* (2001).
90. Repas, T. B. & Ross Tanner, J. Preventing early cardiovascular death in patients with familial hypercholesterolemia. *J. Am. Osteopath. Assoc.* (2014) doi:10.7556/jaoa.2014.023.
91. Rogers, J. T. & Weeber, E. J. Reelin and apoE actions on signal transduction, synaptic function and memory formation. *Neuron Glia Biology* (2008) doi:10.1017/S1740925X09990184.
92. Rader, D. J., Cohen, J. & Hobbs, H. H. Monogenic hypercholesterolemia: New insights in pathogenesis and treatment. *Journal of Clinical Investigation* (2003) doi:10.1172/JCI200318925.
93. Getz, G. S. & Reardon, C. A. Do the Apoe-/- and Ldlr-/- mice yield the same insight on atherogenesis? *Arteriosclerosis, Thrombosis, and Vascular Biology* (2016) doi:10.1161/ATVBAHA.116.306874.
94. Getz, G. S. & Reardon, C. A. Animal models of Atherosclerosis. *Arteriosclerosis, Thrombosis, and Vascular Biology* (2012) doi:10.1161/ATVBAHA.111.237693.
95. Methia, N. *et al.* ApoE deficiency compromises the blood brain barrier especially after injury. *Mol. Med.* (2001) doi:10.1007/bf03401973.
96. Nakashima, Y., Plump, A. S., Raines, E. W., Breslow, J. L. & Ross, R. ApoE-deficient mice develop lesions of all phases of atherosclerosis throughout the arterial tree. *Arterioscler. Thromb.* (1994) doi:10.1161/01.atv.14.1.133.
97. Bjørklund, M. M. *et al.* Induction of atherosclerosis in mice and hamsters without germline genetic engineering. *Circ. Res.* (2014) doi:10.1161/CIRCRESAHA.114.302937.
98. Lu, H. *et al.* Hypercholesterolemia induced by a PCSK9 gain-of-function mutation augments angiotensin II-induced abdominal aortic aneurysms in C57BL/6 mice-brief report. *Arterioscler. Thromb. Vasc. Biol.* (2016) doi:10.1161/ATVBAHA.116.307613.
99. Roche-Molina, M. *et al.* Induction of sustained hypercholesterolemia by single adeno-

associated virus-mediated gene transfer of mutant hPCSK9. *Arterioscler. Thromb. Vasc. Biol.* (2015) doi:10.1161/ATVBAHA.114.303617.

100. Poirier, S. *et al.* The proprotein convertase PCSK9 induces the degradation of low density lipoprotein receptor (LDLR) and its closest family members VLDLR and ApoER2. *J. Biol. Chem.* (2008) doi:10.1074/jbc.M708098200.
101. Weinreich, M. & Frishman, W. H. Antihyperlipidemic therapies targeting PCSK9. *Cardiology in Review* (2014) doi:10.1097/CRD.0000000000000014.
102. Constantinides, A., Kappelle, P. J. W. H., Lambert, G. & Dullaart, R. P. F. Plasma Lipoprotein-associated Phospholipase A 2 Is Inversely Correlated with Proprotein Convertase Subtilisin-kexin Type 9. *Arch. Med. Res.* (2012) doi:10.1016/j.arcmed.2012.01.001.
103. Abifadel, M. *et al.* Mutations in PCSK9 cause autosomal dominant hypercholesterolemia. *Nat. Genet.* (2003) doi:10.1038/ng1161.
104. Zimetti, F. *et al.* Increased PCSK9 cerebrospinal fluid concentrations in Alzheimer's disease. *J. Alzheimer's Dis.* (2016) doi:10.3233/JAD-160411.
105. Sheridan, C. Phase 3 data for PCSK9 inhibitor wows. *Nature biotechnology* (2013) doi:10.1038/nbt1213-1057.
106. Notkola, I. L. *et al.* Serum total cholesterol, apolipoprotein E ε4 allele, and Alzheimer's disease. *Neuroepidemiology* (1998) doi:10.1159/000026149.
107. Chen, Y. L. *et al.* Changes in astrocyte functional markers and β-amyloid metabolism-related proteins in the early stages of hypercholesterolemia. *Neuroscience* (2016) doi:10.1016/j.neuroscience.2015.12.039.
108. Hohsfield, L. A., Daschil, N., Orädd, G., Strömberg, I. & Humpel, C. Vascular pathology of 20-month-old hypercholesterolemia mice in comparison to triple-transgenic and APPSwDI Alzheimer's disease mouse models. *Mol. Cell. Neurosci.* (2014) doi:10.1016/j.mcn.2014.10.006.

The manuscript ends here. The following sections are not part of the above paper, but form part of the rest of Chapter 1. In these sections, I discuss the use of preclinical models to study human disease, namely cardiovascular and cerebrovascular diseases. Furthermore, I discuss the need to generate comorbid models that better reflect the human conditions, as many diseases of ageing are often present with two or more multimorbidities. To date, there are very limited comorbid models (some of which are outlined in the following section), and basic and translational scientists need to develop more representative models if therapies are to succeed clinical trials.

1.10 – Paper Title and Authors

Preclinical Models of Disease and Multimorbidity with Focus upon Cardiovascular Disease and Dementia

Osman Shabir[1,2,4], Tobias A Moll[2,3], Martyna M Matuszyk[2,3], Beth Eyre[1,2], Manmohi D Dake[2,3], Jason Berwick[1,2,5] & Sheila E Francis[2,4,5]*

Author Affiliations:

[1]The Neurovascular Lab, Department of Psychology, Alfred Denny Building, University of Sheffield, Western Bank, Sheffield, S10 2TN

[2]Neuroscience Institute, University of Sheffield, Sheffield, S10 2TN

[3]Sheffield Institute for Translational Neuroscience (SITraN), 385a Glossop Road, Sheffield, S10 2HQ

[4]Department of Infection, Immunity & Cardiovascular Disease (IICD), University of Sheffield Medical School, Royal Hallamshire Hospital, Beech Hill Road, Sheffield, S10 2RX

[5]Healthy Lifespan Institute (HELSI), University of Sheffield, Sheffield, S10 2TN

***Corresponding Author:** Professor Sheila E Francis, Professor of Cardiovascular Biology, Department of Infection, Immunity & Cardiovascular Disease (Healthy Lifespan Institute), University of Sheffield, Medical School, Royal Hallamshire Hospital, Beech Hill Road, Sheffield, S10 2RX (s.francis@sheffield.ac.uk)

1.11 – Abstract

The use of animal models is fundamental to furthering our understanding of human disease mechanisms, as well as identifying potential therapeutic targets. Diseases of ageing often involve multiple body systems; however, multi-systemic features are not fully recapitulated in the many of the animal models available. Therefore, combining pre-clinical models to better reflect the multimorbidities observed at the clinical level is critical. This review will highlight some of the key pre-clinical experimental models associated with **cardiovascular (atherosclerosis, coronary heart disease), cerebrovascular (stroke, vascular dementia),** *metabolic (obesity, type-2 diabetes mellitus) and neurological (amyotrophic lateral sclerosis, frontotemporal dementia, Parkinson's, epilepsy) diseases,* and whether these models encompass known multimorbidities. In addition to this, we discuss established pre-clinical models that combine two or more conditions, within the context of dementia.

1.12 – Introduction

Studying the mechanisms of human disease is a complex and challenging task. Pre-clinical models are necessary in order to fully interrogate and manipulate different pathophysiological processes and to understand the mechanisms involved in disease onset and progression. Whilst cell models provide invaluable insight at the molecular level, animal models are inevitably required to fully recapitulate the complex multisystem involvement of diseases of

ageing. Animal models of human disease have led to significant improvements in our understanding of human diseases as well as allowing us to trial novel therapies. The focus of this review is to describe some of the main pre-clinical models used to study many of the major human diseases (cardiovascular, metabolic & neurological) associated with ageing and dementia, as well as outlining some of the mixed comorbid models combining two or more diseases.

1.13 – Cardiovascular Diseases

Cardiovascular diseases (CVDs) are a leading cause of mortality worldwide (1), with an estimated 30% of all deaths globally being attributed to CVDs. Within the UK, 7.4 million people are currently living with CVDs and these numbers are expected to rise due to the increasing ageing population. CVDs include a range of linked diseases that affect the heart and/or the circulatory system. These include coronary heart disease (CHD), cerebrovascular diseases (CbVDs) including stroke, peripheral arterial disease, aortic aneurysms, thromboembolic disease, renal artery stenosis, cardiomyopathy, pulmonary heart disease, cardiac dysrhythmias, valvular heart disease, inflammatory heart diseases and heart failure. Many of these conditions have similar underlying pathologies including the development of atherosclerosis as well as common modifiable risk factors including hypertension, obesity, hypercholesterolaemia, sedentary lifestyle (inactivity), diabetes mellitus, smoking and excessive alcohol consumption (2). Other non-modifiable factors include genetics (family history), ethnicity, being male and advanced age. As such, many CVDs are preventable through modifying lifestyle risk factors and adopting a healthier and active lifestyle. In this section, models of atherosclerosis and cerebrovascular disease will be discussed, whereas diabetes mellitus and obesity will be covered in depth later.

Atherosclerosis is the main underlying cause of CVD and affects most people over the age of 60 to some degree with around 50% of all people over the age of 40 being in good health having a risk of developing serious atherosclerosis (3). Atherosclerosis is the chronic and progressive thickening and hardening of major arteries by the build-up of atheromatous plaques that can lead to luminal narrowing to restrict blood flow over time (4). Atheromatous plaques may themselves rupture to form a thrombus disrupting blood flow or to cause an embolism or haemorrhage. Atherosclerosis and thromboembolism are the primary causes of CHD, myocardial infarction and stroke. Atherosclerosis whilst itself is a disease, often does not present with overt symptoms until plaques severely limit flow/rupture or a secondary effect of atherosclerosis occurs – such as CHD or stroke. A more detailed discussion of atherosclerosis and its effects on cerebrovascular function can be found in our recent review (5).

Mouse models of human atherosclerosis tend to centre around genetic knockouts of commonly implicated genes in atherogenesis, notably LDLR and APOE mouse knockouts (6). LDL molecules (commonly referred to as “bad cholesterol”) alongside other lipids, triglycerides and cholesterol molecules bind to the LDLR primarily within hepatocytes in the liver leading to lipid endocytosis (7). Mouse models that knockout LDLR have a reduced ability to endocytose LDL molecules thus serum LDL and cholesterol levels become elevated (hypercholesterolemia). The ApoE protein has numerous physiological roles including its ability to bind to chylomicron and VLDL molecules and binding to the LDLR leading to lipid endocytosis. Compared to $LDLR^{-/-}$ mice, $ApoE^{-/-}$ mice are hyperlipidaemic even on a normal rodent diet without the need for a high-fat Western or Paigen diet; which the $LDLR^{-/-}$ mice requires for atherogenesis, however, $ApoE^{-/-}$ mice display much higher serum cholesterol levels and atherosclerotic lesions with a Western diet (6). As such, the $APOE^{-/-}$ mouse model is much more aggressive than the $LDLR^{-/-}$ mouse model on a high-fat diet, although the latter displays hyperlipidaemia profiles that closely resemble the spectrum of lipid levels in humans. The specific differences between the two strains with respect to atherogenesis are discussed in depth elsewhere (6). A third and more recent model of atherosclerosis utilises a single injection of rAAV8-mPCSK9-D377Y that is sufficient to cause robust atherosclerosis in mice and hamsters within 8-12 weeks when combined with a Western diet comparable to $LDLR^{-/-}$ mice (8, 9). PCSK9 typically regulates cholesterol levels homeostatically by interacting with LDLR to cause its internalisation and degradation (10). The murine D377Y mutation confers a gain of function mutation to PCSK9 leading to its constitutive activation at all times permanently reducing LDLR expression, which is analogous to the human D374Y mutation found in familial autosomal dominant hypercholesterolaemia (11). As recently discussed in our previous review (5), the AAV8-mediated virally injected model of atherosclerosis is far cheaper and simpler than maintaining large inbred colonies and breeding genetically modified animals. Not only is the induction of atherosclerosis relatively quick, it can also be induced in almost any strain of mouse at any age. ***Table 1*** outlines the key features of these models.

Of the three mouse models, the $APOE^{-/-}$ has been used more extensively in the research of atherosclerosis and cerebrovascular function than the $LDLR^{-/-}$ or mPCSK9 models. We have previously investigated cerebrovascular changes in the $APOE^{-/-}$ mouse (12), where we found that interleukin-1 (IL1ß) was a key driver of systemically mediated cerebrovascular inflammation. An anti-IL1ß approach can potentially be used to therapeutically intervene in atherosclerosis, dementia and stroke (13). Within the brain, lipid deposition coinciding with inflammation was found in the lateral ventricle and choroid plexus associated with Cd45+ cells as well as significant microglial (Iba1+) activation. Lipid deposition, but not atherosclerotic

lesions, was found within the walls of larger ventricle-associated blood vessels and in some smaller parenchymal arteries. However, focal pathologies were not present within the parenchyma. Using anti-IL1ß antibodies, the number of CD45+ cells were substantially reduced as well as reduced microglial activation (12). It is important to note that the most severe neuroinflammatory changes and lipid deposition was substantially more pronounced in $APOE^{-/-}$ mice fed a Paigen diet (more cholesterol and cholate) than those fed a Western diet. Other work using the $APOE^{-/-}$ model has found impaired cerebrovascular autoregulation and worsened ischemic perfusion deficits (14). In accordance to our previous findings, Ayata et al did not find any evidence of intracranial atherosclerosis despite evidence of scattered foam cells in carotid arteries and fatty streaks within the aorta. Blood pressure was found to be 10% higher compared to controls, and indeed hypertension is a common comorbidity of atherosclerosis/CVD in humans and animal models. Furthermore, reduced vascular reactivity by 30% in $APOE^{-/-}$ mice was observed compared to controls as assessed through a 5% hypercapnia test. In addition, blunted neurovascular haemodynamic responses to sensory whisker stimulations by 64% were also observed despite no cortical activation differences, indicative of impaired neurovascular coupling (14). Other studies have shown cognitive and behavioural changes associated with $ApoE^{-/-}$ mice including deficient spatial memory (assessed by Morris water maze) (15) as well as in the $LDLR^{-/-}$ mouse fed a Western diet (16), which also displayed more anxiety. Furthermore, these mouse models have served as good bases for trialling therapeutic strategies for atherosclerosis in. For example, simvastatin has been shown to reduce atherogenesis and promotes the expression of genes associated with cholesterol uptake using $ApoE^{-/-}$ mice fed high-fat diet (17). In addition, simvastatin has also been shown to improve cognitive deficits in the Tg2576 mouse model of AD due to its anti-inflammatory properties (18). The biggest limitation with mouse models of atherosclerosis is that mice in general are resistant to atherosclerosis; which may in part be due to the fact that LDL-cholesterol can be degraded rapidly from plasma and mice naturally have much higher levels of HDL-cholesterol which is athero-protective (19). Even when atherosclerosis is induced in mouse models such as genetically knocking out ApoE & LDLR, or by virally inducing by rAAV8-mPCSK9-D377Y, the atherosclerosis is often limited to the aorta and aortic sinus without too much further progression to coronary, pulmonary and cerebral circulation. Both $ApoE^{-/-}$ and $LDLR^{-/-}$ mice have extremely limited or completely absent plaque rupture and thrombosis or any coronary arterial occlusion (19), all which are important features of human CVD.

Coronary heart disease (CHD), particularly heart failure, is caused by a reduction of blood flow to the heart muscle due to a build-up of atherosclerosis in coronary arteries and is common affecting around 2.3 million people in the UK. Individuals with CHD have on average a 45%

increased risk of developing cognitive impairment or dementia (20). This is associated with a reduced cerebral perfusion due to reduced cardiac output. This is very difficult to model and ApoE$^{-/-}$ mice fed a Western diet with severe atherosclerosis do not display complete coronary arterial occlusion. However, when ApoE$^{-/-}$ or LDLR-$^{/-}$ mice are crossed with mice deficient for Na+/H+ exchange regulatory cofactor NHE-RF3 (encoded by PDZK1); a protein which binds to a HDL receptor SRB1, or have SRB1 deficiency, these double transgenic mice fed altered fatty diets do present with coronary artery occlusion and myocardial infarction (21, 22) (***Table 1***). It is thought that the mechanism for this is that unesterified cholesterols accumulate in HDL-cholesterol molecules impairing their naturally athero-protective properties alongside HDL-cholesterol increase (toxic forms) causing rapid and robust atherogenesis. These mice often die young due to spontaneous myocardial infarction. Normal rodent chow mice live the longest, followed by Western diet fed mice, and Paigen diet mice living the shortest due to the increased fat and cholesterol levels (22). The mice fed Paigen or Western diets display a significantly increased expression of VCAM-1, ICAM-1 in coronary arteries accompanied by an increased number of monocytes infiltrating the wall. Other models of CHD with human like presentation of symptoms include crossing ApoE$^{-/-}$ mice with those deficient for eNOS (ApoE$^{-/-}$/eNOS$^{-/-}$) (23). These mice develop coronary artery atherosclerosis with heart failure and myocardial infarction as well as the presence of aortic aneurysms. The problem with deleting eNOS is that other isoforms of NOS are upregulated in a compensatory manner. Total NOS knockout (NOS tKO) mice suffer from several comorbidities including hypertension, left ventricular hypertrophy, dysfunctional vascular pulsing, coronary spasm initiated by mast-cell derived histamine release and death (24). Whilst this mouse model is useful for dissecting new mechanisms involving the NOS system and its importance in maintaining normal cardiovascular function, it is highly artificial as humans tend not to have complete NOS deficiency but allows the possibility of NO-donors as potential therapeutic agents for CHD given that NOS deficiency is key in many CVDs (25).

Other models of CVD include rabbit models similar to the rodent models in terms of being fed a high-fat or cholesterol diet. The advantage of rabbits over rodents is that they are medium sized animals that readily present with fibroatheroma lesions, though much like rodents, typically do not exhibit any plaque rupture (26). Rabbits when fed a high-fat diet develop robust atherosclerotic lesions which in part resemble human lesions with respect to the involvement of immune cells and vascular smooth muscle cell proliferation (26) (***Table 1***). In addition, models of plaque rupture have been successfully modelled in rabbits when a high-fat diet was combined with vascular injury modelling leading to vulnerable plaque formation that consist of lipid rich cores, macrophage accumulation and fibrous caps which resemble vulnerable human atherosclerotic lesions (27).

1.14 – Cerebrovascular Disease (CbVD)

Systemic CVD of the type discussed above can lead to impaired blood circulation to the brain and/or to vessels within the brain giving rise to a collection of conditions called CbVDs. These diseases include both haemorrhagic and ischaemic strokes, cerebral aneurysms and vascular dementia. Every 2 seconds, somewhere in the world suffers from a stroke, and there are approximately 100,000 strokes in the UK every year (1 every 5 minutes) and approximately 1.2 million stroke survivors (28) Stroke is the 4th biggest cause of mortality in the UK and the 2nd biggest cause of mortality across the world causing around 5.78 million deaths in 2016. 1 out of 4 affected individuals will suffer from another stroke within 5 years. 85% of all strokes are ischaemic whereas only 15% are haemorrhagic (29). The primary cause of ischaemic strokes are large vessel atherosclerosis, cardioembolism, lacunar infarcts due to small vessel disease (SVD) or rupture of an atherosclerotic plaque, though some strokes remain due to undetermined aetiologies known as cryptogenic strokes (30). Strokes can either be transient (transient ischaemic attacks) or major cerebrovascular incidents (both fatal and non-fatal). Often with non-fatal strokes, cognitive impairment can occur that can lead to vascular dementia (VaD) – the 2nd most common form of dementia after AD, along with SVD and intracranial atherosclerosis; both also causes of stroke (31). Thus, stroke and vascular dementia are tightly linked together with 1 in 3 stroke survivors developing VaD within 5 years and 75% of all dementia cases in stroke survivors being attributed to VaD (32).

Rodent models of stroke tend to either be mechanical (surgical) in nature or pharmacological to predispose animals to clotting, for example. The most common surgical model is that of the middle cerebral artery occlusion (MCAO) model in which a filament is inserted into the internal carotid artery and pushed until the MCA is blocked that can either be permanent, or temporary to allow reperfusion (33) (***Table 1***). This model mimics thromboembolic infarcts seen in patients where the majority of infarcts occur within the MCA. The major issue, however, with this model is that it results in complete occlusion of the MCA whereas ischaemic strokes in patients tend not to be completely occluding and spontaneous reperfusion tends to occur in most patients due to the resolution of the thrombus within 48hrs (33). Nonetheless, this model has provided valuable insights into specific elements of ischaemic stroke including blood-brain-barrier injury, neuroinflammation and reactivity, and cell death – common features of human stroke. Other MCAO techniques include the permanent electrocoagulation of the distal portion of the MCA (dMCA) which leads to consistent infarct volumes of up to around 12% of the cerebral hemisphere affecting somatosensory and motor cortices, which resembles closely a significant proportion of human strokes in terms of area affected (34). Embolic stroke models can be modelled by either spontaneously formed or thrombin-induced material. Thrombin can be injected directly into the MCA to mimic vessel occlusion, or by introducing

an embolic material through the extracranial internal carotid artery or external carotid artery to cause occlusion of potentially multiple vessels (35-38) (***Table 1***). The major advantage of this approach of the complete MCAO model is that there is spontaneous and unpredictable partial or complete occlusion followed by resolution and reperfusion that mimics human embolic stroke more closely. The model is also highly variable, much like clinical strokes and the disease-course can present very differently in different animals. Although there has been steady development over the years with rodent models, none of the drugs so far studied in these models has translated to a successful stroke treatment (39).

Many non-human primate models, unlike rodents, have more complicated and evolved brain structures that resemble human brains better, for example the macaque monkey and baboons. However, many non-human primates including marmosets still have a lissecephalic brain thus in terms of gyri and sulci are not more evolved than rats, for example, despite overall having a more complex organisation of the cortex. Thus, the use of a non-human primate in stroke research for example would be more suitable using a gyrencephalic brain of a baboon or macaque. Endovascular ischaemic stroke has been modelled in rhesus macaques by inflating a balloon attached to a micro-catheter to occlude the MCA for 3hrs; similar to the MCAO rodent model, and by injection of an autologous clot into the MCA for 3hrs (40) (***Table 1***). In line with rodent studies, perfusion deficits and worse prognoses (including hemiparesis and death) was attributed to the full occlusion model compared to the clotting model which displayed better outcomes for some but not all of the monkeys. This variability was due to the positioning of the clot along the MCA where M1 occlusion would be more fatal rather than via M2 segments, allowing M1 reperfusion. The bifurcation (or trifurcation) of MCA branches of such an extent can only be modelled using higher order organisms. Indeed, promising therapeutic trials from rodent studies have been replicated in monkeys (such as PSD-95 inhibitor) (41). Thus, a more natural pre-clinical pipeline would be to assess promising rodent therapies in gyrencepahilc non-human primates before human trials. However, compared to rodent studies, the ethical and legal framework involved in non-human primate research is much more complex and often holds a public stigma associated with it, despite the increasing need to replicate rodent studies in non-human primates due the immense failures of most translational therapies for stroke from rodents.

After non-fatal stroke, VaD can occur in around 75% of all stroke survivors. This second most common form of dementia after Alzheimer's is estimated to affect 150,000 people in the UK and causing around 15,000 deaths each year (42). Individuals with CHD and diabetes are at a particularly high risk of developing VaD (42) therefore with respect to models of VaD and vascular cognitive impairment dementia (VCID), there is a need to effectively recapitulate

hypoxia and inflammation that is associated with deep white matter lesions. In order to do this, similar to the stroke models discussed, bilateral occlusion of the carotid arteries (rather than cerebral arteries) is typically performed (BCAO) to cause generalised hypoperfusion and hypoxia-induced white matter damage (43, 44) (***Table 1***). The original study from 1994 explored neuropathological changes associated with the BCAO rat model and found significant glial (GFAP+) activation associated with increased MHCI/II expression on microglia, and infiltration of CD4+ and CD8+ immune cells were found within the white matter (43). This results in severe, but temporary oligemia, which gradually returns to baseline within a few weeks with a compensatory enlargement of the basilar artery. Behavioural tests on BCAO mice have shown prolonged responses and learning times as well as increased error rates during Morris water maze tests indicative of learning and memory deficits in these mice (44). This occurred alongside a significant reduction in CA1 hippocampal neuronal number/ disorganisation, BBB disruption associated with vasogenic oedema, loss of oligodendrocytes and reductions in myelination density (45). Bilateral carotid arterial partial stenosis (BCAS) methods are preferred in mice as opposed to permanent BCAO (which leads to death in mice) using small coils that lead to hypoperfusion but allow some slow reperfusion (46) (***Table 1***). These mice also display working memory deficits assessed by radial maze tests associated with hippocampal atrophy with widespread evidence of apoptosis (46, 47). This gradual stenosis model compared to a sudden acute oligemia is more reflective of human carotid stenosis implicated in VaD/VCID onset and maybe a better preclinical model as only white matter lesions are reported rather than extensive grey matter damage. Several treatment strategies have emerged using this model including the use of cyclosporin A which has been shown to suppress glial activation and BBB breakdown through inhibition of the MMP-9 pathway in pericytes thus preventing neurodegeneration (48).

Although VaD is linked to stroke, the actual term ‘dementia’ refers to a group of diseases characterised by progressive cognitive decline. Currently, there are no effective treatments to prevent, cure or slow down the disease progression of these diseases. Symptoms include, but are not limited to, behavioural changes, memory loss, difficulties in communicating and impaired executive function interfering with daily activities of affected individuals (49). Dementia is a leading cause of mortality worldwide with over 50 million people affected globally (50). This is set to triple to approximately 152 million by 2050, with nearly 10 million new cases every year (50). Within the UK, there are currently over 537,000 people with a dementia diagnosis, and this figure is projected to increase to 1 million by 2025 (51). In order of prevalence, common types of dementia include Alzheimer’s disease (AD), followed by vascular dementia (VaD, described above), frontotemporal dementia (FTD), and dementia with Lewy bodies (DLB). Up to 20% of all dementia patients often present with more than one

of these diseases leading to a mixed dementia diagnosis (52). Relevant to this review, the most common mixed dementia is AD with VaD or other cerebrovascular disease (CbVD). Since these diseases are associated with age, the prevalence of cardiovascular diseases (CVD) and CbVD increases, which is also the case for dementia. The main pathological hallmarks of AD include amyloid-beta (Aβ) plaques and neurofibrillary tangles of hyperphosphorylated-tau; however, many AD patients also display significant hallmarks of CbVD including white matter lesions (52, 53). Many other diseases of ageing often coexist with other diseases with common overlapping risk factors. For example, dementia is associated with CVD, hypercholesterolaemia/hyperlipidaemia, obesity, diabetes mellitus, hypertension and CbVD (53).

The presence of Aβ plaques and neurofibrillary tangles characterises neuropathological changes in AD (54), and is followed by microglial and astrocytic activation, release of pro-inflammatory mediators and neuronal death, leading to brain atrophy. Familial and sporadic AD cases are observed. Sporadic AD (sAD) is not typically associated with any specific genetic mutations, whilst familial AD (fAD) is typically inherited in an autosomal dominant pattern (55). Mutations associated with familial AD include mutations in the APP gene, which are associated with increased Aβ production (56-58). Other causative mutations include PSEN1 and PSEN2, which can result in abnormal production of Aβ (59-62). Animal models of AD include transgenic mouse lines expressing familial AD mutations. Popular mouse models often focus on modelling Aβ deposition in the brain. Many mouse lines focus on the overexpression of the human amyloid precursor protein (APP), which is a key protein leading to cleavage and secretion of Aβ (63). Additionally, double and triple transgenic mouse models have also been developed, where both APP and PSEN1 mutations are present, further increasing amyloid plaque content in the brain (63). Transgenic AD mice present with age-dependent amyloid deposition in the brain, which include amyloid plaques as well as activated microglia and astrocytes. Furthermore, such mice develop cognitive and memory impairments. However, no existing model of AD exhibits all features of AD, which includes cognitive deficits, amyloid plaques, neurofibrillary tangles, gliosis, synapse loss and neurodegeneration. For example, in many AD-mouse models, tau pathology is not observed. Neurofibrillary tangles are only seen when human tau is expressed, whilst neuronal loss is observed in a few lines (64). For a comprehensive review on mouse models of AD see (65). Other dementia models also use genetic manipulations of commonly implicated human genetic mutations (as in the case of FTD; discussed later), whereas other models use surgical methods to cause a reduction in cerebral blood flow (CBF) as in the case of modelling VaD, discussed above and in ***Table 1***.

Table 1 – Models of CVD and CbVD

Model	Description	Phenotype	Age Ranges	Advantages	Limitations	References
Atherosclerosis *ApoE$^{-/-}$ Mouse*	Homozygous Apoe(tm1Unc) on a C57BL/6J background	Serum cholesterol >500mg/dL on NRC and >1800mg/dL on Western Diet. Aortic fatty streaks from 10wks with intermediate foam cell lesions (with VSMCs) from 15wks. Fibrous plaques at 20wks (NRC)	Can be used from birth, and diet can be induced at any age. Plaques are present from early on.	Hyperlipidaemia without Western diet Severity can be increased by Western diet as well as exacerbating disease course Plaques resemble human lesions	Absence of plaque rupture or thrombosis No coronary artery occlusion/lesions Artificially high serum cholesterol levels on Western diet	Plump et al, 1992 (Plump et al., 1992) Piedrahita et al, 1992 (67) Getz & Reardon, 2016 (6)
LDLR$^{-/-}$ Mouse	Homozygous Ldlr(tm1Her) on a C57BL/6J background	Serum cholesterol 200-400mg/dL on NRC (higher on HFD). Around 3m slight aortic sinus/arch lesions (slow to start), but robustly increase to abdominal aorta (6-9m) Susceptible to obesity due to blunted leptin responsiveness Increased serum glucose levels linking to obesity	Typically, takes up to 6-9m for robust plaques to form – which resembles closer to human age of atherosclerosis onset (midlife) compared to ApoE$^{-/-}$	Hypercholesterolemia resembles human levels more than ApoE$^{-/-}$ mice Plaque development is steady	Requires Western diet to develop robust atherosclerosis Absence of plaque rupture or thrombosis No coronary artery occlusion/lesions	Ishibashi et al, 1993 (68) Getz & Reardon, 2016 (6) Ma et al, 2012 (69) Ngai et al, 2010 (70)
ApoE$^{-/-}$/LDLR$^{-/-}$ 2xTg Mouse	Apoe$^{-/-}$ x Ldlr$^{-/-}$ on Western diet on C57BL/6J background	Serum cholesterol levels matching ApoE$^{-/-}$ mice with advanced aortic lesions Obstructive coronary artery occlusion and myocardial infarction Increased mortality after 7m	Effects are observed between 4-12 months of age, with a Western diet duration of up to 7 weeks. However, after 7m there is high mortality which is young.	Additional stressors exacerbate myocardial infarction (mental stress and hypoxia) – resembling human heart attacks. Evidence that atherosclerosis rather than hyperlipidaemia is needed for CHD. Good model to test myocardial infarction prevention drugs.	High incidence of mortality after 7m	Caligiuri et al, 1999 (71)
AAV8-mPCSK9 Mouse/Hamster	Single injection of rAAV8-mPCSK9-D377Y with HFD (C57BL/6J mice)/Golden Syrian Hamsters	Serum cholesterol 300mg/dL on NRC (higher on HFD) Aortic lesions (plaques) with foam cells and VSMCs after 12wks	Can be induced in most strains at any age and resembles Ldlr$^{-/-}$ profiles.	Atherosclerosis can be induced in almost any strain or species (including hamsters) at any age with a single injection Western diet exacerbates hypercholesterolemia	Requires Western diet for atherogenesis AAV-mediated induction of atherosclerosis varies in different mouse strains	Bjorklund et al, 2014 (8) Roche-Molina et al, 2015 (9)
CHD *LDLR$^{-/-}$/SRB1$^{-/-}$ 2xTg Mouse*	LDLR$^{-/-}$/SRB1$^{-/-}$ fed HFD (Western, high cholesterol & Paigen diets)	Occlusive platelet rich coronary artery atherosclerosis that correlates to dietary fat and cholesterol contents – myocardial	Diets given for a period of 12 weeks, but 2xTg KO mice fed Paigen diets only survived 3.5wks, those on Western	Newer models to study coronary artery disease and occlusion not typically seen in ApoE$^{-/-}$ or LDLR$^{-/-}$ mice	High rates of mortality Unclear mechanisms and interactions of PDZK1 and SRB1 in protective effects and role in hyperlipidaemia	Fuller et al, 2014 (22)

ApoE$^{-/-}$/PDZK1$^{-/-}$ 2xTg Mouse	ApoE$^{-/-}$/PDZK1$^{-/-}$ fed Paigen diet	infarction and death Further increase in plasma cholesterol levels and exacerbated aortic lesions with substantial coronary artery disease & myocardial infarction	11.4wks – very young death. 4wks old animals fed Paigen diet for 3 months (so around 4-5 months of age – which is young)	Elucidation of the role of PDZK1 and SRB1 in the role of CHD development and serving as models for therapies		Yesilaltay et al, 2009 (21)
Stroke *MCAO in Mice or Rats*	Focal cerebral ischemia induced by MCAO with intraluminal nylon filaments (of varying diameters) inserted through internal carotid artery	Cerebral infarction caused by abrupt CBF decline in the temporoparietal cortex and laterocaudal part of caudate putamen Ischaemia accompanied by ATP depletion, acidosis and suppression of protein synthesis	Can be performed at any age. Typically, 60 minutes or 120 minutes of MCAO is performed.	Reproducible focal cerebral ischaemia Avoidance of craniotomy Reperfusion possible Standardization of thread selection by a numerical relationship between thread size and weight of animals	Careful selection of thread material and diameter to advance far enough the arterial branch that is sufficient to occlude leading to inconsistency – however Hata et al use a numerical standardization technique to overcome this	Hata et al, 1998 (33)
	Tying off common carotid artery and using external carotid artery as a side path to suture through the internal carotid artery to lodge in the junction of MCA and ACA	Suture method leads to ischaemic cell death in striatum, overlying frontal, parietal, temporal and occipital cortices producing complex motor, sensory, autonomic and cognitive defects		In the suture method, the suture can be left in place for variable amounts of time and be removed to allow reperfusion – this method does not require craniotomy.	Suture method can have mortality rates of around 12% due to haemorrhage – also poor post-stroke performance due to impaired mastication. Hypothalamic damage can occur typically not seen in humans	Belayev et al, 1996 (72)
Thromboembolism Mouse or Rat	Injection of an autologous thrombus/clot (or microspheres) into extracranial arteries (e.g. common carotid) – typically 60-200µm	Clot occlusion in the proximal part of MCA resulting in the reduction of CBF and focal injury of the cortical territory Ischaemia is more prevalent than infarction, though some animals do develop cerebral infarction	Can be performed at any age or in any genetic strain to model age-different stroke	Model better resembles human stroke as ischaemia is primarily caused by thromboembolism as the occluding agent	Size and site of thromboembolism is difficult to control Chance of microembolization elsewhere (not typical of embolic stroke)	Kudo et al, 1982 (73) Busch et al, 1997 (36) Rapp et al, 2003 (37) Roos et al, 2003 (38)
Permanent Coagulation of dMCA in Mice	Transcranial electrocoagulation of the distal MCA (high frequency 7W) using electrocoagulation forceps proximal and distal to MCA bifurcation	Coagulation of dMCA leads to consistent infarct volumes (~15.4mm^3; 12% of hemisphere) within somatosensory and motor cortices with limited subcortical lesions. Asymmetrical limb use (assessed by cylinder test)	Can be performed at any age or in any strain, and due to low mortality can give better survivability rates to study long-term effects	Technique has a very short operation time (10min) with limited anaesthesia. Stroke ischaemic lesion volume (5-15% of hemisphere) and localisation resembles better human lesions compared to other coagulation methods Very low mortality rate and high reproducibility	No spontaneous reperfusion – a clinical feature in a large proportion of cases Mechanical damage to the cortex cannot be excluded – but can be limited Risk of recanalization of MCA – but can mitigated by 2 or 3 occlusion sites	Llovera et al, 2014 (34)

Rhesus Macaque Monkey	Micro-catheter (on inflatable balloon) to occlude M1-MCA (like rodent MCAO) Autologous clot injected via micro-catheter into M1-MCA	Occlusion model resulted in larger infarct sizes, lower Spetzler neurological scores, more profound hemiparesis and increased mortality rates compared to thromboembolism model Clots that end up in M2-MCA survive, with clots that remain in M1-MCA having 50% mortality rate due to lack of collateral flow	8-10-year-old monkeys used in the study (adult males) which is equivalent of midlife in humans	Two distinct models of ischaemic stroke easily reproducible in monkeys Macaques have gyrencephalic brains	Ethical and legal guidelines around non-human primates in many countries As with rodent thromboembolism models, reproducibility of embolism is poor	Wu et al, 2016 (40)
VaD *BCAO Mouse/Rat*	BCAO by ligation in Kunming mice for 10 minutes, loosened and repeated 3 times BCAO (permanent) in rats	Cognitive performance (errors and response times) Hippocampal CA1 neuronal death and disorganized arrangement with irregular glia – with gliosis Glial activation, immune cell infiltration & white matter changes within a couple of days after BCAO	Can be performed at any age, like MCAO in any strain	Good reproducibility with high success rates of inducing VaD-like phenotypes Model reflects SVD pathological changes seen in humans	Human VaD is more complex often with SVD and complex neuroinflammatory changes Permanent BCAO in mice is lethal, but not in rats – species specific differences	Wakita et al, 1994 (43) Wang et al, 2014 (44)
BCAS Mouse	BCAS in C57BL/6J mice using micro coils (0.16-0.22mm)	CBF reduction, white matter lesions (after 2wks), with some mice developing grey matter changes Microglial and astrocytic activation in white matter beyond 3 days post-BCAS	Can be performed at any age	Better mouse model of VaD than BCAO due to more complex pathological changes that occur resembling rat BCAO in human VaD involving white matter	Mortality rates of around 13-75% depending on size of coil within 2wks post-BCAS due to infarction	Shibata et al, 2004 (46)

1.15 – Comorbid CVD/CbVD Models

According to the British Heart Foundation, up to 80% of people with a form of CVD also have at least one other comorbidity, with the most common being cerebrovascular disease (42). Due to the nature of CVDs affecting the circulatory system, inevitably, there are secondary effects that can develop in almost any organ or area – notably to the brain. The human brain weighs just 2% of total body weight but receives 20% of cardiac output (5). The brain therefore is susceptible to global circulatory changes either originating directly due to cardiac disease, or due to atherosclerosis of peripheral and cerebral vessels, leading to many cerebrovascular disease (5) (discussed in depth later). As with all CVDs and CbVDs, multiple comorbidities present alongside these conditions creating a more complex aetiological and pathophysiological nature. One of the most common comorbidities associated with CVDs and

CbVDs is hypertension, in addition to diabetes mellitus, obesity and infection. The other, and perhaps more important non-modifiable factor, is that of advanced age. Typically, younger rodents have been used for stroke research, for example, whereas older animals would be more appropriate, combined with one or two more comorbidities to better replicate the human conditions. It is for this reason many promising stroke therapies that have worked in traditional models have failed to translate effectively in clinical settings (74).

Investigators are now starting to consider preclinical models with co-morbidities. As discussed earlier, MCAO is a common model of (acute) stroke and this 'mechanical' model was applied to atherosclerotic APOE$^{-/-}$ mice by Ayata et al (discussed earlier) to test perfusion deficit differences between controls and ApoE$^{-/-}$ mice fed a high-fat diet (14) (***Table 2***). MCAO abruptly reduced regional CBF, however, the perfusion reduction was more severe in the area of the affected penumbra of ApoE$^{-/-}$ mice compared to controls, leading to significantly larger infarct volumes in ApoE$^{-/-}$ mice (14). Thus, this study highlights the susceptibility of worsened stroke outcomes in patients with atherosclerosis. By combining an atherosclerosis model (ApoE$^{-/-}$) with an acute stroke model (MCAO), a comorbid mouse model was created providing novel and comprehensive insights into cerebrovascular dysfunction in stroke with underlying CVD.

As mentioned previously, hypertension is also major risk factor for dementia, stroke and CVD and is, perhaps, the most modifiable too, and easy to induce in pre-clinical models. This has been modelled using a spontaneously hypertensive rat (SHR) model, normotensive at birth but which gradually develops hypertension due to overactive renin-angiotensin systems by 6m of age (75) (***Table 2***). These animals when fed with a high-salt diet rapidly increased their blood pressure to above 240mmHg making a stroke-prone SHR (spSHR), with cortical strokes and SVD (75). This model remains the best stroke model for lacunar stroke due to the development of SVD, although the model itself is often very unpredictable. Another study combined the spSHR rat model with the mutated familial-Alzheimer's disease (fAD) APPswe/PS1ΔE9 transgene resulting in a comorbid fAD-spSHR mixed dementia rat model (76) (Table 2). The level of phosphorylated-tau was substantially higher in fAD-spSHR rats compared to spSHR, fAD rats alone. This corresponded to an increased microglial cell number and soma size (reactive states), increased astrogliosis and increased expression of aquaporin-4. Furthermore, there was evidence of SVD such as increased collagen IV and PECAM1/CD31 expression in cerebral vessels. Interestingly, the number of amyloid plaques was reduced in the fAD-spSHR rat compared to fAD alone (76). Neuronal damage was much higher in the fAD-spSHR rats with increased caspase-cleaved actin levels as well as loss of myelin and reduced calbindin staining in neurons, in addition to the loss of mitochondrial

complex I & II (76). This truly mixed comorbid rat model is one of the very few and limited models to combine multiple diseases alongside successfully recapitulating features of the human conditions. Such models will be important in driving future pre-clinical research into understanding the complex pathophysiology of comorbid disease and serving as excellent stable models for therapeutics research.

Other interesting murine comorbid models include diabetes-accelerated atherosclerosis models in which ApoE$^{-/-}$ or LDLR$^{-/-}$ mice are given streptozotocin; STZ (a pancreatic beta-cell cytotoxin) to induce type-1 diabetes mellitus in (77-79) (***Table 2***). In the diabetic ApoE$^{-/-}$ mouse model, there was an acceleration of large vessel atherosclerosis of the aortic sinus and carotid arteries with the presence of foam cells and increased oxidised-LDL uptake without further increases in plasma lipid levels, as seen in diabetic CVD patients (79). This also explains why many diabetic individuals have a higher risk of developing CHD. This however, was not the case in diabetic LDLR$^{-/-}$ mice despite elevated hyperglycaemia and enhanced advanced glycation end-product (AGE) in arterial walls of these mice including the presence of elevated serum IgG's against AGE epitopes (77). Thus, these two diabetic atherosclerotic models display differences in the effect of hyperglycaemia on atherogenesis and may in part reflect the severity of the atherosclerotic model i.e. more aggressive ApoE$^{-/-}$ mediated atherogenesis is exacerbated by higher hyperglycaemia whereas milder LDLR$^{-/-}$ mediated atherogenesis is not hugely affected by milder hyperglycaemia. In the ApoE$^{-/-}$ diabetic model, 200mg/kg STZ was used compared to 160mg/kg for LDLR-/- mice, again reflecting the severity of diabetes induction. As will be discussed later in more detail, metabolic syndrome comprising of hypertension, hyperglycaemia, diabetes mellitus and obesity are all linked to a substantially increased risk of developing dementia, thus models combining diabetes and atherosclerosis may better reflect the human condition, and more research needs to be done on the neuropathological, behavioural (cognitive) and neurovascular function in these models.

Other non-murine models include rabbit atherosclerotic models (high-fat diet induced) alongside a chronic antigen-induced arthritis (AIA) by injection of ovalbumin with vessel injury in the study of the effect of arthritis (inflammation) on atherosclerosis (80) (***Table 2***). Compared to controls, atherosclerosis alone or AIA alone, the new comorbid model showed much higher levels of inflammation marked by substantially higher IL-6, CRP, COX2 & PGE2. Although the intima-media thickness of both atherosclerotic rabbits and comorbid rabbits remained the same, the mixed model had a higher level of infiltrating macrophages in their lesions. Furthermore, only 27% of rabbits fed a high-fat diet displayed significant aortic lesions whereas 60% of comorbid atherosclerotic and AIA rabbits had aortic lesions (80). This study shows how arthritis can exacerbate atherosclerosis by added inflammation and metabolic

pathways. It has relevance to humans since midlife rheumatoid arthritis increases the risk of developing cognitive impairment and dementia in patients within 2 decades (81), perhaps by increasing vascular pathology as modelled in the above study. Modelling disease in rabbits could therefore serve to be an important model to test therapeutics for patients that have both diseases.

Table 2 – Comorbid CVD/CbVD Models

Model	Description	Phenotype	Age Ranges	Advantages	Limitations	References
ApoE$^{-/-}$ MCAO Mouse Model of Atherosclerosis & Stroke	Transient MCAO performed using microvascular clip on ApoE$^{-/-}$ mice (with and without Western) up to maximum 14wks	MCAO causes CBF reductions in dorsolateral cortex in all groups – penumbral perfusion reduction more severe in ApoE$^{-/-}$ fed Western diet compared to ApoE$^{-/-}$ fed NC and non-ApoE$^{-/-}$ undergoing MCAO Worse perfusion deficits lead to increased infarct volumes in ApoE$^{-/-}$ (HFD) MCAO eNOS phosphorylation at S1176 reduced and T494 increased in ApoE$^{-/-}$ mice with Western diet	Mice fed normal or Western diet for up to 12wks starting at 4wks of age.	Well established atherosclerosis model Well established stroke model Transient MCAO allows longitudinal and chronic assessment Comparison of diet on cerebrovascular outcomes	No flow limiting atherosclerotic lesions in aorta or cervical arteries, or circle of Willis at 14wks – however, these would confound CBF and at this age, the effect of ApoE$^{-/-}$ is being determined as a predisposition for greater cerebrovascular dysfunction/ischaemia	Ayata et al, 2013 (14)
Stroke Prone Spontaneous Hypertensive Rat (spSHR) Model	Inducible model of large artery stroke in rats when combined with a high-salt diet	Hypertension around 240mm/Hg with high-salt diet caused by overactive renin-angiotensin system Arteriolar wall thickening, subcortical lesions, enlarged perivascular spaces, cortical infarcts and haemorrhages with BBB leakage	5-21wk old rats (very young) and not reflective of age-related disease	Multiple cortical strokes and subcortical SVD (lacunar strokes|) with neuroinflammation Similar features to human lacunar stroke and models complex human disease features	Often unpredictable strokes make studying strokes difficult	Bailey et al, 2011 (75)
Familial AD with Stroke Prone Hypertension Rat	fAD-APPswe/PS1ΔE9 transgene inserted unto spSHR to create a mixed vascular dementia fAD-spSHR rat model	Exacerbated neuroinflammation (astrocytosis and gliosis) and increased tau-phosphorylation – subtle alterations to amyloid plaques SVD features including increased collagen-IV (dissociated from vessels) and	16-18month old rats – which reflects older adult age-related disease presentation	Multiple comorbidities of stroke, hypertension, Alzheimer's disease, vascular dementia (mixed dementia) that is reliably reproducible SVD alongside amyloid and tau pathology One of very limited 'true' mixed models of	As with spSHR, the strokes themselves are often unpredictable Rat genetic tools are poorer compared to mice; thus the creation of other AD-rats may be challenging	Denver et al, 2019 (76)

		PECAM1/CD31 expression Loss of myelin and neuronal calbindin with specific mitochondrial deficits (complex I & II)		cerebrovascular disease		
Diabetic LDLR$^{-/-}$ Mouse	Streptozotocin-induced hyperglycaemia in LDLR$^{-/-}$ & 21% HFD C57BL/6J mice	Blood glucose 257mg/dL in diabetic mice compared to 111mg/dL in non-diabetic. Plasma cholesterol similar in both groups (966mg/dL vs 1002mg/dL) – VLDL-cholesterol higher in diabetic mice. Higher AGE in arterial walls of diabetic group, with higher IgG autoantibodies in sera that bind to AGE epitopes. Similar extent of atherosclerosis in aorta suggesting diabetes does not accelerate atherogenesis in LDLR$^{-/-}$ mice.	HFD was fed for 6 months from mice aged 6-10wks	Inducible diabetes model by streptozotocin injection in any strain at any time-point – induction can be done in a dose-dependent manner Well established atherosclerosis models Does not require additional high-sugar content food to cause hyperglycaemia	The two different atherosclerotic models present with contradictory results with respect to atherogenesis Diabetes induced in BALB/c mice does exacerbate lesion formation thus there may be murine strain-specific differences in susceptibility to proatherogenic effects	Reaven et al, 1997 (77)
Diabetic ApoE$^{-/-}$ Mouse	Streptozotocin-induced hyperglycaemia in ApoE$^{-/-}$ mice	Aortic atherosclerotic lesion significantly higher in diabetic mice. Mouse peritoneal macrophages (MPM) exhibit higher lipid peroxidase contents. Ox-LDL uptake by MPM increased in diabetic mice with greater foam cells suggesting diabetes does accelerate atherogenesis in ApoE$^{-/-}$ mice	Diabetes induced for up to 3 months from 6wks of age	Duration of hyperglycaemia correlates with atherosclerosis exacerbation in ApoE$^{-/-}$ mice – this exacerbates coronary artery atherosclerosis which is a common comorbidity in diabetics		Hayek et al, 2005 (79)
Arthritic AIA & Hyperlipidaemic High-Fat Diet Rabbit	HFD rabbit with endothelial lesion combined with AIA by ovalbumin injection	Increased levels of serum IL6, CRP & PGE2 NFκB binding, CCL2 & COX2 expression higher in peripheral blood mononuclear cells, vessels & synovial membranes Higher level of macrophage infiltration in blood vessel walls with much higher aortic lesions	Procedure takes up 6wks to cause endothelial lesion, atherogensis along with OVA injections – can be done at any age	Model of plaque instability Convergence of inflammatory and metabolic pathways that synergistically drive and exacerbate atheorgenesis and arthritis – common comorbidity in humans	Limitations with the use of rabbits as opposed to rodents in terms of costs, housing and technical assistance	Largo et al, 2008 (80)

It is clear that there are many overlapping risk factors and interactions between several cardiovascular, metabolic and neurological processes that lead to the synergistic interactions between CVD, CbvD and dementia (summarised in ***Figure 1.8***). For example, diabetes and arthritis can exacerbate atherogenesis, CHD and dementia. As atherosclerosis is implicated in CHD, CbVD, VaD and AD, having metabolic or inflammatory disorders can greatly influence the onset and progression of dementia and therefore, models addressing such comorbidities to reflect the clinical prevalence of these are desperately needed.

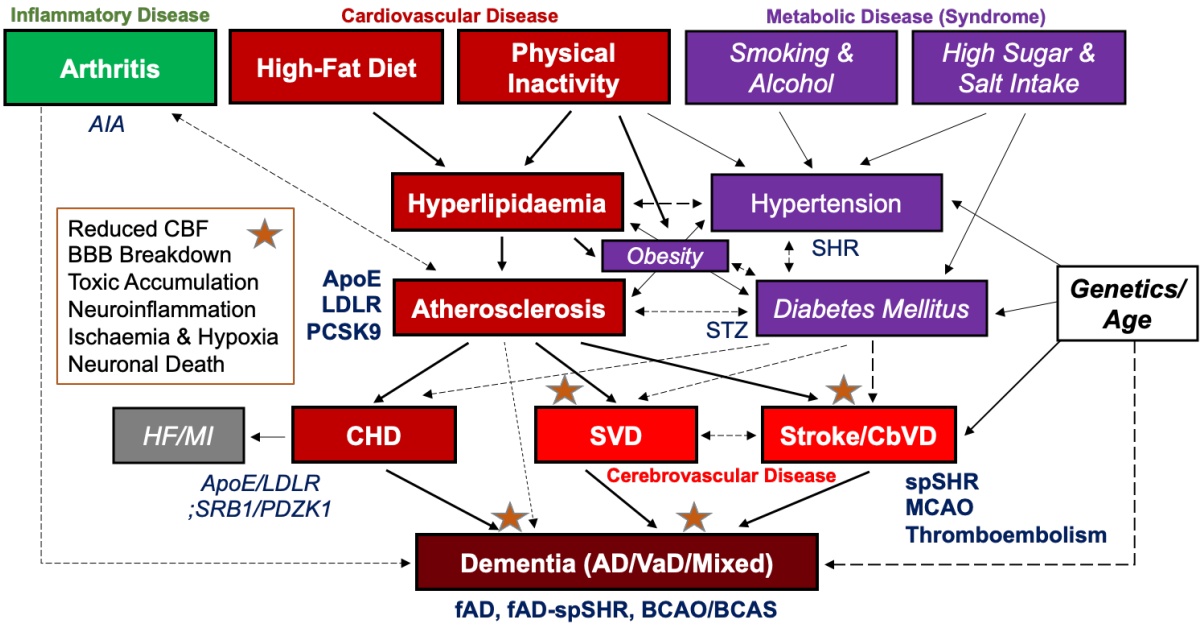

Figure 1.8 - CVD, CbVD and Dementia Overlap. Hyperlipidaemia is the primary cause of atherosclerosis (ApoE$^{-/-}$, LDLR$^{-/-}$, mPCSK9 models), which in the heart can lead to coronary artery occlusion (CHD) (ApoE$^{-/-}$/LDLR$^{-/-}$;PDZK1$^{-/-}$/SRB1$^{-/-}$ models) and by affecting both extracranial and intracranial arteries can lead to reduced global or regional CBF. This can lead to ischaemia within the brain and cause stroke (MCAO, embolism and spSHR models), alongside other CbVDs – one of which is VaD (BCAS model). Metabolic disorders such as diabetes mellitus (STZ models) and obesity, in addition to systemic inflammatory disorders such as arthritis can also greatly influence cerebrovascular dysfunction as well as exacerbating or contributing to AD (fAD models). The common mechanisms implicated in dementia onset as a result of CVD/CbVD are global or regional oligemia (reduced CBF) leading to hypoxia and ischemia, neuroinflammation, SVD and subsequent BBB breakdown. Mismatch between neuronal metabolic expenditure and energy/oxygen provision (breakdown of neurovascular coupling) can lead to dementia. Specific risk factors such as APOE4-allele coupled with pre-existing CVD and metabolic disorders can exacerbate beta-amyloid and tau accumulation leading to AD. Inevitably, as we age, the coexistence of two or more diseases leads to synergistic interactions between different pathological mechanisms contributing to complications or exacerbation of disease. (Adapted from Shabir et al, 2018 (5)).

1.16 – Conclusions and Future Directions

The use of preclinical models in the study of human diseases is an invaluable method to understand the pathobiological mechanisms underlying different disease processes. Genetic manipulation, surgical techniques and chemical exposure have allowed us to interrogate different aspects of disease at the molecular, cellular, tissue, organ and systemic levels. Whilst models of disease tend to generally focus on one aspect e.g. genetic knockouts, and have hugely improved our understanding of disease, these models inherently lack the true complexity associated with human disease – which tends to be multifactorial and involves the coexistence of many multimorbidities. Thus, the generation of comorbid models combining two or more diseases may more accurately reflect the human condition, help us understand the synergy and interactions between different conditions, as well as developing novel therapeutics that have previously failed using conventional pure models. Thus, future research involving comorbid models is essential if therapeutics are to pass clinical trials, especially with respect to dementia – which, as of yet, has no curative or preventative treatment. Models incorporating fAD/fFTD mutations, for example, in combination with CVD, or T2DM to better reflect human comorbidity, may be more appropriate if therapies are to succeed.

1.17 – References:

1. K. Mc Namara, H. Alzubaidi, J. K. Jackson, Cardiovascular disease as a leading cause of death: how are pharmacists getting involved? *Integr Pharm Res Pract* **8**, 1-11 (2019).
2. G. B. D. Mortality, C. Causes of Death, Global, regional, and national age-sex specific all-cause and cause-specific mortality for 240 causes of death, 1990-2013: a systematic analysis for the Global Burden of Disease Study 2013. *Lancet* **385**, 117-171 (2015).
3. E. M. Tuzcu *et al.*, High prevalence of coronary atherosclerosis in asymptomatic teenagers and young adults: evidence from intravascular ultrasound. *Circulation* **103**, 2705-2710 (2001).
4. A. J. Lusis, Atherosclerosis. *Nature* **407**, 233-241 (2000).
5. O. Shabir, J. Berwick, S. E. Francis, Neurovascular dysfunction in vascular dementia, Alzheimer's and atherosclerosis. *BMC Neurosci* **19**, 62 (2018).
6. G. S. Getz, C. A. Reardon, Do the Apoe-/- and Ldlr-/- Mice Yield the Same Insight on Atherogenesis? *Arterioscler Thromb Vasc Biol* **36**, 1734-1741 (2016).
7. T. B. Repas, J. R. Tanner, Preventing early cardiovascular death in patients with familial hypercholesterolemia. *J Am Osteopath Assoc* **114**, 99-108 (2014).
8. M. M. Bjorklund *et al.*, Induction of atherosclerosis in mice and hamsters without germline genetic engineering. *Circ Res* **114**, 1684-1689 (2014).
9. M. Roche-Molina *et al.*, Induction of sustained hypercholesterolemia by single adeno-associated virus-mediated gene transfer of mutant hPCSK9. *Arterioscler Thromb Vasc Biol* **35**, 50-59 (2015).

10. S. Poirier *et al.*, The proprotein convertase PCSK9 induces the degradation of low density lipoprotein receptor (LDLR) and its closest family members VLDLR and ApoER2. *J Biol Chem* **283**, 2363-2372 (2008).
11. M. Abifadel *et al.*, Mutations in PCSK9 cause autosomal dominant hypercholesterolemia. *Nat Genet* **34**, 154-156 (2003).
12. A. Denes *et al.*, Interleukin-1 mediates neuroinflammatory changes associated with diet-induced atherosclerosis. *J Am Heart Assoc* **1**, e002006 (2012).
13. C. J. Smith *et al.*, SCIL-STROKE (Subcutaneous Interleukin-1 Receptor Antagonist in Ischemic Stroke): A Randomized Controlled Phase 2 Trial. *Stroke* **49**, 1210-1216 (2018).
14. C. Ayata *et al.*, Hyperlipidemia disrupts cerebrovascular reflexes and worsens ischemic perfusion defect. *J Cereb Blood Flow Metab* **33**, 954-962 (2013).
15. J. Grootendorst *et al.*, Stress alleviates reduced expression of cell adhesion molecules (NCAM, L1), and deficits in learning and corticosterone regulation of apolipoprotein E knockout mice. *Eur J Neurosci* **14**, 1505-1514 (2001).
16. G. A. Elder *et al.*, Increased locomotor activity in mice lacking the low-density lipoprotein receptor. *Behav Brain Res* **191**, 256-265 (2008).
17. G. Song *et al.*, Simvastatin reduces atherogenesis and promotes the expression of hepatic genes associated with reverse cholesterol transport in apoE-knockout mice fed high-fat diet. *Lipids Health Dis* **10**, 8 (2011).
18. L. Li, D. Cao, H. Kim, R. Lester, K. Fukuchi, Simvastatin enhances learning and memory independent of amyloid load in mice. *Ann Neurol* **60**, 729-739 (2006).
19. J. Liao, W. Huang, G. Liu, Animal models of coronary heart disease. *J Biomed Res* **30** (2015).
20. K. Deckers *et al.*, Coronary heart disease and risk for cognitive impairment or dementia: Systematic review and meta-analysis. *PLoS One* **12**, e0184244 (2017).
21. A. Yesilaltay, K. Daniels, R. Pal, M. Krieger, O. Kocher, Loss of PDZK1 causes coronary artery occlusion and myocardial infarction in Paigen diet-fed apolipoprotein E deficient mice. *PLoS One* **4**, e8103 (2009).
22. M. Fuller *et al.*, The effects of diet on occlusive coronary artery atherosclerosis and myocardial infarction in scavenger receptor class B, type 1/low-density lipoprotein receptor double knockout mice. *Arterioscler Thromb Vasc Biol* **34**, 2394-2403 (2014).
23. P. J. Kuhlencordt *et al.*, Accelerated atherosclerosis, aortic aneurysm formation, and ischemic heart disease in apolipoprotein E/endothelial nitric oxide synthase double-knockout mice. *Circulation* **104**, 448-454 (2001).
24. M. Tsutsui, H. Shimokawa, T. Morishita, Y. Nakashima, N. Yanagihara, Development of genetically engineered mice lacking all three nitric oxide synthases. *J Pharmacol Sci* **102**, 147-154 (2006).
25. H. Katsumi, M. Nishikawa, M. Hashida, Development of nitric oxide donors for the treatment of cardiovascular diseases. *Cardiovasc Hematol Agents Med Chem* **5**, 204-208 (2007).
26. C. Zaragoza *et al.*, Animal models of cardiovascular diseases. *J Biomed Biotechnol* **2011**, 497841 (2011).

27. T. Shimizu *et al.*, Simple rabbit model of vulnerable atherosclerotic plaque. *Neurol Med Chir (Tokyo)* **49**, 327-332; discussion 332 (2009).
28. S. Audit (2020).
29. G. A. Donnan, M. Fisher, M. Macleod, S. M. Davis, Stroke. *Lancet* **371**, 1612-1623 (2008).
30. E. L. Bailey, C. Smith, C. L. Sudlow, J. M. Wardlaw, Pathology of lacunar ischemic stroke in humans--a systematic review. *Brain Pathol* **22**, 583-591 (2012).
31. C. Iadecola, The pathobiology of vascular dementia. *Neuron* **80**, 844-866 (2013).
32. D. Leys, H. Henon, M. A. Mackowiak-Cordoliani, F. Pasquier, Poststroke dementia. *Lancet Neurol* **4**, 752-759 (2005).
33. R. Hata *et al.*, A reproducible model of middle cerebral artery occlusion in mice: hemodynamic, biochemical, and magnetic resonance imaging. *J Cereb Blood Flow Metab* **18**, 367-375 (1998).
34. G. Llovera, S. Roth, N. Plesnila, R. Veltkamp, A. Liesz, Modeling stroke in mice: permanent coagulation of the distal middle cerebral artery. *J Vis Exp* 10.3791/51729, e51729 (2014).
35. A. Durukan, T. Tatlisumak, Acute ischemic stroke: overview of major experimental rodent models, pathophysiology, and therapy of focal cerebral ischemia. *Pharmacol Biochem Behav* **87**, 179-197 (2007).
36. E. Busch, K. Kruger, K. A. Hossmann, Improved model of thromboembolic stroke and rt-PA induced reperfusion in the rat. *Brain Res* **778**, 16-24 (1997).
37. J. H. Rapp *et al.*, Cerebral ischemia and infarction from atheroemboli <100 microm in Size. *Stroke* **34**, 1976-1980 (2003).
38. M. W. Roos *et al.*, Functional evaluation of cerebral microembolization in the rat. *Brain Res* **961**, 15-21 (2003).
39. I. M. Macrae, S. M. Allan, Stroke: The past, present and future. *Brain Neurosci Adv* **2**, 2398212818810689 (2018).
40. D. Wu *et al.*, Endovascular ischemic stroke models of adult rhesus monkeys: a comparison of two endovascular methods. *Sci Rep* **6**, 31608 (2016).
41. D. J. Cook, L. Teves, M. Tymianski, Treatment of stroke with a PSD-95 inhibitor in the gyrencephalic primate brain. *Nature* **483**, 213-217 (2012).
42. B. H. Foundation (2020) Heart Statistics.
43. H. Wakita, H. Tomimoto, I. Akiguchi, J. Kimura, Glial activation and white matter changes in the rat brain induced by chronic cerebral hypoperfusion: an immunohistochemical study. *Acta Neuropathol* **87**, 484-492 (1994).
44. H. Wang, Establishment of an animal model of vascular dementia. *Exp Ther Med* **8**, 1599-1603 (2014).
45. F. Y. Jalal, Y. Yang, J. Thompson, A. C. Lopez, G. A. Rosenberg, Myelin loss associated with neuroinflammation in hypertensive rats. *Stroke* **43**, 1115-1122 (2012).
46. M. Shibata, R. Ohtani, M. Ihara, H. Tomimoto, White matter lesions and glial activation in a novel mouse model of chronic cerebral hypoperfusion. *Stroke* **35**, 2598-2603 (2004).

47. K. Nishio *et al.*, A mouse model characterizing features of vascular dementia with hippocampal atrophy. *Stroke* **41**, 1278-1284 (2010).
48. R. D. Bell *et al.*, Apolipoprotein E controls cerebrovascular integrity via cyclophilin A. *Nature* **485**, 512-516 (2012).
49. S. Duong, T. Patel, F. Chang, Dementia: What pharmacists need to know. *Can Pharm J (Ott)* **150**, 118-129 (2017).
50. WHO (2020) Infographic on dementia.
51. A. s. R. U. (ARUK) (2020) Dementia Statisitics Hub - Prevalence of Dementia.
52. N. Custodio *et al.*, Mixed dementia: A review of the evidence. *Dement Neuropsychol* **11**, 364-370 (2017).
53. C. Y. Santos *et al.*, Pathophysiologic relationship between Alzheimer's disease, cerebrovascular disease, and cardiovascular risk: A review and synthesis. *Alzheimers Dement (Amst)* **7**, 69-87 (2017).
54. R. Aleksis, F. Oleskovs, K. Jaudzems, J. Pahnke, H. Biverstal, Structural studies of amyloid-beta peptides: Unlocking the mechanism of aggregation and the associated toxicity. *Biochimie* **140**, 176-192 (2017).
55. G. D. Schellenberg, T. J. Montine, The genetics and neuropathology of Alzheimer's disease. *Acta Neuropathol* **124**, 305-323 (2012).
56. G. Di Fede *et al.*, A recessive mutation in the APP gene with dominant-negative effect on amyloidogenesis. *Science* **323**, 1473-1477 (2009).
57. Z.-d. Zhou *et al.*, The roles of amyloid precursor protein (APP) in neurogenesis: Implications to pathogenesis and therapy of Alzheimer disease. *Cell Adh Migr* **5**, 280-292 (2011).
58. W.-T. Chen *et al.*, Amyloid-beta (Aβ) D7H mutation increases oligomeric Aβ42 and alters properties of Aβ-zinc/copper assemblies. *PloS one* **7**, e35807-e35807 (2012).
59. R. Sherrington *et al.*, Cloning of a gene bearing missense mutations in early-onset familial Alzheimer's disease. *Nature* **375**, 754-760 (1995).
60. E. Levy-Lahad *et al.*, Candidate gene for the chromosome 1 familial Alzheimer's disease locus. *Science* **269**, 973-977 (1995).
61. M. Cacquevel, L. Aeschbach, J. Houacine, P. C. Fraering, Alzheimer's disease-linked mutations in presenilin-1 result in a drastic loss of activity in purified gamma-secretase complexes. *PLoS One* **7**, e35133 (2012).
62. R. Potter *et al.*, Increased in vivo amyloid-beta42 production, exchange, and loss in presenilin mutation carriers. *Science translational medicine* **5**, 189ra177 (2013).
63. E. Drummond, T. Wisniewski, Alzheimer's disease: experimental models and reality. *Acta Neuropathol* **133**, 155-175 (2017).
64. A. M. Hall, E. D. Roberson, Mouse Models of Alzheimer’s Disease. *Brain Res Bull* **88**, 3-12 (2012).
65. G. Esquerda-Canals, L. Montoliu-Gaya, J. Guell-Bosch, S. Villegas, Mouse Models of Alzheimer's Disease. *J Alzheimers Dis* **57**, 1171-1183 (2017).

66. A. S. Plump *et al.*, Severe hypercholesterolemia and atherosclerosis in apolipoprotein E-deficient mice created by homologous recombination in ES cells. *Cell* **71**, 343-353 (1992).
67. J. A. Piedrahita, S. H. Zhang, J. R. Hagaman, P. M. Oliver, N. Maeda, Generation of mice carrying a mutant apolipoprotein E gene inactivated by gene targeting in embryonic stem cells. *Proc Natl Acad Sci U S A* **89**, 4471-4475 (1992).
68. S. Ishibashi *et al.*, Hypercholesterolemia in low density lipoprotein receptor knockout mice and its reversal by adenovirus-mediated gene delivery. *J Clin Invest* **92**, 883-893 (1993).
69. M. Decressac, B. Mattsson, M. Lundblad, P. Weikop, A. Bjorklund, Progressive neurodegenerative and behavioural changes induced by AAV-mediated overexpression of alpha-synuclein in midbrain dopamine neurons. *Neurobiol Dis* **45**, 939-953 (2012).
70. Y. F. Ngai *et al.*, Ldlr-/- mice display decreased susceptibility to Western-type diet-induced obesity due to increased thermogenesis. *Endocrinology* **151**, 5226-5236 (2010).
71. G. Caligiuri, B. Levy, J. Pernow, P. Thoren, G. K. Hansson, Myocardial infarction mediated by endothelin receptor signaling in hypercholesterolemic mice. *Proc Natl Acad Sci U S A* **96**, 6920-6924 (1999).
72. L. Belayev, O. F. Alonso, R. Busto, W. Zhao, M. D. Ginsberg, Middle cerebral artery occlusion in the rat by intraluminal suture. Neurological and pathological evaluation of an improved model. *Stroke* **27**, 1616-1622; discussion 1623 (1996).
73. M. Kudo, A. Aoyama, S. Ichimori, N. Fukunaga, An animal model of cerebral infarction. Homologous blood clot emboli in rats. *Stroke* **13**, 505-508 (1982).
74. C. J. Sommer, Ischemic stroke: experimental models and reality. *Acta Neuropathol* **133**, 245-261 (2017).
75. E. L. Bailey, C. Smith, C. L. Sudlow, J. M. Wardlaw, Is the spontaneously hypertensive stroke prone rat a pertinent model of sub cortical ischemic stroke? A systematic review. *Int J Stroke* **6**, 434-444 (2011).
76. P. Denver *et al.*, A Novel Model of Mixed Vascular Dementia Incorporating Hypertension in a Rat Model of Alzheimer's Disease. *Front Physiol* **10**, 1269 (2019).
77. P. Reaven, S. Merat, F. Casanada, M. Sutphin, W. Palinski, Effect of streptozotocin-induced hyperglycemia on lipid profiles, formation of advanced glycation endproducts in lesions, and extent of atherosclerosis in LDL receptor-deficient mice. *Arterioscler Thromb Vasc Biol* **17**, 2250-2256 (1997).
78. X. Shen, K. E. Bornfeldt, Mouse models for studies of cardiovascular complications of type 1 diabetes. *Ann N Y Acad Sci* **1103**, 202-217 (2007).
79. T. Hayek *et al.*, Macrophage foam-cell formation in streptozotocin-induced diabetic mice: stimulatory effect of glucose. *Atherosclerosis* **183**, 25-33 (2005).
80. R. Largo *et al.*, Chronic arthritis aggravates vascular lesions in rabbits with atherosclerosis: a novel model of atherosclerosis associated with chronic inflammation. *Arthritis Rheum* **58**, 2723-2734 (2008).
81. K. Wallin *et al.*, Midlife rheumatoid arthritis increases the risk of cognitive impairment two decades later: a population-based study. *J Alzheimers Dis* **31**, 669-676 (2012).

The manuscript section that I authored ends here. *The following sections are not part of the above paper, but form part of the rest of chapter 1. In brief, the next section describes the background on the neuroimaging, the genesis of my PhD project including the knowledge gaps that existed when I began my project, my hypotheses and project aims.*

1.18 – 2D-Optical Imaging Spectroscopy Background

2D-optical imaging spectroscopy (2D-OIS) is a technique that allows measurements in the changes in total haemoglobin (HbT); akin to cerebral blood volume (CBV) changes, in addition to blood oxygenation (Kennerley et al., 2005, Kennerley et al., 2009, Kennerley et al., 2012). Compared to fMRI, 2D-OIS has a higher spatial and temporal resolution in the investigation of cerebral haemodynamics and the BOLD response. A more detailed overview of the methodology (biophysics) and experimental paradigm is given in ***section 2.2.3*****.**

In previous work (Kennerley et al., 2012), baseline oxygen saturation values of 50% were used (based on rats breathing air), however, mice breathing oxygen were approximated to have a baseline oxygen saturation of 70%, and varying this value in the different physiological ranges between 40-70% had little effect on the BOLD signal magnitude (Kennerley et al., 2012). In our most recent publication (Sharp et al., 2019), varying the HbT baseline micromolar value (from 60-120μM) results in different peak HbT values if comparing micromolar changes, however, if presented as a fractional change (or % change), then the fractional change is identical as it is scaled by itself and is not different. Throughout the imaging protocol, I will be measuring changes in baseline volume and saturation in the animals when switching from breathing 100% oxygen to air. Moreover, even if estimates of volume and saturation were wrong (which is not likely the case), the fractional change in HbT response would be unaffected.

With respect to the total haemoglobin concentration in the superficial areas of the cortex (the area being imaged by 2D-OIS), the value of 100μM was determined as:

$$HbT_0 = v_f \cdot Hct \cdot R_{c/l} \cdot \frac{[Hb]_{RBC}}{Mm_{Hb}}$$

The profile of blood volume fractionation (v_f) can be converted into baseline haemoglobin concentration (HbT_0) in brain tissue by where Hct is the fraction of the haematocrit (0.46), $R_{c/l}$ is the ratio of cerebral tissue to large vessels (0.69; based on Wyatt et al, 1990), $[Hb]_{RBC}$ is the concentration of haemoglobin in red blood cells (340g/l) and Mm_{Hb} is the molecular mass of haemoglobin (64,450g/M) (Kennerley et al., 2009). Thus, the haemoglobin concentration value of 100μM is used throughout.

In other previous work (Kennerley et al., 2005), direct comparisons of MRI measurements of CBV changes with concurrent 2D-OIS measurements of HbT changes were found to be identical in the superficial layers of the cortex assuming a constant haematocrit level, thus CBV and HbT changes can be used interchangeably and the profile of normalised haemoglobin changes is identical to the profile of measured CBV changes:

$$\frac{HbT}{HbT_0} = \frac{CBV}{CBV_0}$$

from which the profile of normalised changes in HbT can be found:

$$\frac{\Delta HbT}{HbT_0} = \frac{HbT}{HbT_0} - 1$$

Changes in CBV (determined by 2D-OIS) and CBF (determined by LDF) follow a scaling relationship $CBV=CBF^a$, with the mean alpha being 0.38+/-0.06 (Kennerley et al., 2005), based on Grubb et al 1974. In Jones et al, the alpha value was found to be 0.29 for stimulation and 0.31 for hypercapnia (Jones et al., 2001). Thus, the relationship between CBF-CBV is similar regardless of how a change in flow is achieved. As illustrated in Jones et al, the time series for flow and volume changes from stimulation onset to peak are very similar; although there is a slight 0.2s lag between volume and flow that is only detectable due to a high temporal resolution of the data collection (Jones et al., 2001). Post-peak, whilst flow returns to baselines, volume changes remain elevated for a little while before returning to baseline slower. Using CBF measurements (from LDF), HbT and HbR can be used to calculate $CMRO_2$. However, since I will not be measuring CBF, I will not be able to calculate $CMRO_2$.

The spectrographic analysis is based upon the path length scaling algorithm (PLSA) described in detail elsewhere (Mayhew et al., 1999). The 4 wavelength image data set (*discussed in **section 2.2.3***) is analysed against the known absorption coefficients for HbR and HbO in addition to parametrising Monte Carlo Simulations (MCS) of light transport through a homogenous tissue model with the baseline volume and blood oxygen saturation values (derived from Kennerley et al., 2009). The MCS tracks photon transport by incorporating an array of different parameters such as absorption, remittance, scattering in the tissue and undisturbed propagation to provide an approximation of the path length through with the photon has travelled (Kennerley et., 2012). The computed data is entered into a lookup table which uses a modified Beer-Lambert law which relates light attenuation to the path length, absorption coefficients and concentrations of the specific chromophores to determine changes and produce 2D-maps of HbO, HbR and HbT concentration as a mean across all stimulations within a given experiment. For this algorithm to work, values for baseline concentrations and

saturation have to be inputted. For this, the haemoglobin concentration was inputted as 100μM and oxygen saturation was 70% (as discussed earlier). As reported in (Jones et al., 2001), the results of the analysis are qualitatively the same over a range of haemoglobin concentrations (50-200μM).

To summarise, changes in neuronal activity produce changes in the relative concentrations of HbO and HbR chromophores, and OIS exploits the differences in absorption by HbO and HbR as a function of wavelength (λ). The Beer-Lambert law states that the attenuation of light $(A(\lambda))$ is linearly related to the concentrations (c_i) of the absorbers in the medium by:

$$A(\lambda) = L \sum_i \varepsilon_i(\lambda) c_i$$

where $\varepsilon_i(\lambda)$ is the specific extinction coefficient of the *i*th absorbent. However, in brain tissue, this linear relationship is no longer accurate as the path length within a scattering medium (brain tissue) is longer than that of non-scattering media, thus the likelihood of the photon being absorbed is increased. Therefore, the relationship between $(A(\lambda))$ and c_i becomes non-linear and dependent on the properties of the medium. Consequently, the OIS algorithm uses a differential path length $L_d(\lambda)$ which relates changes in attenuation (ΔA) to changes in the concentrations of absorbents (Δc):

$$\Delta A(\lambda) = L_d\,(\lambda) \sum_i \varepsilon_i(\lambda) \Delta c_i$$

The differential path length defined is related to the mean and partial path lengths. Changes in neuronal activity alter the concentrations of HbO and HbR. The path length is dependent only on the absorption coefficient $\mu a(\lambda) \propto (\varepsilon HbO(\lambda) HbO + \varepsilon HbR(\lambda) HbR)$ and the reduced scattering coefficient $\mu' s(\lambda)$ of the tissue. Once the path length is estimated, changes in HbT and oxygen saturation (Y) due to evoked changes in neural activity are calculated as follows:

$$\Delta A(\lambda) = L_d\,(\lambda)\,(\varepsilon HbO\,(\lambda)\,\Delta HbO + \varepsilon HbR\,(\lambda)\,\Delta HbR$$

The relationship between Y and [HbR] concentration is defined by:

$$\frac{(1-Y)}{(1-Y_0)} = \frac{HbR}{HbR_0} \cdot \frac{HbT_0}{HbT}$$

A more detailed discussion about the spectroscopy algorithms and assumptions are detailed in Kennerley et al., 2009, and validated using fMRI in Kennerley et al., 2012.

1.19 – Work Leading to my PhD Project

In 2015, the lab published a paper outlining an anaesthetised mouse surgical and imaging preparation method that was optimised for the best neurovascular responses to sensory stimulations, that had similar profiles to an awake preparation (Sharp et al., 2015). The surgically implanted chronic imaging window allowed longitudinal imaging up to 3-6 months. The anaesthetic regimen was optimised to combine midazolam and fentanyl-fluanisone in sterile water in a 1:1:2 ratio injected into the mouse i.p. Furthermore, all imaging and experiments began at least 1-hour post anaesthetic induction to allow neurovascular responses to return to normal after an initial 'inverted response' (Sharp et al., 2015). Using this novel chronic preparation, the lab investigated neurovascular coupling in the J20-$hAPP_{(Sw,Ind)}$ mouse model of AD between the ages of 9-12m (Sharp et al., 2019), and published these data in a paper that I co-authored. I will summarise this briefly. Based on the literature investigating neurovascular function in this mouse model, which suggested impaired neurovascular responses, we sought to validate these findings accordingly using our new method. Contrary to expectation, we found no significant differences in terms of stimulus-evoked haemodynamic and neural responses in the J20-mouse compared to WT controls when imaging was performed using the novel chronic setup (Sharp et al., 2019). We only saw significantly perturbed responses in acute imaging sessions where the skull was drilled, and an electrode inserted to record neural responses simultaneously, thus leading to the hypothesis that electrode insertion causes cortical spreading depression to occur in all animals. Thus, that study highlights the importance of methodology and animal preparation methods in the study of neurovascular coupling. Chapter 3 aims to follow up on the findings of Sharp et al, 2019 with the same approach but at an earlier time point. A more detailed analysis of this is made in the discussion section of chapter 3 (Shabir et al., 2020) and the mechanisms underlying this presented and discussed in chapter 4.

In 2015, the University of Sheffield took a strategic decision to fund 3 PhD students as part of the (then) new Neuroimaging in Cardiovascular Disease (NICAD) network – a collaboration of neuroscientists & cardiovascular scientists across the Faculty of Medicine and Faculty of Science. Human imaging analysis in diabetes (Dounavi/Wilkinson/Martin), zebrafish models of hyperglycaemia (Chhabria/Chico/Howarth) and mouse models of dementia (Shabir/Berwick/Francis) were the three projects, the latter which I applied to and was awarded the studentship for (in 2017). The NICAD mouse project aimed to investigate neurovascular function and interactions between neurological disease and cardiovascular disease – an increasingly popular and important research area at the nexus of neuroscience and cardiovascular science. With respect to models of atherosclerosis, a novel virally inducible

method (rAAV8-mPCSK9) (Bjorklund et al., 2014) – mentioned earlier in chapter 1, and discussed in detail in chapter 4 – was used to investigate neurovascular function.

The gaps in knowledge prior to my PhD are summarised below:

- Reliability of surgical and imaging preparations in models of AD
- Neurovascular function in a novel model of atherosclerosis (PCSK9)
- The lack of comorbid models to better reflect human disease

1.20 – Hypothesis

The central hypothesis is that neurovascular coupling is impaired in the Alzheimer's, atherosclerosis and comorbid models of human disease. There will be increased neuropathology in the mixed comorbid model. Furthermore, based on previous observations, electrode insertion into the brain causes cortical spreading depression to occur in all animals that impairs evoked-haemodynamic responses. These findings will provide an insight into any potential biomarkers, novel disease mechanisms and therapeutic targets or strategies that could lead to clinical therapies in the future.

1.21 – Aims

The overall aims of this thesis were to investigate neurovascular function in pre-clinical mouse models of human disease. In order to achieve this, a combination of pre-clinical neuroimaging techniques and electrophysiology were performed to investigate neurovascular coupling, functionally. Furthermore, post-mortem cellular and molecular studies were used to validate *in vivo* findings to provide a more comprehensive overview of changes to neurovascular function. Specific aims of the different studies were:

1. To investigate neurovascular coupling in young 6-9m old J20-hAPP(Sw,Ind) mouse model of Alzheimer's disease (AD) compared to healthy wild-type (WT) controls using 2D-optical imaging spectroscopy (2D-OIS) and neural electrophysiology (***Chapter 3***).
2. To investigate neurovascular coupling in mid-age 9-12m old rAAV8-mPCSK9-D377Y mouse model of atherosclerosis compared to WT controls using 2D-OIS and neural electrophysiology. To further investigate the cellular expression of cells of the neurovascular unit (NVU) by performing immunohistochemistry (IHC) on fixed post-mortem tissue, as well as markers of neuroinflammation by performing qRT-PCR on snap-frozen brains (***Chapter 4***).
3. To induce atherosclerosis in the J20-hAPP mouse model of AD (AAV-mPCSK9 injection) to form a novel comorbid mixed model of disease, and to characterise neurovascular function in this novel model (***Chapter 4***).

Chapter 2 – Materials & Methods

2.1 – Materials

2.1.1 – Commercial Kits & Reagents

Description	Details	Company
Tris-Buffered Saline (TBS)	85g NaCl, 60.5g Tris-base in 10L d.H_2O	NA
Trisodium Citrate (TSC)	3g TSC in 1L d.H_2O pH6.5	Fisher Scientific
Ethylenediaminetetra acetic acid (EDTA)	0.372g in 1L d.H_2O pH8	
VectaStain ABC Immunohistochemistry Kits	Mouse, Goat & Rabbit Kits: *Blocking solution – 3 drops normal serum in 10ml TBS. Secondary – 3 drops biotinylated IgG secondary antibody in 10ml TBS. ABC reagent – 2 drops Avidin (A), 2 drops biotinylated HRP (B) in 10ml TBS*	Vector Laboratories, US
DAB Substrate Kit	3.3'-diaminobenzidine (DAB) substrate kit SK-4100: *2 drops buffer, 2 drops H_2O_2 & 4 drops DAB in 5ml d.H_2O*	Vector Laboratories, US
3% Hydrogen Peroxide (H_2O_2)	12ml H_2O_2 in 388ml methanol	VWR Chemicals
Scott's Tap Water	50g $MgSO_4$, 7.75g $NaHCO_3$ in 2.5L d.H_2O	NA

2.1.2 – Diets

Description	Details	Company/Stock
Western Diet	21% fat, 0.15% cholesterol, 0.03% cholate, 0.296% sodium	#829100 Special Diet Services (SDS)-Witham, UK

2.1.3 – Viruses

Description	Details	Company/Stock
AAV-Virus for Atherosclerosis Induction	$6.1x10^{12}$ virus molecules/ml rAAV8-mPCSK9-D377Y dialysed w/350mM NaCl & 5% D-Sorbitol in PBS	Lot#AV8541 University of North Carolina (UNC) GTC Vector Core (US)

2.1.4 – Antibodies & Immunohistochemistry Conditions

Description	Details	Company/Stock
Antibody for Astrocytes	Rabbit anti-GFAP (glial fibrillary acidic protein) 1:500 (microwave antigen retrieval pH6.5 TSC) – *2 minutes with DAB*	Dako Z0334
Antibody for Microglia	Goat anti-Iba1 (allograft inflammatory factor 1) 1:250 (microwave antigen retrieval pH6.5 TSC) – *2.5 minutes with DAB*	Abcam ab5076
Antibody for Neurons	Rabbit anti-NeuN (neuronal nuclei) 1:3000 (microwave pH9 EDTA) – *2.5 minutes with DAB*	Abcam ab177487
Antibody for Pericytes	Goat anti-PDGFRb (Platelet-derived growth factor receptor beta) 1:250 (microwave pH9 EDTA) – *2 minutes with DAB*	R&D Systems AF1042-SP
Antibody for Amyloid Plaques	Mouse anti-Beta-Amyloid 1:100 (microwave pH6.5 TSC) – *5.5 minutes with DAB*	Dako M0872

2.1.5 – RNA Extraction

Description	Details	Company
RNA Extraction Kit	Direct-Zol RNA MiniPrep Kit	Zymo Research (US)
TRI Reagent	Trizol	Zymo Research (US)

2.1.6 – PCR and Primers

Description	Details	Company
cDNA Synthesis Kit	UltraScript 2.0 cDNA Synthesis Kit	BioSystems
qPCR Mix	Luna qRT-PCR Master Mix	BioLabs
qRT-PCR Primer for beta-actin *(ACTB)*	Primer (fwd) 1 5'-GCGAGCACAGCTTCTTTG-3' Primer 2 (rev) 5'-ATGCCGGAGCCGTTGTC-3' *Exons 1-2*	Integrated DNA Technologies (IDT) US
qRT-PCR Primer for interleukin-1-beta *(IL1b)*	Primer 1 (fwd) 5'-GCAAGTGTCTGAAGCAGCTAT-3' Primer 2 (rev) 5'-GTCCGTCAACTTCAAAGAACAG-3' *Exons 1-3*	Integrated DNA Technologies (IDT) US

qRT-PCR Primer for tumour necrosis factor-alpha *(TNFa)*	Primer 1 (fwd) 5'-AGACCCTCACACTCAGATCA-3' Primer 2 (rev) 5'-TCTTTGAGATCCATGCCGTTG-3' *Exons 2-4*	Integrated DNA Technologies (IDT) US
qRT-PCR Primer for nitric oxide synthase-1 *(NOS1)*	Primer 1 (fwd) 5'-TCAACTACATCTGTAACCACGTC-3 Primer 2 (rev) 5'-AGTCATGCTTGCCATCAGTC-3' *Exons 6-7*	Integrated DNA Technologies (IDT) US
qRT-PCR Primer for nitric oxide synthase-3 *(NOS3)*	Primer 1 (fwd) 5'-CTTGAGGATGTGGCTGTGT-3' Primer 2 (rev) 5'-TGGTCCACTATGGTCACTTTG-3' *Exons 8-10*	Integrated DNA Technologies (IDT) US

2.1.7 – Laboratory Equipment

Description	Details	Company
Nikon Microscope	Nikon Eclipse Ni (Brightfield) with DS-Ri1 camera	Nikon
Centrifuge	1-15PK Centrifuge	Sigma
Thermal Cycler (Incubator)	PTC-200 Peltier Thermal Cycler	MJ Research
qRT-PCR	CFX384 Real-Time System with C1000 Touch Thermal Cycler	Bio-Rad

2.1.8 – Software

Description	Details	Company
Nikon microscope capture and editing software	NIS-elements	Nikon
MATLAB for 2D-OIS and electrophysiology analysis	MATLAB R2019a	MathWorks
GraphPad for Bar graphs and statistics	Prism v8.3.1	Graphpad

2.1.9 – Statement of Ethics

All animal procedures were performed with approval from the UK Home Office in accordance to the guidelines and regulations of the Animal (Scientific Procedures) Act 1986 and were approved by the University of Sheffield ethical review and licensing committee. This work was licenced to PPL: 70/8547/M (J Berwick) and PIL: I4CEF849C (O Shabir), under University of Sheffield ISP: JB-13 (all moderate severity procedures).

2.1.10 – Animals

Description	Details	Company
Wild-Type (WT) Mice	Male C57BL/6J *Normal Rodent Chow*	Charles River
Mouse Model of Alzheimer's Disease (AD)	Male J20 B6.(PDGFB-hAPP(Sw,Ind) *Normal Rodent Chow*	JAX
Mouse Model of Atherosclerosis (ATH)	Male C57BL/6J injected i.v. rAAV8-mPCSK9-D377Y *Western Diet*	Charles River
Mixed Comorbid Mouse Model of AD & ATH	Male J20 B6.(PDGFB-hAPP(Sw,Ind) injected i.v. rAAV8-mPCSK9-D377Y *Western Diet*	JAX

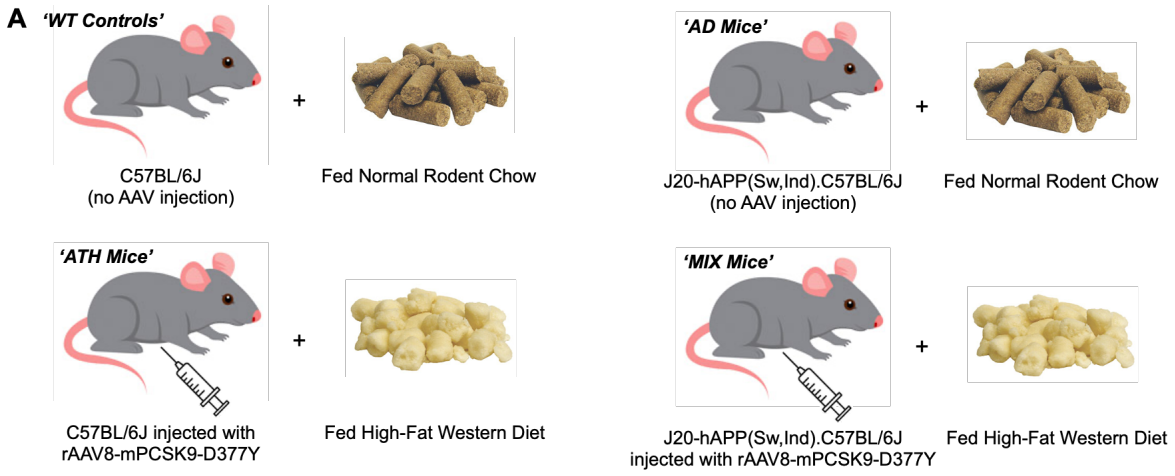

Figure 2.1 – Mouse Models Used.

Mice were housed with littermates in a 12hr dark/light cycle at a temperature of 23^{O}C, with food and water supplied *ad-libitum*. Western diet pellets were replaced twice a week to prevent them from drying out.

2.2 – In Vivo Neuroimaging

2.2.1 – Experimental Overview

In order to investigate neurovascular coupling *in vivo,* a combination of haemodynamic imaging with 2D-optical imaging spectroscopy (2D-OIS) and neural multichannel electrophysiology was used. To allow access and visualisation of cortical vasculature, surgery was performed to chronically implant a thinned cranial window, and mice were recovered for a minimum of 2 weeks. All chronic imaging sessions (with the skull intact) were performed 3 weeks post-surgery, and a final terminal acute experimental session was performed 1 week after chronic sessions where the skull was drilled, and a multichannel electrode was inserted to simultaneously record neural activity in combination with 2D-OIS.

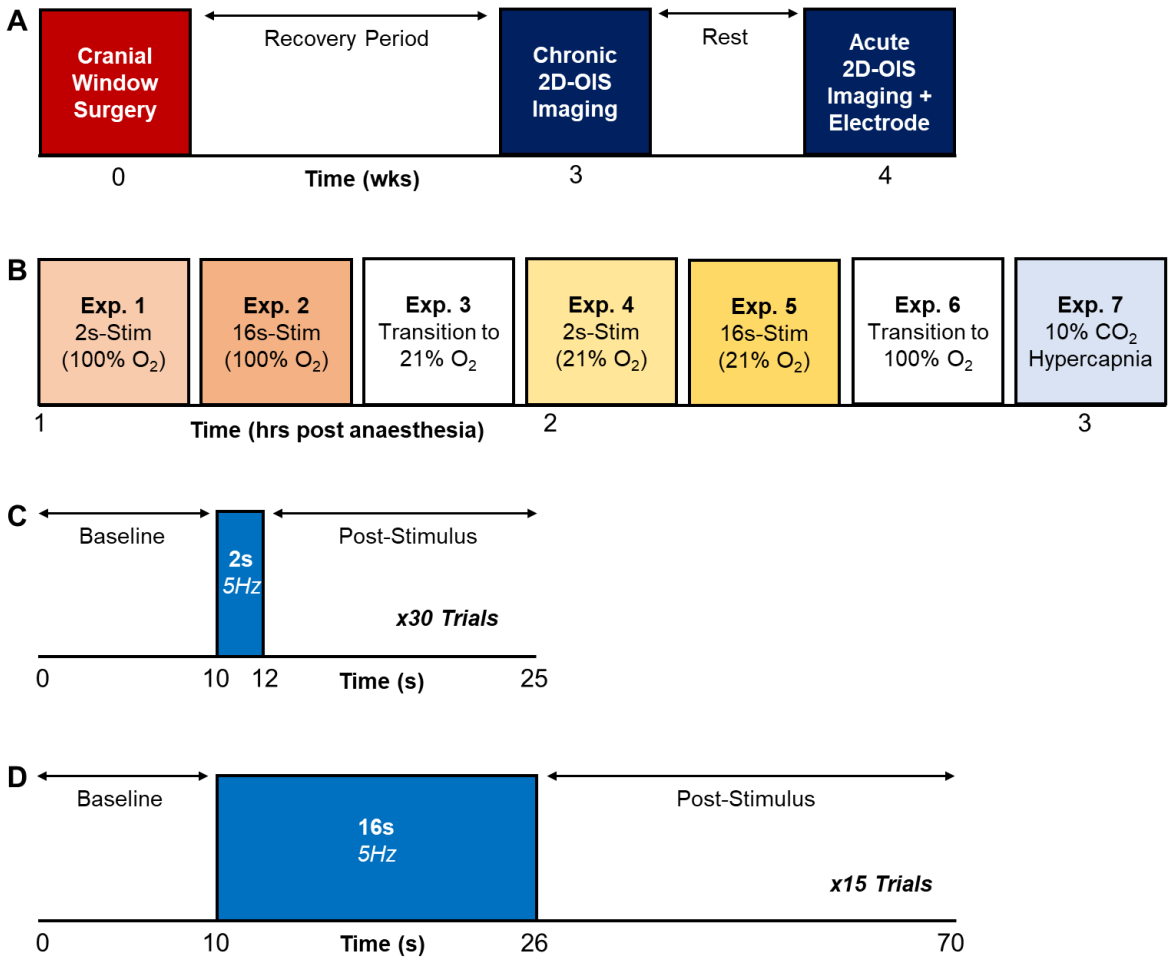

Figure 2.2 - Experimental Plan/Paradigms.

A – Thinned cranial window surgery was performed on all mice which were then given 3 weeks to recover. 1 initial chronic imaging session was performed 3 weeks post-surgery with the skull intact. 1 week later, a final acute imaging (terminal) session was performed with an electrode inserted into the brain. After terminal experiments, mice were sacrificed for tissue.

B – Each imaging session performed had the same set of experiments with the same timings (post anaesthesia/drilling) and within each experiment. The first stimulation began at least 1-hour post-anaesthesia. All experiments took around 3 hours to complete. The Shabir Paradigm (illustrated) was used in Chapters 4 & 5. The Sharp Paradigm: 1) 2s-O_2, 2) 2s-O_2, 3) >Air, 4) 2s-Air, 5) 16s-Air, 6) >O_2, 7) 16s-O2 & 8) CO_2) for Chapter 3.

C – Each 2s-whisker stimulation (5Hz/5V) had baselines of 10s and a post-stimulus period of 13s. 2s-stimulations consisted of 30 trials.

D– Each 16s-whisker stimulation (5Hz/5V) had baselines of 10s and a post-stimulus period of 44s. 16s-stimulations consisted of 15 trials.

2.2.2 – Thinned Cranial Window Surgery

Mice were anaesthetised with 7ml/kg i.p. injection of fentanyl-fluanisone (Hypnorm, Vetapharm Ltd, Leeds, UK), midazolam (Hypnovel, Roche Ltd, Welwyn Garden City, UK), diluted in sterile water in a 1:1:2 by volume ratio for surgery induction, and subsequently maintained in surgical anaesthesia by the inhalation of 0.5-0.8% isoflurane in 100% oxygen (flow rate of 1L/min). Core body temperature was maintained at 36.5-37.0^{O}C using a homoeothermic blanket (Harvard Apparatus, Cambridge, UK) through rectal temperature monitoring. Eyes were protected from drying out by the application of an ophthalmic ointment; Viscotears® (Novartis, Surrey, UK). Mice were placed in a stereotaxic frame (Kopf Instruments, Tujunga, US) ensuring the head was stable before the scalp was excised using surgical scissors (***Figure 2.3-I***). After exposing the skull, bone overlying the right somatosensory cortex was thinned to translucency using a dental drill to form a thinned cranial optical window (measuring ~3mm^2) (***Figure 2.3-II***). A thin layer of clear cyanoacrylate glue was applied over the cranial window to reduce specularities and to reinforce the surface of the window. A circular wall of dental cement (Super Bond C&B, Sun Medical, Shiga, Japan) was made around the perimeter of the window to which a metal head-plate was fixed to allow chronic imaging over several weeks (***Figure 2.3-III***). Mice were given a saline injection (s.c. 250µl) to re-hydrate and placed into an incubator at 29^{O}C until the resumption of normal awake behaviour, as well as being continually monitored for signs of pain and abnormal behaviour. All mice were given 3 weeks to rest and recover before the first imaging session was performed, in addition to allowing time for any bruising and inflammation to subside.

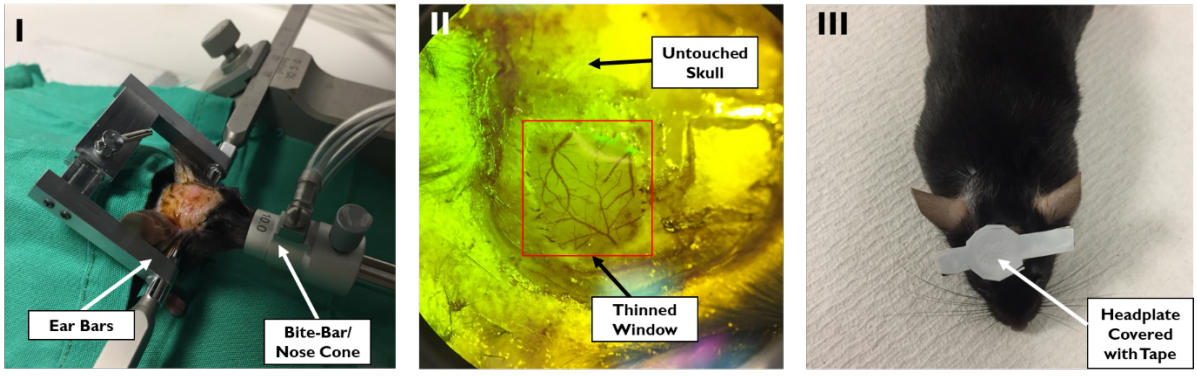

Figure 2.3 – Thinned Cranial Window Surgery.

I – Mice were anaesthetised, scalp was shaved, and mice placed in a stereotaxic frame before scalp was excised.

II – The skull overlying the right somatosensory cortex was thinned to translucency and a thin layer of acrylate was applied to reinforce the window and remove specularities.

III – Dental cement was applied to the periphery of the window to form a chamber to which a metal headplate was attached to. A covering of sticky-tape was applied to cover the window.

2.2.3 – 2D-Optical Imaging Spectroscopy (2D-OIS)

2D-OIS measures changes in cortical haemodynamics by estimating changes in total haemoglobin (HbT), oxyhaemoglobin (HbO) and deoxyhaemoglobin (HbR) concentrations as described previously[38]. For the experimental session, mice were anaesthetised (as described above) and placed into a stereotaxic frame with heads fixed using attached headplates. Anaesthesia was maintained using low-levels of isoflurane (0.3-0.6%) (***Figure 2.4***). For imaging, the right somatosensory cortex was illuminated using 4 different wavelengths of light appropriate to the absorption profiles of the differing haemoglobin states; see ***Figure 2.5*** *below*: (495nm ± 31, 559nm ± 16, 575nm ± 14 & 586nm ± 9) using a Lambda DG-4 high-speed galvanometer (Sutter Instrument Company, US). A Dalsa 1M60 CCD camera with a frame rate of 32Hz operating in a 4x4 binning mode acquired images at 184x184 pixels; giving a pixel resolution of 75x75µm, was used to capture the re-emitted light from the cortical surface.

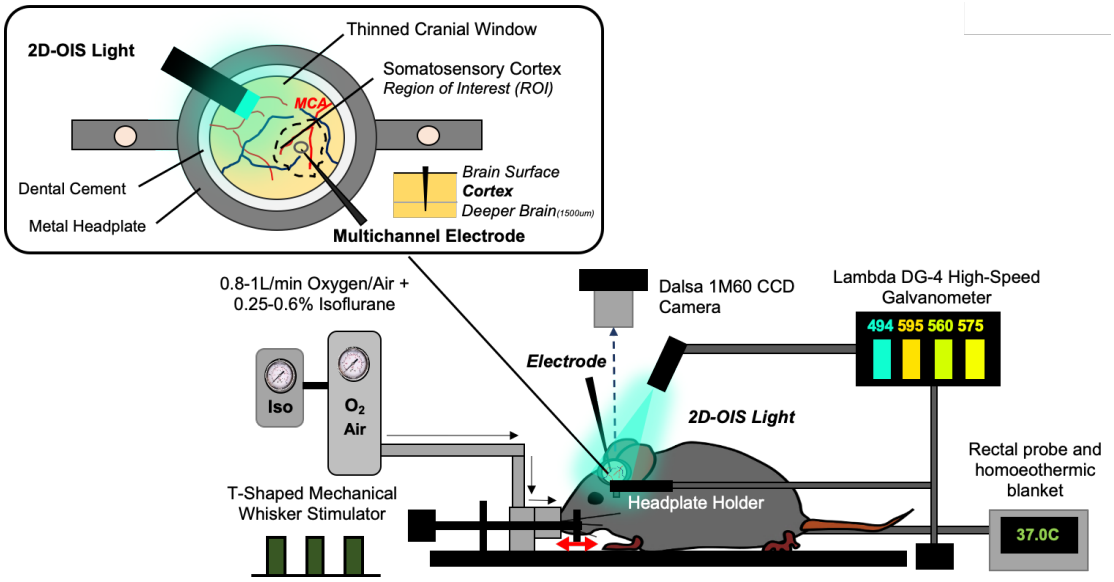

Figure 2.4 – 2D-OIS Imaging Setup. Adapted from (Lee et al., 2020); *Figure authored by me.*

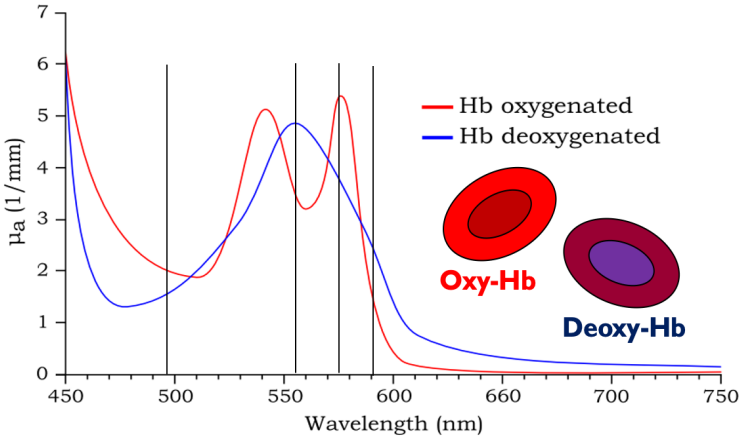

Figure 2.5 – 2D-OIS Wavelength and Absorption Co-Efficient for HbO & HbR. Figure Adapted from (Saka et al., 2010). Oxy-Hb (HbO) & Deoxy-Hb (HbR) summate for HbT.

All spatial images recorded from the re-emitted light underwent spectral analysis based on the path length scaling algorithm (PLSA) as described previously (Berwick et al., 2005, Mayhew et al., 1999), which uses a modified Beer-Lambert law with a path-length correction factor converting detected attenuation from the re-emitted light with a predicted absorption value. Relative HbT, HbR and HbO concentration estimates were generated from baseline values in which the concentration of haemoglobin in the tissue was assumed to be 100μM and O_2 saturation to be 70%. The spectral analysis produced 2D-images of micromolar changes in volume of HbT, HbO & HbR over each stimulation period. Analysis was performed using MATLAB (MathWorks). An automated region of interest (ROI) was selected using the stimulation data from spatial maps generated using 2D-OIS. The threshold for a pixel to be included within the ROI was set at 1.5xSTD, therefore the automated ROI for each session per animal represents the area of the cortex with the largest haemodynamic response, as determined by the HbT. For each experiment, the response across all pixels within the ROI was averaged and used to generate a time-series of the haemodynamic response against time for HbT, HbO & HbR.

2.2.4 – Neural Multichannel Electrode Electrophysiology

In order to assess neurovascular function in its entirety, both haemodynamic and neural measures were obtained. Simultaneous measures of neural activity alongside 2D-OIS were performed in a final acute imaging session 1-week after the 1st imaging. A small burr-hole was drilled through the skull overlying the barrel cortex (as defined by the biggest HbT changes from 2D-OIS imaging) and a 16-channel microelectrode (100μm spacing, 1.5-2.7MΩ impedance, site area 177μm^2) (NeuroNexus Technologies, USA) was inserted into the whisker barrel cortex to a depth of ~1500μm. The microelectrode was connected to a TDT preamplifier and a TDT data acquisition device (Medusa BioAmp/RZ5, TDT, USA). All data collected was sampled at 24kHz and downsampled to 6kHz for analysis of multi-unit activity (MUA) and local-field potentials (LFPs). Multi-unit analysis (MUA) was performed on the data. All channels were depth aligned to ensure twelve electrodes covered the depth of the cortex in each animal. The data was filtered above 300Hz to remove all low frequency components and then split into 100ms temporal bins. Within each bin any data crossing a threshold of 1.5SD above the mean baseline was counted and the results presented in the form of spikes per 100ms of data, or fractional changes in MUA.

2.3 – Cellular Studies

2.3.1 – Tissue Harvest & Perfusion

After terminal acute experiments, mice were given an overdose of pentobarbital (0.13ml per mouse via i/p injection) and after the loss of the pedal reflex, were transcardially perfused. Briefly, the ribcage was cut and removed from the chest, a butterfly-clip needle attached to a syringe of 5ml warm saline (0.9%) was inserted into the bottom of the left-ventricle of the heart followed by snipping of the right-atrium/vena cava allowing blood to be gently expelled from the body. Post-perfusion, mice were decapitated, and the brains were manually dissected from the skull. Once the brains were isolated, the brains were cut into 2 hemispheres with the right hemisphere being placed in 4%v/v formalin for fixation, and the left hemispheres snap-frozen in isopentane at -20^{O}C for 2 minutes before being stored at -80^{O}C. The formalin-fixed hemispheres were then subsequently embedded in paraffin-wax and stored at room temperature.

2.3.2 – Immunohistochemistry (IHC)

Right hemispheres that were formalin-fixed paraffin-embedded (FFPE) underwent standard dewaxing and antigen retrieval steps (as described in 2.1.4) before immunohistochemistry was performed according to the avidin-biotin complex (ABC) staining method (2.1.1). Briefly, sections deparaffinated in xylene (10min) and rehydrated through increasing gradients of ethanol to water (2min each) before being placed in 3% peroxide/methanol for 20min. Following this step, sections underwent the necessary antigen retrieval steps (described in 2.1.4) before sections were blocked for 30min. Primary antibodies (described in 2.1.4) were applied for the necessary timings and temperatures before being washed and secondary biotinylated antibodies applied for 1hr. After washing, ABC reagent was applied for 30min, followed by washing and the application of DAB for the necessary timings. All sections were then counterstained using haematoxylin (30sec) followed by Scott's water for 10sec. Finally, all slides were dehydrated to absolute ethanol through increasing ethanol gradients (2min each), then xylene (2min) before being mounted with coverslips using DPX.

2.3.3 – Imaging and Analysis

All sections were imaged using a brightfield setting on a Nikon Eclipse Ni-microscope attached to a DS-Ri1 camera. 5 random and non-overlapping regions within the hippocampus and cortex were taken for each condition and animal (20x magnification). Computer software (ANALYsis^D) was used to quantify % area coverage of staining of each image. All experimentation, imaging and analysis was performed blinded. Mean % coverage (out of 5 sections per animal per antibody) was calculated for hippocampus and cortex respectively.

2.4 – Genetic Studies

2.4.1 – RNA Extraction

Left hemispheres from the snap-frozen brains *(described above in 2.3.2)* had cerebellums excised off using a scalpel. The remaining cerebrums of each brain were placed in tubes along with 300µl of TRI-reagent™ and RNA extraction was performed as per the manufacturer's guidelines (Direct-Zol™ RNA MiniPrep Kit; *Zymo Research, US*). Briefly, brain samples were homogenised and centrifuged (10,000g; 50sec) before 250µl abs. ethanol was added to the supernatant in a fresh tube. The supernatant was transferred to an IIC-filtered column tube and this was centrifuged (10,000g; 50sec). Next, 400µl RNA Pre-Wash (Direct-Zol™) was added to the column and the contents centrifuged again (10,000g; 50sec) with this step being repeated twice. After centrifugation, 700µl of RNA-wash buffer was added to the column and centrifuged (10,000g; 120sec) before finally eluting the RNA into a 1.5ml Eppendorf tube applying 25µl nuclease-free water to the column and then centrifuging (10,000g; 50sec). The quality of the extracted RNA was determined using a NanoDrop™ ND-100 spectrophotometer by adding 1µl of the eluted RNA from each sample.

2.4.2 – cDNA Synthesis

cDNA synthesis from the extracted RNA was performed as to the manufacturer's guidelines using the UltraScript™ 2.0 cDNA Synthesis Kit (BioSystems®). Briefly, master mixes were made up for each RNA sample by adding 4µl of 5x cDNA Synthesis Mix, 1µl UltraScript™ 2.0 and a minimum of 3.5µg RNA by adding the respective volume of nuclease-free water, with ratios of RNA to water being calculated from minimum [RNA] being 47ng/µl. Samples were mixed and spun-down briefly before being incubated at 53^{O}C (PTC-200) for 30min for reverse transcription, and finally at 95^{O}C for 10min to denature before being stored at -20^{O}C.

2.4.3 – Real-Time Quantitative Polymerase Chain Reaction (qRT-PCR)

qRT-PCR was performed using PrimeTime™ qPCR assay tubes according the manufacturer's guidelines (IDT, US). Briefly, primers for *IL1b*, *TNFa*, *NOS1* & *NOS3* (including *ACTB* as a housekeeping gene for normalisation) were resuspended in 100µl IDTE buffer to produce a 20x stock solution. Primer sequences are described in 2.1.6. A master mix for each gene was made up by adding 13µl of primer, 52µl Luna® qPCR Master Mix (SYBR Green) (BioLabs™) and 52µl nuclease-free water from which 9µl of the primer/qPCR mix was added to 1µl cDNA for each sample. 4µl of the sample mix was then pipetted in duplicates in a 384-well plate, covered and centrifuged (1760g; 60sec) before placing in a C1000 Touch Thermal Cycler attached to a CFX384 Real-Time System (BioRad) incubated at 95^{O}C for 3min, before 48 cycles (95^{O}C; 10sec, 60^{O}C; 30sec).

2.5 – Analysis and Statistics

To compare haemodynamic & neural responses, analysis was performed using Graphpad Prism v8 and SPSS v25. Statistical comparisons were made on HbT, HbO, HbR & MUA values using two-way repeated measures ANOVAs as well as 2-tailed unpaired t-tests. P-values <0.05 were considered statistically significant. For chapter 5, SPSS v25 was used to perform statistical analyses. Shapiro-Wilks test was used to check for normality and Levene's test was used to assess equality of variances. 2-way mixed design ANOVA, 1-way ANOVA or Kruskal-Wallis tests were used, as appropriate. The Shapiro-Wilks test suggested that, for chronic experiments, peak values of HbT and HbO are normally distributed, however, HbR values are significantly non-normal. 2-way mixed design was used to compare peak values for HbT, HbO & HbR (although HbR failed the S-W test for normality, an ANOVA was used as they were considered fairly robust against small deviations from normality). Dunnett's (two-sided) multiple comparisons test was used to compare disease models to WT, and for HbR, Games-Howell multiples comparisons were used.

For immunohistochemistry, analysis was performed using GraphPad Prism v8. All data sets were found to be normally distributed after performing a Shapiro-Wilk normality test (p=>0.05 for all conditions and animals). Due to the data being normally distributed in all cases, statistical analyses were performed using single t-tests (between WT vs disease for each condition) and two-way ANOVAs (with post-hoc Dunnett's multiple comparisons).

For the qRT-PCR data, all the Ct values were inputted into a Microsoft Excel spreadsheet and the data was analysed according to the well-established 'delta-delta-Ct' method by normalisation of all Ct values to *ACTB* for each gene in each mouse sample. All the data was found to be normally distributed using the Shapiro-Wilk test, and all WT vs disease comparisons were performed using multiple t-tests and two-way ANOVAs (with post-hoc Dunnett's multiple comparisons).

Chapter 3 – Neurovascular Function in Young J20-hAPP Mouse Model of Alzheimer's Disease

This chapter is a published research paper (Shabir et al, 2020. Sci Rep. 10(1), 7518).

3.1 – Paper Title and Authors

Enhanced Cerebral Blood Volume under Normobaric Hyperoxia in the J20-hAPP Mouse Model of Alzheimer's Disease

Osman Shabir[1], Paul Sharp[1], Monica A Rebollar[2], Luke Boorman[1], Clare Howarth[1], Stephen B Wharton[2], Sheila E Francis[3] & Jason Berwick*[1]

[1]The Neurovascular & Neuroimaging Group (Department of Psychology), Alfred Denny Building, University of Sheffield, Western Bank, Sheffield, S10 2TN

[2]Sheffield Institute for Translational Neuroscience (SITraN), 385a Glossop Road, University of Sheffield, Sheffield, S10 2HQ

[3]Department of Infection, Immunity & Cardiovascular Disease (IICD), University of Sheffield, Medical School, Beech Hill Road, Sheffield, S10 2RX

*Corresponding Author (j.berwick@sheffield.ac.uk) University of Sheffield, Western Bank, Sheffield, S10 2TN (United Kingdom)

I, Osman Shabir, am the sole author of the manuscript. I performed the majority of the experiments. Paul Sharp performed some of the experiments (4 animals). Monica Rebollar helped with the IHC. Luke Boorman helped make the analysis code. Jason Berwick helped with MATLAB data analysis. Clare Howarth, Stephen Wharton, Sheila Francis and Jason Berwick supervised the research, proofread and helped edit the manuscript.

3.2 – Abstract

Early impairments to neurovascular coupling have been proposed to be a key pathogenic factor in the onset and progression of Alzheimer's disease (AD). Studies have shown impaired neurovascular function in several mouse models of AD, including the J20-hAPP mouse. In this study, we aimed to investigate early neurovascular changes using wild-type (WT) controls and J20-hAPP mice at 6 months of age, by measuring cerebral haemodynamics and neural activity to physiological sensory stimulations. A thinned cranial window was prepared to allow access to cortical vasculature and imaged using 2D-optical imaging spectroscopy (2D-OIS). After chronic imaging sessions where the skull was intact, a terminal acute imaging session was performed where an electrode was inserted into the brain to record simultaneous neural activity. We found that cerebral haemodynamic changes were significantly enhanced in J20-hAPP mice compared with controls in response to physiological stimulations, potentially due to the significantly higher neural activity (hyperexcitability) seen in the J20-hAPP mice. Thus, neurovascular coupling remained preserved under a chronic imaging preparation. Further, under hyperoxia, the baseline blood volume and saturation of all vascular compartments in the brains of J20-hAPP mice were substantially enhanced compared to WT controls, but this effect disappeared under normoxic conditions. This study highlights novel findings not previously seen in the J20-hAPP mouse model, and may point towards a potential therapeutic strategy.

3.3 – Introduction

Alzheimer's disease (AD) is the most prevalent form of dementia worldwide and is characterised by a progressive decline in cognition. AD is pathologically characterised by the presence of extracellular amyloid beta (Aβ) plaques and intracellular neurofibrillary tangles composed of hyperphosphorylated-tau, which are associated with the progressive neurodegeneration and synaptic dysfunction seen in AD[1]. At present there are limited disease modifying or curative treatments for AD and studying disease mechanisms in human subjects is difficult. Therefore, pre-clinical models of AD; mainly mouse models, have been generated to study AD mechanisms in vivo. Whilst numerous mouse models of AD exist, they do not fully recapitulate the human disease in its entirety[2,3]. However, these mouse models can effectively model specific aspects of AD pathology, such as amyloid plaque deposition and toxicity where smaller oligomers (8-24-mers) have been shown to be more toxic than larger matured fibrils[4]. The J20-hAPP mouse model of AD over-expresses human amyloid precursor protein (hAPP) with the Swedish (K670N and M671L) and the Indiana (V7171F) familial mutations[5]. These mice produce more Aβ1-42 and plaques begin to readily form in the hippocampus from around 5-6 months of age[5,6]. The J20-hAPP mouse model displays significant neuroinflammation

characterised by gliosis of both astrocytes and microglia[6]. They also display significant long-term memory impairment[6].

The brain is extremely metabolically demanding, and the neurophysiological process of neurovascular coupling ensures that neurons receive an efficient and adequate blood supply to match the metabolic demands that neurons exert. The neurovascular degeneration hypothesis; as proposed by Zlokovic[7,8], suggests that neurovascular breakdown is an important step in the pathogenesis of cerebrovascular and neurodegenerative disease, especially in AD. Evidence suggests that vascular dysregulation is the earliest feature of late-onset AD, preceding Aβ deposition, metabolism and structural deficits[9]. Therefore, studying neurovascular coupling and neurovascular degeneration is important to identify early biomarkers or treatment strategies. Using a chronic mouse preparation, previous research from our laboratory found no significant neurovascular deficits in the J20-hAPP mouse between 9-12m age[10], despite neuroinflammation and memory deficits[6]. This is contrary to what other laboratories have shown with the J20-mouse at the same age[11–13]. Such deficits have only been reported in acute experimental preparation sessions where the measurement of neurovascular function is performed on the same day as surgery, and not in chronic sessions where the effects of surgery have been mitigated. Based on these observations, we hypothesised that neurovascular function will not be altered in 6m old J20-hAPP mice using a chronic imaging preparation. The aim of the study therefore was to investigate neurovascular function at an earlier stage (around 6m) in the J20-hAPP mouse model to investigate whether there were neuronal or vascular abnormalities at an earlier disease stage when amyloid-plaques start to form, or whether they would remain intact as seen in 9-12m old J20-hAPP mice.

3.4 – Results

3.4.1 – Enhanced Blood Volume (HbT) Responses in J20-hAPP Mice

Imaging of the cortex through a thinned cranial window using 2D-OIS allows estimation of cortical haemodynamics in terms of relative changes of HbT (total haemoglobin, blood volume), HbR (deoxyhaemoglobin) & HbO (oxyhaemoglobin) concentration (***Figure 3.1***). Mechanical whisker stimulations at 5Hz evoke a haemodynamic response within the branches of the middle cerebral artery (MCA) and the immediately surrounding regions from which an active region of interest (ROI) can be determined (***Figure 3.1B***). From the ROI, an average time-series of the haemodynamics can be produced showing percentage changes of HbT, HbR & HbO over time; before, during and post-stimulation (***Figure 3.1D***).

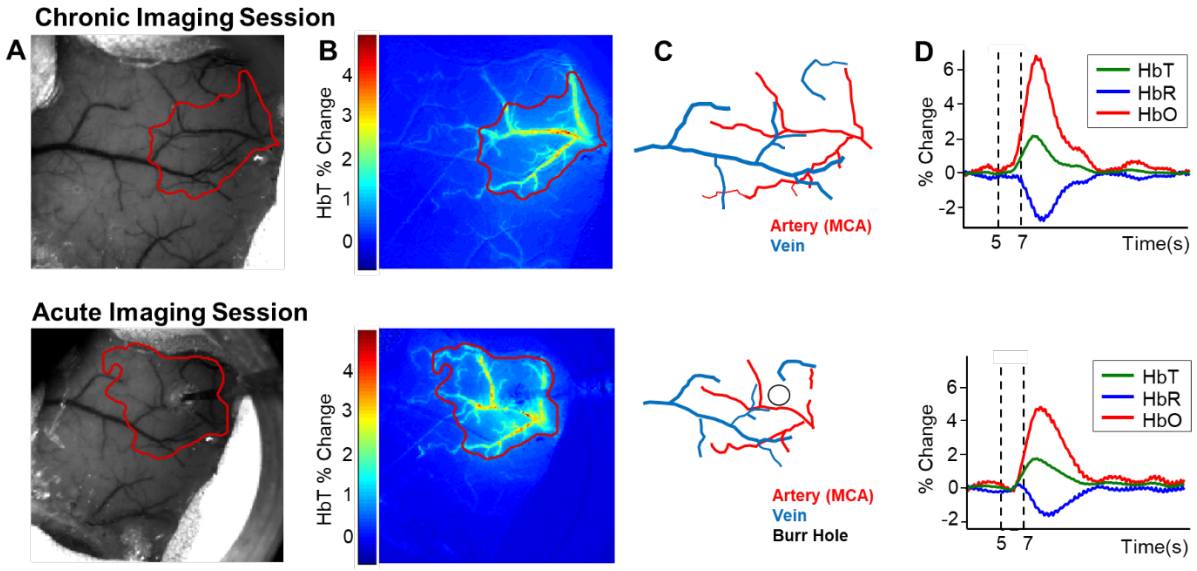

Figure 3.1 - Representative 2D-OIS haemodynamic data from an AD mouse to a 2s-mechanical whisker stimulation. Top: chronic imaging sessions. Bottom: Acute imaging sessions with electrode. A) Raw grayscale image of thinned cranial window overlaid with the active region of interest (ROI; red) as defined from B. B) Spatial map of HbT activation across a stimulation trial with colour-bar representing the % change of HbT from baseline. C) Vessel map showing arteries and veins within the window and active ROI. D) Time-series profiles of the haemodynamic data showing increases to HbT & HbO and a decrease (washout) in HbR. Dotted lines represent start and end time of whisker stimulation.

A week after chronic imaging sessions (in which the skull remains intact), a small burr-hole was drilled through the skull in the centre of the barrel cortex; determined from 2D-OIS data on a previous chronic imaging session, and a micro-electrode was inserted through the brain as a terminal experiment (***Figure 3.1, bottom row***).-Using the chronic thinned cranial window preparation (as shown in ***Figure 3.1-top***) and imaging through an intact skull 2 weeks after surgery, the first question addressed was whether stimulation-evoked haemodynamic responses were different in J20-hAPP mice compared to WT controls. We found that stimulation-evoked HbT (blood volume) responses were significantly higher (on average by a +2% change in absolute values) in J20-AD mice compared to WT controls under both 100% O_2 (hyperoxia) and 21% O_2 (normoxia) conditions (2-way repeated-measures ANOVA of peak response: F=11.6, p=0.001) (***Figure 3.2***). HbO peak responses were also significantly increased (2-way repeated measures ANOVA: F=8.42, p=0.005). The washout of HbR was always significantly smaller in both WT and J20-AD mice in normoxic conditions (2-way repeated measures ANOVA: F=5.96, p=0.01), though not significantly more impaired in J20-hAPP mice compared to WTs (F=0.95, p=0.34). Irrespective of gas condition, HbT and HbO were always substantially higher in J20-hAPP mice compared to WTs in all experiments (***Figure 3.2***).

As part of the experimental paradigm, a test of global vascular reactivity was performed at the end of the experiment using 10% hypercapnia (***Figure 3.6***). We found no significant differences between WT and J20-hAPP mice (HbT: 2-tailed unpaired t-test p=0.53) suggesting that vessels in WT and J20-hAPP mice are able to dilate maximally to the same extent. In 6 WT and 5 J20-hAPP mice, acute imaging sessions were performed where an electrode was inserted into the brain one week after chronic imaging sessions. In these sessions, there were no significant differences in the haemodynamic responses between WT and J20-hAPP mice: HbT (F=3.09, p=0.087), HbO (F=1.42, p=0.24) & HbR (F=3.73, p=0.06) (***Figure 3.7***).

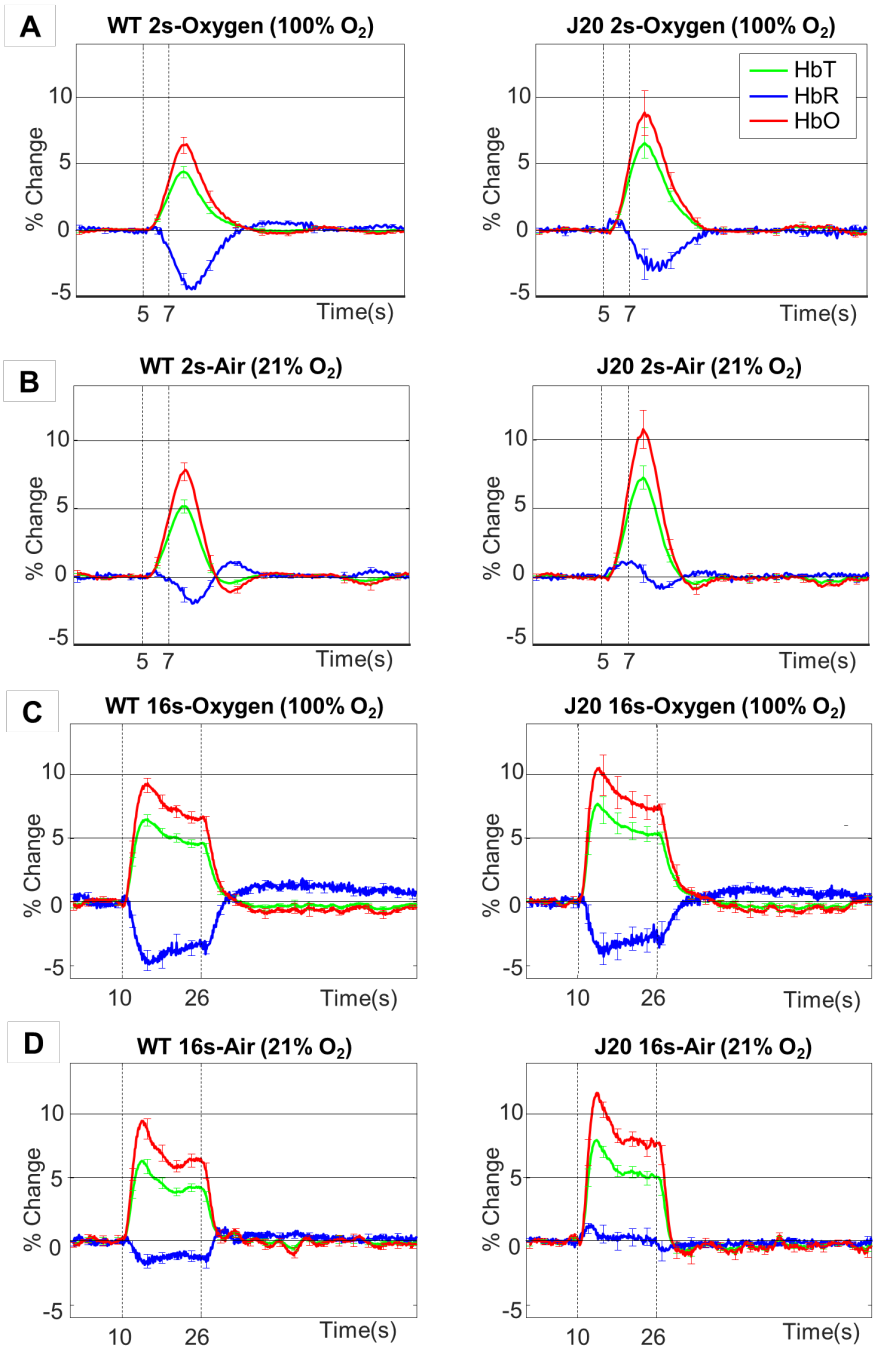

Figure 3.2 – Mean stimulation-evoked haemodynamic responses in WT and J20-hAPP mice. WT (n=8) [left column] and J20-hAPP (n=9) [right column] with graphs showing mean % changes in the peak values of HbT, HbR & HbO. Error bars ±SEM. **A)** 2s stimulation in 100% oxygen: WT-HbT 4.48±0.4, J20-HbT 6.7±1.09, WT-HbO 6.64±0.58, J20-HbO 9.06±1.57, WT-HbR -3.82±1.12, J20-HbR -3.99±1.09. **B)** 2s stimulation in 21% oxygen: WT-HbT 5.3±0.47, J20-HbT 7.38±0.8, WT-HbO 8.04±0.6, J20-HbO 11.04±1.25, WT-HbR -3.19±0.34, J20-HbR -1.62±0.4. **C)** 16s stimulation in 100% oxygen: WT-HbT 6.62±0.4, J20-HbT 8.09±1.04, WT-HbO 9.44±0.52, J20-HbO 11.04±1.55, WT-HbR -4.92±0.65, J20-HbR -4.15±1.15. **D)** 16s stimulation in 21% oxygen WT-HbT 6.44±0.49, J20-HbT 8.36±0.68, WT-HbO 9.64±0.68, J20-HbO 12.22±0.99, WT-HbR -2.06±0.42, J20-HbR -1.18±0.48. Dotted vertical lines indicate start and end time of whisker stimulation.

3.4.2 – Neural Activity is Substantially Higher in J20-hAPP Mice

Next, we investigated whether the J20-hAPP mice had altered neural activity early in the disease course. We inserted a multichannel microelectrode into the centre of the barrel cortex (***Figure 1-bottom row***) and recorded neural data simultaneously with 2D-OIS. We found that stimulation-evoked multi-unit activity (MUA) was significantly higher in J20-hAPP mice compared to WT mice across all stimulation durations and gas conditions (2-way repeated measures ANOVA: $F=8.82$, $p=0.005$) (***Figure 3.3***). The enhanced neural activity was indicative of neural hyperexcitability in J20-hAPP mice. MUA responses were averaged from channels 3-8 (***Figure 3.3A***) which were at the depth of the somatosensory cortex.

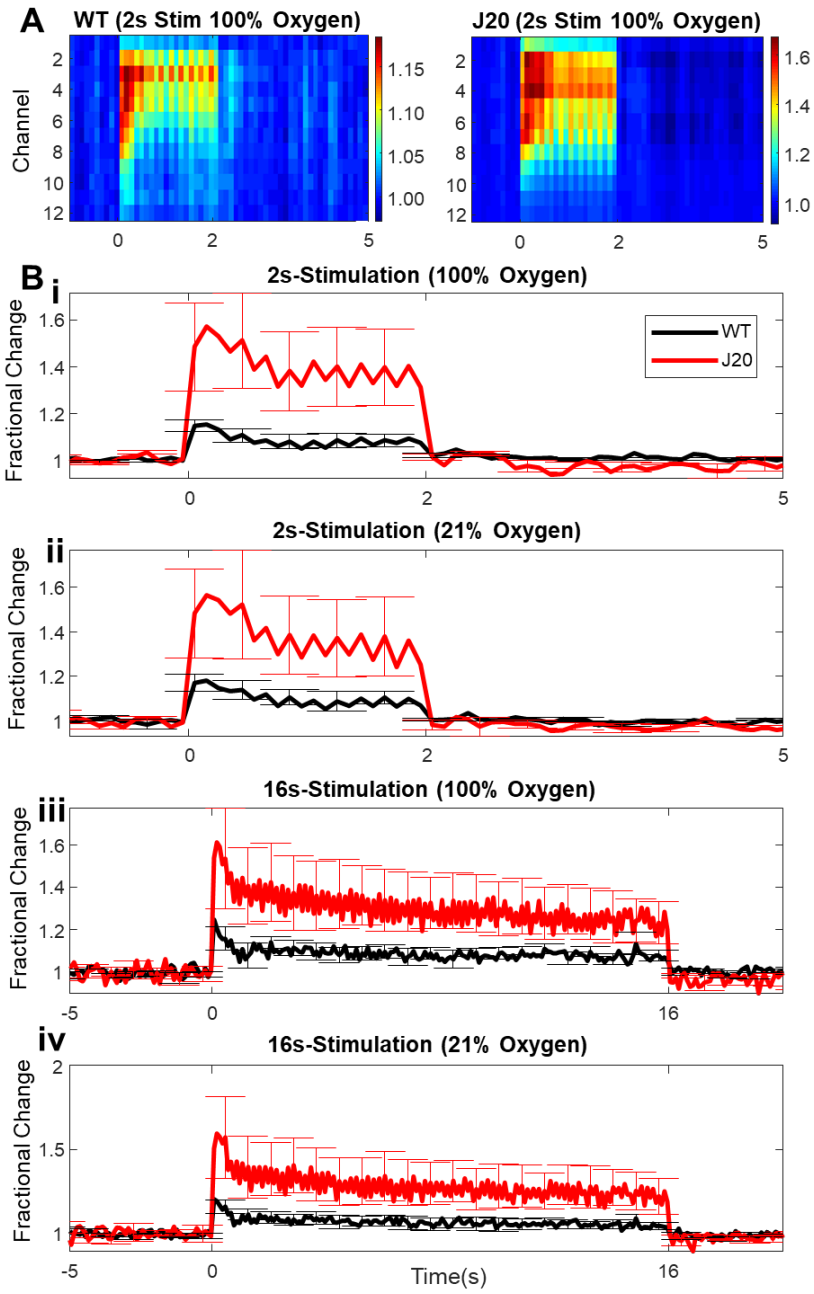

Figure 3.3 – Multi-Unit Activity (MUA) Data. A) MUA activity (fractional changes of number of spikes/100ms) along depth of the microelectrode and time (stimulation periods) for 2s-stimulation in 100% oxygen. Cortical regions are at the depth of channels 3-8 (biggest responses in MUA). B) Time-series of mean total responses of MUA (fractional changes in spikes/100ms) ±SEM. **i)** 2s-stimulation in 100% oxygen: WT-MUA 547.52±98.7 spikes/100ms, J20-MUA 2260.78±710.8 spikes/100ms. **ii)** 2s-stimulation in 21% oxygen: WT-MUA 676.1±143.35 spikes/100ms, J20-MUA 2318.16±932.9 spikes/100ms. **iii)** 16s-stimulation in 100% oxygen: WT-MUA 4722.73±914.8 spikes/100ms, J20-MUA 14,158.4±4753.2 spikes/100ms. **iv)** 16s-stimulation in 21% oxygen: WT-MUA 3974.8±796.8 spikes/100ms, J20-MUA 13,592.8±5184.6 spikes/100ms. WT n=6, J20-hAPP n=5.

3.4.3 – Baseline Blood Volume is Substantially Higher in J20-hAPP Mice under Hyperoxia

As part of the experimental protocol, baseline haemodynamics during transition experiments (from 100% oxygen to 21% oxygen/air and vice versa) were recorded and quantified. We found that the baseline blood volume (HbT) was significantly enhanced in J20-hAPP mice under hyperoxic conditions (2-tailed unpaired t-test p=0.0002), but not in WT mice (***Figure 3.4B***). Upon transition from 100% oxygen to air (21% oxygen), there was a substantial decrease in HbT in J20-AD mice (-6.2% change on average) characterised by the enhanced vasoconstriction of all vascular compartments (***Figure 3.4A/C***).

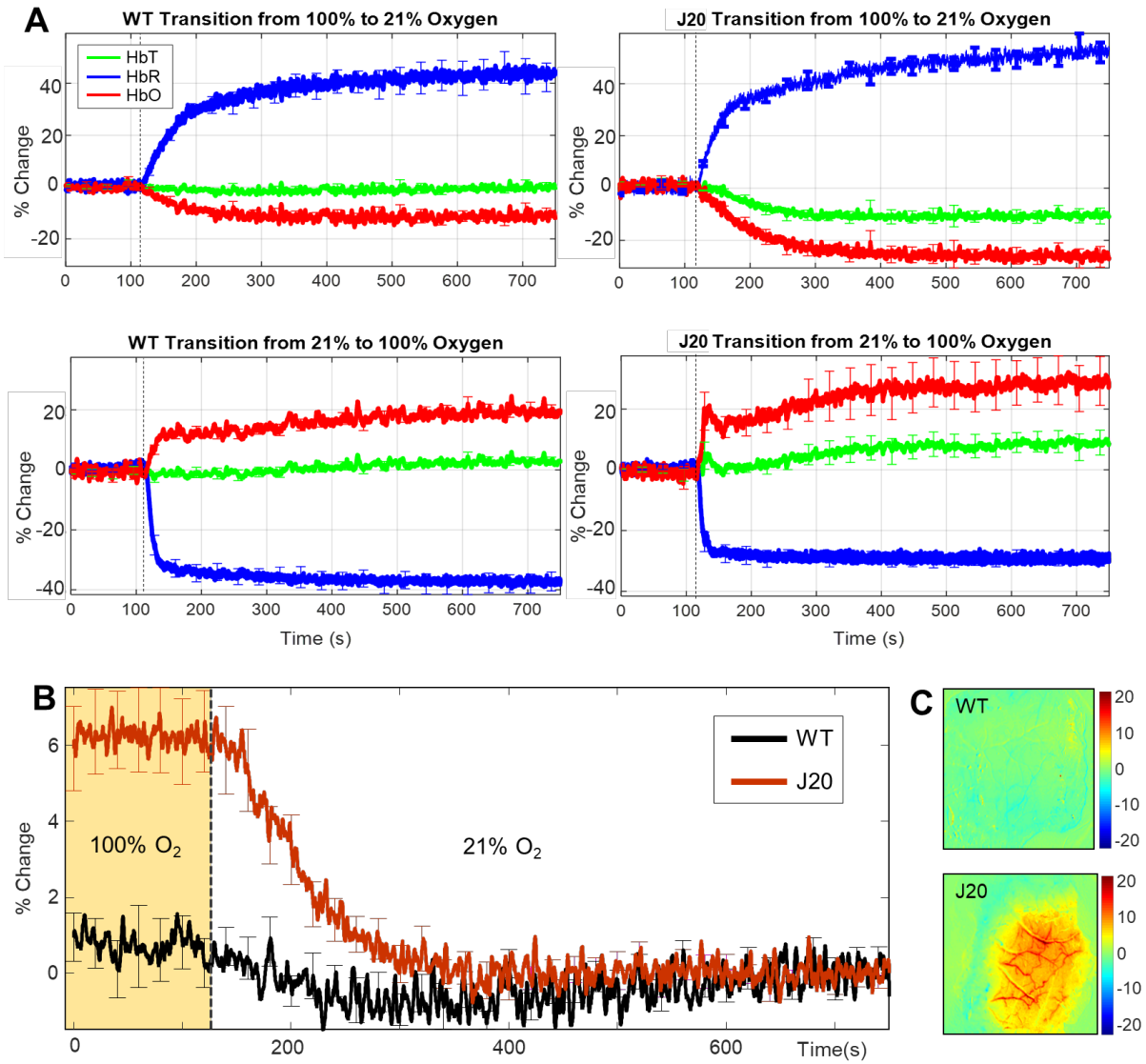

Figure 3.4 – Average gas transitions between hyperoxic and normoxic conditions in WT and J20-hAPP mice. A) Time-series of gas transition experiments: top; transition from 100% oxygen to 21% oxygen & bottom; transition from 21% oxygen to 100% oxygen. B) Time-series of HbT at baseline at 100% oxygen and during gas transition to 21% oxygen with % change in HbT: WT-HbT 0.5%±1.8%STD, J20-HbT 6.2%%±3%STD. *Error bars* ±*SEM*. **(**C) Representative spatial map showing the differences in HbT across all vascular compartments in a J20-hAPP mouse (bottom), but not WT mouse (top) under normobaric hyperoxia.

3.4.4 – Amyloid-Plaques Begin to Form in the Hippocampus of 6m J20-hAPP Mice

Amyloid plaques are a key pathological hallmark of AD and begin to form in the hippocampus in the J20-hAPP AD mouse at around 6m of age[6]. The progression of plaque pathology and subsequent inflammatory changes have been well characterised in the J20-hAPP mouse[6]. We confirmed that in our cohort, by the age of 6m, the hippocampus has numerous medium sized plaques (***Figure 3.5***) with fewer and smaller diffuse ones forming within the deeper cortex, but none within the upper layers of the cortex.

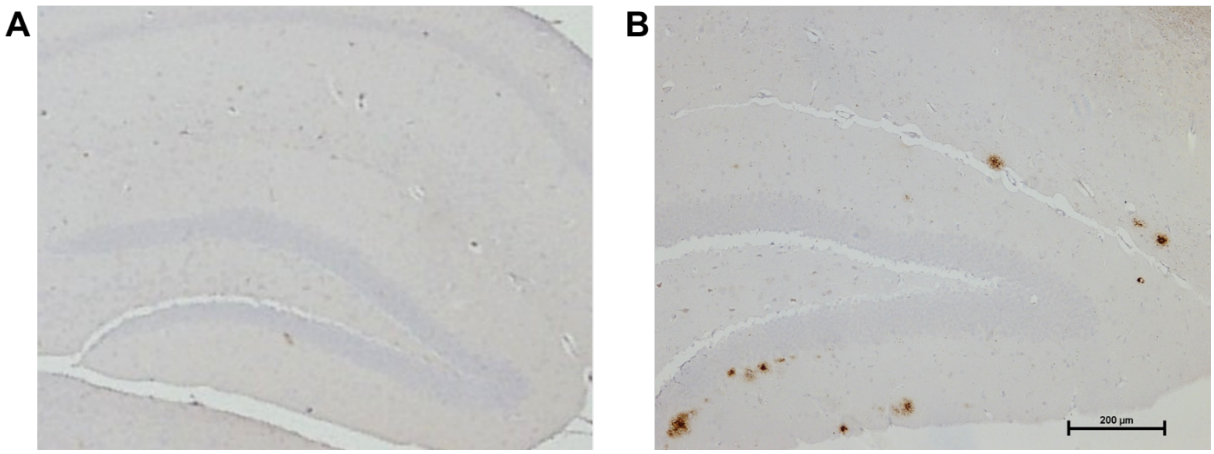

Figure 3.5 – Representative hippocampal sections. A) WT mice do not develop any amyloid plaques. B) In the J20-hAPP mouse, diffuse plaques can be found predominantly forming in the dentate gyrus of the hippocampus by 6m, with one or two developing in the deep cortex, but not in the superficial layers.

3.5 – Discussion

The present study aimed to investigate neurovascular function in the J20-hAPP mouse model of AD to establish whether there were any haemodynamic and neural differences at am early time point (6 months) compared to WT mice. Stimulation-evoked cerebral haemodynamics responses (blood volume and HbO) were significantly enhanced in J20-hAPP mice as measured in a stable chronic cranial window preparation (***Figure 3.2***). This consistent and remarkable finding was irrespective of stimulation duration (2s/16s) or gas condition (hyperoxia/normoxia). The washout of HbR was always smaller in J20-hAPP mice, but much smaller under normoxia. These responses were consistent across all experimental setups and the timing of experiments post-anaesthesia. These findings are contrary to the majority of the published literature with respect to neurovascular function in the J20-hAPP mouse[11–13] which all reveal diminished haemodynamic responses in terms of HbT (blood volume) in the J20-hAPP mouse at a similar age. However, one study has previously reported augmented haemodynamics in the APP/PS1 double transgenic model[14]. In that study, a multi-modal approach was used to investigate cerebral haemodynamics in response to electrical stimulation of the hind-paw. Laser-Doppler flowmetry, multi-photon laser scanning microscopy and intrinsic optical imaging (similar to 2D-OIS) all confirmed enhanced HbT in 7m APP/PS1 mice and not earlier than 5m, similar to our data from the J20-hAPP mice around 6m of age. However, Kim and colleagues did not measure neural activity and speculated that the enhanced haemodynamic responses could be attributed to either increased neuronal activity or increased vascular reactivity. Our data along with others investigating neural activity confirm that there is neuronal hyperexcitability around 6m of age in the J20-hAPP mouse, but that there is no difference in vascular reactivity between WT controls and J20-hAPP mice as demonstrated by the response to hypercapnia. Previous research from our laboratory has shown no significant differences in either haemodynamics or neural activity between 9-12m in the same J20-mouse model unless an electrode is inserted into the brain[10]. Using exactly the same approach, we present here novel findings of hyperexcitability and enhanced evoked haemodynamic responses at an earlier age, around 6m, in the J20-mouse model of AD. Combined, these studies suggest that these effects are only seen at an earlier age point and are, therefore, time-dependent.

A major finding from this study was that under normobaric hyperoxia, the baseline blood volume and saturation across the entire cortex was substantially higher in J20-hAPP mice compared to control mice, and this effect disappeared upon transitioning to normoxia, where J20-hAPP mice displayed a significant decrease in HbT to match the baseline of WT controls (***Figure 3.4***). This enhanced blood volume could be seen across all vascular compartments across the observable cortical regions. This oxygen-specific effect on cerebral

haemodynamics was only observed in the J20-hAPP mice and was not a feature of WT mice and did not seem to affect stimulation-evoked haemodynamics in terms of HbT volume. In early stages of AD, soluble Aβ fragments can be cleared from the brain through paravascular pathways in the brain, including the glymphatic system[15] and the intramural periarterial drainage system[16]. It may be possible that naturally increasing cerebral blood flow could potentially enhance the clearance of soluble Aβ in the early stages of AD onset, though this would require further work to establish if true. Since our data show that normobaric hyperoxia can elevate baseline blood volume across the cortex in young J20-hAPP mice, this mechanism may provide a potential disease prevention strategy enhancing the clearance of Aβ before plaques begin to form, as well as reducing the formation and concentration of Aβ oligomers. As we can visualise plaques from around the age these J20-hAPP mice, these observations could be related to early Aβ deposition. In terms of corroboration and translatability of these findings, it has previously been demonstrated that hyperbaric oxygen therapy reduces neuroinflammation in the 3xTg AD mouse model[17].

Another finding from this study was that the J20-hAPP mice were hyperexcitable, as indicated by the enhanced MUA evoked by whisker stimulation (***Figure 3.3***) consistent with other studies showing neural hyperexcitability in the J20 mouse[18]. The cause of hyperexcitability in J20-hAPP mice, and indeed some AD patients, may be due to neurophysiological abnormalities caused by the presence of Aβ[19–22], or by aberrant APP processing resulting in different intracellular domain fragments[23–25]. Unprovoked seizures can occur in 10-22% of AD patients[26], especially myoclonic seizures, which are specifically due to the hyperexcitability of the cortex. For unknown reasons, the prevalence of seizures in AD-patients, including the myoclonic type, are more frequent in younger AD-patients, especially that of early-onset AD[27]. This hyperexcitability at a young age is also reflected in our data from the J20-hAPP mouse. Furthermore, another study showed a higher incidence of epileptiform-like discharges in the APP/PS1 mouse model compared to controls which were correlated to the number of Aβ plaques between 4-9m of age[28]. The hyperexcitability and epileptic activity of the J20-hAPP mice dissipates by the age of 8m[23]. Therefore, the hyperexcitability seen in the J20-hAPP mouse, APP/PS1 mice and younger AD-patients may be related to the brains initial reaction to the emerging presence of Aβ oligomers, or that of aberrant APP processing. Whisker deflection in APP/PS1 mice also resulted in much higher neural responses in the cortex, also supporting our findings[29]. In our study, the observed enhanced neural activity couples well with the enhanced haemodynamic responses, suggesting that neurovascular coupling in the J20-hAPP mouse is intact and functioning well at this younger age of 6m.

In J20-hAPP mice, amyloid plaques begin to form around 6m of age within the dentate gyrus of the hippocampus as well as in some areas of the neocortex[30]. These mice do not exhibit any neurofibrillary tangles of hyperphosphorylated tau at any stage of their life. Neuronal loss within CA1 as well as synaptic loss begins around 3m of age within the hippocampus, significant neuroinflammation from 6m[1,6], with cognitive impairment starting around 4m where J20-hAPP mice display spatial memory deficits as measured by the radial arm maze[1]. In human patients with AD, memory deficits come secondary to Aβ deposition[9], although important pathological hallmarks such as neuroinflammation and hippocampal sclerosis are present early on during early mild cognitive impairment (EMCI), in addition to tau pathology. Thus the 6m time point of the J20-hAPP mouse could be considered as an equivalent of EMCI in humans; characterised by some memory deficits, structural and functional alterations within the brain including Aβ deposits, neuronal & synaptic loss in hippocampus as well as neuroinflammation, though with the notable exception of any tau pathology as well as displaying cognitive impairments before significant Aβ deposition.

In our acute experimental sessions, the intactness of NVC was masked by the technical procedure used and a mismatch between neural activity and haemodynamic response was recorded (***Figure 3.7***). As described in our previous research using the J20-hAPP mouse between 9-12m of age[10], insertion of an electrode into the mouse brain can cause cortical spreading depression (CSD) to occur across the cortex[31]. CSD is characterised by prolonged vasoconstriction that can persist for some time (in some cases over an hour) and this generally dampens haemodynamic responses and overall cerebral blood flow across a wide area of the cerebral cortex[32]. During this time, neural activity often recovers quickly, however the recovery rate of haemodynamics varies and there is a considerable lag[33]. As such, despite the enhanced MUA seen in our J20-hAPP mice to stimulations, the haemodynamics measured are comparable to WT controls due to CSD. Although cerebral haemodynamics recover in both WT and J20-hAPP mice, the rate of recovery between these varies, and J20-hAPP mice take longer as previously demonstrated[10]. By the end of the experimental period (16s-stimulaton 100% O_2), HbT increases in J20-hAPP mice to match that of WT controls (***Figure 3.7 bottom***). Our data, along with our previous research, highlight the major impact that acute imaging sessions have on neurovascular studies. Future experiments could combine 2D-OIS with non-invasive optical neural readouts (such as genetically encoded calcium indicators (GECIs) e.g. GCaMP in neurons, although these have their own technical and physiological considerations, discussed in depth elsewhere[34].

A limitation of the study was that animals were lightly anaesthetised throughout. While it is increasingly argued that all neurovascular studies should be performed using awake animals[35]

due to the effects of anaesthesia on neurovascular function, previous research from our laboratory has determined an optimal anaesthetic regimen that has minimal effect on cerebrovascular function and reactivity[36]. Performing experiments at 1-hour post induction of anaesthesia, and maintaining sedation via low levels of isoflurane (<0.5%), is comparable to awake imaging in terms of haemodynamic responses and profiles to whisker stimulation[36]. Use of such an anaesthetic regime avoids the multiple confounds associated with behavioural state (arousal, locomotion, stress, grooming etc.), which are present in the awake animal. A second limitation is that our estimates of blood volume and saturation may be inaccurate especially for the J20-hAPP mouse. Our recent study[10] using older age groups of mice discussed this issue in detail, which showed that regardless of the baseline blood volume estimation used, our percentage change was scaled by it (i.e. always the same change). Therefore the observation in this paper that blood volume is increased in the J20-hAPP mice under oxygen compared to air is robust. A third limitation was that blood flow measurements were not quantified and therefore we were unable to assess perfusion in the brain as a whole. Most other studies however indicate chronic hypoperfusion in patients and the J20-hAPP mouse[37].

In conclusion, using a stable chronic imaging preparation, we have shown that, at early time points, the J20-hAPP mouse model of AD exhibits enhanced haemodynamics in the brain marked by an increased blood volume response to sensory stimulations compared to WT controls. The likely cause of such increased blood volume responses in young J20-AD mice is neural hyperexcitability, suggesting that neurovascular function is preserved in these mice. A key finding from this study was that under normobaric hyperoxia, baseline blood saturation and volume is enhanced in all vascular compartments in the brain of J20-AD mice. This effect did not present under normoxia, with transition from hyperoxia to normoxia resulting in a large decrease of HbT/blood volume in J20-hAPP, but not WT mice. The enhancement of blood volume in normobaric hyperoxia may provide a time-dependent therapeutic strategy by driving enhanced paravascular clearance pathways in the brain. Future work should investigate the effect of regular normobaric hyperoxia on the levels of beta-amyloid in the J20-hAPP mouse.

3.6 – Materials & Methods

3.6.1 – Animals

All animal procedures were performed with approval from the UK Home Office in accordance to the guidelines and regulations of the Animal (Scientific Procedures) Act 1986, as well as being approved by the University of Sheffield ethical review and licensing committee. 6m old male wild-type (WT) C57BL/6J mice (n=8) and male heterozygous transgenic J20-hAPP B6.Cg-Zbtb20Tg(PDGFB-APPSwInd)20Lms/2Mmjax) (MMRRC Stock No: 34836-JAX | J20)

mice (n=9) were used. All mice were housed with littermates in a 12hr dark/light cycle at a temperature of 23C, with food and water supplied *ad-libitum*.

3.6.2 – Chronic Thinned Cranial Window Preparation

Mice were anaesthetised with 7ml/kg i.p. injection of fentanyl-fluanisone (Hypnorm, Vetapharm Ltd, UK), midazolam (Hypnovel, Roche Ltd, UK), diluted in sterile water in a 1:1:2 by volume ratio for surgery induction, and maintained in a surgical anaesthetic plane by inhalation of 0.5-0.8% isoflurane. Core body temperature was maintained at 36.5-37.0C through rectal temperature monitoring. Mice were placed in a stereotaxic frame (Kopf Instruments, US) and the scalp was excised. The bone overlying the right somatosensory cortex was thinned to translucency forming a thinned cranial optical window (measuring ~9mm^2). A thin layer of clear cyanoacrylate glue was applied over the cranial window to reduce specularities and to reinforce the window. Dental cement (Super Bond C&B, Sun Medical, Japan) was applied around the window to which a metal head-plate was chronically attached. WT mice were 5.85 months ±3.5 days at surgery, and J20 mice were 5.47 months ±5.4 days at surgery. All mice were given 2 weeks to recover before the first imaging session was performed.

3.6.3 – 2D-Optical Imaging Spectroscopy (2D-OIS)

2D-OIS measures changes in cortical haemodynamics by estimating changes in total haemoglobin (HbT), oxyhaemoglobin (HbO) and deoxyhaemoglobin (HbR) concentrations as described previously[38]. For the experimental session, mice were anaesthetised (as described above) and placed into a stereotaxic frame with heads fixed using attached headplates. Anaesthesia was maintained using low-levels of isoflurane (0.3-0.6%). For imaging, the right somatosensory cortex was illuminated using 4 different wavelengths of light appropriate to the absorption profiles of the differing haemoglobin states (495nm ± 31, 559nm ± 16, 575nm ± 14 & 587nm ± 9) using a Lambda DG-4 high-speed galvanometer (Sutter Instrument Company, US). A Dalsa 1M60 CCD camera with a frame rate of 32Hz operating in a 4x4 binning mode acquired images at 184x184 pixels; giving a pixel resolution of 75x75μm, was used to capture the re-emitted light from the cortical surface.

All spatial images recorded from the re-emitted light underwent spectral analysis based on the path length scaling algorithm (PLSA) as described previously[38,39], which uses a modified Beer-Lambert law with a path-length correction factor converting detected attenuation from the re-emitted light with a predicted absorption value. Relative HbT, HbR and HbO concentration estimates were generated from baseline values in which the concentration of haemoglobin in the tissue was assumed to be 100μM and O_2 saturation to be 70%. The spectral analysis

produced 2D-images of micromolar changes in volume of HbT, HbO & HbR over each stimulation period.

3.6.4 – Stimulation Paradigm & Experimental Overview

A mechanical whisker stimulation paradigm was used. Whiskers were mechanically deflected for a 2s duration and a 16s duration at 5Hz using a plastic T-shaped stimulator which caused a 1cm deflection of the left-whisker pad in the rostro-caudal direction. Each individual experiment consisted of 30 stimulation trials (for 2s) or 15 stimulation trials (for 16s) from which a mean trial was generated after spectral analysis of 2D-OIS (as described previously). Stimulations were performed in 100% O_2 (normobaric hyperoxia), a gas transition to medical air (normobaric normoxia; 21% O_2) as well as an additional 10% CO_2-hypercapnia test of vascular reactivity. The same set of experiments with the same timings were performed on all mice on all experimental days. 2-weeks post-surgery the 1st imaging session was performed with 2D-OIS alone (a chronic session as imaging was through an intact skull). 1-week after the 1st imaging session a 2nd terminal imaging session was performed in combination with neural electrophysiology.

3.6.5 – Neural Electrophysiology

In order to assess neurovascular function in its entirety, both haemodynamic and neural measures were obtained. Simultaneous measures of neural activity alongside 2D-OIS were performed in a final acute imaging session 1-week after the 1st imaging. A small burr-hole was drilled through the skull overlying the barrel cortex (as defined by the biggest HbT changes from 2D-OIS imaging) and a 16-channel microelectrode (100µm spacing, 1.5-2.7MΩ impedance, site area 177µm^2) (NeuroNexus Technologies, USA) was inserted into the whisker barrel cortex to a depth of ~1500µm. The microelectrode was connected to a TDT preamplifier and a TDT data acquisition device (Medusa BioAmp/RZ5, TDT, USA). All data collected was sampled at 24kHz and downsampled to 6kHz for analysis of multi-unit activity (MUA) and local-field potentials (LFPs).

3.6.6 – Region Analysis

Analysis was performed using MATLAB (MathWorks). An automated region of interest (ROI) was selected using the stimulation data from spatial maps generated using 2D-OIS. The threshold for a pixel to be included within the ROI was set at 1.5xSTD, therefore the automated ROI for each session per animal represents the area of the cortex with the largest haemodynamic response, as determined by the HbT. For each experiment, the response across all pixels within the ROI was averaged and used to generate a time-series of the haemodynamic response against time for HbT, HbO & HbR.

3.6.7 – Statistical Analysis

Statistical analyses were performed using GraphPad Prism v8. To compare haemodynamic & neural responses, statistical comparisons were made on HbT, HbO, HbR & MUA values using two-way repeated measures ANOVAs as well as 2-tailed unpaired t-tests. P-values <0.05 were considered statistically significant. All the data are presented as mean values ± standard error of mean (SEM), unless otherwise stated.

3.6.8 – Immunohistochemistry

At the end of terminal experiments, mice were euthanized with an overdose of pentobarbital (100mg/kg, Euthatal, Merial Animal Health Ltd) and transcardially perfused with 0.9% saline followed by 4% ice-cold paraformaldehyde (0.1M, pH7.4). Brains were dissected and embedded in paraffin wax. 5µm coronal sections were obtained using a cryostat. Immunohistochemistry was performed using an avidin-biotin complex (ABC) method (as described previously[6]). Briefly, sections were deparaffinised, rehydrated and quenched of endogenous peroxidase activity in 0.3% H_2O_2/methanol solution. Following antigen retrieval (pressure cooker at 20psi at 120C for 45s (pH6.5)) sections underwent additional pre-treatment in 70% formic acid. Sections were incubated with 1.5% normal serum followed by incubation with the primary antibody (biotinylated anti-Aβ – 1:100, BioLegend, USA) for 1 hour. Horseradish peroxidase avidin-biotin complex (Vectastain Elite Kit, Vector Laboratories, UK) was used to visualise antibody binding along with 3,3-diaminobenzidine tetrahydrochloride (DAB) (Vector Laboratories, UK). All sections were counterstained with haematoxylin, dehydrated and mounted in DPX. Sections were imaged using a Nikon Eclipse Ni-U microscope attached to a Nikon DS-Ri1 camera.

3.7 – Acknowledgments

We would like to thank Prof Lennart Mucke (Gladstone Institute of Neurological Disease & Department of Neurology, UCSF, CA, US) as well as the J. David Gladstone Institutes for the J20-hAPP mice. We wold like to thank Michael Port for building and maintaining the whisker stimulation device and 2D-OIS apparatus.

3.8 – Competing Interests

There are no competing interest do declare.

3.9 – Funding

Osman Shabir's PhD studentship and consumables were funded by the Neuroimaging in Cardiovascular Disease (NICAD) network scholarship (University of Sheffield). The J20-mouse colony was in part funded and supported by Alzheimer's Research UK (Grant R/153749-12-1). The remainder of the work was funded by Medical Research Council (MRC)

UK (Grant Number MR/M013553.1). Clare Howarth is funded by a Sir Henry Dale Fellowship jointly funded by the Wellcome Trust and the Royal Society (Grant Number 105586/Z/14/Z).

3.10 – References

1. Wright, A. L. *et al.* Neuroinflammation and Neuronal Loss Precede Aβ Plaque Deposition in the hAPP-J20 Mouse Model of Alzheimer's Disease. *PLoS One* (2013) doi:10.1371/journal.pone.0059586.
2. Ameen-Ali, K. E. *et al.* Review: Neuropathology and behavioural features of transgenic murine models of Alzheimer's disease. *Neuropathology and Applied Neurobiology* (2017) doi:10.1111/nan.12440.
3. Webster, S. J., Bachstetter, A. D., Nelson, P. T., Schmitt, F. A. & Van Eldik, L. J. Using mice to model Alzheimer's dementia: An overview of the clinical disease and the preclinical behavioral changes in 10 mouse models. *Front. Genet.* (2014) doi:10.3389/fgene.2014.00088.
4. Sengupta, U., Nilson, A. N. & Kayed, R. The Role of Amyloid-β Oligomers in Toxicity, Propagation, and Immunotherapy. *EBioMedicine* (2016) doi:10.1016/j.ebiom.2016.03.035.
5. Mucke, L. *et al.* High-level neuronal expression of Aβ(1-42) in wild-type human amyloid protein precursor transgenic mice: Synaptotoxicity without plaque formation. *J. Neurosci.* (2000) doi:10.1523/jneurosci.20-11-04050.2000.
6. Ameen-Ali, K. E. *et al.* The Time Course of Recognition Memory Impairment and Glial Pathology in the hAPP-J20 Mouse Model of Alzheimer's Disease. *J. Alzheimer's Dis.* (2019) doi:10.3233/JAD-181238.
7. Zlokovic, B. V. Neurovascular mechanisms of Alzheimer's neurodegeneration. *Trends in Neurosciences* (2005) doi:10.1016/j.tins.2005.02.001.
8. Zlokovic, B. V. Neurovascular pathways to neurodegeneration in Alzheimer's disease and other disorders. *Nature Reviews Neuroscience* (2011) doi:10.1038/nrn3114.
9. Iturria-Medina, Y. *et al.* Early role of vascular dysregulation on late-onset Alzheimer's disease based on multifactorial data-driven analysis. *Nat. Commun.* (2016) doi:10.1038/ncomms11934.
10. Sharp, P. S. *et al.* Neurovascular coupling preserved in a chronic mouse model of Alzheimer's disease: Methodology is critical. *J. Cereb. Blood Flow Metab.* **In Press**, (2019).
11. Lacoste, B., Tong, X. K., Lahjouji, K., Couture, R. & Hamel, E. Cognitive and cerebrovascular improvements following kinin B1 receptor blockade in Alzheimer's disease mice. *J. Neuroinflammation* (2013) doi:10.1186/1742-2094-10-57.
12. Ongali, B. *et al.* Angiotensin II type 1 receptor blocker losartan prevents and rescues cerebrovascular, neuropathological and cognitive deficits in an Alzheimer's disease model. *Neurobiol. Dis.* (2014) doi:10.1016/j.nbd.2014.04.018.
13. Royea, J., Zhang, L., Tong, X. K. & Hamel, E. Angiotensin IV receptors mediate the cognitive and cerebrovascular benefits of losartan in a mouse model of Alzheimer's disease. *J. Neurosci.* (2017) doi:10.1523/JNEUROSCI.0329-17.2017.
14. Kim, J. & Jeong, Y. Augmentation of sensory-evoked hemodynamic response in an early

alzheimer's disease mouse model. *J. Alzheimer's Dis.* (2013) doi:10.3233/JAD-121900.

15. Nedergaard, M. Garbage truck of the brain. *Science* (2013) doi:10.1126/science.1240514.
16. Aldea, R., Weller, R. O., Wilcock, D. M., Carare, R. O. & Richardson, G. Cerebrovascular smooth muscle cells as the drivers of intramural periarterial drainage of the brain. *Front. Aging Neurosci.* (2019) doi:10.3389/fnagi.2019.00001.
17. Shapira, R., Solomon, B., Efrati, S., Frenkel, D. & Ashery, U. Hyperbaric oxygen therapy ameliorates pathophysiology of 3xTg-AD mouse model by attenuating neuroinflammation. *Neurobiol. Aging* (2018) doi:10.1016/j.neurobiolaging.2017.10.007.
18. Palop, J. J. & Mucke, L. Network abnormalities and interneuron dysfunction in Alzheimer disease. *Nature Reviews Neuroscience* (2016) doi:10.1038/nrn.2016.141.
19. Ping, Y. *et al.* Linking Aβ42-Induced Hyperexcitability to Neurodegeneration, Learning and Motor Deficits, and a Shorter Lifespan in an Alzheimer's Model. *PLoS Genet.* (2015) doi:10.1371/journal.pgen.1005025.
20. Minkeviciene, R. *et al.* Amyloid β-induced neuronal hyperexcitability triggers progressive epilepsy. *J. Neurosci.* (2009) doi:10.1523/JNEUROSCI.5215-08.2009.
21. Palop, J. J. & Mucke, L. Amyloid-B-induced neuronal dysfunction in Alzheimer's disease: From synapses toward neural networks. *Nature Neuroscience* (2010) doi:10.1038/nn.2583.
22. Busche, M. A. *et al.* Critical role of soluble amyloid-β for early hippocampal hyperactivity in a mouse model of Alzheimer's disease. *Proc. Natl. Acad. Sci. U. S. A.* (2012) doi:10.1073/pnas.1206171109.
23. Palop, J. J. *et al.* Aberrant Excitatory Neuronal Activity and Compensatory Remodeling of Inhibitory Hippocampal Circuits in Mouse Models of Alzheimer's Disease. *Neuron* (2007) doi:10.1016/j.neuron.2007.07.025.
24. Lalonde, R., Fukuchi, K. I. & Strazielle, C. Neurologic and motor dysfunctions in APP transgenic mice. *Rev. Neurosci.* (2012) doi:10.1515/revneuro-2012-0041.
25. Kobayashi, D. *et al.* BACE1 gene deletion: Impact on behavioral function in a model of Alzheimer's disease. *Neurobiol. Aging* (2008) doi:10.1016/j.neurobiolaging.2007.01.002.
26. Sherzai, D., Losey, T., Vega, S. & Sherzai, A. Seizures and dementia in the elderly: Nationwide inpatient sample 1999-2008. *Epilepsy Behav.* (2014) doi:10.1016/j.yebeh.2014.04.015.
27. Vossel, K. A. *et al.* Seizures and epileptiform activity in the early stages of Alzheimer disease. *JAMA Neurol.* (2013) doi:10.1001/jamaneurol.2013.136.
28. Reyes-Marin, K. E. & Nuñez, A. Seizure susceptibility in the APP/PS1 mouse model of Alzheimer's disease and relationship with amyloid β plaques. *Brain Res.* **1677**, 93–100 (2017).
29. Maatuf, Y., Stern, E. A. & Slovin, H. Abnormal Population Responses in the Somatosensory Cortex of Alzheimer's Disease Model Mice. *Sci. Rep.* (2016) doi:10.1038/srep24560.
30. Hong, S. *et al.* Complement and microglia mediate early synapse loss in Alzheimer mouse models. *Science (80-.).* (2016) doi:10.1126/science.aad8373.
31. Eles, J. R., Vazquez, A. L., Kozai, T. D. Y. & Cui, X. T. In vivo imaging of neuronal calcium during electrode implantation: Spatial and temporal mapping of damage and recovery.

Biomaterials (2018) doi:10.1016/j.biomaterials.2018.04.043.

32. Piilgaard, H. & Lauritzen, M. Persistent increase in oxygen consumption and impaired neurovascular coupling after spreading depression in rat neocortex. *J. Cereb. Blood Flow Metab.* (2009) doi:10.1038/jcbfm.2009.73.
33. Chang, J. C. *et al.* Biphasic direct current shift, haemoglobin desaturation and neurovascular uncoupling in cortical spreading depression. *Brain* (2010) doi:10.1093/brain/awp338.
34. Knöpfel, T. Genetically encoded optical indicators for the analysis of neuronal circuits. *Nature Reviews Neuroscience* (2012) doi:10.1038/nrn3293.
35. Gao, Y. R. *et al.* Time to wake up: Studying neurovascular coupling and brain-wide circuit function in the un-anesthetized animal. *NeuroImage* (2017) doi:10.1016/j.neuroimage.2016.11.069.
36. Sharp, P. S. *et al.* Comparison of stimulus-evoked cerebral hemodynamics in the awake mouse and under a novel anesthetic regime. *Sci. Rep.* (2015) doi:10.1038/srep12621.
37. Hébert, F. *et al.* Cortical atrophy and hypoperfusion in a transgenic mouse model of Alzheimer's disease. *Neurobiol. Aging* (2013) doi:10.1016/j.neurobiolaging.2012.11.022.
38. Berwick, J. *et al.* Neurovascular coupling investigated with two-dimensional optical imaging spectroscopy in rat whisker barrel cortex. *Eur. J. Neurosci.* (2005) doi:10.1111/j.1460-9568.2005.04347.x.
39. Mayhew, J. *et al.* Spectroscopic analysis of changes in remitted illumination: The response to increased neural activity in brain. *Neuroimage* (1999) doi:10.1006/nimg.1999.0460.

3.11 – Supplemental Data

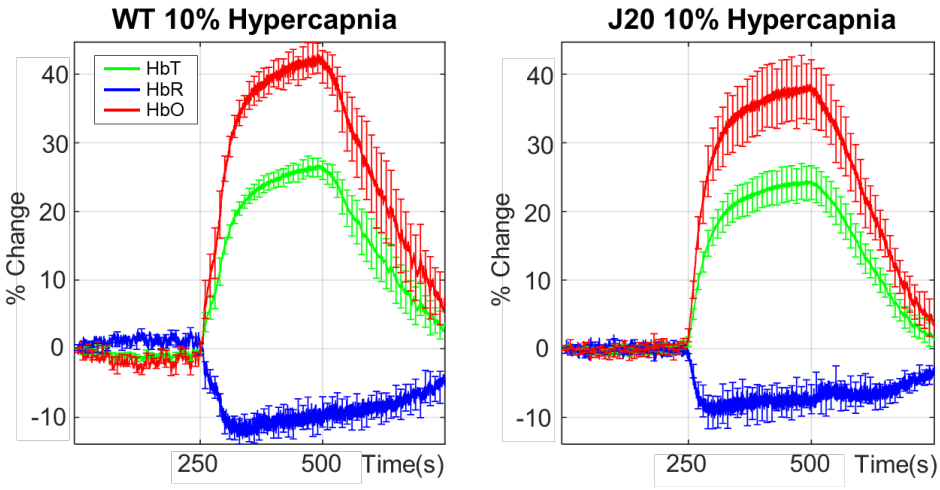

Figure 3.6(S) – 10% Hypercapnia Responses. Chronic data for WT (n=8) and J20-hAPP (n=9) hypercapnia responses showed no significant differences between groups. Hypercapnia was performed in 100% oxygen.

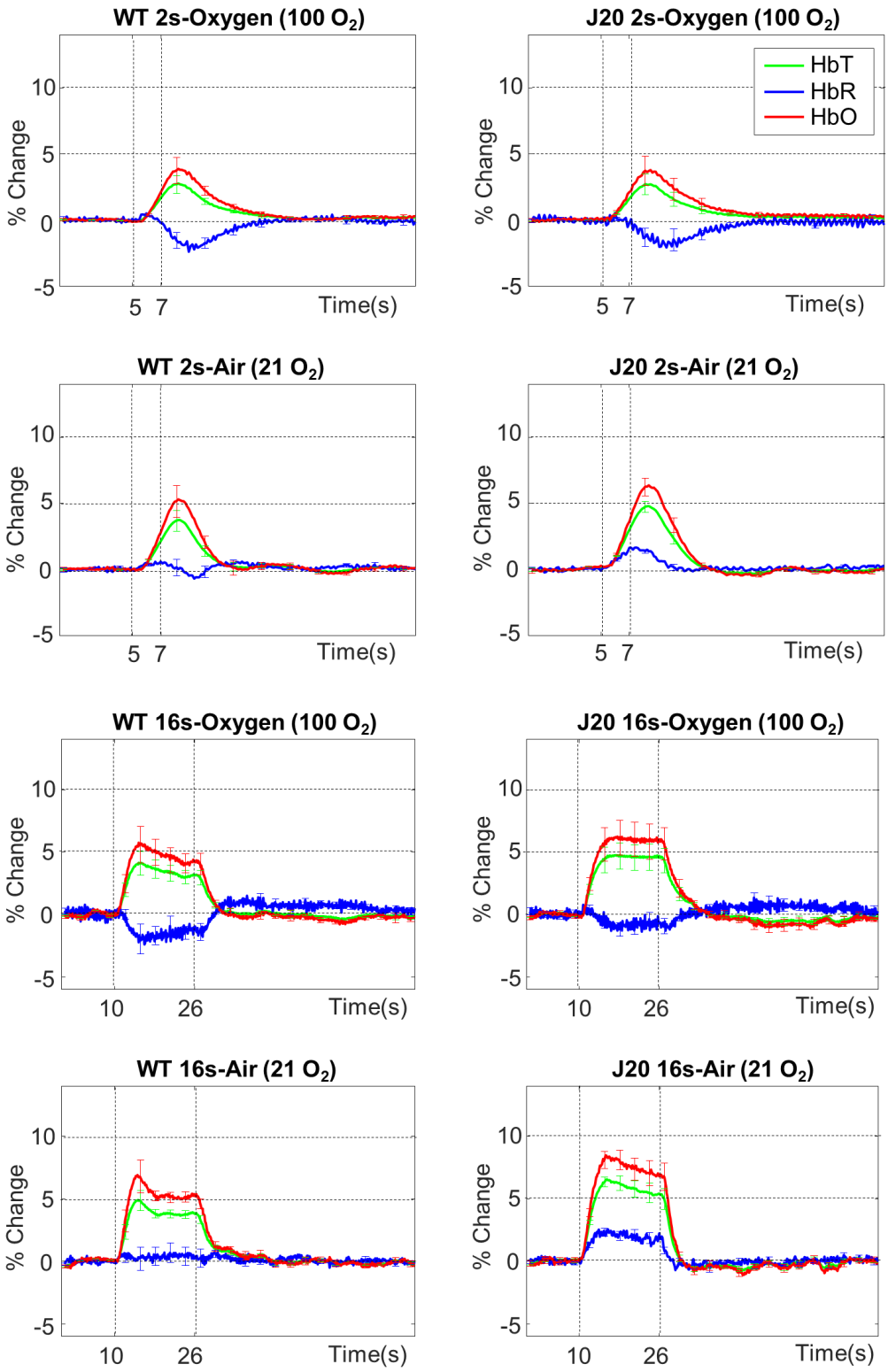

Figure 3.7(S) – Haemodynamic Responses During Acute Imaging Session (with Electrode Inserted). There are no significant differences in HbT between WT (n=6) and J20-hAPP (n=5). HbT/blood volume recovers in both groups as a result of time post-electrode insertion. Washout of HbR is impaired under 21% oxygen conditions in both WT and J20-hAPP mice.

Chapter 4 – Neurovascular Function in Experimental Models of Atherosclerosis (PCSK9), Alzheimer's Disease (J20-hAPP) and a Novel Mixed Comorbid Model (J20-PCSK9)

This chapter is a paper submitted to a mid-tier journal and is currently available as a preprint on bioRxiv (Shabir et al, 2020. bioRxiv. 10.1101/2020.08.13.249987)

4.1 – Paper Title and Authors

Assessment of Neurovascular Coupling & Cortical Spreading Depression in Mixed Models of Atherosclerosis & Alzheimer's Disease

Osman Shabir[1,2,4], Ben Pendry[3], Llywelyn Lee[1,2], Beth Eyre[1,2], Paul Sharp[1], Monica A Rebollar[2,3], Clare Howarth[1,2], Paul R Heath[2,3], Stephen B Wharton[2,3], Sheila E Francis[2,4,5†] & Jason Berwick[1,2,5†*]

[†]*Authors Contributed Equally.*

*Corresponding Author: Dr Jason Berwick, Sheffield Neurovascular Lab, Department of Psychology, The University of Sheffield, Alfred Denny Building, Western Bank, Sheffield, S10 2TN (United Kingdom). Email: j.berwick@sheffield.ac.uk Phone: (+44) 0114 222 6597

Author Affiliations:

[1]Sheffield Neurovascular Lab, Department of Psychology, University of Sheffield, Alfred Denny Building, Western Bank, Sheffield, S10 2TN (United Kingdom)

[2]Neuroscience Institute, University of Sheffield, Sheffield, S10 2TN (United Kingdom)

[3]Sheffield Institute for Translational Neuroscience (SITraN), University of Sheffield, 385a Glossop Road, Sheffield, S10 2HQ (United Kingdom)

[4]Department of Infection, Immunity & Cardiovascular Disease (IICD), University of Sheffield Medical School, Royal Hallamshire Hospital, Beech Hill Road, Sheffield, S10 2RX (United Kingdom)

[5]Healthy Lifespan Institute (HELSI), University of Sheffield, Sheffield, S10 2TN (United Kingdom)

Classification: Biological Sciences – Neuroscience

I, Osman Shabir, am the sole author of the manuscript. I performed the majority of *in vivo* experiments. Ben Pendry performed some of the histological and genetic experiments under my supervision and training. Monica Rebollar helped with training Ben and analysis. I performed qPCR. Paul Heath helped with qPCR. Llywelyn Lee & Beth Eyre performed some *in vivo* experiments (4 & 1 animals respectively). Clare Howarth helped with data analysis using SPSS due to the complex datasets. Jason Berwick helped with MATLAB data analysis & figure generation. Clare Howarth, Stephen Wharton, Sheila Francis and Jason Berwick proofread and helped edit the manuscript.

4.2 – Abstract

Neurovascular coupling is a critical brain mechanism whereby changes to blood flow accompany localised neural activity. The breakdown of neurovascular coupling is linked to the development and progression of several neurological conditions including dementia. However, experimental data commonly arise from preclinical models in young mice with one disease only. In this study, we examined cortical haemodynamics in preparations that modelled common co-existing conditions namely Alzheimer's disease (J20-AD) combined with atherosclerosis (PCSK9-ATH) between 9-12m of age. We report novel findings with atherosclerosis where neurovascular decline is characterised by significantly reduced blood volume (HbT), levels of oxyhaemoglobin (HbO) & deoxyhaemoglobin (HbR), in addition to global neuroinflammation. In the comorbid mixed model (J20-PCSK9-MIX), we report a highly significant increase (3x fold) in hippocampal amyloid-beta plaques, without any further alterations to neurovascular function. There were no significant changes in evoked neural activity in any of the disease models, suggesting a breakdown of neurovascular coupling in PCSK9-ATH mice with inadequate oxygen delivery. A key finding was that cortical spreading depression (CSD) due to electrode insertion into the brain was worse in the diseased animals and led to a prolonged period of hypoxia and potentially ischaemia. The inflammatory environment in the brain was also perturbed, with interleukin-1 beta raised up to 2-fold and tumour necrosis factor raised up to 7-fold in brain tissues from these mice. Taken together, these findings suggest that systemic atherosclerosis can be detrimental to neurovascular health and that having cardiovascular comorbidities can exacerbate pre-existing Alzheimer's-related amyloid-plaques.

4.3 – Significance Statement

The development of therapies for dementia is one of the biggest scientific priorities as many amyloid-targeting treatments have failed clinical trials in the past, and to date, we have no disease modifying therapies. Understanding the different disease mechanisms involved in the onset of dementia is important if therapies are to succeed. Evidence has pointed to vascular dysfunction as a key potential mechanism involved in dementia onset and many preclinical studies have highlighted the role of impaired neurovascular coupling in such models. In this study we report novel findings with respect to neurovascular dysfunction in disease models, as well as describing how brain state plays a role in worsened outcomes of brain injury and migraine in the context of dementia onset.

4.4 – Key Words

Neurovascular coupling, atherosclerosis, Alzheimer's disease, CSD, comorbid

4.5 – Author Contributions

OS performed the majority of the *in vivo* experiments and authored the manuscript. OS & JB designed the experiments. OS, BP, LL, BE, PS & MAR performed experiments. OS, CH & JB performed data analysis. JB, SEF, CH, PRH & SBW supervised the research and provided editorial guidance. All authors proofread the final version of the manuscript.

4.6 – Introduction

Neurovascular coupling (NVC) is the neurophysiological process that ensures active regions of the brain receive an increased local cerebral blood flow (CBF) to match the metabolic demands neuronal activity exerts. Cell types including neurons, astrocytes, endothelial cells, vascular smooth muscle cells, and pericytes are involved in the facilitation of NVC during which local blood vessels dilate (1). The vasodilation of cerebral arterioles causes an influx of oxygenated blood (HbO) coupled to a decrease in deoxyhaemoglobin (HbR), that is the source of the blood-oxygen-level-dependent (BOLD) fMRI signal (2, 3). The breakdown of NVC is thought to be an important and early pathogenic mechanism in the onset and progression of a range of neurological conditions (4).

Alzheimer's disease (AD) is the most common form of dementia worldwide, with the vast majority of cases being sporadic and occurring 65 years and over. Population based studies have shown that AD and vascular pathologies commonly coexist in the brains of elderly individuals (5-8). A major cardiovascular pathology that affects as many as up to 60% of all individuals after the age of 55 is atherosclerosis. Atherosclerosis is the progressive thickening, hardening and narrowing of major arteries, including those that supply the brain, such as the carotids (9). Intracranial atherosclerosis does not occur until much later in life, around 75 years and above. As such, Alzheimer's disease that begins around the 8th decade of life is usually present with other comorbidities such as atherosclerosis (10). There is also evidence that, not only do these often exist as comorbidities, but they may interact pathogenically with vascular disease and neurovascular unit changes contributing to AD (11, 12). To date, there are very limited models of comorbidity with respect to preclinical studies, and instead models have been very specific and 'pure', and not reflective of the clinical pathology in humans. Atherosclerosis is known to be a major risk factor for the development of dementia. The progressive atheromatous plaque build-up within cerebral arteries that supply the cortex over time can lead to stenosis producing insufficient oxygen delivery to the brain parenchyma, potentially resulting in neuronal death and symptoms of dementia (1). Indeed, the vascular cognitive impairment (VCI) which precedes the onset of dementia may be attributed to a variety of different vascular pathologies affecting either systemic or intracranial vasculature (both large or small vessels) (13). Due to the complexity of atherosclerosis and dementia

pathogenesis, understanding the mechanisms of their mutual interactions is necessary if efforts to develop therapeutics to prevent VCI and vascular dementia, which currently has no disease-modifying cure, are to succeed.

In the present study, we aimed to investigate neurovascular function in mid-aged (9-12m old) mice where atherosclerosis was a comorbidity. We used a novel model of atherosclerosis that utilises a single adeno-associated virus (AAV) i.v. injection of a gain of function mutation (D377Y) to proprotein convertase subtilisin/kexin type 9 (rAAV8-mPCSK9-D377Y), combined with a high-fat Western diet to induce atherosclerosis in most adult mouse strains (14, 15). This leads to the constitutively active inhibition of the LDL-receptor preventing cholesterol internalisation and degradation by hepatocytes, leading to hypercholesterolaemia to occur and the development of robust atherosclerotic lesions within 6-8 weeks (14). Furthermore, in order to address the effect atherosclerosis could have on mild Alzheimer's pathology, we combined the atherosclerosis with the mild J20-hAPP mouse model of familial Alzheimer's disease (fAD) to create a mixed comorbid mouse model (J20-PCSK9-MIX). The J20-hAPP mouse model of fAD over-expresses human amyloid precursor protein (hAPP) with the Swedish (K670N and M671L) and the Indiana (V7171F) familial mutations (16), which begin to develop amyloid-beta (Aβ) plaques around 5-6 months of age, and show signs of cognitive impairments from 4 months (17). We hypothesised that atherosclerosis would exacerbate Alzheimer's disease pathology in the brain and that neurovascular function would be further worsened compared to AD or ATH models alone. We have previously reported no significant alterations to evoked-haemodynamics in the J20-AD model of the same age (9-12m); however, under acute imaging sessions where an electrode was inserted into the brain, we found significantly perturbed haemodynamics (18). We hypothesised that electrode insertion causes cortical spreading depression (CSD). Based on recent data linking migraine with aura with cardiovascular disease (19), we hypothesised that experimental CSD might be heightened in all disease models. We report that experimentally induced atherosclerosis in the J20-AD model increased the number of Aβ plaques by 300%. Furthermore, experimental CSD is more severe in all diseased groups compared to WT controls.

4.7 – Results

4.7.1 – 2D-Optical Imaging Spectroscopy (2D-OIS) Measures Brain Cortical Haemodynamics Through a Thinned Cranial Window

We performed chronic imaging of the brain cortex 3-weeks post-surgery, where the thinned cranial window remained intact (***Figure 4.1A/B***), as described previously (18, 20). We deployed a range of stimulations (2s & 16s mechanical whisker stimulations) with the mouse breathing both 100% oxygen (hyperoxia) and 21% oxygen (normoxia), in addition to recording

transitions between conditions and performing a 10% hypercapnia test to test the maximum dilation of vessels. Each experimental day consisted of the same set of experiments with consistent timings to ensure reliability across all animal groups. First, a 2s-whisker stimulation (5Hz) with the mouse breathing 100% oxygen; hyperoxia, consisting of 30 trials, second, a 16s-whisker stimulation consisting of 15 trials. Animals were then transitioned from hyperoxia to 21% oxygen; normoxia, and the baseline haemodynamic changes were recorded. The same set of stimulations were deployed under normoxia (2s & 16s stimulations), before transitioning back to hyperoxia for a final 10% hypercapnia test. Using these stimulations, activation maps of blood volume; total haemoglobin (HbT), can be generated (***Figure 4.1C***). Mice were allowed to recover and after 1-week, a final acute imaging session was performed. In this setup, a small burr-hole was drilled through the thinned skull overlying the active region of interest (ROI) as determined from the chronic imaging sessions (***Figure 4.1D***), and a multichannel electrode was inserted into the brain (***Figure 4.1E***) to record neural activity simultaneously. We then imaged and recorded the baseline haemodynamics for a 35-minute period to observe the effect electrode insertion, before commencing the first stimulation. This was also done to record baselines on chronic imaging sessions.

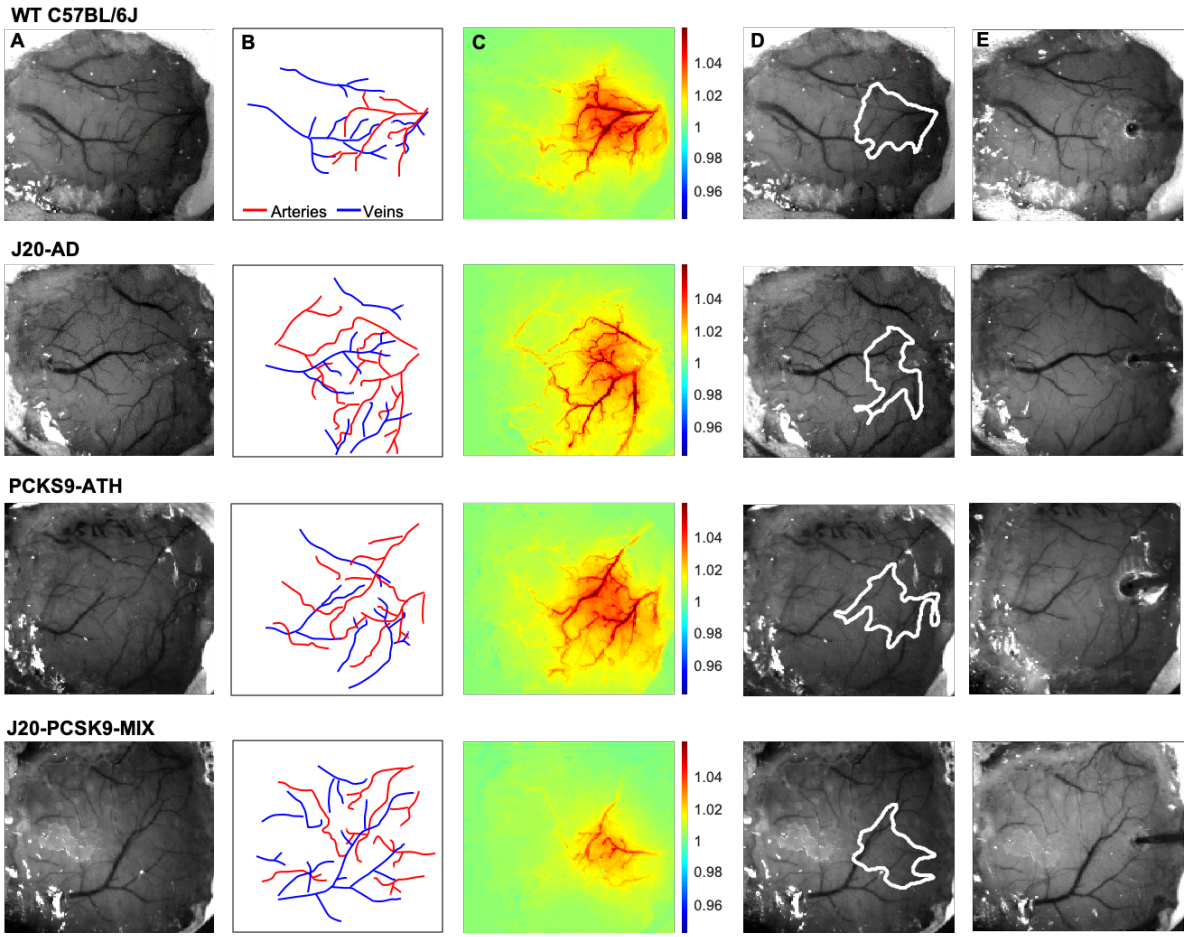

Figure 4.1 – Experimental Setup and Data Derivation. A) Raw image of representative thinned cranial windows for WT, J20-AD, PCKS9-ATH AND J20-PCSK9-MIX mice (chronic imaging session). B) Vessel map outlining the major arteries and veins within the thinned cranial window. C) HbT spatial activation map showing fractional changes in HbT in response to a 16s-whisker stimulation. D) Automated computer-generated region of interest (ROI) determined from the HbT activation response in C from which time-series for HbT, HbO & HbR are generated. E) Raw image of the same animals in terminal acute imaging sessions with multichannel electrodes inserted into the active ROI determined from chronic imaging session.

4.7.2 – Chronic Haemodynamic Responses in the Brain are Reduced in PCSK9-ATH Mice.

Cortical haemodynamics were imaged through a thinned cranial window to determine whether evoked cortical haemodynamics were different between 9-12m old wild-type (WT), atherosclerotic (PCSK9-ATH), Alzheimer's (J20-AD) & mixed (J20-PCSK9-MIX) mouse models (***Figure 4.2***). Across all stimulations and conditions, ATH-PCSK9 mice displayed a significant reduction of evoked blood volume responses (HbT; peak value) compared to WT controls. J20-AD mice and J20-PCSK9-MIX mice did not exhibit a significant change in HbT across all stimulation conditions compared to WT mice. Evoked HbT responses; although initially are smaller in J20-PCSK9-MIX mice, recovered to match that of J20-AD mice later in the experimental protocol under normoxia (***Figure 4.2D***). Levels of oxyhaemoglobin (HbO) were significantly reduced in PCSK9-ATH mice but showed a reduced trend in J20-PCSK9-MIX mice too. The washout of deoxyhaemoglobin (HbR) was significantly reduced in PCSK9-ATH mice compared to WT, but also showed a reduced trend across all diseased groups across all conditions compared to WT mice. All mice displayed stable and robust haemodynamic responses across the experimental protocol (***Figure 4.7***). Finally, vascular reactivity as determined by the response to 10% hypercapnia was not significantly different between any of the diseased groups (***Figure 4.8).***

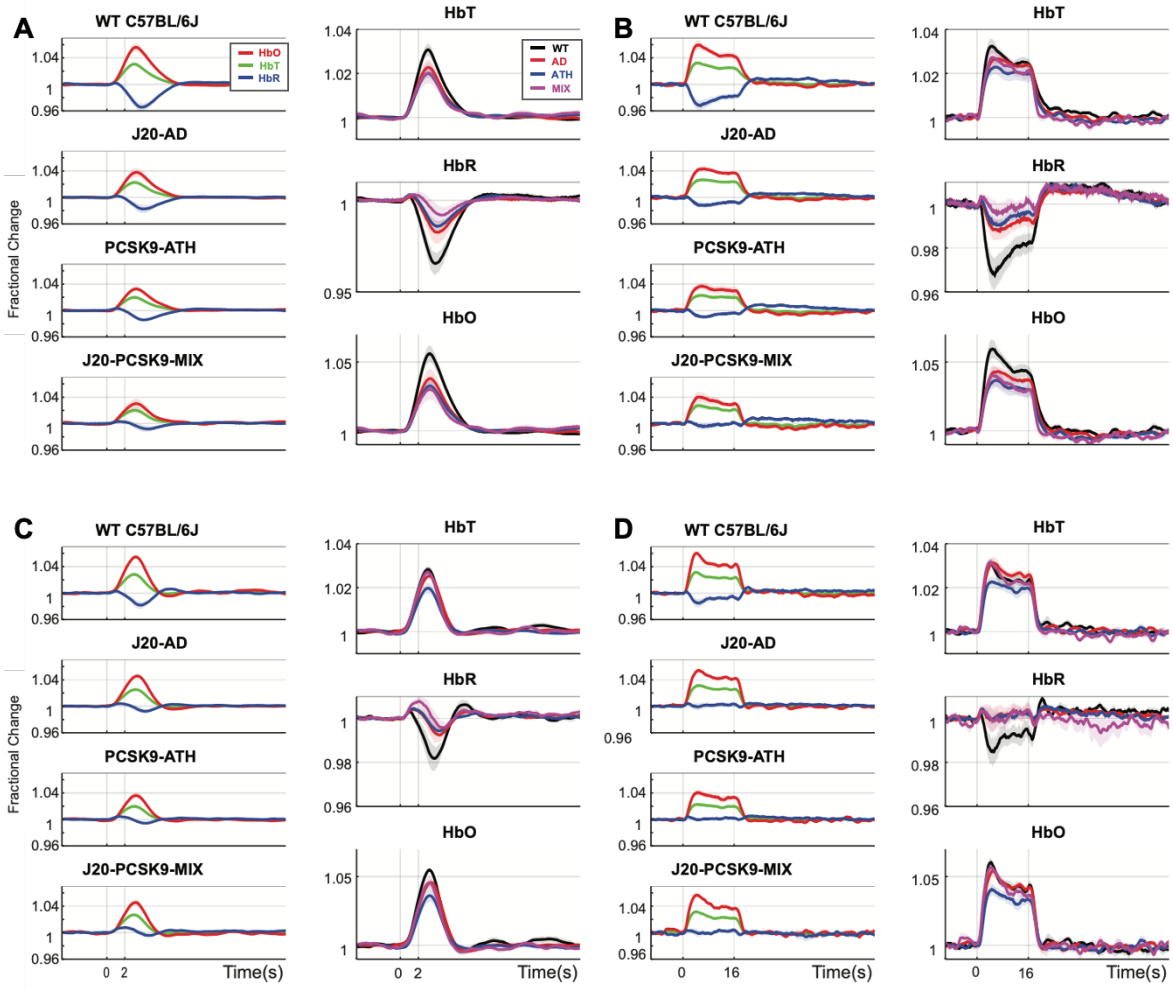

Figure 4.2 – Fractional Changes in Chronic Stimulus-Evoked (Peak) Haemodynamic Responses. A) 2s-stimulation in 100% oxygen. B) 16-stimulation in 100% oxygen. C) 2s-stimulation in 21% oxygen. D) 16s-stimulation in 21% oxygen. All animals aged 9-12m: WT (n=6), J20-AD (n=9), PCSK9-ATH (n=8), J20-PCSK9-MIX (n=6). **HbT:** There was no significant overall effect of disease $F(3,25)=2.83$, $p=0.059$. However, Dunnett's (two-sided) multiple comparisons test revealed there was a significant difference between WT and ATH ($p=0.023$). As expected, there was a significant effect of experiment, $F(1.65,41.14)=13.64$, $p<0.001$. There was also no significant interaction effect between experiment and disease, $F(4.94,41.14)=1.50$, $p=0.211$. **HbO:** There was a significant overall effect of disease $F(3,25)=4.84$, $p=0.009$. Dunnett's (two-sided) multiple comparisons test revealed there was a significant difference between WT and ATH ($p= 0.002$). There was a significant effect of experiment, $F(1.47,36.72)=15.348$, $p<0.001$. There was no significant interaction effect between experiment and disease, $F(4.41,36.72)=1.64$,$p=0.181$. **HbR:** There was a significant overall effect of disease $F(3,25)=4.86$, $p=0.008$. Games-Howell multiple comparisons reveal HbR peak is significantly different for WT vs ATH ($p=0.040$). There was a significant effect of experiment, $F(1.69,42.28)=17.33$, $p<0.001$. There was a significant interaction between experiment and disease interaction: $F(5.07, 42.28)=3.19$, $p=0.015$. All error bars (lightly shaded) are ±SEM. Vertical dotted lines indicate start and end of stimulations.

4.7.3 – CSD is Worse in Diseased Animals and Impacts Haemodynamic Recovery to Baseline

1-week after recovery from the chronic imaging protocol, an acute imaging experiment was performed wherein a small-burr hole was drilled into the skull overlying the active region (determined from HbT responses from chronic experiments) and a microelectrode was inserted into the brain to a depth of 1500-1600μm to obtain neural electrophysiology data in combination with the imaging of cortical haemodynamics by 2D-OIS. Electrode insertion into the brain resulted in a wave of haemodynamic changes that occurred in all mice (CSD) (***Figure 4.3***). In WT mice, electrode insertion led to a small decrease in HbT (vasoconstriction) followed by a robust HbT bounce back (vasodilation), immediately followed by a small sustained vasoconstriction (reduced HbT) that persisted for some time (***Figure 4.3A-top***). In J20-AD mice, electrode insertion caused a large vasoconstriction to occur which spread across the cortex in a strong wave of vasoconstriction that was followed by a very small attempted recovery. This was masked by a large sustained and prolonged vasoconstriction of contiguous vessels that persisted for some time (***Figure 4.3A-bottom***). The largest vasoconstriction post-CSD occurred in J20-AD mice, followed by PCSK9-ATH mice, then J20-PCSK9-MIX mice compared to WT controls. The smallest of all CSD occurred in WT mice (***Figure 4.3B***). A prolonged and sustained constriction below baseline persisted in all mice post-CSD, however, this effect was recovered to baseline in WT mice during the first stimulation experiment 35 minutes after the CSD occurred (***Figure 4.3B***). In all disease mouse models, the constriction below baseline was more severe and persisted for a much longer time with a slower haemodynamic recovery. Following CSD, stimulation-evoked haemodynamic changes were not significantly different in any of the diseased groups overall, although they were initially smaller in the first two stimulations for PCSK9-ATH mice (***Figure 4.6***).

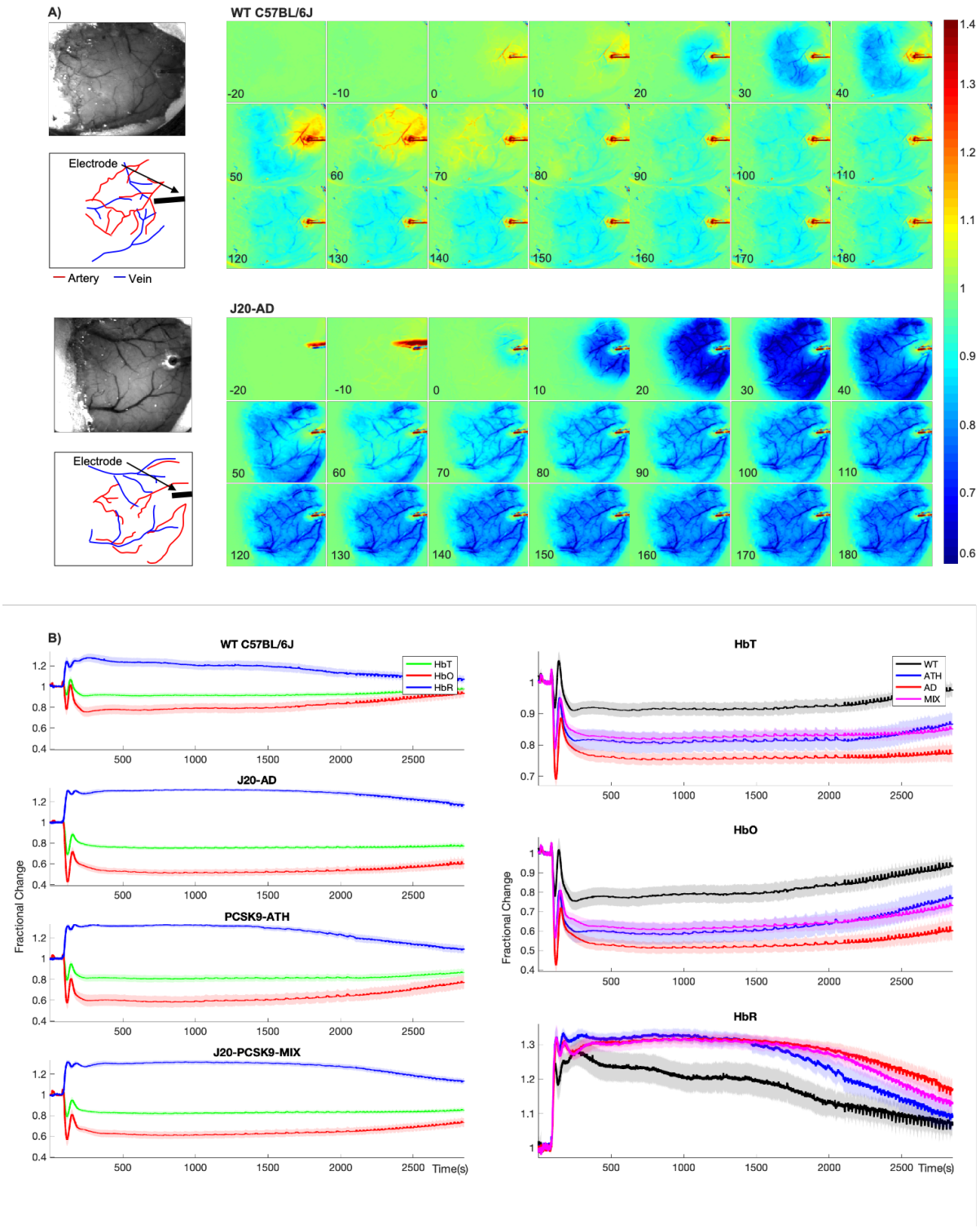

Figure 4.3 – Cortical Spreading Depression (CSD) in WT, diseased and comorbid animals. A) Representative montage time-series of WT and J20-AD mice showing HbT changes post-electrode insertion. Colour bar represents fractional changes in HbT from baseline. B) Left: Average CSD haemodynamics profiles for control animals (WT C57BL/6J & nNOS-ChR2) (n=7), J20-AD (n=7), PCSK9-ATH (n=5) & J20-PCSK9-MIX (n=6) mice. Right: Averaged changes to HbT (top), HbO (middle) & HbR (bottom) upon CSD in the different mouse groups compared to WT. [cont.]

[cont.] **HbT:** A 1-way ANOVA showed significant effect of disease for HbT ($F(3,21)=9.62$, $p=0.001$. Dunnett's 2-sided multiple comparisons showed that AD vs WT $p<0.001$, ATH vs WT $p=0.012$ & MIX vs WT $p=0.020$. **HbO:** 1-way ANOVA showed significant effect of disease for HbO ($F(3,21)=8.51$, $p<0.001$. Dunnett's 2-sided multiple comparisons showed that AD vs WT $p<0.001$, ATH vs WT $p=0.01$ & MIX vs WT $p=0.017$. **HbR:** Kruskal-Wallis test revealed no significant effect of disease $H(3)=6.58$, $p=0.087$. All error bars (lightly shaded) are ±SEM.

4.7.4 – Stimulus-Evoked Neural Activity is Not Significantly Altered in Any Disease Groups Compared to WT Mice

In the final imaging session and after a 35-minute period of recovery post-electrode insertion, the first experimental stimulation was performed (2s-stimulation in 100% oxygen) where evoked cortical haemodynamics were imaged simultaneously with the recording of neural multi-unit activity (MUA). Evoked-MUA response were not significantly different in any of the diseased groups compared to WT mice (***Figure 4.4***), suggesting that the significantly different evoked-HbT in PCSK9-ATH mice (observed on chronic imaging sessions) was due to neurovascular breakdown. Initially, the MUA was slightly lower for J20-AD, PCSK9-ATH & J20-PCSK9-MIX mice compared to WT mice (***Figure 4.4A***), however, later in the experimental session by the last stimulation, there was no observable difference in MUA between any of the groups (***Figure 4.4D***). Thus, this suggests that the neural MUA was initially smaller after the CSD had occurred, however, recovered fully with time. The haemodynamic responses in the acute experimental session were not significantly different across all stimulations for any of the diseased groups (***Figure 4.6***).

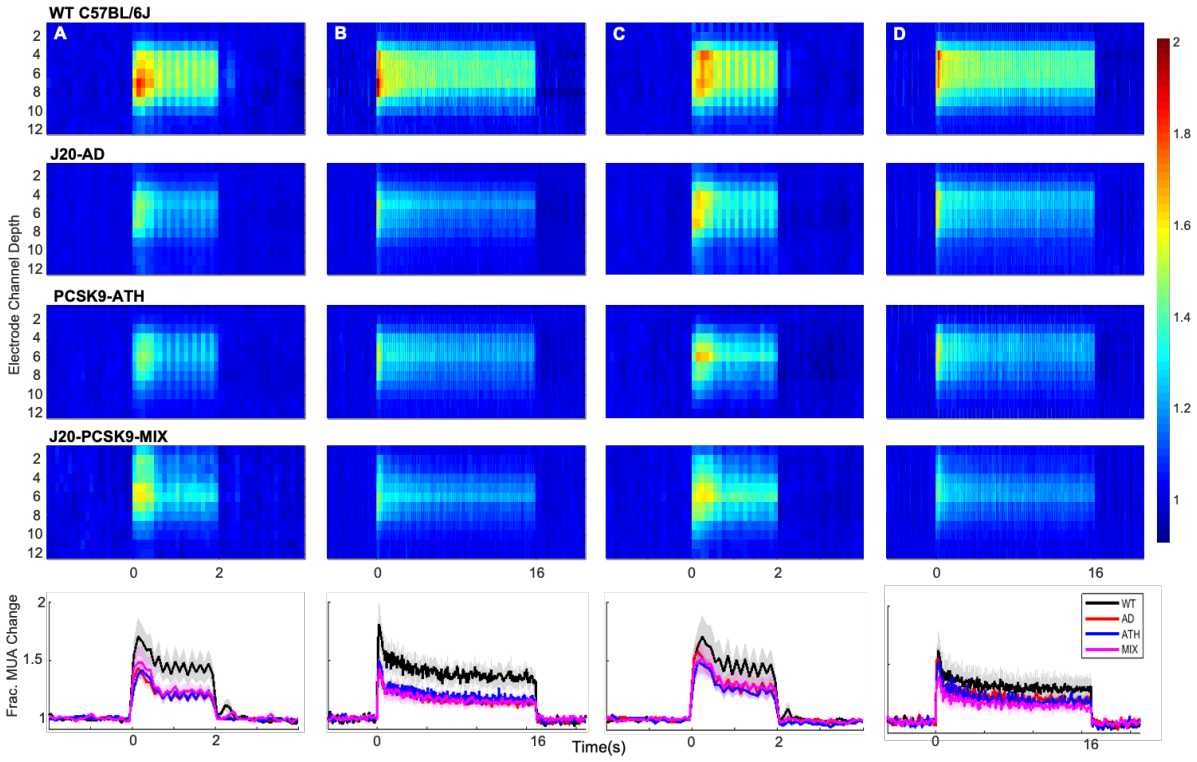

Figure 4.4 – Evoked Neural Multi-Unit Activity (MUA) Responses. MUA heat maps showing fractional changes in MUA along the depth of the cortex (channels 4-8) in response to stimulations in WT C57BL/6J (n=6), J20-AD (n=9), PCSK9-ATH (n=7) & J20-PCSK9-MIX (n=6) mice. Overall effect of disease on MUA $F(3,24)=2.24$, $p=0.109$ (2-way mixed design ANOVA). There was a significant effect of experiment, as expected, $F(2.26, 54.16)=6.83$, $p=0.002$. There was no significant interaction between experiment and disease $F(6.77, 54.16)=0.70$, $p=0.670$. All error bars (lightly shaded) are ±SEM.

4.7.5 – Increased Number of Hippocampal Aβ Plaques in J20-PCSK9-MIX Mice. Increased Neuroinflammation in J20-AD and PCSK9-ATH Mice

Immunohistochemistry was performed on J20-AD and J20-PCSJK9-MIX mice to assess whether there were any specific differences in AD neuropathology changes. Staining was performed for Aβ plaques and these were quantified within the hippocampus and the cortex. Aβ plaques were significantly increased by 3-fold in the hippocampi of J20-PCSK9-MIX mice compared to J20-AD mice (***Figure 4.5A/B***). Within the cortex, there was no significant difference in Aβ plaques between the 2 groups (***Figure S7***). Next, neuroinflammation was assessed by qRT-PCR for 2 key inflammatory markers: interleukin-1β (IL1β) and tumour necrosis factor-α (TNFα) to assess the degree of neuroinflammation present globally within the brain. IL1β mRNA was significantly upregulated in J20-AD and PCSK9-ATH mice (***Figure 4.5C***). TNFα mRNA was significantly upregulated in PCSK9-ATH mice only (***Figure 4.5D***). J20-PCSK9-MIX mice displayed the lowest inflammatory changes in IL1β & TNFα compared to the other diseased groups, though this was still higher than WT mice.

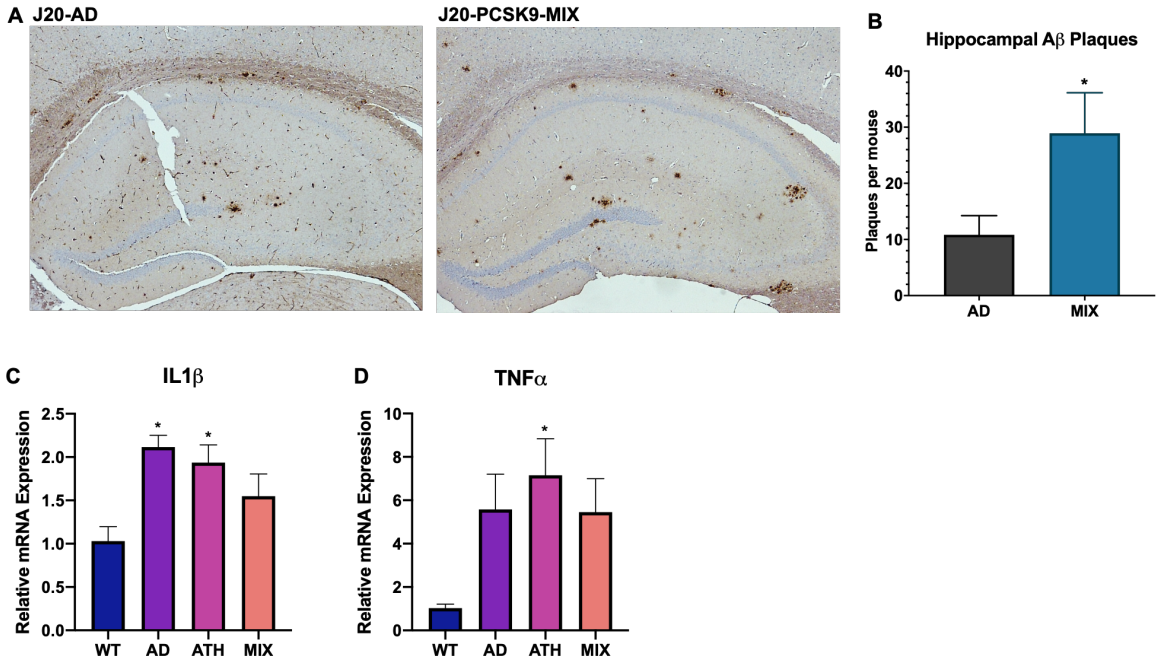

Figure 4.5 – Neuropathology and Neuroinflammation. A) Representative histological coronal hippocampal sections for J20-AD and J20-PCSK9-MIX mice stained with anti-Aβ to visualise Aβ plaques. B) Increased number of amyloid-beta plaques in the hippocampus of J20-PCSK9-MIX mice compared to J20-AD mice (p=0.036; unpaired t-test) (n=4 each). Cortical plaques p=0.3372 (data not shown). D) qRT-PCR for 1L1β: AD vs WT p=0.011, ATH vs WT p=0.0278, MIX vs WT p=0.218 (1-way ANOVA with post-hoc Dunnett's multiple comparisons test). E) qRT-PCR for TNFα: AD vs WT p=0.1197, ATH vs WT p=0.0370, MIX vs WT p=0.1313 with post-hoc Dunnett's multiple comparisons test. All error bars are ±SEM.

4.8 – Discussion

The present study investigated neurovascular function in a novel experimental model of ATH (PCSK9-ATH) and for the first time, in a comorbid setting whereby ATH was experimentally induced in a well characterised model of AD; J20-hAPP(Sw,Ind), to create a mixed comorbid model (J20-PCSK9-MIX). These mice were compared to age-matched (9-12m) WT C57BL/6J controls, and J20-AD mice. Given that systemic ATH is a major risk factor for dementia, the mechanisms underpinning the relationship between ATH, neurovascular decline and dementia are still largely unclear. In the study, we utilised a chronic mouse preparation to image cortical haemodynamics through an intact skull surface, followed by an acute terminal imaging session where the skull was drilled, and the brain penetrated with a multichannel electrode. In our experimental paradigm, we deployed a range of stimulations (both short 2s and long 16s durations) and different respiratory conditions (hyperoxia & normoxia) to assess neurovascular coupling to mechanical whisker stimulations, in addition to measuring neural activity within the active region defined from the chronic imaging.

In the first part of the study, we characterised evoked-haemodynamic responses using a chronic skull-intact & surgery-recovered mouse preparation. We found that PCSK9-ATH mice displayed significantly reduced evoked blood volume (HbT) responses, in addition to reduced levels of oxyhaemoglobin (HbO) and notably, an impaired washout of deoxyhaemoglobin (HbR) across all stimulations and conditions. The J20-PCSK9-MIX mice did not display a significant reduction in HbT, nor in HbO or HbR levels. With respect to J20-AD mice, we did not observe any significant alterations to HbT as previously published (18). Another important finding from the present study was that 10%-hypercapnia responses were not significantly different in any of the mice compared to WT controls (***Figure 4.8***), thus suggesting that vascular reactivity was not impaired in any of the mice, indicating that cerebral arterioles were unaffected by atherosclerosis at this time-point (9-12m). Thus, the basis of reduced HbT in PCSK9-ATH mice cannot be attributed to intracranial atherosclerosis. Previous work examining experimental atherosclerosis in the $ApoE^{-/-}$ model of ATH only showed extravascular lipid pools in large ventricle-associated and parenchymal blood vessels (21). Other work has found hypercapnia differences in the $ApoE^{-/-}$ model (22), however, this may be due to the severity differences in the mouse models where $ApoE^{-/-}$ is more severe compared to PCSK9-mice which resemble more closely the milder and more 'human-like' $LDLR^{-/-}$ model.

In the second part of the study, we obtained neural multi-unit activity (MUA) by inserting a multichannel electrode into the active region defined from the chronic imaging experiments. In order to do this, we carefully drilled a small burr-hole without penetrating the dura, followed by

a gentle insertion of the electrode into the brain whilst simultaneously recording the baseline haemodynamics by 2D-OIS. As we showed in our previous reports (18, 20), the technical procedure of electrode insertion causes a cortical spreading depression (CSD) to occur in all animals. Here, we describe the CSD and its recovery on the different disease groups. CSD has two distinct phases: 1) a wave of depolarisation within the grey matter characterised by neuronal distortion leading to a large change of the membrane potential whereby neuronal activity is silenced (spreading depression) & 2) haemodynamic changes that accompany neuronal spreading depolarisation which typically result in a wave of prolonged reduced perfusion that persists for some time (23, 24). CSD does not typically occur in healthy brain tissue, however, it is a common neurophysiological occurrence in certain pathological conditions including migraine, epilepsy, brain injury, hyperthermia, chemically induced neurotoxicity, hypoxia & ischaemia (24). In WT mice, the initial constriction wave is small, and a robust haemodynamic recovery occurs which allows for neurovascular coupling to occur to sustain neurons metabolically. Although WT mice exhibit a slight constriction below baseline, levels of HbO and HbR are not greatly affected, thus suggesting that CSD in WT mice does not result in severe hypoxia or ischaemia. This is a marked difference to the diseased animals, which upon electrode insertion to cause a CSD, exhibit profound vasoconstriction with an extremely limited haemodynamic recovery resulting in a prolonged constriction, severe reductions to blood volume and HbO & HbR levels indicating profound hypoxia and ischaemia. Thus, the haemodynamic response to CSD in diseased mice is severely inappropriate and can lead to long lasting devastating effects such as widespread cortical pannecrosis of neurons and astrocytes (24). As our data shows, baseline blood volumes do not recover in the diseased animals for a much longer period compared to WT animals, with the most profound CSD occurring in J20-AD mice, followed by PCSK9-ATH mice. The least severe CSD of the disease groups occurs in the J20-PCSK9-MIX animals. This surprising effect may be related to the levels of neuroinflammation within the brain (see below).

CSD is a reflection of whole brain state and disease burden effects, such as global neuroinflammation and in relation to certain pathologies including migraines or TBI, especially in the context of pre-existing disease (24). CSD may be the neuropathological link between migraine, stroke, cardiovascular disease and dementia in which cardiovascular risk factors, genetics and other lifestyle factors which prime the onset of migraine to occur lead to vascular vulnerability within the brain predisposing affected individuals to an increased risk of cerebral ischaemia and haemorrhagic stroke (25). There is accumulating evidence to suggest that shared genetic and associated clinical features observed in migraine patients are involved in the increased vulnerability to cerebral ischaemia, therefore, predisposing affected individuals to stroke and white matter lesions associated with dementia (26). The underlying mechanism

being CSD; the neurophysiological feature of aura in migraines, whose induction threshold can be reduced by genetic mutations and systemic comorbidities that contribute to vascular dysfunction and neuroinflammation (26). Indeed, mouse models of cerebral autosomal dominant arteriopathy with subcortical infarcts and leukoencephalopathy syndrome (CADASIL); a genetic cerebrovascular disease caused by *NOTCH3* mutations that has a high frequency of migraines with aura, have enhanced CSD linking a dysfunctional neurovascular unit with migraine with aura (27). Furthermore, a recent study examined women who suffered from migraines with and without aura and found that those that suffered migraines with aura had a higher incidence rate of cardiovascular disease compared to women without aura or any migraines (19). In addition, another recent study found that migraine history was positively associated with an increased risk of developing both all-cause dementia and AD, but not VaD (28). Our study, along with the previously discussed studies provide an explanation for these recent findings and highlights how systemic disease can prime the brain to allow profound CSDs to occur in the context of migraine, and as such, migraine frequency and intensity may be related to the onset of neurological disease by later in life including dementia. CSD is not limited to migraines, but also suggests that those with cardiovascular disease or genetic mutations that suffer a brain injury may also suffer from worse effects due to increased severity of CSD, as modelled in our experimental protocol by electrode insertion. CSD may also be an effective and robust biomarker to assess brain states as well as testing the efficacy of therapies in both preclinical studies and in neurological patients.

Surprisingly, neural MUA data was not significantly altered across any of the stimulations or conditions for any of the disease groups compared to WT controls. Although the MUA for J20-AD, PCSK9-ATH & J20-PCSK9-MIX mice does appear to be smaller in the first stimulation (***Figure 4.4***), it was not significant after post-hoc tests were performed. Furthermore, this effect disappears under the normoxia conditions (in 21% oxygen) where there is no longer such an indicative difference. The similar MUA across all groups, coupled with impaired HbO & HbR levels in PCSK9-ATH mice, and to some extent in the other disease models may indicate that neurovascular coupling is inefficient and metabolically compromised. A consistent finding irrespective of stimulation and condition was that PCSK9-ATH mice display consistently reduced evoked-HbT responses (observed in chronic experiments) compared to WT controls, which suggests an advanced level of neurovascular breakdown and inefficiency. Other groups have found similarly reduced blood flow in the $ApoE^{-/-}$ model without altered cortical activation, however, unlike in the present study, reduced hypercapnia response (22). A recent study found decreased tissue oxygenation in the $LDLR^{-/-}$ mouse model of atherosclerosis (29), and this is most likely to be the case in the PCSK9 model. This is also the case for the J20-AD and J20-PCSK9-MIX mice which also display a trend towards reduced HbR washout which

suggests that although neurovascular coupling is still present in these mice, it could be less efficient resulting in inadequate oxygen delivery to active neurons. PCSK9-ATH mice on the other hand display reduced evoked-HbT to normal levels of cortical activation in addition to reduced HbR washout indicating neurovascular breakdown and metabolic inefficiency.

A question that arises is why the J20-PCSK9-MIX mice HbT responses are not more severely impaired than J20-AD and PCSK9-ATH? There may be redundancies that occur physiologically to compensate for mild hypoxia in the brain, such as the possible angiogenesis within the brain. Angiogenesis is known to be triggered in cerebral microvessels in AD in response to increased Aβ and neuroinflammation and may initially reflect a compensatory mechanism to increase perfusion (30). However, neovascularisation in AD is eventually thought to be pathogenic and damaging to the brain due to enhanced endothelial Aβ secretion that leads to increased ROS and endothelial damage (30). In addition, the levels of neuroinflammation seen in these mice may be due to an altered disease-course and examining temporospatial expression may reveal much higher levels of inflammation in this mixed model at an earlier time-point. Other markers of inflammation may be upregulated compared to those that we assessed, and future studies would incorporate transcriptomic approaches to identify other mechanisms or markers. Nevertheless, a key translational finding from our study was that J20-PCSK9-MIX mice displayed a significant increase in the number of hippocampal plaques, and this confirms other studies that have used APP/PS1 mice (31). However, the number of cortical plaques were not significantly increased between J20-AD and J20-PCSK9-MIX mice, again confirming findings from the previously discussed study (31). Furthermore, other research has found that high-fat diet in APP/PS1 double transgenic mouse model of AD is able to increase neuropathological changes as well as worsen behavioural abnormalities, however, without any further alterations to CBF (32), as seen in our study. Our neurovascular data focuses on the cortex, and we do not see worsened responses in J20-PCSK9-MIX mice compared to J20-AD (or PCSK9-ATH) mice potentially reflecting the similar number of amyloid-plaques in the cortex. It is plausible that neurovascular coupling in the hippocampus in J20-PCSK9-MIX may be more perturbed than in J20-AD and PCSK9-ATH, however, our imaging system does not allow for us to image the hippocampus in vivo. We can also hypothesise that inducing atherosclerosis in a more moderate or severe fAD model such as the APP/PS1 or 5xfAD could worsen neurovascular coupling and neuropathological and neuroinflammation changes compared to the very mild J20-AD model that we have used. In the more extreme setting, neurovascular function may be severely perturbed and dysfunctional reflecting the later disease-course in humans, whereas the J20-AD model reflects a midlife stage.

There are several notable limitations with the present study. Firstly, all imaging was performed on lightly anaesthetised animals, which is known to compromise neurovascular function (33). However, previous research from our laboratory has developed an anaesthetic regimen that is comparable to awake imaging in terms of the haemodynamic responses to physiological whisker stimulation with little effect on vascular reactivity (34). The benefits of lightly anaesthetised preparations over awake preparations is that we can avoid the multiple considerations of behavioural state in which the animals may be whisking, grooming as well as their arousal and stress states which may be present in awake animals. Furthermore, we report the stability and robustness of our imaging preparation in this study. We present the average of all the raw stimulation trials from each animal across the whole experimental session (***Figure 4.7***), showing the stability and robustness of our preparation, as well as easily identifying any changes. Secondly, our imaging analysis assumes O_2 saturation to be 70% with a baseline haemoglobin concentration of 100μM. This may be important if the assumed baselines are different in the diseased animals compared to WT controls; however, our recent study (18) using the same J20-AD mouse model discussed this issue in detail, in which we showed that regardless of the baseline blood volume estimation used, our percentage change was scaled by it (i.e. always the same change). Therefore, the observations in this paper with respect to the different diseased animals are robust. Finally, we only performed qRT-PCR for 2 inflammatory targets, whereas performing RNA-seq on specific cell types or wider transcriptomic studies would allow us to investigate the expression of other inflammatory targets and cellular pathways that could be important. In addition, examining levels of circulating plasma and CSF cytokines may be useful in examining neuroinflammatory changes in these mice.

In conclusion, we report novel findings of impaired neurovascular function in a novel experimental model of atherosclerosis (PCSK9-ATH) characterised by reduced stimulus-evoked blood volume without any significant alterations to evoked neural activity. We induced atherosclerosis in a mild fAD model (J20-AD) to create a mixed comorbid model (J20-PCSK9-ATH) in which we report a significant increase in the number of hippocampal Aβ plaques, however, without any significant changes to evoked haemodynamic or neural responses compared to WT or J20-AD mice. A key finding from this study was CSD was more severe in diseased animals. This may reflect the global inflammatory state of the brain and could also serve to be an effective preclinical and human clinical biomarker for baseline state and to assess therapies. Future studies should include assessment of other inflammatory markers and cellular pathway changes by a genome wide transcriptomics approach from single cell populations, as well as from sera and CSF. It would also be prudent to induce atherosclerosis

in a more severe fAD model to provide a severity continuum of mixed models that reflect clinical presentations of dementia.

4.9 – Materials & Methods

4.9.1 – Animals

All animal procedures were performed with approval from the UK Home Office in accordance to the guidelines and regulations of the Animal (Scientific Procedures) Act 1986 and were approved by the University of Sheffield ethical review and licensing committee. Male C57BL/6J mice were injected i.v at 6wks with 6x1012 virus molecules/ml rAAV8-mPCSK9-D377Y (Vector Core, Chapel Hill, NC) and fed a Western diet (21% fat, 0.15% cholesterol, 0.03% cholate, 0.296% sodium; #829100, Special Diet Services UK) for 8m (PCSK9-ATH). These mice were compared to age-matched wild-type C57BL/6J mice (with no AAV injection fed normal rodent chow) that were used as controls (WT C57BL/6J). In addition, male heterozygous transgenic J20-hAPP B6.Cg-Zbtb20Tg(PDGFB-APPSwInd)20Lms/2Mmjax) (MMRRC Stock No: 34836-JAX) mice were used. Atherosclerosis was induced in J20-hAPP mice alongside WT mice at 6wks of age combined with a Western diet to create a comorbid mixed model (J20-PCSK9-MIX). For the CSD imaging experiments, 4 nNOS-ChR2 mice (M/F, 16-40 weeks old) were included in the WT group. [nNOS-ChR2 mice: heterozygous nNOS-CreER (Jax 014541, (35)) x homozygous Ai32 mice (Jax 024109, (36)), given tamoxifen (100mg/kg, i.p., 3 injections over 5 days) at 1-2 months old]. All mice were imaged between 9-12m of age. All mice were housed in a 12hr dark/light cycle at a temperature of 23C, with food and water supplied ad-libitum.

4.9.2 – Thinned Cranial Window Surgery

Mice were anaesthetised with 7ml/kg i.p. injection of fentanyl-fluanisone (Hypnorm, Vetapharm Ltd), midazolam (Hypnovel, Roche Ltd) and maintained in a surgical anaesthetic plane by inhalation of isoflurane (0.6-0.8% in 1L/min O2). Core body temperature was maintained at 37oC through use of a homeothermic blanket (Harvard Apparatus) and rectal temperature monitoring. Mice were placed in a stereotaxic frame (Kopf Instruments, US) and the bone overlying the right somatosensory cortex was thinned forming a thinned cranial optical window. A thin layer of clear cyanoacrylate glue was applied over the cranial window to reinforce the window. Dental cement was applied around the window to which a metal head-plate was chronically attached. All mice were given 3 weeks to recover before the first imaging session.

4.9.3 – 2D-Optical Imaging Spectroscopy (2D-OIS)

2D-OIS measures changes in cortical haemodynamics: total haemoglobin (HbT), oxyhaemoglobin (HbO) and deoxyhaemoglobin (HbR) concentrations (37). Mice were lightly

sedated and placed into a stereotaxic frame. Sedation was induced as described above and maintained using low levels of isoflurane (0.3-0.6%). For imaging, the right somatosensory cortex was illuminated using 4 different wavelengths of light appropriate to the absorption profiles of the differing haemoglobin states (495nm ± 31, 559nm ± 16, 575nm ± 14 & 587nm ± 9) using a Lambda DG-4 high-speed galvanometer (Sutter Instrument Company, US). A Dalsa 1M60 CCD camera was used to capture the re-emitted light from the cortical surface. All spatial images recorded from the re-emitted light underwent spectral analysis based on the path length scaling algorithm (PLSA) as described previously (37, 38). which uses a modified Beer-Lambert law with a path light correction factor converting detected attenuation from the re-emitted light with a predicted absorption value. Relative HbT, HbR and HbO concentration estimates were generated from baseline values in which the concentration of haemoglobin in the tissue was assumed to be 100μM and O2 saturation to be 70%. For the stimulation experiments, whiskers were mechanically deflected for a 2s-duration and a 16s-duration at 5Hz using a plastic T-shaped stimulator which caused a 1cm deflection of the left-whisker. Each individual experiment consisted of 30 stimulation trials (for 2s) and 15 stimulation trials (for 16s) of which a mean trial was generated after spectral analysis of 2D-OIS. Stimulations were performed with the mouse breathing in 100% O2 or 21% O2, and a gas transition to medical air (21% O2) as well as an additional 10% CO2-hypercapnia test of vascular reactivity.

4.9.4 – Neural Electrophysiology

Simultaneous measures of neural activity alongside 2D-OIS were performed in a final acute imaging session 1-week after the 1st imaging session. A small burr-hole was drilled through the skull overlying the active region (as defined by the biggest HbT changes from 2D-OIS imaging) and a 16-channel microelectrode (100μm spacing, 1.5-2.7MΩ impedance, site area 177μm2) (NeuroNexus Technologies, USA) was inserted into the whisker barrel cortex to a depth of ~1500μm. The microelectrode was connected to a TDT preamplifier and a TDT data acquisition device (Medusa BioAmp/RZ5, TDT, USA). Multi-unit analysis (MUA) was performed on the data. All channels were depth aligned to ensure we had twelve electrodes covering the depth of the cortex in each animal. The data were high passed filtered above 300Hz to remove all low frequency components and split into 100ms temporal bins. Within each bin any data crossing a threshold of 1.5SD above the mean baseline was counted and the results presented in the form of fractional changes to MUA.

4.9.5 – Region Analysis

Analysis was performed using MATLAB (MathWorks). An automated region of interest (ROI) was selected using the stimulation data from spatial maps generated using 2D-OIS. The threshold for a pixel to be included within the ROI was set at 1.5xSD, therefore the automated

ROI for each session per animal represents the area of the cortex with the largest haemodynamic response, as determined by the HbT. For each experiment, the response across all pixels within the ROI was averaged and used to generate a time-series of the haemodynamic response against time.

4.9.6 – Statistical Analysis

Statistical analyses were performed using SPSS v25 & GraphPad Prism v8. Shapiro-Wilks test was used to check for normality and Levene's test was used to assess equality of variances. 2-way mixed design ANOVA, 1-way ANOVA or Kruskal-Wallis tests were used, as appropriate. For 1-way ANOVA, if variances were unequal, Welch's F was reported. Results were considered statistically significant if $p<0.05$. The Shapiro-Wilks test suggested that, for chronic experiments, peak values of HbT and HbO are normally distributed, however, HbR values are significantly non-normal. 2-way mixed design was used to compare peak values for HbT, HbO & HbR (although HbR failed the S-W test for normality, an ANOVA was used as they were considered fairly robust against small deviations from normality). Inspection of Levene's test suggested that variances were equal, therefore, Dunnett's (two-sided) multiple comparisons test was used to compare disease models to WT, and for HbR, Games-Howell multiples comparisons were used. If the Greenhouse-Geisser estimate of sphericity showed deviation from sphericity (chronic experiments: HbT ($\varepsilon=0.55$), HbO ($\varepsilon = 0.49$) & HbR ($\varepsilon=0.564$), results are reported with Greenhouse-Geisser correction applied. qRT-PCR data was analysed by performing 1-way ANOVAs with Dunnett's multiple comparisons test used to compare disease models to WT. P-values <0.05 were considered statistically significant. All the data are presented as mean values ± standard error of mean (SEM).

4.9.7 – Immunohistochemistry

At the end of terminal experiments, mice were euthanized with an overdose of pentobarbital (100mg/kg, Euthatal, Merial Animal Health Ltd) and transcardially perfused with 0.9% saline and brains were dissected. One half-hemisphere of the brains were fixed in formalin and embedded in paraffin wax, with the other half snap-frozen using isopentane and stored at -80C. 5µm coronal sections were obtained using a cryostat. Immunohistochemistry was performed using an avidin-biotin complex (ABC) method (as described previously (Ameen-Ali et al., 2019)). Following slide preparation and antigen retrieval (pressure cooker at 20psi at 120C for 45s (pH6.5)), sections underwent additional pre-treatment in 70% formic acid. Sections were incubated with 1.5% normal serum followed by incubation with the primary antibody (biotinylated anti-Aβ – 1:100, BioLegend, USA) for 1 hour. Horseradish peroxidase avidin-biotin complex (Vectastain Elite Kit, Vector Laboratories, UK) was used to visualise antibody binding along with 3,3-diaminobenzidine tetrahydrochloride (DAB) (Vector

Laboratories, UK). All sections were counterstained with haematoxylin, dehydrated and mounted in DPX. Sections were imaged using a Nikon Eclipse Ni-U microscope attached to a Nikon DS-Ri1 camera. Plaques were identified at x40 magnification and manually counted per section.

4.9.8 – qRT-PCR

Snap-frozen hemispheres were homogenised, and RNA was extracted using Direct-zol RNA MiniPrep kit with TRI-reagent as per the manufacturer's guidelines (Zymo) and RNA quality checked using NanoDropTM (ThermoFisher Scientific). cDNA was synthesised from the extracted RNA using the UltraScript 2.0 cDNA synthesis kit (PCR BioSystems) according to the manufacturer's guidelines. qRT-PCR was performed using PrimeTime qRT-PCR assay primers (IDT) for *IL1β* & *TNFα* with *ACTB* as the reference housekeeping gene. Luna qRT-PCR Master Mix (NEB) was used with the primers, cDNA and nuclease free water and each gene for each sample was duplicated. CFX384 Real-Time System (BioRad) with a C1000 Touch Thermal Cycler (BioRad) was used to perform qRT-PCR consisting of 40 cycles. Data was analysed using the well-established delta-Ct method (Livak and Schmittgen, 2001) by normalising against *ACTB*.

4.10 – Acknowledgments

OS's PhD studentship and consumables were funded by the Neuroimaging in Cardiovascular Disease (NICAD) network scholarship (University of Sheffield). A British Heart Foundation (BHF) project grant was awarded to SEF to carry out the work using the PCSK9 model (PG/13/55/30365). The J20-mouse colony was in part funded and supported by Alzheimer's Research UK (Grant R/153749-12-1). CH is funded by a Sir Henry Dale Fellowship jointly funded by the Wellcome Trust and the Royal Society (Grant Number 105586/Z/14/Z). MAR is funded by a Conacyt scholarship. We would like to thank Prof Lennart Mucke (Gladstone Institute of Neurological Disease & Department of Neurology, UCSF, CA, US) as well as the J. David Gladstone Institutes for the J20-hAPP mice. Finally, we would like to thank Mr Michael Port for building and maintaining the imaging apparatus and Dr Luke Boorman for producing MATLAB code for data analysis.

4.11 – Conflicts of Interest.

The authors have no conflicts of interests to declare.

4.12 – References:

1. O. Shabir, J. Berwick, S. E. Francis, Neurovascular dysfunction in vascular dementia, Alzheimer's and atherosclerosis. *BMC Neurosci* **19**, 62 (2018).

2. K. R. Thulborn, J. C. Waterton, P. M. Matthews, G. K. Radda, Oxygenation dependence of the transverse relaxation time of water protons in whole blood at high field. *Biochim Biophys Acta* **714**, 265-270 (1982).
3. S. Ogawa, T. M. Lee, A. R. Kay, D. W. Tank, Brain magnetic resonance imaging with contrast dependent on blood oxygenation. *Proc Natl Acad Sci U S A* **87**, 9868-9872 (1990).
4. B. V. Zlokovic, Neurovascular pathways to neurodegeneration in Alzheimer's disease and other disorders. *Nat Rev Neurosci* **12**, 723-738 (2011).
5. F. Neuropathology Group. Medical Research Council Cognitive, S. Aging, Pathological correlates of late-onset dementia in a multicentre, community-based population in England and Wales. Neuropathology Group of the Medical Research Council Cognitive Function and Ageing Study (MRC CFAS). *Lancet* **357**, 169-175 (2001).
6. F. E. Matthews *et al.*, Epidemiological pathology of dementia: attributable-risks at death in the Medical Research Council Cognitive Function and Ageing Study. *PLoS Med* **6**, e1000180 (2009).
7. J. Rahimi, G. G. Kovacs, Prevalence of mixed pathologies in the aging brain. *Alzheimers Res Ther* **6**, 82 (2014).
8. A. Kapasi, C. DeCarli, J. A. Schneider, Impact of multiple pathologies on the threshold for clinically overt dementia. *Acta Neuropathol* **134**, 171-186 (2017).
9. A. J. Lusis, Atherosclerosis. *Nature* **407**, 233-241 (2000).
10. C. Napoli *et al.*, Intracranial arteries of human fetuses are more resistant to hypercholesterolemia-induced fatty streak formation than extracranial arteries. *Circulation* **99**, 2003-2010 (1999).
11. A. Kapasi, J. A. Schneider, Vascular contributions to cognitive impairment, clinical Alzheimer's disease, and dementia in older persons. *Biochim Biophys Acta* **1862**, 878-886 (2016).
12. C. Iadecola, The Neurovascular Unit Coming of Age: A Journey through Neurovascular Coupling in Health and Disease. *Neuron* **96**, 17-42 (2017).
13. C. Iadecola *et al.*, Vascular Cognitive Impairment and Dementia: JACC Scientific Expert Panel. *J Am Coll Cardiol* **73**, 3326-3344 (2019).
14. M. M. Bjorklund *et al.*, Induction of atherosclerosis in mice and hamsters without germline genetic engineering. *Circ Res* **114**, 1684-1689 (2014).
15. M. Roche-Molina *et al.*, Induction of sustained hypercholesterolemia by single adeno-associated virus-mediated gene transfer of mutant hPCSK9. *Arterioscler Thromb Vasc Biol* **35**, 50-59 (2015).
16. L. Mucke *et al.*, High-level neuronal expression of abeta 1-42 in wild-type human amyloid protein precursor transgenic mice: synaptotoxicity without plaque formation. *J Neurosci* **20**, 4050-4058 (2000).
17. K. E. Ameen-Ali *et al.*, The Time Course of Recognition Memory Impairment and Glial Pathology in the hAPP-J20 Mouse Model of Alzheimer's Disease. *J Alzheimers Dis* **68**, 609-624 (2019).

18. P. S. Sharp *et al.*, Neurovascular coupling preserved in a chronic mouse model of Alzheimer's disease: Methodology is critical. *J Cereb Blood Flow Metab* 10.1177/0271678X19890830, 271678X19890830 (2019).
19. T. Kurth *et al.*, Association of Migraine With Aura and Other Risk Factors With Incident Cardiovascular Disease in Women. *JAMA* **323**, 2281-2289 (2020).
20. O. Shabir *et al.*, Enhanced Cerebral Blood Volume under Normobaric Hyperoxia in the J20-hAPP Mouse Model of Alzheimer's Disease. *Sci Rep* **10**, 7518 (2020).
21. A. Denes *et al.*, Interleukin-1 mediates neuroinflammatory changes associated with diet-induced atherosclerosis. *J Am Heart Assoc* **1**, e002006 (2012).
22. C. Ayata *et al.*, Hyperlipidemia disrupts cerebrovascular reflexes and worsens ischemic perfusion defect. *J Cereb Blood Flow Metab* **33**, 954-962 (2013).
23. C. Ayata, M. Lauritzen, Spreading Depression, Spreading Depolarizations, and the Cerebral Vasculature. *Physiol Rev* **95**, 953-993 (2015).
24. J. P. Dreier, The role of spreading depression, spreading depolarization and spreading ischemia in neurological disease. *Nat Med* **17**, 439-447 (2011).
25. P. Ripa, R. Ornello, F. Pistoia, A. Carolei, S. Sacco, Spreading depolarization may link migraine, stroke, and other cardiovascular disease. *Headache* **55**, 180-182 (2015).
26. M. Yemisci, K. Eikermann-Haerter, Aura and Stroke: relationship and what we have learnt from preclinical models. *J Headache Pain* **20**, 63 (2019).
27. K. Eikermann-Haerter *et al.*, Cerebral autosomal dominant arteriopathy with subcortical infarcts and leukoencephalopathy syndrome mutations increase susceptibility to spreading depression. *Ann Neurol* **69**, 413-418 (2011).
28. R. E. Morton, P. D. St John, S. L. Tyas, Migraine and the risk of all-cause dementia, Alzheimer's disease, and vascular dementia: A prospective cohort study in community-dwelling older adults. *Int J Geriatr Psychiatry* **34**, 1667-1676 (2019).
29. B. Li *et al.*, Atherosclerosis is associated with a decrease in cerebral microvascular blood flow and tissue oxygenation. *PLoS One* **14**, e0221547 (2019).
30. W. A. Jefferies *et al.*, Adjusting the compass: new insights into the role of angiogenesis in Alzheimer's disease. *Alzheimers Res Ther* **5**, 64 (2013).
31. M. S. Grames *et al.*, Gene Transfer Induced Hypercholesterolemia in Amyloid Mice. *J Alzheimers Dis* **65**, 1079-1086 (2018).
32. O. Bracko *et al.*, High fat diet worsens Alzheimer's disease-related behavioral abnormalities and neuropathology in APP/PS1 mice, but not by synergistically decreasing cerebral blood flow. *Sci Rep* **10**, 9884 (2020).
33. Y. R. Gao *et al.*, Time to wake up: Studying neurovascular coupling and brain-wide circuit function in the un-anesthetized animal. *Neuroimage* **153**, 382-398 (2017).
34. P. S. Sharp *et al.*, Comparison of stimulus-evoked cerebral hemodynamics in the awake mouse and under a novel anesthetic regime. *Sci Rep* **5**, 12621 (2015).
35. H. Taniguchi *et al.*, A resource of Cre driver lines for genetic targeting of GABAergic neurons in cerebral cortex. *Neuron* **71**, 995-1013 (2011).

36. L. Madisen *et al.*, A toolbox of Cre-dependent optogenetic transgenic mice for light-induced activation and silencing. *Nat Neurosci* **15**, 793-802 (2012).
37. J. Berwick *et al.*, Neurovascular coupling investigated with two-dimensional optical imaging spectroscopy in rat whisker barrel cortex. *Eur J Neurosci* **22**, 1655-1666 (2005).
38. J. Mayhew *et al.*, Spectroscopic analysis of changes in remitted illumination: the response to increased neural activity in brain. *Neuroimage* **10**, 304-326 (1999).
39. K. J. Livak, T. D. Schmittgen, Analysis of relative gene expression data using real-time quantitative PCR and the 2(-Delta Delta C(T)) Method. *Methods* **25**, 402-408 (2001).

4.13 – Supplemental Information:

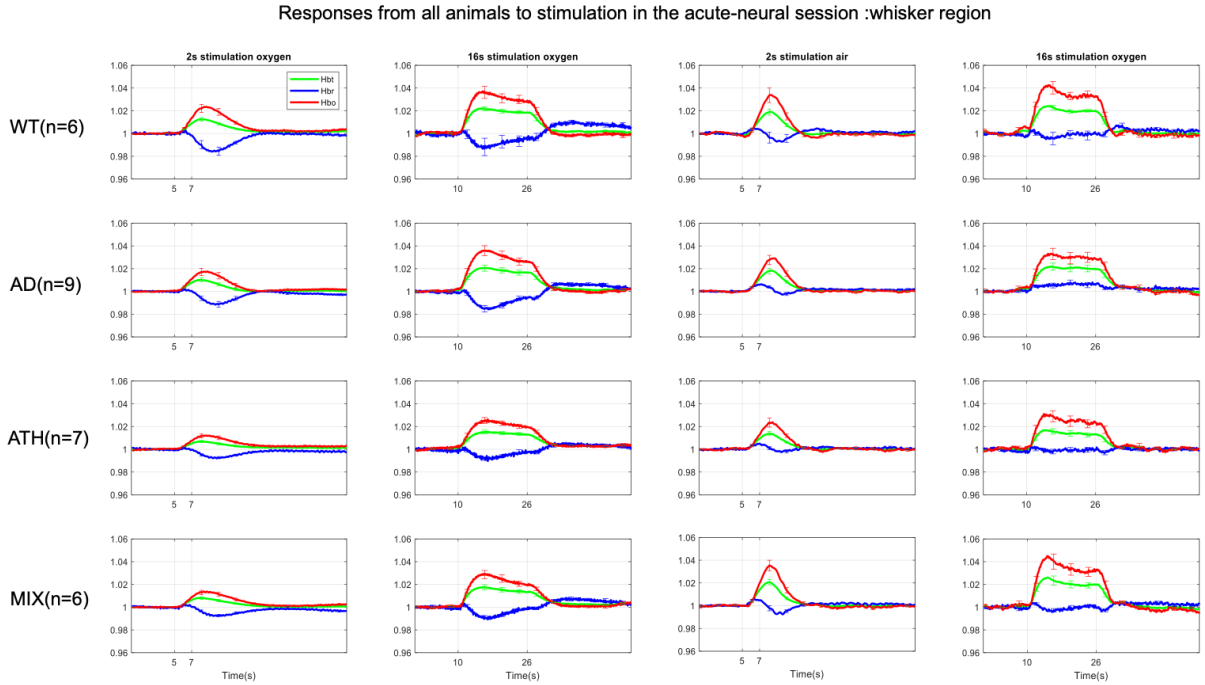

Figure 4.6(S) – Fractional Changes in Acute Stimulus-Evoked Haemodynamic Responses. **HbT:** There was no significant overall effect of disease $F(3,24)=1.69$, $p=0.196$. As expected, there was a significant effect of experiment, $F(2.16,51.73)=76.72$, $p<0.001$. There was no significant interaction effect between experiment and disease, $F(6.47,51.73)=1.73$, $p=0.127$. **HbO:** There was no significant overall effect of disease $F(3,24)=1.36$, $p=0.280$. There was a significant effect of experiment, $F(2.02,48.57=62.10$, $p<0.001$. There was no significant interaction effect between experiment and disease, $F(6.07,48.57)=2.08$, $p=0.072$. **HbR:** There was no significant overall effect of disease $F(3,24)=1.42$, $p=0.262$. As expected, there was a significant effect of experiment, $F(2.18,52.42)=17.54$, $p<0.001$. There was a significant interaction effect between experiment and disease $F(6.55, 52.42)=2.54$, $p=0.028$. All error bars (lightly shaded) are ±SEM. Vertical dotted lines indicate start and end of stimulations.

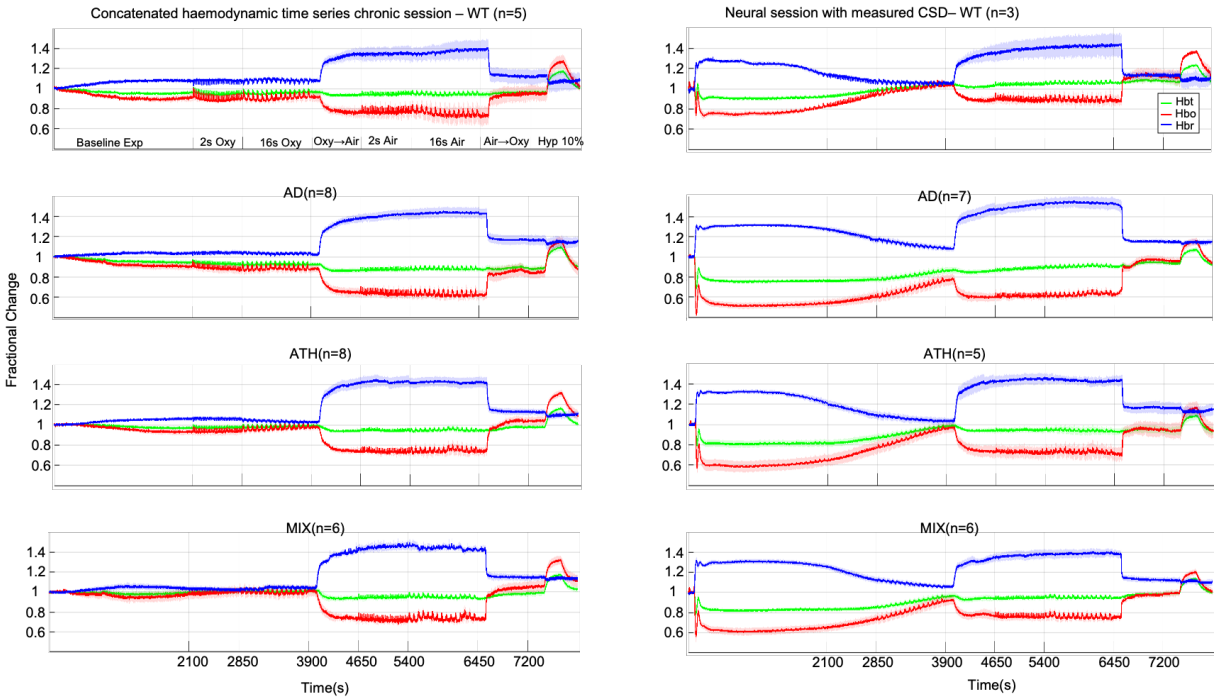

Figure 4.7(S) – Concatenated data showing stability and robustness of the mouse imaging preparation. Left) Chronic imaging sessions including a 35-minute haemodynamics baseline before first stimulation. Right) Acute imaging sessions including CSD plus 35-minute haemodynamics recovery before first stimulation.

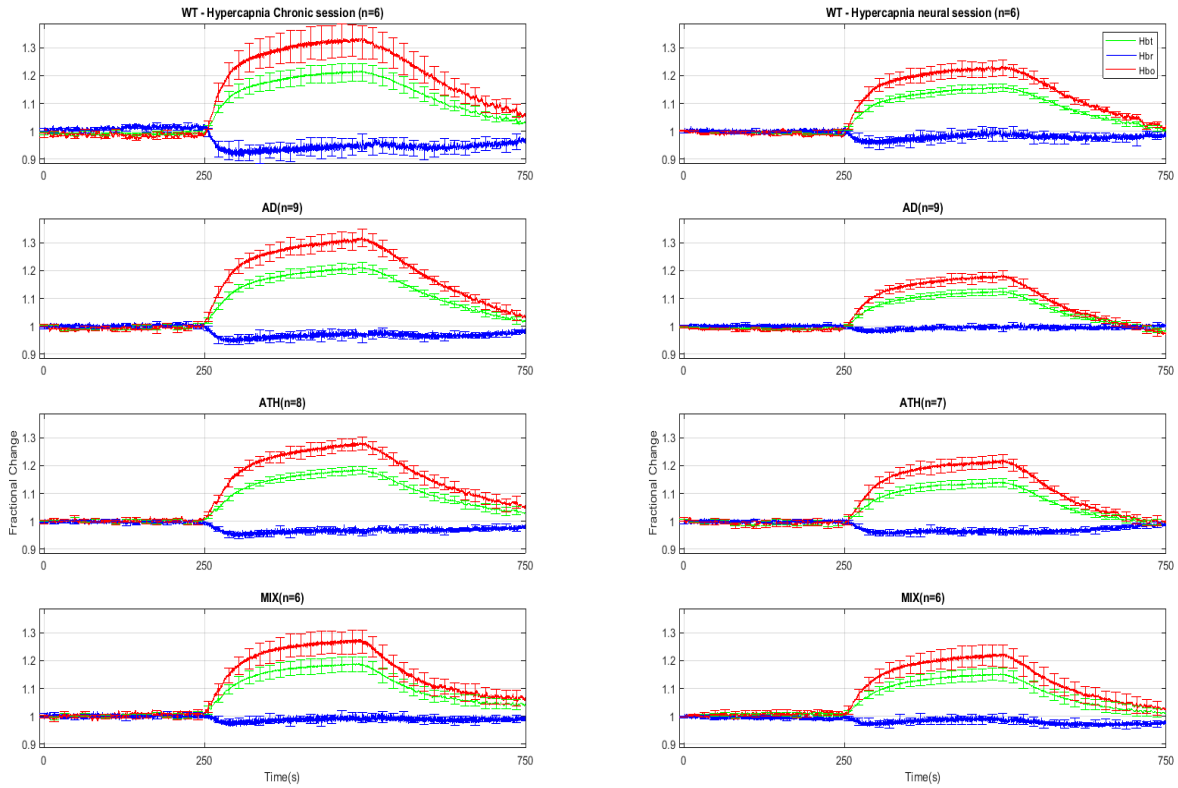

Figure 4.8(S) – Chronic & Acute Hypercapnia. Chronic: A 1-way ANOVA showed no significant effect of disease for HbT ($F(3,12.06)=0.49$, $p=0.694$), HbO ($F(3,11.98)=0.44$, $p=0.732$) nor HbR ($F(3,12.081)=0.98$, $p=0.436$). **Acute:** A 1-way ANOVA showed no significant effect of disease for HbO $F(3,12.00)=0.74$, $p=0.549$ but there was a significant effect of disease for HbR $F(3,11.01)=3.77$, $p=0.044$. Games-Howell multiple comparisons showed that, for HbR, there was a significant difference between AD and ATH ($p=0.019$). Kruskal-Wallis test showed no significant effect of disease for HbT: $H(3)=2.87$, $p=0.412$. Error bars ±SEM.

Chapter 5 – Conclusions & Future Directions

5.1 – Overview

Dementia is one of the biggest medical and scientific priorities of our time. There are currently approximately 50 million worldwide cases of dementia, with over 9.9 million new cases being diagnosed each year; that is one new case every 3 seconds (International, 2020). It is estimated that globally, cases will rise to 152 million by 2050 ((ARUK), 2020). Within the UK, there are currently nearly a million affected individuals with this estimated to double to 2 million by 2050. Harrowingly, the leading cause of death for women in the UK was dementia in 2017, and the second leading cause of death for men. Most worryingly, compared to the top 10 leading causes of death in the UK, dementia is the only one that currently does not have any disease modifying treatments or therapies to reverse, cure or slow down its progression. Within the UK, 10-15% of all dementia cases are mixed with the most common mixed dementia being the combination of AD and VaD, and this prevalence increases in patients over 75 years of age. Comorbidities are extremely common in older individuals, with the most common comorbidities being cardiovascular disease and cerebrovascular disease (Wolters and Ikram, 2019). Thus, understanding the mechanisms connecting cardiovascular, cerebrovascular and neurological disease (heart-brain-axis) is essential if therapies are to succeed. To date, the vast majority of AD treatments have focused on targeting Aβ or the cholinergic system. However, none have succeeded at the clinical level owing to the sheer complexity of dementia in older adults, that is so often complicated by the presence of two or more comorbidities.

Whilst the amyloid-hypothesis of AD still largely dominates the field and remains the biggest target for AD treatments, many amyloid-targeting therapies have previously failed clinical trials, and to date, there are still no disease-modifying treatments available. Furthermore, the notion that AD is purely a neurodegenerative disease has become increasingly more obsolete, with evidence that AD is multifactorial and has a large cerebrovascular element to it. Evidence has shown that there may be a crucial early role for vascular dysregulation in late-onset AD (Iturria-Medina et al., 2016). Vascular dysregulation appears prior to observable increases in Aβ deposition, metabolic alterations, structural and behavioural changes that occur between healthy individuals and those with EMCI-stage of AD. As described in chapter 1, the need for preclinical models to study human disease is necessary to understand the different pathomechanisms of disease if effective treatments are to be found. The vast majority of AD models have modelled fAD mutations (such as the J20 mouse incorporating hAPPSw,Ind familial mutations) and model aspects of Aβ overexpression (Mucke et al., 2000). Whilst many of these models replicate aspects of human disease including time-dependent pathological and behavioural differences (Ameen-Ali et al., 2019), they remain limited due to their incomplete recapitulation of the human condition that tends to be multifactorial and complex.

Thus, in order to better replicate the human condition (especially with respect to age-related conditions), it is important that we consider the use of models that closely resemble the human condition (such as the PCSK9 model over the ApoE$^{-/-}$ model of atherosclerosis) as well as creating comorbid models that incorporate 2 or more overlapping conditions that are typically seen in older human patients.

In my PhD project, I characterised neurovascular function in 2 different mouse models of human disease: J20-hAPP(Sw,Ind) model of fAD, rAAV8-mPCSK9-D377Y model of atherosclerosis and created a novel comorbid J20-hAPP(Sw,Ind) + rAAV8-mPCSK9-D377Y mixed model of fAD and atherosclerosis. Here, I describe the differential phenotypes of the 3 different disease models and link them to cellular and molecular changes in brain tissue. Moreover, I describe novel findings relating to the PCSK9-model of atherosclerosis and report a trebling of Aβ plaques in the novel mixed model. These findings strongly support the 2-hit neurovascular degeneration hypothesis proposed by Zlokovic and confirm the notion that systemic cardiovascular disease is related to impaired neurovascular function and associated with the onset of dementia later in life. Furthermore, the evidence of increased plaques in J20-PCSK9-MIX mice confirms that atherosclerosis exacerbates pre-existing AD-related neuropathology and may accelerate disease-course.

5.2 – Enhanced Evoked-HbT Is Associated with Neural Hyperexcitability in 6m J20-AD Mice. Under Hyperoxia, J20-AD Mice Exhibit Enhanced Baseline HbT and Saturation.

In the first part of the project, I characterised neurovascular function in 6m old J20-AD mice using a stable chronic imaging protocol as described previously in our study which used the same mice at 9-12m of age (Sharp et al., 2019). Between the ages of 4-8 months, J20-AD mice exhibit neural hyperexcitability and up to 15% die due to seizures (Palop et al., 2007). This is of a translational interest as many up to 22% of early-onset fAD patients also exhibit seizures specifically due to cortical hyperexcitability (Vossel et al., 2013). This is thought to be in response to the earliest depositions of Aβ in the brain (Minkeviciene et al., 2009), or as a result of aberrant processing of APP (Palop et al., 2007). Whilst I did not observe any seizures in these mice, 17% of all my J20-AD mice died unexpectedly presumably due to seizures, and many others may have had non-fatal seizures. However, all 6m J20-AD mice exhibited neural hyperexcitability compared to matched WT controls, and this was associated with an increased evoked-HbT. However, the washout of HbR was impaired, especially under normoxic conditions. This HbR observation was also present in older 9-12m J20-AD mice (discussed in section 5.7.2), and suggests that from an earlier age, these mice may have some degree of neurovascular metabolic inefficiency. This may also be indicative of the earliest form of vascular dysregulation as proposed by Itturia-Medina (Iturria-Medina et al., 2016). The main

translational finding from this study was that under normobaric hyperoxic conditions, the baseline blood volume (HbT) and saturation was significantly higher compared to WT controls, and this effect disappeared upon transitioning to normoxia (***Figure 3.4***). This surprising and interesting phenomenon was not present in WT controls, and as reported in our previous paper (Sharp et al., 2019), this effect is not present in 9-12m old J20-AD mice. As such, this hyperoxic effect is a time-dependent phenomenon that occurs at approximately the age of the initial Aβ deposition (5/6m), and last until the hyperexcitable phase fades out by around 8m (Palop et al., 2007). This was a serendipitous finding as it was not initially hypothesised. However, the finding is consistent and reliable (very significant), and the appropriate 2-tailed statistical tests were used in the analysis. This also raises an important discussion with respect to hypothesis-driven findings compared to serendipitous findings, and caution must be exercised when drawing conclusions from such findings, ensuring that the data is presented wholly and not cherry-picked, with the appropriate statistical tests being used.

Waste clearance mechanisms in the brain are directly linked to CBF changes. The glymphatic system (identified by Nedergaard) is a waste clearance pathway of the central nervous system that is formed by glial cells and perivascular channels that is predominantly active during sleep (Rasmussen et al., 2018, Jessen et al., 2015). Para-arterial influx of CSF causes it to enter the brain parenchyma which leads to solute exchange between CSF and interstitial fluid (ISF) within the parenchyma. This fluid and solute exchange is mediated by arterial pulsation (Kiviniemi et al., 2016), and the clearance of waste products and excess extracellular fluid (ECF) is achieved by the bulk flow of ISF which is mediated by AQP4 channels on astrocyte end-feet, which is then eventually drained out of the brain into cervical lymphatic vessels. Glymphatic clearance is impaired as we age and may be related to gliosis that occurs as part of healthy ageing. Those with unhealthy ageing including those who are at risk of developing AD may suffer worse gliosis and inflammation in the brain further worsening glymphatic clearance, coupled with increased Aβ production can lead to amyloid plaque development, tau pathological changes and subsequent neurodegeneration (Rasmussen et al., 2018) (***Figure 5.1***). However, it is important to highlight that the glymphatic system is controversial as some studies have found no evidence of solute clearance in the parenchyma, but suggest a different perivascular mechanism that runs in the opposite direction to paravascular flow (Bacyinski et al., 2017). Irrespective of the contradictions in the literature, waste clearance from the brain, is an important mechanism by which toxic products including Aβ are cleared from the brain. In support of glymphatic clearance; which is thought to be more active during sleep, recent studies have shown enhanced CSF-mediated Aβ clearance overnight, and sleep disturbances can impede this clearance to pose a higher risk of developing AD due to increased Aβ deposition (Shokri-Kojori et al., 2018, Lucey et al., 2018).

My findings of enhanced baseline blood volume and saturation across the cortex under normobaric hyperoxia in 6m J20-AD mice suggests that an increased CBF at baseline may enhance the activity of the glymphatic system to drive an increased clearance (bulk flow) of soluble Aβ, therefore, delaying amyloid deposition in the brain and subsequently delaying the onset of AD (***Figure 5.1***). This, however, needs to be investigated in future studies to determine whether a) normobaric hyperoxia can enhance glymphatic clearance & b) drive an enhanced clearance of Aβ from the brain. My hypothesis is that normobaric hyperoxia will be able to do both and delay amyloid deposition in the brain to delay the onset of both neuropathological and behavioural changes associated with AD. If these preclinical studies are successful in clearing Aβ from the brain from early-stage AD mice, and delay the onset of cognitive decline, then this may be a simple but extremely effective preventative therapeutic strategy to trial in a subset of prodromal AD patients. Hyperbaric hyperoxia, or hyperbaric oxygen therapy, is a commonly used clinical intervention for decompression sickness, mountain sickness, as well as in cases of ischaemic stroke and some traumatic brain injuries (Xu et al., 2012). Recent evidence has shown that hyperbaric oxygen therapy (HBOT) is able to reduce the pathophysiology associated with AD (reduced hypoxia, amyloid burden and tau-phosphorylation) in the 3xTg model of AD in addition to reducing levels of neuroinflammation (IL1β & TNFα as well as reducing astrogliosis and microgliosis) and improving behavioural outcomes (Shapira et al., 2018). Whilst this study corroborates clinical uses of hyperbaric hyperoxia and shows the efficacy of such a therapy in AD, hyperbaric therapies do come with additional risks that are mitigated by normobaric hyperoxia and can be used more routinely by clinics and easily at home. Interestingly, hypoxia usually results in vasodilation to compensate for lower oxygen saturation, whereas normobaric hyperoxia leads to some degree of vasoconstriction in healthy individuals (Johnston et al., 2003), although this effect is minimal and not as profound as for hypoxia. However, the intriguing and surprising observation that hyperoxia is able to elevate baseline blood volume in the cortex of 6m J20-AD mice seems counterintuitive. Thus, the exact mechanism underlying this response is unknown and needs to be investigated at the cellular level. Trialling the therapeutic applications of this research as well understanding the mechanisms underlying the effect have been submitted as a project grant application.

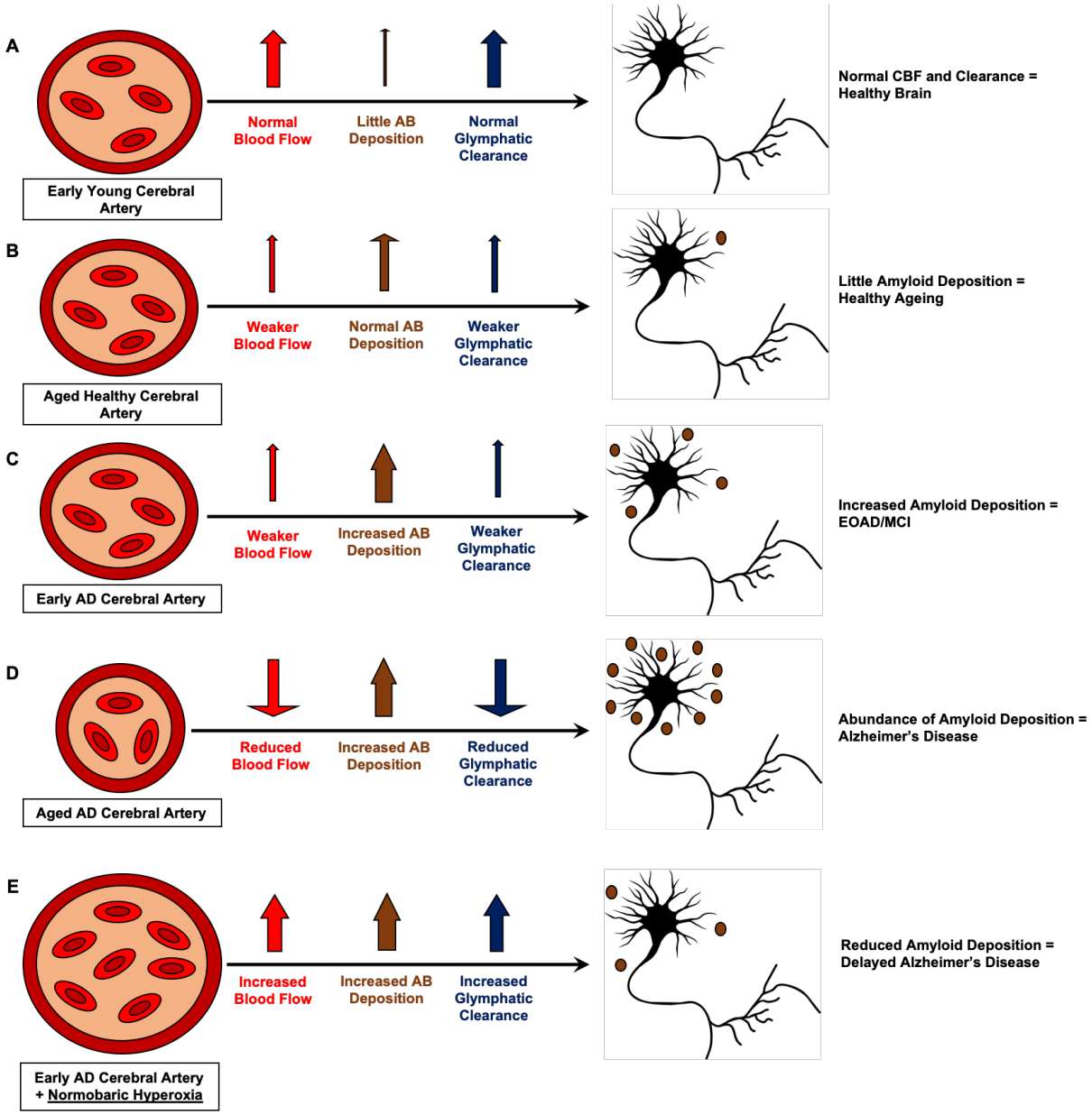

Figure 5.1 – Schematic Summary of Hyperoxia as a Potential Preventative Treatment for AD. A) Healthy cerebral arteries in younger individuals allow for an efficient CBF and glymphatic clearance in the brain efficiently clearing toxic products preventing any neurological toxicity to occur. B) Healthy brain ageing is characterised by weak disruptions to CBF. Whilst Aβ deposition may occur, it occurs minimally, and plaques do not tend to readily develop. Glymphatic clearance, although weakened, is not as drastically reduced in healthy ageing and allows much of the soluble Aβ to be cleared from cerebral tissue. C) In the early stages of EOAD/MCI, CBF begins to be disrupted, also impacting on the efficiency of glymphatic clearance. Coupled with a pathological increase in Aβ production, weaker clearance pathways allow Aβ to slowly accumulate in the brain and blood vessels. D) In AD, there is an increased Aβ production and deposition both in the cerebral parenchyma as well as around vessels (CAA) which leads to an overall constriction of cerebral vessels reducing CBF. Furthermore, pathological changes impair fluid dynamics in the brain (such as altered AQP4 expression). This is coupled to a reduced efficiency of glymphatic clearance of Aβ, thus Aβ plaques build up readily to cause neurodegeneration and cognitive decline. E) Normobaric hyperoxia elevates baseline CBF and oxygen saturation in prodromal stages of AD thus increasing the efficiency of glymphatic clearance which allows excess Aβ to be cleared away from the brain, potentially slowing down the development and progression of AD.

5.3 – Impaired Neurovascular Function in PCSK9-ATH Mice Characterised by Consistently Reduced Evoked-HbT and Potential Neurovascular Breakdown.

In the second part of the project, I characterised neurovascular function in a novel experimental model of atherosclerosis; 9-12m old rAAV8-mPCSK9-D377Y mice fed a Western diet using the same stable chronic imaging protocol as described previously. Whilst there are several neurovascular studies using the more aggressive ApoE$^{-/-}$ model (Denes et al., 2012, Ayata et al., 2013), and the more-human like Ldlr$^{-/-}$ model (Jahrling et al., 2018), to the best of my knowledge, no group has previously studied neurovascular coupling in the PCSK9 model. Whilst this model is similar to the Ldlr$^{-/-}$ model, the fact that it can be induced in any major mouse strain of any genotype at any age is the major advantage of this model, and results in robust atherosclerotic plaques forming by 8-9 weeks post-induction (Bjorklund et al., 2014, Roche-Molina et al., 2015). Robust atherosclerotic plaques (stained by Oil Red O) from a representative PCSK9-ATH mouse can be seen in ***Figure S1*****.**

My data show that PCSK9-ATH mice consistently displayed reduced evoked-HbT responses compared to WT controls, thus confirming my initial hypothesis. This was irrespective of stimulation duration (2s/16s) or gaseous composition (hyperoxia/normoxia) and was a consistent observation not attributable to any baseline haemodynamic shifts that may have occurred (***Figure 4.7***). Furthermore, the hypercapnia data show no significant differences between WT and PCSK9-ATH mice, suggesting that vascular reactivity was intact, and all observations were due to neurovascular abnormalities. This may be due to a degree of neurovascular breakdown and/or reduced cortical activation. The reduced evoked-HbT responses were associated with neurovascular breakdown with the haemodynamic responses not being reflective of the overall neural activity. However, as ***Figure 4.4*** shows, there was still a trend for reduced evoked-MUA in PCSK9-ATH mice, especially under hyperoxia. The evidence suggests that in both cases, there are hints at reduced evoked-MUA, but more importantly, the consistently reduced evoked-HbT is indicative of perfusion and saturation problem. ***Figure S1*** clearly illustrates the extent of atherosclerotic plaques within the aorta and subsequent branches. One can speculate that as these mice age, neurovascular function would worsen and that neurons would suffer from widespread pannecrosis. My results show that systemic atherosclerosis is detrimental to cerebrovascular health at midlife stages, and greatly predispose the brain to ischaemic vulnerabilities later in life.

Histological validation of brain tissue revealed small but significant reduction in cortical neurons (***Figure S6***), and a trend in reduced neurons in chapter 5 when comparing to different multiple comparisons, as well as the presence of reactive astrocytes and shorter processes on microglial. These reactive states were confirmed to be associated with significant IL1β and

TNFα mediated neuroinflammation (determined by qRT-PCR), and taken together, these observations may explain the impaired neurovascular responses and cerebrovascular function in PCSK9-ATH mice. This is summarised in ***Figure 5.2*** below. PCSK9-ATH mice develop hypercholesterolaemia (from 82mg/dL to 820mg/dL within a week post atherosclerosis induction (Goettsch et al., 2016). Atherosclerotic plaque lesion size is comparable to $Ldlr^{-/-}$ mice including aortic calcification. Both $Ldlr^{-/-}$ and AAV-PCSK9 mice display significantly reduced LDLR protein expression in the liver; confirming the role of the g.o.f. D377Y mutation to PCSK9 in inhibiting LDLR (Goettsch et al., 2016). Not only do plaques readily develop and calcify within 20 weeks, there is also extensive collagen remodelling and macrophage infiltration and accumulation that occurs in high-fat diet mice subsequently given AAV-PCSK9. In mice, HFD alone is not sufficient to cause atherosclerosis (as it is in humans). I fed a WT C57BL/6J mouse Western diet for 12wks and compared its neurovascular responses to a WT C57BL/6J counterpart as well as an PCSK9-ATH mouse fed a Western diet for 12wks and found no differences in evoked-responses between WT and WT + HFD mice (***Figure S2***), however, the PCSK9-ATH mouse did exhibit reductions to HbT, HbO and HbR. It is important to note that whilst these atherosclerotic effects are robust and highly reproducible in C57BL/6J mice, there are differences between male and female mice, with atherosclerotic induction being significantly weaker and highly inconsistent in female mice (Aimee E Vozenilek, 2019). This is also the case with cardiovascular diseases generally being more prevalent in men than women clinically. For this reason, all male mice were used in my project to allow for robust and highly consistent atherosclerosis induction, given the time constraints and funding shortfalls. It is important to use mice of both sexes in future studies in accordance to ARRIVE guidelines and to observe any potential sex-specific differences that may be behind the greater prevalence of AD in females and CVD in males.

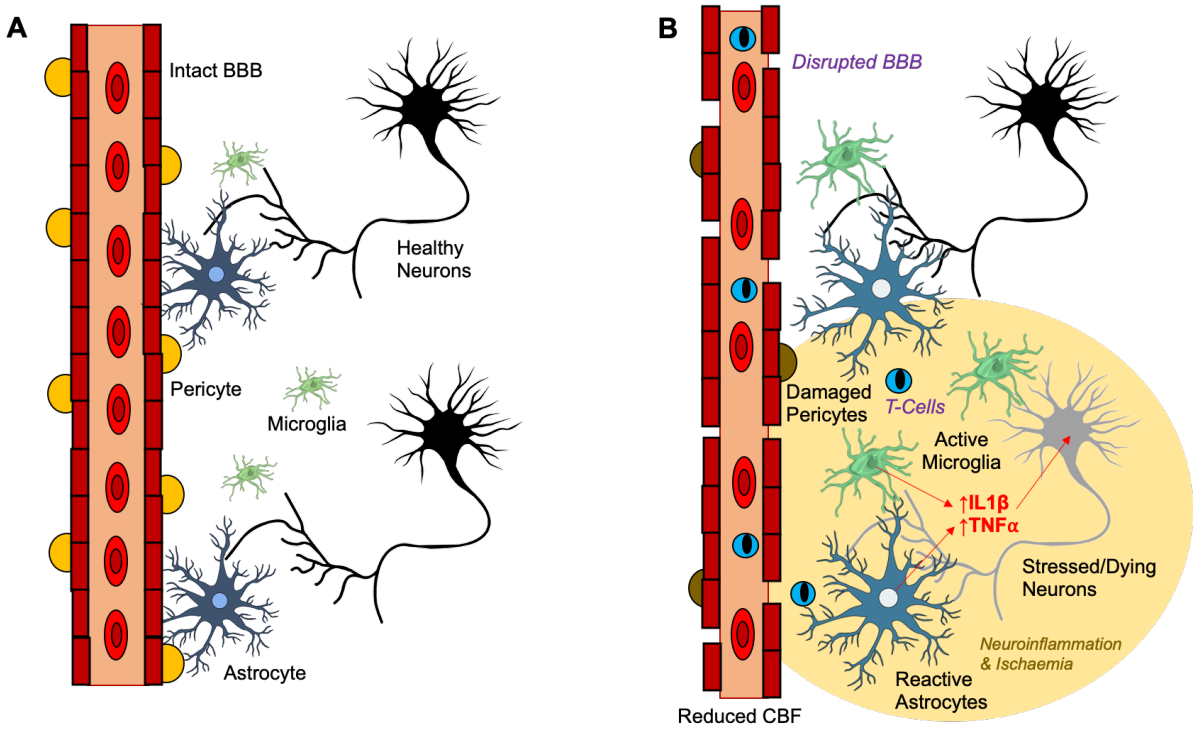

Figure 5.2 – Proposed Neurovascular Dysfunction Mechanism in Atherosclerosis. A) Healthy cerebral arterioles/capillaries have an intact BBB, NVU and very little neuroinflammation allowing for efficient NVC. B) In atherosclerosis, there is impaired neurovascular coupling, characterised by neuroinflammation, reactive astrogliosis, microgliosis, damaged pericytes, as well as potential BBB breakdown, immune cell infiltration and ischaemia. *Text in purple indicates hypothesised mechanisms not currently identified from my PhD, however, will be the bases for future studies.*

5.4 – Increased Aβ plaques in J20-PCSK9-MIX Mice Without Further Impairments to Neurovascular Coupling.

In the final part of my PhD, I generated a mixed comorbid mouse model of fAD and ATH (J20-PCSK9-MIX) by injecting rAAV8-mPCSK9-D377Y in J20-hAPP(Sw,Ind) mice. This was performed at 6wks of age, and all mice were put on a high-fat Western diet. To the best of my knowledge, I am the first to generate a mixed comorbid model of J20-hAPP with atherosclerosis and study its neurovascular function. One study has previously induced atherosclerosis using the AAV-PCSK9 method in a different fAD mouse model: APP/PS1 (Grames et al., 2018), but they did not characterise neurovascular function. In my model, neurovascular coupling was not significantly impaired compared to WT controls; matching the data from J20-AD mice, however, J20-PCSK9-MIX mice did display a trend in reduced HbR washouts (***Figure 4.2***), suggesting a degree of neurovascular metabolic inefficiency with inadequate oxygen delivery to neurons.

The biggest translational finding from the J20-PCSK9-mixed comorbid model was that there was a trebling of Aβ plaques in the hippocampi compared to J20-AD mice alone (***Figure 4.5A***). As proposed as an initial hypothesis in ***Figure 1.6*** (chapter 1); as well proposed by the 2-hit degeneration hypothesis by Zlokovic (Zlokovic, 2005, Zlokovic, 2011), these findings that I have reported confirm these assumptions and prove that vascular factors ("hit-1") exacerbate neurological factors ("hit-2") to accelerate, or worsen neurological outcomes. Although this finding was not significant in the cortex (***Figure S7-left***), there was an upwards trend, and if the plaque counts are combined for the whole coronal sections incorporating hippocampi and cortices, then the overall increase in plaques is still significant (***Figure S7-right***). Furthermore, the size of each plaque in the J20-PCSK9-MIX mice is much larger than in J20-AD mice alone, although this morphological assessment needs to be verified at a higher resolution. This novel comorbid mouse model is not an aggressive phenotype compared to the other fAD and atherosclerotic models; such as 3xTg fAD (APP/PS1/Tau) or the ApoE$^{-/-}$ model of atherosclerosis. I hypothesise that inducing atherosclerosis using the AAV-PCSK9 method in APP/PS1, 3xTg, 5xfAD models of AD, or crossbreeding these models with ApoE$^{-/-}$ strains fed a Western diet would lead to severe phenotypes, that could equate to aggressive forms of fAD that occur earlier in life. However, despite the mild nature of this comorbid mouse model, the trebling of plaques in the hippocampus is indicative of an accelerated disease-course, and as such proves that comorbid factors; namely atherosclerosis, can worsen pre-existing AD-related neuropathology. I further hypothesise that this trebling of plaques could worsen behavioural outcomes, which would be assessed in future studies. Aβ plaques can wrap around cerebral blood vessels; cerebral amyloid angiopathy (CAA), which can lead to impeded vasodilatory responses (***Figure S9***), and this would be worse in such models.

A consistent finding irrespective of stimulation and condition was that PCSK9-ATH mice display stability throughout the imaging sessions, and all responses are similar across the session. J20-AD and J20-PCSK9-MIX, on the other hand, exhibited a baseline HbT shift throughout the imaging session, especially after transitioning to air and after CSD (in a time dependent manner) (***Figure S4***). This highlights the critical importance of methodology in determining the true reflection of disease-dependent effects, where timing (post-anaesthesia and CSD) and procedure (acute vs chronic) are important considerations for preclinical neurovascular studies. It is important to note, on acute imaging sessions haemodynamic responses were compromised due to the effect of CSD and were no longer significantly different in any of the mice in such circumstances, especially as I began my first stimulations after a 35-minute period of recovery post-CSD. This is in contrast to the labs previous work (Sharp et al., 2019), in which on acute imaging sessions, there was a significant difference in HbT between WT and J20-AD mice as we did not wait the additional time period to allow the CSD to recover. However, as presented in chapter 4, I have allowed the effects of CSD to somewhat subdue and baselines to partially recover thus the initial stimulation is no longer significantly different across any of the groups (***Figure 4.6***). Using the labs preparation and my paradigm, I am able to tease apart the effects of disease but there are added confounds such as baseline state of J20-based animals that dependent on anaesthesia and disease. As the concatenated data shows (***Figure 4.7***), any of these observations can be made easily due to the attention to such details. I also presented the average of all the raw stimulation trials from each animal across the whole experimental session (***Figure 4.7***), showing the stability and robustness of the preparation, as well as easily identifying any changes; such as baseline shifts, which are apparent in J20-based animals. A question may arise as to why would J20-based animals exhibit such a baseline drift at this age? As chapter 3 discusses in detail, hyperexcitability is seen in all J20-animals up to around the age of 8/9 months. Since I used animals starting at this age group, it may be that the hyperexcitability related oxygen effect may still be present in these animals, albeit to a smaller extent, and this may be the cause of such a baseline dilation at the start as my paradigm begins using hyperoxia.

During the experimental stage, two J20-PCSK9-MIX mice died due to anaesthetic induction and a further mouse had to be humanely euthanised after it became paralysed after anaesthesia for surgery. One PCSK9-ATH mouse also died after recovery from surgery. Common in all these mice was their excessive weight (***Figure S3***). None of the WT or J20-AD mice died due to anaesthesia. In humans, carrying excessive body weight, fat and increased BMI >30 leads to several complications especially with respect to sudden death, pulmonary, cardiac and cerebrovascular incidents (Adams and Murphy, 2000). This risk is further exacerbated in anaesthetic conditions where the risk of hypoventilation, hypoxaemia,

hypercapnia and cardiac failure greatly increases. It may be that these mice suffered from such effects causing their deaths. Furthermore, the incidence of stroke causing paralysis is also raised post-anaesthesia especially with existing comorbidities (Wong et al., 2000).

5.5 – CSD Is More Severe in Diseased Mice and Relates to Levels of Neuroinflammation.

As part of the experimental protocol, the final experimental session included an acute imaging session where a small burr-hole was drilled into the skull overlying the active region (determined from the chronic imaging sessions), and a multichannel microelectrode inserted into the brain to record neural activity in combination with haemodynamic activity by 2D-OIS. As discussed throughout chapter 3 and chapter 4, whenever an electrode was inserted into the brain, the initial stimulation resulted in a much smaller haemodynamic response compared to the first stimulation on chronic imaging days. As suggested in a previous paper that I co-authored (Sharp et al., 2019), the technical process of electrode insertion may cause a CSD that leads to the impaired phenotypes observed (a hypothesis that I tested in my PhD project and subsequently confirmed). To test this, I recorded the baseline haemodynamics prior to and after electrode insertion to assess what changes occurred in the cortex. In all mice, the haemodynamic correlate of CSD occurred. This is characterised by a triphasic S-shaped change in HbT; an initial decrease (constriction), followed by an increase (dilation), then decrease again, that persists for some time in all mice (***Figure 4.3*****).** The observed CSD began at the site of electrode insertion and spread unidirectionally across the observable cortical surface to the opposite end in a wave of this characteristic triphasic change in HbT. However, CSD profiles were significantly different in the diseased groups compared to WT mice. Compared to WT mice, the initial constriction was more profound in the 3 diseased groups; with the strongest constriction in J20-AD mice, and the dilatory bounce back was minimal as this phase was quickly succumbed to a prolonged and profound constriction below the baseline that persisted for a significantly longer time compared to WT controls. These observations may be related to IL1β neuroinflammatory changes (***Figure 4.5***), where J20-AD mice display the most significant upregulation of IL1β mRNA and display the most severe CSD, followed by PCSK9-ATH, followed by J20-PCSK9-MIX mice, although this needs to be further validated to prove causation. This will be discussed in more detail later (*section 5.6*).

In the experimental protocol, the insertion of an electrode is akin to a pin-prick model of minimal brain damage which causes CSD. However, as this trigger causes CSD, it can also be a proxy model for migraine with aura and epilepsy spread. As discussed extensively in chapter 5, the frequency of migraines is higher in those with cardiovascular disease (Kurth et al., 2020), those at risk of developing AD (Morton et al., 2019), and epilepsy is a more common occurrence in EOAD/EMCI (Sherzai et al., 2014). Furthermore, recurrent sports-related

injuries (concussions causing TBI) can lead to an increased risk of developing severe neurological conditions including Parkinson's and AD (Henry et al., 2017). The strongest CSDs occurred in brains with the highest levels of IL1β (AD and ATH respectively), thus confirming previous epidemiological and clinical observations that migraine frequency is associated with cardiovascular disease and an increased risk of dementia. My data show that brains with the highest levels of global neuroinflammation are primed for a more devastating effect of CSD – whether it occurs as a result of migraine, epilepsy or TBI – and lead to prolonged ischaemic and potentially hypoxic periods characterised with long period of neurovascular uncoupling and metabolic shifts that cause neuronal stress and potentially pannecrosis of both neurons and glia. This, over time, would lead to widespread neurodegeneration and lead to the onset of dementia. Although the CSD in J20-PCSK9-MIX mice was the least severe of the other 2 disease groups, it directly relates to the levels of neuroinflammation (i.e. reduced compared to J20-AD and PCSK9, but still higher than WT), and as I have suggested that these mice may have an altered and accelerated disease-course, it may be that observing CSD at an earlier timepoint may reveal more profound changes. Due to prolonged periods of reduced CBF and ischaemia, coupled with increased Aβ deposition, I would hypothesise that AD-onset would be exacerbated in these mice coupled with more severe behavioural deficits.

5.6 – Cellular & Molecular Mechanisms Underpinning the Observed Phenotypes – Potential Therapeutic Implications by Targeting Neuroinflammation?

Understanding the cellular and molecular basis for the observed phenotypes is essential in finding viable and prominent therapeutic targets. In order to assess cellular & molecular alterations in the different mouse groups, I dissected the brains from the mice after terminal acute imaging experiments and processed one half hemisphere in formalin to use for immunohistochemistry, whereas the other half hemisphere was snap-frozen using isopentane and stored at -80^{o}C for genetic studies. Firstly, I performed immunohistochemistry for the major cell types of the NVU: neurons (NeuN), astrocytes (GFAP), microglia (Iba1) & pericytes (PDGFRb). With respect to neuronal counts, there was a small trend towards a reduction in the number of cortical neurons in PCSK9-ATH mice compared to WT controls (***Figure S6***). J20-AD mice do not exhibit any significant neuronal loss. J20-PCSK9-ATH mice also display reduced cortical neuronal counts which was significant in the cortex (***Figure S6***), although the baseline drift of HbT throughout the imaging protocol confounds the earlier observed impairments overall (***2s-oxygen; Figure 4.2***). These results are indicative of the beginnings of potential neuronal decline at this age-group; exacerbated by comorbidity, and longitudinal assessments after this age group may reveal enhanced neurodegeneration in all diseased mice, especially PCSK9-ATH and J20-PCSK9-MIX mice.

All diseased mice showed evidence of reactive astrocytes and alterations to microglial morphology, though none exhibited a clear cellular proliferation (***Figure S6***). Furthermore, all 3 diseased groups exhibited altered microglial morphologies that may relate to a reactive state. Together with astrogliosis and microgliosis, these are indicative of potential nervous system damage in all 3 disease mouse groups (especially with reduced neuronal counts in the cortex of PCSK9-ATH and J20-PCSK9-MIX mice). Although I do not report a significant increase in Iba1+ microglia (i.e. no proliferation at this stage), the presence of shorter processes and some ameboid cells is indicative of microglial transitioning in response to neuroinflammation. Furthermore, the clustering of active microglia in J20-AD and J20-PCSK9-MIX mice may be around Aβ plaques (***Figure S6***), although this needs to be validated by dual staining in future studies. Other studies have shown increased cell number of microglia in the more severe $ApoE^{-/-}$ model (Denes et al., 2012). The findings of the PCSK9-ATH model may be more reflective of a milder disease-course in both mice and humans. Another interesting observation from the histological analysis was a reduction in pericyte coverage in PCSK9-ATH and J20-PCSK9-MIX mice compared to WT and J20-AD mice (***Figure S6***), although this effect was non-significant after correcting for multiple comparisons. Despite this, this suggests a trend towards reduced pericyte numbers in these diseased mice and may be causative in microvascular dysfunction associated with small vessel disease and ischaemia in cortical tissue. Many other studies have found decreased pericyte coverage and capillary length in the ApoE4 model of sporadic AD (Halliday et al., 2016), and show evidence of pericyte-loss mediated neurodegeneration (Sagare et al., 2013).

As alluded to in the previous discussion in chapter 4, there may be several reasons why the J20-PCSK9-MIX mice displayed lower levels of neuroinflammation compared to J20-AD and PCSK9-ATH mice. Firstly, this new phenotype may be reflective of an altered disease-course (temporal changes) with an advanced stage phenotype compared to the age-matched pure models. Thus, the peak of neuroinflammation may have been at an earlier time-point. It may be that increased levels of neuroinflammation (in PCSK9-ATH and J20-AD mice) are representative of an initial phase of disease that leads to the profound changes seen in both human patients and model organisms, and that over time these significantly higher levels begin to resolved by the time-point I investigated (in J20-PCSK9-MIX mice), and other factors could be upregulated**.** Secondly, it is not necessarily the case that 2 distinct inflammatory diseases ‘add-up’ their levels of inflammation in a comorbid setting, due to different mechanisms involved. Interestingly, neurovascular coupling is impaired in PCSK9-ATH mice the most, and this corresponds to these mice having the highest levels of TNFα in the brain, however, this also needs to be validated. TNFα may be a crucial cytotoxic chemokine leading to neuronal and glial dysfunction in the brain. Astrocytes are able to secrete TNFα induced by

circulating cytokines, including IL1β (Chung and Benveniste, 1990), which itself is the key inflammatory driver of systemic atherosclerosis (Rader, 2012). Furthermore, a study showing the pharmacological inhibition of reactive astrogliosis by *withaferin A* was able to protect against neuronal loss by limiting the production of TNFα (Livne-Bar et al., 2016). The *de novo* production of TNFα by glial cells within the CNS is part of the neuro-inflammatory response in the presence of neuropathology (Olmos and Llado, 2014). TNFα can lead to glutamate-mediated excitotoxicity as well as increased calcium-mediated excitotoxicity within neurons thus leading to a progressive neuronal loss within the brain (Olmos and Llado, 2014), as seen in my data. Behaviourally, it has been shown that systemic TNFα can produce cognitive dysfunction and symptoms of sickness behaviour (Hennessy et al., 2017). Symptoms of delirium are also highly exacerbated by the presence of neuroinflammation, importantly due to high levels of TNFα within the brain (van Gool et al., 2010). Though I have not performed any behavioural tests on these mice, performing cognitive tests may confirm signs of early dementia and sickness behaviour in future studies. I also saw a significant increase in IL1β levels in the brains of PCSK9-ATH mice. It has been demonstrated that hypoxia is able to induce IL1β expression in macrophages, in addition to enhanced secretion of IL1β in the presence of cholesterol crystals (Folco et al., 2014). However, it is important to note that my findings of neuroinflammation are related to global changes across the brain (whole homogenates) rather than being cell-specific, thus the origin of TNFα in my study cannot be determined. Future work would investigate the cell specific origins of inflammation in the brain of these mice to provide a more comprehensive outlook as to the exact mechanisms underlying the observed phenotypes of neuronal loss.

Whilst the CSD haemodynamic changes were significant for PCSK9-ATH mice compared to WT (***Figure 4.3***), the most profound CSD occurred in J20-AD mice, and this may relate to the levels of IL1β (***Figure 4.5***). However, another interesting observation relating to the MUA changes immediately post-CSD seemed to be more related to levels of TNFα with the highest surge in MUA followed by the strongest silencing of MUA happening in PCSK9-ATH mice (***Figure S8***). The exact physiological relevance of this observation is not immediately apparent; however, it is likely that this surge phase (200s) is related to the 'bounce back' phase of the CSD-haemodynamic recovery (upwards HbT during the triphasic response). The period of MUA silencing after this phase is also interesting as it may be reflective of the sustained vasoconstriction below baseline that occurs and may be related to neuronal exhaustion due to the metabolic mismatch during the initial CSD phase where periods of neurovascular uncoupling lead to massive metabolic deficits (i.e. severely reduced perfusion and saturation not able to sustain neuronal function) leading to this period of silencing in order to recuperate.

Finally, a surprising finding was the upregulation of *NOS1* and *NOS3* mRNA in J20-AD, PCSK9-ATH and J20-PCSK9-MIX mice (***Figure S5***). *NOS1* encodes neuronal nitric oxide synthase (nNOS) and *NOS3* encodes endothelial NOS (eNOS). qRT-PCR revealed the highest upregulation of *NOS1* mRNA in J20-AD mice, whilst the highest upregulation of *NOS3* mRNA was in PCSK9-ATH mice. These observations reflect the pathology, AD being neurological in origin (nNOS) whereas atherosclerosis is vascular in origin (eNOS). Whilst the literature surrounding NOS expression in clinical and preclinical studies is often contradictory and inconclusive, my finings of upregulated NOS mRNA may be indicative of two distinct possibilities: i) increased functional hyperaemia from lowered baseline by increased NOS (i.e. vasodilatory) to compensate for perceived ischaemia, or ii) the production of toxic NO^- radicals by NOS uncoupling. eNOS, releasing NO, can influence vessel tone and diameter via cGMP signalling, however, in excessive amounts, the enzyme can uncouple leading to the production of NO and $O2^-$ reactive oxygen species (ROS) which subsequently react to form $OONO^-$, a major cause of oxidative damage (Huang, 2009). It has been demonstrated that TNFα is able to induce both eNOS in HeLa cells (Barsacchi et al., 2003) and iNOS in macrophages under experimental inflammatory conditions (Fonseca et al., 2003). Thus, there may be a toxic vicious cycle of induction and synergy between TNFα and NOS under pathological conditions such as atherosclerosis that can contribute to neuronal death. The enhanced levels of eNOS, along with iNOS, may be a compensatory mechanism to sustain baseline vasodilation in the presence of diminished cerebral blood flow and hypoxia in the PCSK9-ATH mice, but also inadvertently damaging to neurons due to the potential production of ROS and interactions with TNFα. Thus, the potentially toxic combination of enhanced glial TNFα as well as eNOS may/could be the cause of the neurovascular deficits seen in PCSK9-ATH mice, though this would be investigated in future studies to define a mechanism.

Whilst the initial upregulation, seen here, may be related to compensatory mechanisms, it may be that over time toxic NO^- radical contribute to neurovascular decline. A recent study published in Nature found that caveolae within brain arterioles play a key role in regulating neurovascular coupling (Chow et al., 2020). Caveolae are membrane invaginations found within cells (to allow transcytosis) and tissues (including arterioles), and are formed by caveolin-1, encoded by *Cav1*. In their study, $Cav1^{-/-}$ mice displayed impaired caveolae, and subsequently exhibited impaired haemodynamic responses; both arteriolar diameter changes and capillary blood flow, to whisker stimulation compared to controls (Chow et al., 2020). *Cav1* interacts with eNOS, and $NOS3^{-/-}$ mice display similar levels of evoked-arteriolar dilation and capillary blood flow compared to $Cav1^{-/-}$ mice, but $NOS3^{-/-}/Cav1^{-/-}$ mice exhibit completely ablated evoked-responses, suggesting both mediate their effects independently. Thus, this study highlights not only novel mechanisms of NVC but also the importance of assessing

redundant mechanisms that may allow for continued physiological processes to occur. Furthermore, the recent identification of NO-containing endothelial notches in zebrafish, called *Kugelns* (identified by Elizabeth Kugler & Tim Chico here at the University of Sheffield) (Kugler et al., 2019), which may also play a role in endothelial function and NO signalling is of great interest, however, these need to be identified in mammals to understand their function in health and disease models. As discussed in chapter 4, the interactions between TNFα and eNOS can cause a vicious cycle of detrimental effects, thus targeting neuroinflammation may allow for the resumption of normal NOS function.

5.7 – Conclusion

In conclusion, I have found key neurovascular, neuropathological and neuroinflammatory changes in 3 different mouse models of human disease: J20-AD (hAPPSw,Ind), PCSK9-ATH (rAAV8-mPCSK9-D377Y) and a novel comorbid J20-PCSK9-MIX model.

The **4 key translational findings** from my PhD are summarised below:

1. **Normobaric hyperoxia can elevate baseline blood volume** and oxygen saturation in the brain in young 6m J20-AD mice. Increasing baseline blood volume, flow and saturation may enhance the glymphatic clearance of Aβ from the brain. This effect could also be used clinically to elevate baseline blood flow and saturation in prodromal/early-onset AD patients to increase glymphatic mediated Aβ clearance.
2. **Systemic atherosclerosis leads to reduced evoked-haemodynamic responses** in the cortex characterised by impairments to neurovascular coupling and neurovascular inefficiency. These findings are associated with elevated cerebral neuroinflammation: IL-1β and TNFα, and therapeutically antagonising these may reverse these phenotypes and work as effective treatments in patients with cardiovascular disease.
3. **Cortical spreading depression (CSD) is more severe in diseased animals** and relates to global neuroinflammation levels. Furthermore, this is highly related to increased migraine and seizure frequency. In addition, CSD could be an effective clinical biomarker in the assessment of brain-state in determining cerebral vulnerabilities in the potential development of dementia and may also be an effective assessment of therapeutic interventions in preclinical neurovascular studies.
4. **Systemic atherosclerosis exacerbates pre-existing AD-related neuropathology**, especially Aβ plaques in the brain, and lead to an accelerated disease-course. Treating and managing midlife cardiovascular diseases is of vital importance for cerebral health later in life. This needs to be implemented as an urgent public health policy in countries with high incidences of both dementia and cardiovascular diseases, including the UK.

Recently, a new form of dementia, limbic-predominant age-related TDP-43 encephalopathy (LATE), was identified that may actually account for up to a third of all presumed AD-diagnoses over the age of 85 (Nelson et al., 2019). This may also be a reason as to why so many AD-related drugs that initially were successful preclinically (modelled in fAD animals) did not succeed clinical trials of larger and older AD clinical cohorts. Preclinical research, therefore, is absolutely vital in elucidating mechanisms of disease and pathophysiological processes, as well as in the development of novel and effective treatments. Recently, aducanumab; a monoclonal antibody against Aβ developed by Biogen (currently in Phase III trials), was sent for FDA approval for use in prodromal stages of AD to inhibit Aβ deposition after evidence emerged of successful Aβ reduction with some clinical benefits with as much as up to 23% reduction in the rate of cognitive decline (Schneider, 2020). This was not a definitive clinical treatment in a parallel clinical trial. Whilst both of these new discoveries have been the two single most important advancements in the field of AD research, there still remain no definitive disease modifying or curative treatment. The findings from my PhD suggest novel findings with respect to prodromal AD and midlife atherosclerosis and mixed pathology, which need to be considered if new therapies are to succeed clinically. Namely, normobaric hyperoxia could work similar to aducanumab in terms of reducing early-Aβ, and that the targeting of neuroinflammation early in life may be critical in stabilising neurovascular, neuropathological and subsequent clinical decline associated with VaD, AD and mixed dementia. Furthermore, and importantly, the presence of one comorbidity can greatly exacerbate neuropathology at the same age, thus therapies aiming to reduce Aβ; such as aducanumab, may not be as effective in comorbid patients due to the higher levels of overall Aβ. This is why it is absolutely crucial to investigate comorbid models to better reflect the clinical presentation, and if any novel therapy is able to target the enhanced effects of comorbidity that is present in large proportions of patients.

5.7 – Future Directions

The findings from my PhD have several translational implications and testing them in preclinical settings are needed before implementing such strategies in clinical trials. Firstly, trialling normobaric hyperoxia in J20-AD and related fAD-models to assess i) the effectiveness of the therapy on Aβ clearance & ii) assess behavioural outcomes by performing simple cognitive tests to determine the effectiveness of this simple approach. Finally, iii) to understand the mechanisms by which normobaric hyperoxia leads to enhanced baseline CBF in prodromal AD mice. This proposal has been submitted to Alzheimer's Society as a project grant by JB. Secondly, the findings of IL1β and TNFα mRNA upregulation in disease mice suggests that neuroinflammation may be one of the major causative factors in neurovascular decline and targeting these with antagonists: Anakinra (IL1) and Infliximab (TNFα), may

improve neurovascular function, neuropathological and behavioural outcomes. Both of these proposals have been submitted as a project grant (to BHF for IL1 by SEF; which was awarded in August 2020 to start in October 2020 as me as the post-doc) and a postdoctoral fellowship application (to ARUK & AlzSoc for TNFα by OS). These applications will seek to investigate the cellular & molecular mechanisms underlying the observed phenotypes, and to confirm some of the previously mentioned associations e.g. links to IL1β and TNFα inflammation, assessment of BBB damage and immune system involvement in the brain. Furthermore, performing behavioural studies will be important in assessing both the extent of cognitive decline in these models, but also to test the effect of the anti-inflammatory treatments (and oxygen therapy). The implications of my research findings have exciting and potentially important therapeutic applications both preclinically and clinically.

References

(ARUK), A. S. R. U. 2020. *Dementia Statisitics Hub - Prevalence of Dementia* [Online]. Available: https://www.dementiastatistics.org/statistics-about-dementia/prevalence/ [Accessed 2020].

ADAMS, J. P. & MURPHY, P. G. 2000. Obesity in anaesthesia and intensive care. *Br J Anaesth,* 85**,** 91-108.

AIMEE E VOZENILEK, S. C., CASSIDY M BLACKBURN, RENEAU CASTORE, RONALD L KLEIN, MATTHEW D WOOLARD 2019. Abstract 433: Difference in pAAV/D377Y-mPCSK9-induced Expression of mPCSK9 Between Male and Female Mice. *Arteriosclerosis, Thrombosis, and Vascular Biology,* 38.

AMEEN-ALI, K. E., SIMPSON, J. E., WHARTON, S. B., HEATH, P. R., SHARP, P. S., BREZZO, G. & BERWICK, J. 2019. The Time Course of Recognition Memory Impairment and Glial Pathology in the hAPP-J20 Mouse Model of Alzheimer's Disease. *J Alzheimers Dis,* 68**,** 609-624.

AYATA, C., SHIN, H. K., DILEKOZ, E., ATOCHIN, D. N., KASHIWAGI, S., EIKERMANN-HAERTER, K. & HUANG, P. L. 2013. Hyperlipidemia disrupts cerebrovascular reflexes and worsens ischemic perfusion defect. *J Cereb Blood Flow Metab,* 33**,** 954-62.

BACYINSKI, A., XU, M., WANG, W. & HU, J. 2017. The Paravascular Pathway for Brain Waste Clearance: Current Understanding, Significance and Controversy. *Front Neuroanat,* 11**,** 101.

BARSACCHI, R., PERROTTA, C., BULOTTA, S., MONCADA, S., BORGESE, N. & CLEMENTI, E. 2003. Activation of endothelial nitric-oxide synthase by tumor necrosis factor-alpha: a novel pathway involving sequential activation of neutral sphingomyelinase, phosphatidylinositol-3' kinase, and Akt. *Mol Pharmacol,* 63**,** 886-95.

BERWICK, J., JOHNSTON, D., JONES, M., MARTINDALE, J., REDGRAVE, P., MCLOUGHLIN, N., SCHIESSL, I. & MAYHEW, J. E. 2005. Neurovascular coupling investigated with two-dimensional optical imaging spectroscopy in rat whisker barrel cortex. *Eur J Neurosci,* 22**,** 1655-66.

BJORKLUND, M. M., HOLLENSEN, A. K., HAGENSEN, M. K., DAGNAES-HANSEN, F., CHRISTOFFERSEN, C., MIKKELSEN, J. G. & BENTZON, J. F. 2014. Induction of atherosclerosis in mice and hamsters without germline genetic engineering. *Circ Res,* 114**,** 1684-9.

CHOW, B. W., NUNEZ, V., KAPLAN, L., GRANGER, A. J., BISTRONG, K., ZUCKER, H. L., KUMAR, P., SABATINI, B. L. & GU, C. 2020. Caveolae in CNS arterioles mediate neurovascular coupling. *Nature,* 579**,** 106-110.

CHUNG, I. Y. & BENVENISTE, E. N. 1990. Tumor necrosis factor-alpha production by astrocytes. Induction by lipopolysaccharide, IFN-gamma, and IL-1 beta. *J Immunol,* 144**,** 2999-3007.

DENES, A., DRAKE, C., STORDY, J., CHAMBERLAIN, J., MCCOLL, B. W., GRAM, H., CROSSMAN, D., FRANCIS, S., ALLAN, S. M. & ROTHWELL, N. J. 2012. Interleukin-1 mediates neuroinflammatory changes associated with diet-induced atherosclerosis. *J Am Heart Assoc,* 1**,** e002006.

FOLCO, E. J., SUKHOVA, G. K., QUILLARD, T. & LIBBY, P. 2014. Moderate hypoxia potentiates interleukin-1beta production in activated human macrophages. *Circ Res,* 115**,** 875-83.

FONSECA, S. G., ROMAO, P. R., FIGUEIREDO, F., MORAIS, R. H., LIMA, H. C., FERREIRA, S. H. & CUNHA, F. Q. 2003. TNF-alpha mediates the induction of nitric oxide synthase in macrophages but not in neutrophils in experimental cutaneous leishmaniasis. *Eur J Immunol,* 33**,** 2297-306.

GOETTSCH, C., HUTCHESON, J. D., HAGITA, S., ROGERS, M. A., CREAGER, M. D., PHAM, T., CHOI, J., MLYNARCHIK, A. K., PIEPER, B., KJOLBY, M., AIKAWA, M. & AIKAWA, E. 2016. A single injection of gain-of-function mutant PCSK9 adeno-associated virus vector induces cardiovascular calcification in mice with no genetic modification. *Atherosclerosis,* 251**,** 109-118.

GRAMES, M. S., DAYTON, R. D., LU, X., SCHILKE, R. M., ALEXANDER, J. S., ORR, A. W., BARMADA, S. J., WOOLARD, M. D. & KLEIN, R. L. 2018. Gene Transfer Induced Hypercholesterolemia in Amyloid Mice. *J Alzheimers Dis,* 65**,** 1079-1086.

HALLIDAY, M. R., REGE, S. V., MA, Q., ZHAO, Z., MILLER, C. A., WINKLER, E. A. & ZLOKOVIC, B. V. 2016. Accelerated pericyte degeneration and blood-brain barrier breakdown in apolipoprotein E4 carriers with Alzheimer's disease. *J Cereb Blood Flow Metab,* 36**,** 216-27.

HENNESSY, E., GORMLEY, S., LOPEZ-RODRIGUEZ, A. B., MURRAY, C., MURRAY, C. & CUNNINGHAM, C. 2017. Systemic TNF-alpha produces acute cognitive dysfunction and exaggerated sickness behavior when superimposed upon progressive neurodegeneration. *Brain Behav Immun,* 59**,** 233-244.

HENRY, L. C., TREMBLAY, S. & DE BEAUMONT, L. 2017. Long-Term Effects of Sports Concussions: Bridging the Neurocognitive Repercussions of the Injury with the Newest Neuroimaging Data. *Neuroscientist,* 23**,** 567-578.

HUANG, P. L. 2009. eNOS, metabolic syndrome and cardiovascular disease. *Trends Endocrinol Metab,* 20**,** 295-302.

INTERNATIONAL, A. S. D. 2020. *Dementia Statistics* [Online]. Available: https://www.alz.co.uk/research/statistics [Accessed 2020].

ITURRIA-MEDINA, Y., SOTERO, R. C., TOUSSAINT, P. J., MATEOS-PEREZ, J. M., EVANS, A. C. & ALZHEIMER'S DISEASE NEUROIMAGING, I. 2016. Early role of vascular dysregulation on late-onset Alzheimer's disease based on multifactorial data-driven analysis. *Nat Commun,* 7**,** 11934.

JAHRLING, J. B., LIN, A. L., DEROSA, N., HUSSONG, S. A., VAN SKIKE, C. E., GIROTTI, M., JAVORS, M., ZHAO, Q., MASLIN, L. A., ASMIS, R. & GALVAN, V. 2018. mTOR drives cerebral blood flow and memory deficits in LDLR(-/-) mice modeling atherosclerosis and vascular cognitive impairment. *J Cereb Blood Flow Metab,* 38**,** 58-74.

JESSEN, N. A., MUNK, A. S., LUNDGAARD, I. & NEDERGAARD, M. 2015. The Glymphatic System: A Beginner's Guide. *Neurochem Res,* 40**,** 2583-99.

JOHNSTON, A. J., STEINER, L. A., GUPTA, A. K. & MENON, D. K. 2003. Cerebral oxygen vasoreactivity and cerebral tissue oxygen reactivity. *Br J Anaesth,* 90**,** 774-86.

JONES, M., BERWICK, J., JOHNSTON, D. & MAYHEW, J. 2001. Concurrent optical imaging spectroscopy and laser-Doppler flowmetry: the relationship between blood flow, oxygenation, and volume in rodent barrel cortex. *Neuroimage,* 13**,** 1002-15.

KENNERLEY, A. J., BERWICK, J., MARTINDALE, J., JOHNSTON, D., PAPADAKIS, N. & MAYHEW, J. E. 2005. Concurrent fMRI and optical measures for the investigation of the hemodynamic response function. *Magn Reson Med,* 54**,** 354-65.

KENNERLEY, A. J., BERWICK, J., MARTINDALE, J., JOHNSTON, D., ZHENG, Y. & MAYHEW, J. E. 2009. Refinement of optical imaging spectroscopy algorithms using concurrent BOLD and CBV fMRI. *Neuroimage,* 47**,** 1608-19.

KENNERLEY, A. J., MAYHEW, J. E., BOORMAN, L., ZHENG, Y. & BERWICK, J. 2012. Is optical imaging spectroscopy a viable measurement technique for the investigation of the negative BOLD phenomenon? A concurrent optical imaging spectroscopy and fMRI study at high field (7 T). *Neuroimage,* 61**,** 10-20.

KIVINIEMI, V., WANG, X., KORHONEN, V., KEINANEN, T., TUOVINEN, T., AUTIO, J., LEVAN, P., KEILHOLZ, S., ZANG, Y. F., HENNIG, J. & NEDERGAARD, M. 2016. Ultra-fast magnetic resonance encephalography of physiological brain activity - Glymphatic pulsation mechanisms? *J Cereb Blood Flow Metab,* 36**,** 1033-45.

KUGLER, E. C., VAN LESSEN, M., DAETWYLER, S., CHHABRIA, K., SAVAGE, A. M., SILVA, V., PLANT, K., MACDONALD, R. B., HUISKEN, J., WILKINSON, R. N., SCHULTE-MERKER, S., ARMITAGE, P. & CHICO, T. J. 2019. Cerebrovascular endothelial cells form transient Notch-dependent cystic structures in zebrafish. *EMBO Rep,* 20**,** e47047.

KURTH, T., RIST, P. M., RIDKER, P. M., KOTLER, G., BUBES, V. & BURING, J. E. 2020. Association of Migraine With Aura and Other Risk Factors With Incident Cardiovascular Disease in Women. *JAMA,* 323**,** 2281-2289.

LEE, L., BOORMAN, L., GLENDENNING, E., CHRISTMAS, C., SHARP, P., REDGRAVE, P., SHABIR, O., BRACCI, E., BERWICK, J. & HOWARTH, C. 2020. Key Aspects of Neurovascular Control Mediated by Specific Populations of Inhibitory Cortical Interneurons. *Cereb Cortex,* 30**,** 2452-2464.

LIVAK, K. J. & SCHMITTGEN, T. D. 2001. Analysis of relative gene expression data using real-time quantitative PCR and the 2(-Delta Delta C(T)) Method. *Methods,* 25**,** 402-8.

LIVNE-BAR, I., LAM, S., CHAN, D., GUO, X., ASKAR, I., NAHIRNYJ, A., FLANAGAN, J. G. & SIVAK, J. M. 2016. Pharmacologic inhibition of reactive gliosis blocks TNF-alpha-mediated neuronal apoptosis. *Cell Death Dis,* 7**,** e2386.

LUCEY, B. P., HICKS, T. J., MCLELAND, J. S., TOEDEBUSCH, C. D., BOYD, J., ELBERT, D. L., PATTERSON, B. W., BATY, J., MORRIS, J. C., OVOD, V., MAWUENYEGA, K. G. & BATEMAN, R. J. 2018. Effect of sleep on overnight cerebrospinal fluid amyloid beta kinetics. *Ann Neurol,* 83**,** 197-204.

MAYHEW, J., ZHENG, Y., HOU, Y., VUKSANOVIC, B., BERWICK, J., ASKEW, S. & COFFEY, P. 1999. Spectroscopic analysis of changes in remitted illumination: the response to increased neural activity in brain. *Neuroimage,* 10**,** 304-26.

MINKEVICIENE, R., RHEIMS, S., DOBSZAY, M. B., ZILBERTER, M., HARTIKAINEN, J., FULOP, L., PENKE, B., ZILBERTER, Y., HARKANY, T., PITKANEN, A. & TANILA, H. 2009. Amyloid beta-induced neuronal hyperexcitability triggers progressive epilepsy. *J Neurosci,* 29**,** 3453-62.

MORTON, R. E., ST JOHN, P. D. & TYAS, S. L. 2019. Migraine and the risk of all-cause dementia, Alzheimer's disease, and vascular dementia: A prospective cohort study in community-dwelling older adults. *Int J Geriatr Psychiatry,* 34**,** 1667-1676.

MUCKE, L., MASLIAH, E., YU, G. Q., MALLORY, M., ROCKENSTEIN, E. M., TATSUNO, G., HU, K., KHOLODENKO, D., JOHNSON-WOOD, K. & MCCONLOGUE, L. 2000. High-level neuronal expression of abeta 1-42 in wild-type human amyloid protein precursor transgenic mice: synaptotoxicity without plaque formation. *J Neurosci,* 20**,** 4050-8.

NELSON, P. T., DICKSON, D. W., TROJANOWSKI, J. Q., JACK, C. R., BOYLE, P. A., ARFANAKIS, K., RADEMAKERS, R., ALAFUZOFF, I., ATTEMS, J., BRAYNE, C., COYLE-GILCHRIST, I. T. S., CHUI, H. C., FARDO, D. W., FLANAGAN, M. E., HALLIDAY, G., HOKKANEN, S. R. K., HUNTER, S., JICHA, G. A., KATSUMATA, Y., KAWAS, C. H., KEENE, C. D., KOVACS, G. G., KUKULL, W. A., LEVEY, A. I., MAKKINEJAD, N., MONTINE, T. J., MURAYAMA, S., MURRAY, M. E., NAG, S., RISSMAN, R. A., SEELEY, W. W., SPERLING, R. A., WHITE III, C. L., YU, L. & SCHNEIDER, J. A. 2019. Limbic-predominant age-related TDP-43 encephalopathy (LATE): consensus working group report. *Brain,* 142**,** 1503-1527.

OLMOS, G. & LLADO, J. 2014. Tumor necrosis factor alpha: a link between neuroinflammation and excitotoxicity. *Mediators Inflamm,* 2014**,** 861231.

PALOP, J. J., CHIN, J., ROBERSON, E. D., WANG, J., THWIN, M. T., BIEN-LY, N., YOO, J., HO, K. O., YU, G. Q., KREITZER, A., FINKBEINER, S., NOEBELS, J. L. & MUCKE, L. 2007. Aberrant excitatory neuronal activity and compensatory remodeling of inhibitory hippocampal circuits in mouse models of Alzheimer's disease. *Neuron,* 55**,** 697-711.

PLUMP, A. S., SMITH, J. D., HAYEK, T., AALTO-SETALA, K., WALSH, A., VERSTUYFT, J. G., RUBIN, E. M. & BRESLOW, J. L. 1992. Severe hypercholesterolemia and atherosclerosis in apolipoprotein E-deficient mice created by homologous recombination in ES cells. *Cell,* 71**,** 343-53.

RADER, D. J. 2012. IL-1 and atherosclerosis: a murine twist to an evolving human story. *J Clin Invest,* 122**,** 27-30.

RASMUSSEN, M. K., MESTRE, H. & NEDERGAARD, M. 2018. The glymphatic pathway in neurological disorders. *Lancet Neurol,* 17**,** 1016-1024.

ROCHE-MOLINA, M., SANZ-ROSA, D., CRUZ, F. M., GARCIA-PRIETO, J., LOPEZ, S., ABIA, R., MURIANA, F. J., FUSTER, V., IBANEZ, B. & BERNAL, J. A. 2015. Induction of sustained hypercholesterolemia by single adeno-associated virus-mediated gene transfer of mutant hPCSK9. *Arterioscler Thromb Vasc Biol,* 35**,** 50-9.

SAGARE, A. P., BELL, R. D., ZHAO, Z., MA, Q., WINKLER, E. A., RAMANATHAN, A. & ZLOKOVIC, B. V. 2013. Pericyte loss influences Alzheimer-like neurodegeneration in mice. *Nat Commun,* 4**,** 2932.

SAKA, M., BERWICK, J. & JONES, M. 2010. Linear superposition of sensory-evoked and ongoing cortical hemodynamics. *Front Neuroenergetics,* 2.

SCHNEIDER, L. 2020. A resurrection of aducanumab for Alzheimer's disease. *Lancet Neurol,* 19**,** 111-112.

SHABIR, O., SHARP, P., REBOLLAR, M. A., BOORMAN, L., HOWARTH, C., WHARTON, S. B., FRANCIS, S. E. & BERWICK, J. 2020. Enhanced Cerebral Blood Volume under Normobaric Hyperoxia in the J20-hAPP Mouse Model of Alzheimer's Disease. *Sci Rep,* 10**,** 7518.

SHAPIRA, R., SOLOMON, B., EFRATI, S., FRENKEL, D. & ASHERY, U. 2018. Hyperbaric oxygen therapy ameliorates pathophysiology of 3xTg-AD mouse model by attenuating neuroinflammation. *Neurobiol Aging,* 62**,** 105-119.

SHARP, P. S., AMEEN-ALI, K. E., BOORMAN, L., HARRIS, S., WHARTON, S., HOWARTH, C., SHABIR, O., REDGRAVE, P. & BERWICK, J. 2019. Neurovascular coupling preserved in a chronic mouse model of Alzheimer's disease: Methodology is critical. *J Cereb Blood Flow Metab***,** 271678X19890830.

SHARP, P. S., SHAW, K., BOORMAN, L., HARRIS, S., KENNERLEY, A. J., AZZOUZ, M. & BERWICK, J. 2015. Comparison of stimulus-evoked cerebral hemodynamics in the awake mouse and under a novel anesthetic regime. *Sci Rep,* 5**,** 12621.

SHERZAI, D., LOSEY, T., VEGA, S. & SHERZAI, A. 2014. Seizures and dementia in the elderly: Nationwide Inpatient Sample 1999-2008. *Epilepsy Behav,* 36**,** 53-6.

SHOKRI-KOJORI, E., WANG, G. J., WIERS, C. E., DEMIRAL, S. B., GUO, M., KIM, S. W., LINDGREN, E., RAMIREZ, V., ZEHRA, A., FREEMAN, C., MILLER, G., MANZA, P., SRIVASTAVA, T., DE SANTI, S., TOMASI, D., BENVENISTE, H. & VOLKOW, N. D. 2018. beta-Amyloid accumulation in the human brain after one night of sleep deprivation. *Proc Natl Acad Sci U S A,* 115**,** 4483-4488.

VAN GOOL, W. A., VAN DE BEEK, D. & EIKELENBOOM, P. 2010. Systemic infection and delirium: when cytokines and acetylcholine collide. *Lancet,* 375**,** 773-5.

VOSSEL, K. A., BEAGLE, A. J., RABINOVICI, G. D., SHU, H., LEE, S. E., NAASAN, G., HEGDE, M., CORNES, S. B., HENRY, M. L., NELSON, A. B., SEELEY, W. W., GESCHWIND, M. D., GORNO-TEMPINI, M. L., SHIH, T., KIRSCH, H. E., GARCIA, P. A., MILLER, B. L. & MUCKE, L. 2013. Seizures and epileptiform activity in the early stages of Alzheimer disease. *JAMA Neurol,* 70**,** 1158-66.

WOLTERS, F. J. & IKRAM, M. A. 2019. Epidemiology of Vascular Dementia. *Arterioscler Thromb Vasc Biol,* 39**,** 1542-1549.

WONG, G. Y., WARNER, D. O., SCHROEDER, D. R., OFFORD, K. P., WARNER, M. A., MAXSON, P. M. & WHISNANT, J. P. 2000. Risk of surgery and anesthesia for ischemic stroke. *Anesthesiology,* 92**,** 425-32.

XU, F., LIU, P., PASCUAL, J. M., XIAO, G. & LU, H. 2012. Effect of hypoxia and hyperoxia on cerebral blood flow, blood oxygenation, and oxidative metabolism. *J Cereb Blood Flow Metab,* 32**,** 1909-18.

ZLOKOVIC, B. V. 2005. Neurovascular mechanisms of Alzheimer's neurodegeneration. *Trends Neurosci,* 28**,** 202-8.

ZLOKOVIC, B. V. 2011. Neurovascular pathways to neurodegeneration in Alzheimer's disease and other disorders. *Nat Rev Neurosci,* 12**,** 723-38.

Appendix

Figure S1 – Oil Red O Staining of Atherosclerotic Aorta. Dissected aorta from an atherosclerotic mouse was stained for fatty (lipid) deposits using Oil Red O to reveal the extent of aortic atherosclerosis. Deposits can be found bilaterally primarily in aortic arch, including the branches of the common carotids (supplying to head, neck and brain) and brachiocephalic branches. Aorta was dissected by Dr Celine Souilhol.

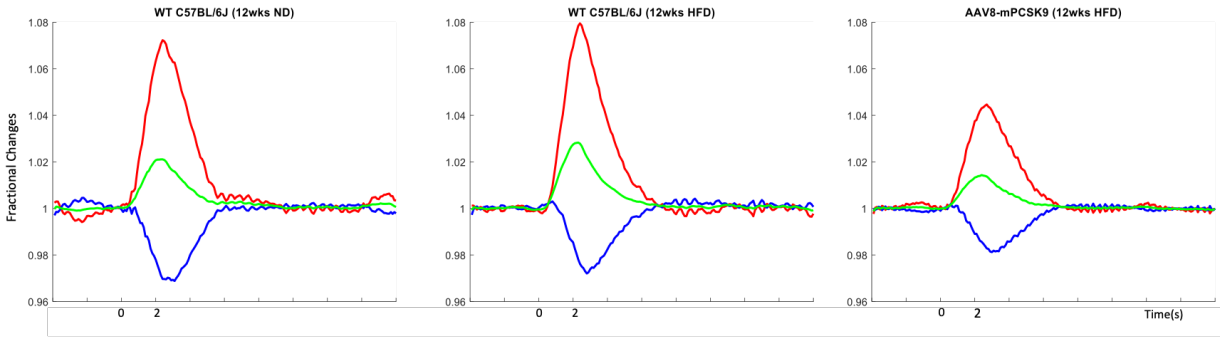

Figure S2 – 2s-Stimulation for WT, WT + HFD and AAV-PCSK9 Mice. 2s-duration evoked haemodynamic response for WT + Normal Diet (ND) (n=1), WT + High-Fat Western Diet (HFD) (n=1) & AAV8-mPCSK9/ATH (n=1). There is no difference in evoked HbT, HbO and HbR between WT and WT + HFD. ATH mice displays reduced HbT, HbO and HbR compared to both. This suggests that in mice, HFD alone (chronic) does not lead to impaired responses. All mice had 12 weeks of treatment; either no HFD (WT), HFD or with AAV-injection.

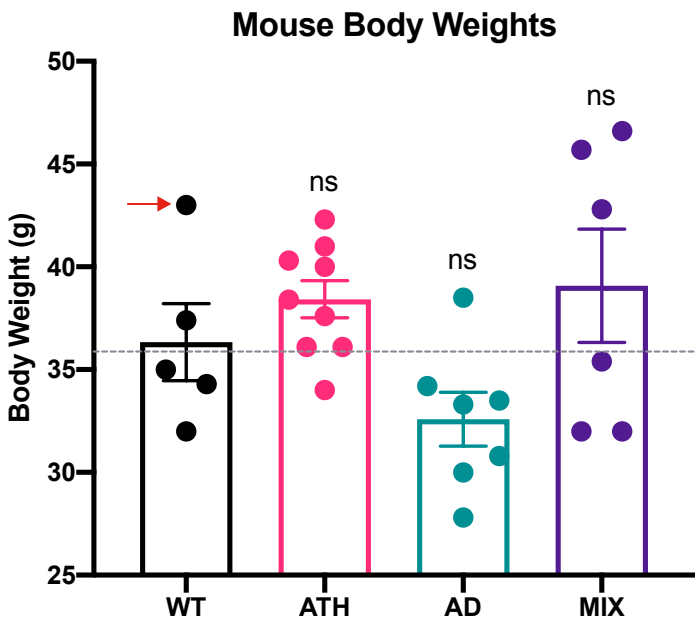

Figure S3 – Mouse Body Weights. Individual and mean body weights (g) of all mouse groups (used in chapter 6) showing. No overall significant difference between any of the groups. All HFD mice were given no more than 5g/day/mouse worth of pellets to prevent overeating and obesity. The trend for ATH and half of the MIX mice is increased weight, whereas for almost all AD and 2 MIX mice is decreased weight. The average weight of a C57BL/6J is 36g at this age group (dotted horizontal line). Error bars ±SEM. Red arrow indicates large WT mouse, without including ATH vs WT becomes significant.

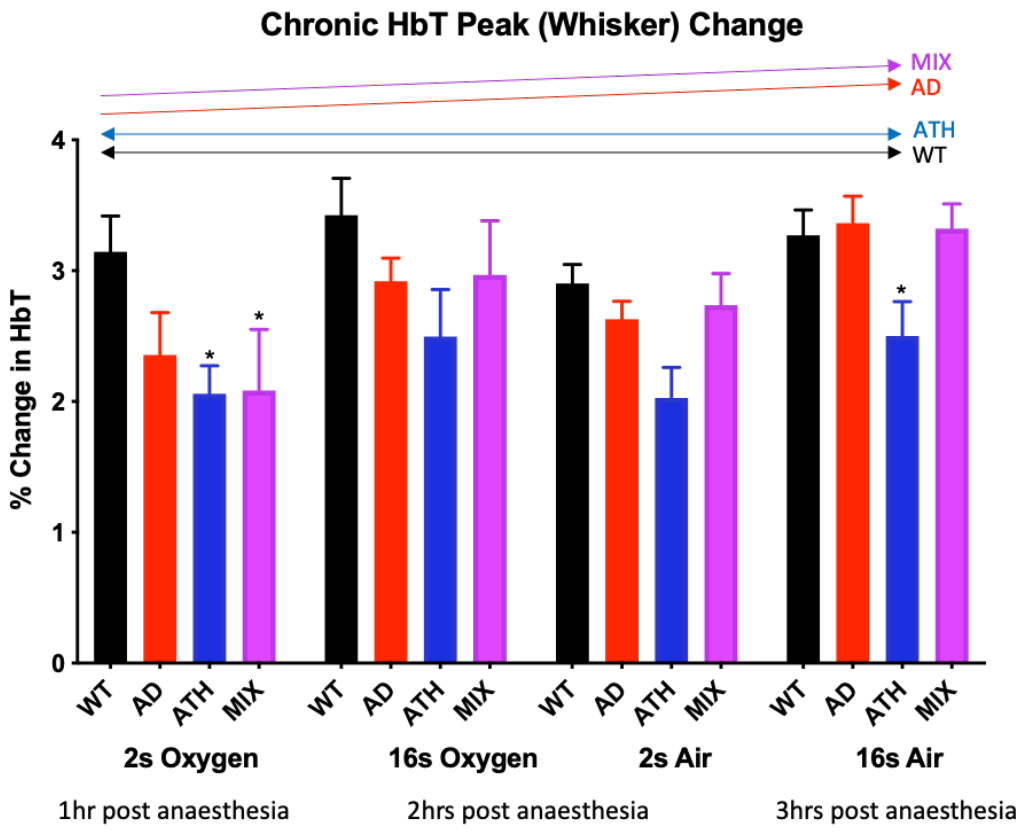

Figure S4 – Bar Graph of Mean HbT for Mouse Groups Across all Stimulations. WT and ATH mice display consistent responses across the experimental period whereas AD and MIX mice exhibit and upwards drift in baseline and evoked responses by the end of the experimental protocol. Where MIX mice display significant HbT differences compared to WT in the first stimulation, they do not by the end of the experimental protocol. Error bars ±SEM.

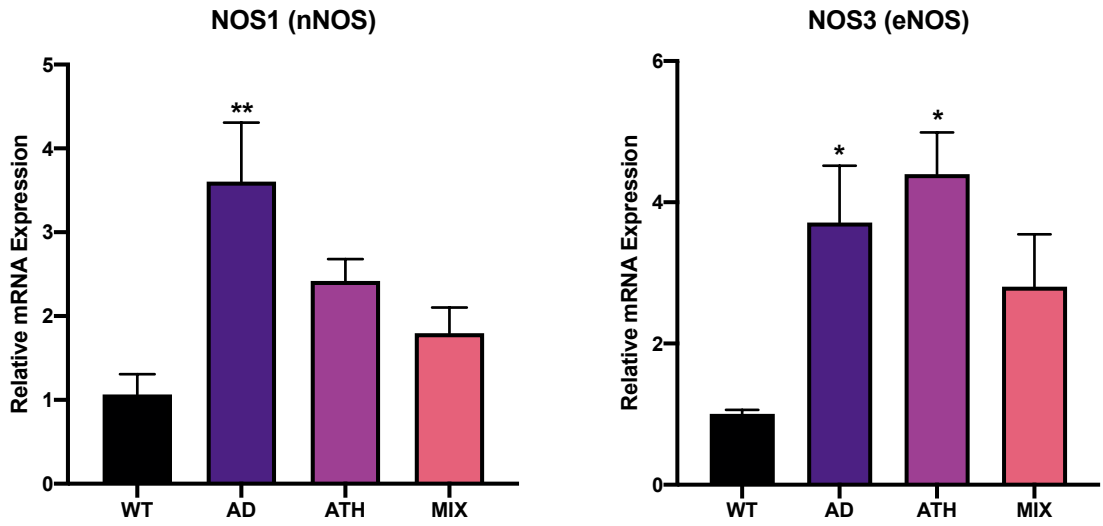

Figure S5 – NOS1 and NOS3 qRT-PCR. Left) *NOS1* (nNOS) mRNA is significantly upregulated in AD mice compared to WT (p=0.0048), ATH p=0.056(ns, but close to significance) (1-way ANOVA with post-hoc Dunnett's multiple comparisons test). Right) *NOS3* (eNOS) mRNA is significantly upregulated in AD mice (p=0.0368) and ATH mice (p=0.012) compared to WT (1-way ANOVA with post-hoc Dunnett's multiple comparisons test). Error bars ±SEM.

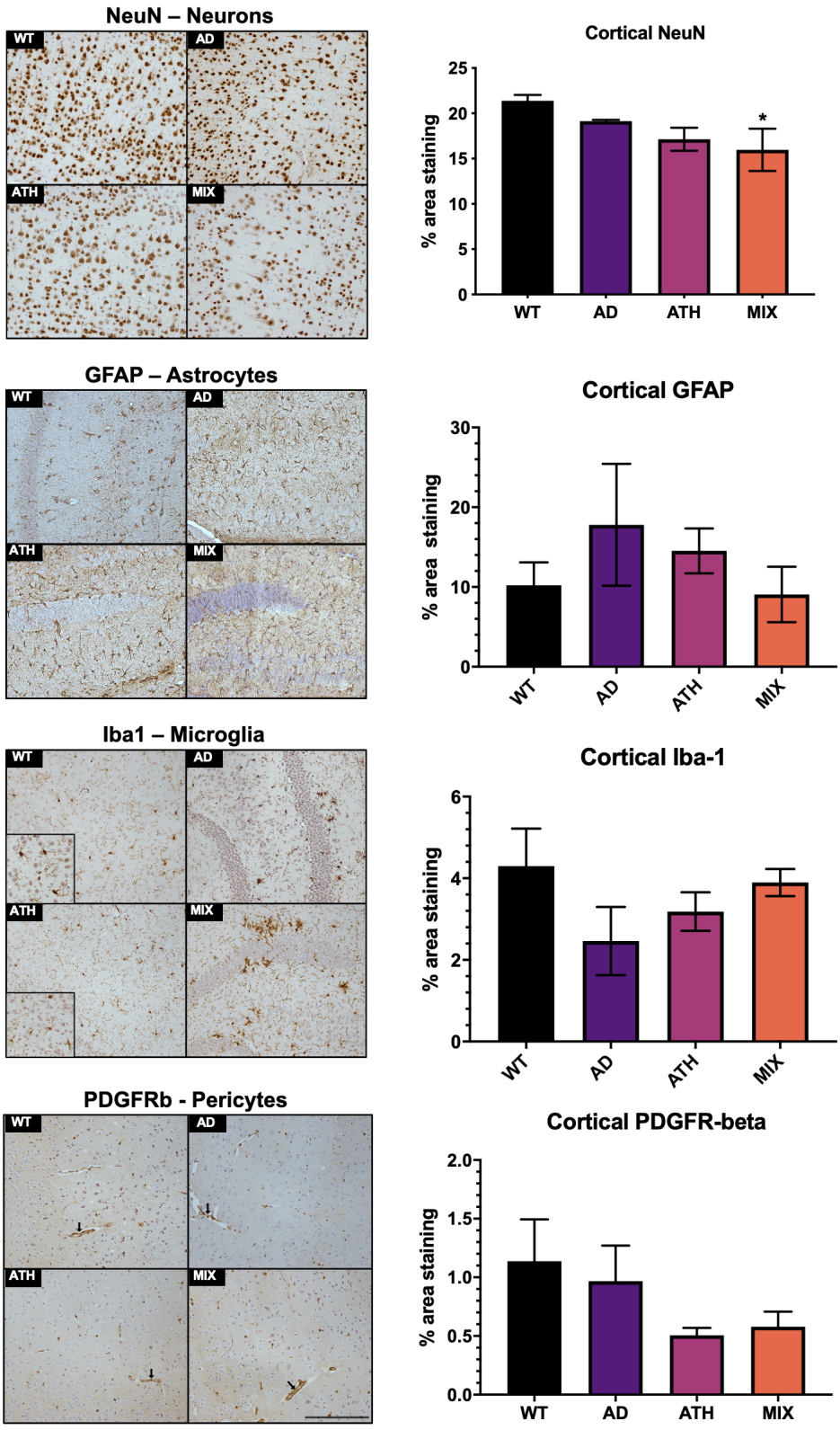

Figure S6 – Qualitative & Quantitative Histological Analysis (Cortical). Neurons (NeuN) MIX p=0.0424(*) (1-way ANOVA post-hoc Dunnett's test), astrocytes (GFAP), microglia (Iba1), pericytes (PDGFRb). N=4 each. Reduction in astrocytes in MIX may be related to neuronal and glial loss. Scale bar 200µm. Error bars ±SEM. Experiments jointly performed by Ben Pendry under my training and supervision for his MSc in Translational Neuropathology.

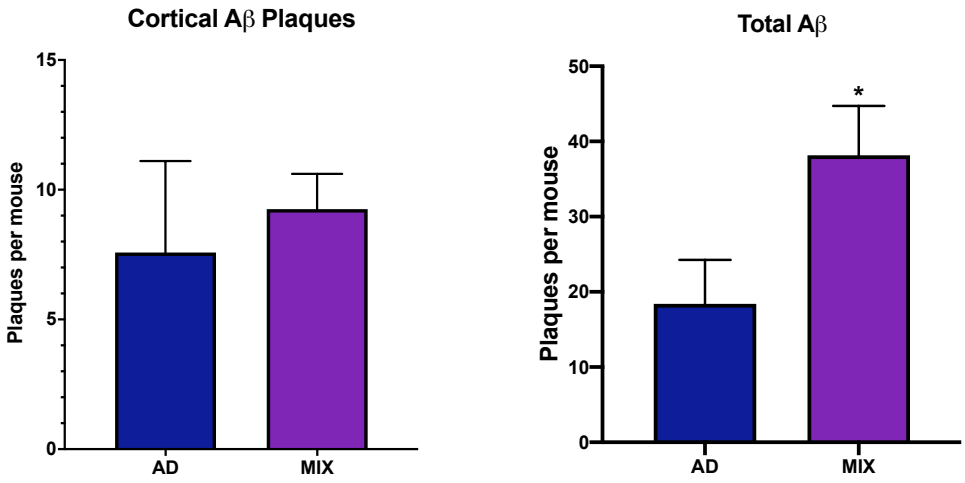

Figure S7 – Aβ Plaques. Left) Cortical Aβ plaques p=0.3372(ns). Right) Total Aβ plaques (hippocampal and cortical) p=0.0328(*). Unpaired t-tests (n=4 each). Error bars ±SEM.

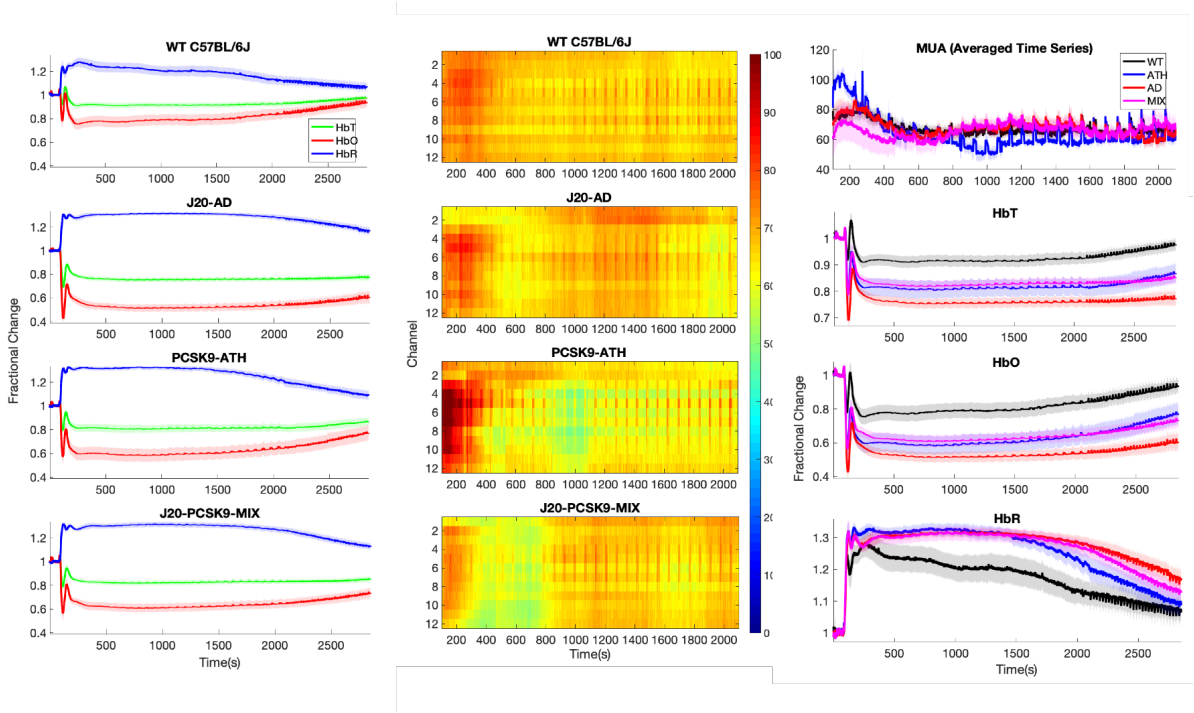

Figure S8 – CSD Haemodynamic and MUA Profiles. Left) CSD haemodynamic changes upon electrode insertion in WT, J20-AD, PCSK9-ATH & J20-PCSK9-MIX mice. Middle) CSD MUA changes immediately after electrode insertion (200s) characterised by an initial surge (strongest being in PCSK9-ATH mice), followed by MUA silencing in PCSK9-ATH and J20-PCSK9-MIX mice. Right) Timeseries for MUA (top), HbT/HbO/HbR for all 4 mouse groups. Error bars ±SEM.

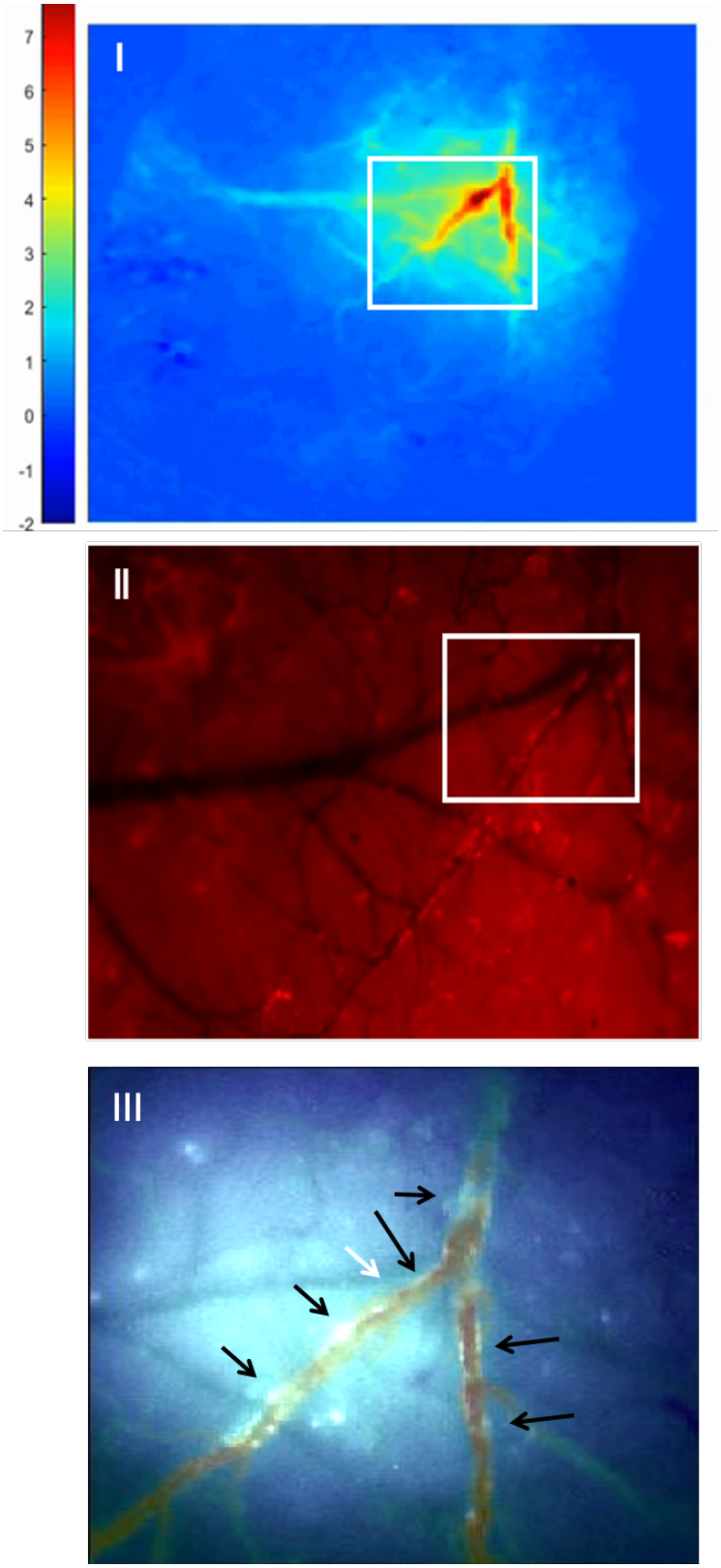

Figure S9 – Cerebral Amyloid Angiopathy in 15m J20-AD Mouse. I) 2s-stimulation evoked HbT response over zoomed in branch of MCA showing an irregular vasodilatory response characterised by a full dilation 'blob' juxtaposed to adjacent areas of less dilation. II) MCA region visualised by methoxy-X04 to label Aβ *in vivo*. III) Superimposition of A & B (using 2D-OIS and UV illumination).

Sample	Ng/µl	A260	A280	260/280	260/230	Absorption
WT5	792.24	19.806	10.561	1.88	1.41	14.082
WT4	66.28	1.657	0.952	1.74	0.73	2.257
WT2	115.77	2.894	1.73	1.67	0.79	2.648
MIX1	58.53	1.463	0.832	1.76	0.89	1.637
MIX3	12.36	0.309	0.142	2.18	1.15	0.268
MIX4	1375.26	34.381	17.096	2.01	2.11	16.318
ATH3	46.62	1.166	0.658	1.77	0.78	1.496
ATH4	144.65	3.616	1.792	2.02	1.79	2.019
ATH5	564.02	14.101	7.917	1.78	2.09	6.751
AD2	343.32	8.583	4.33	1.98	1.65	5.216
AD3	1507.02	37.675	19.844	1.9	2.23	16.886
AD4	2404.48	60.112	33.49	1.79	2.29	26.205

Table S1 – RNA Concentration and Quality (NanoDrop).
All RNA was of good usable quality and quantity and all concentrations made up to 700ng/µl (to match the lowest concentration isolated.

Doctoral Development Training (DDP)

Additional papers that I contributed to (co-authored) during my PhD:

1. **Sharp et al, 2019.** Neurovascular coupling preserved in a chronic mouse model of Alzheimer's disease: Methodology is critical. *Journal of Cerebral Blood Flow & Metabolism.* doi: 10.1177/0271678X19890830.
2. **Lee et al, 2019.** Key aspects of neurovascular control mediated by specific populations of inhibitory cortical interneurons. *Cerebral Cortex.* pii: bhz251.

I have presented my doctoral work at the following conferences/seminars:

- **Society for Neuroscience (SfN) Annual Conference**, McCormick Place, Chicago, IL, US – October 2019. I presented the majority of my PhD work at a 4-hour poster session.
- **Dementia Futures**, SITraN – July 2018 and July 2019. I presented my PhD work in a lay fashion to patients and caregivers as well as the general public. I won an award for the best oral presentation in 2018.
- **Public Health England (PHE)'s Clinical Network for Older People's Mental Health & Dementia Event**, Cedar Court Hotel, Wakefield, August 2019. I presented my PhD work and discussed the interactions of the heart-brain axis to a group of clinicians, scientists and PHE representatives. I was invited to give a talk by a representative for PHE who attended Dementia Futures.
- **Sheffield Glia Symposium 2019**, Sheffield Hallam University (Collegiate Crescent) – April 2019. I gave a talk on neurovascular methodology and the importance of considering a stable mouse preparation to observe accurate results.
- **Alzheimer's Disease & Vascular Dementia Symposium**, INOX, University of Sheffield – June 2019. I presented my PhD work to Sheffield dementia researchers.
- I have also presented my PhD work at **departmental seminars and postgraduate conferences** in the Departments of Psychology & IICD as well as SITraN, in addition to faculty-wide conferences in the Faculties of Medicine & Science.

I have delivered the following lectures/seminars:

- **'BOLD and it's Applications'**. I have given a 2-hour formal lecture twice for the MRes Research Methods course outlining key BOLD-related neuroimaging techniques and their application in clinical and preclinical research.
- **Research Seminar**. I have given a 1-hour research seminar twice to MSc Cognitive Neuroscience & Human Neuroimaging course outlining my research.

I have supervised and taught the following:

- **Day-to-Day & Academic Supervisor (2018-19)**. Mr Ben Pendry, MSc Translational Neuropathology, Department of Neuroscience (SITraN). I planned and supervised the entirety of Ben's MSc project who received a distinction in his thesis and MSc overall. Ben is also an author on the atherosclerosis and mixed model chapters/papers.
- **Day-to-Day & Academic Supervisor (2019-20).** Ms Paige Wolverson, MSc Translational Neuropathology, Department of Neuroscience (SITraN). I planned and supervised the entirety of Paiges's MSc project – but due to COVID-19, the project had to be changed from a lab-based project to an extensive literature review.
- **Neuroanatomy Demonstrator (2017-20).** I have been a neuroanatomy demonstrator at the Medical Teaching Unit (MTU) teaching to first year medical students and MSc neuroscience students.

I have organised:

- **Principal Organiser of 'Alzheimer's Disease & Vascular Dementia Symposium'**, INOX, University of Sheffield – 2019. I organised and planned the symposium which was the first such symposium to happen in Sheffield. I invited Professor Nigel Hooper (Vice Dean for R&I & Head of Dementia Research, University of Manchester) to be the keynote speaker. I secured over £2000 from ARUK, Proteintech, University of Sheffield's Think Ahead Scheme & the Company of Biologists. The purpose of this inaugural event was to showcase the range of neuroscience-related dementia research happening across Sheffield. The morning session comprised of senior academics discussing their research and methods, with the afternoon session having PhD students presenting their research. This was a hugely successful event with excellent feedback.
- **Principal Organiser of Sheffield Dementia Symposium 2020**, INOX, University of Sheffield – 2020. Due to the huge success of the inaugural symposium, I decided to organise a second event for 2020 with Professor John Hardy FRS (University College London) as the keynote speaker. This event has been postponed due to the COVID-19 pandemic.

Extracurricular DDP activities include:

Freelance Medical Writer, AzoNetworks' News-Medical. I have authored 90+ medical articles on topics primarily focusing on neuroscience, but also other biomedical disciplines including immunity, cardiovascular diseases, cell & molecular biology, neurology & psychiatry. The link to my profile: https://www.news-medical.net/medical/authors/osman-shabir